A linelist for the hydrogen sulphide molecule

Ala'a A. A. Azzam

Department of Physics and Astronomy

University College London

A thesis submitted for the degree of

Doctor of Philosophy

29 July 2013

I, Ala'a A. A. Azzam, confirm that the work presented in this thesis is my own. Where information has been derived from other sources, I confirm that this has been indicated in the thesis.

Acknowledgements

I would like to thank the University of Jordan for the financial support. Where I have been fortunate and privileged to have been selected by the physics department for having a PhD degree in atomic and molecular physics, and to convey my knowledge to my community as a lecturer in the University of Jordan.

I thank my family with all of my heart for their continuous support and encouragement without which this thesis would not have been possible. My father who did not hesitate to present our house as a grantee for my Jordanian scholarship. My mother who was indefatigable in keeping tracking my life and my study abroad day by day. My brother Mohammad-Kher, and my sisters, Dunia and her husband Omar, Isra'a and her husband Mohammad, and Sumaya and her husband Khaled, who kept motivating and strengthening me at the moments of tiredness and weakness. Also my best brother Ala'a-Aldeen my source of inspiration of hope. I will not forget to thank my nephews from eldest to youngest, Abd Allah, Rashid, Ahmad, Zaid and Qutaiba for keeping calling me and inspiring me by their smiles and very nice comments.

It is of my pleasure of having been supervised by professor Jonathan Tennyson, one of the outstanding researchers in the molecular spectroscopy field. His very long experience and unequalled knowledge made him guiding me to achieve the aims of this research successfully meeting the dead line of my Jordanian scholarship. I would like to thank him also for his financial support through the ERC advanced investigator project 267219, partial support for my salary which made my life much easier in a very expensive city such as London, and full support for attending scientific conferences during my study.

Thanks are also due to all the members of ExoMol group and my other colleagues. I am particularly grateful for, my co-adviser Sergey Yurchenko who I consider as a good example of enthusiastic and very organised researcher, Pavlos G. Galiatsatos who taught me in very good way the basics of the programming using FORTRAN when I had no idea about any programming language before, Lorenzo Lodi who did not hesitate to answer my questions and to discuss some problematic situations during this research giving very valuable advices.

Thanks are also due to Marie-Aline Martin-Drumel and Olivier Pirali, with whom I have collaborated during the experimental work at SOLEIL synchrotron in Paris.

Among my many friends who I met during my study in London, I would like to thank my best friend, Bedoor Alkurtass who shared me my happiest moments and my saddest ones.

Abstract

The main aim of this study is to calculate a high temperature line list for $H_2{}^{32}S$. The results will form an important addition to the databases used for space applications, as well as laboratory investigations and pollution studies. The Dvr3d program suite is used to calculate the bound ro-vibrational energy levels, and dipole moment transition intensities. The most accurate available potential energy surface is empirically determined. This surface is used in our calculations after refining it by fitting to the up-to-date experimental data. For accurate line intensities, an accurate dipole moment surface (DMS) is needed. Constructing an accurate DMS for H_2S is well known to be difficult. A systematic *ab initio* study for the DMS has been performed. Different methods were tested in conjunctions with different basis sets taking into account the relativistic corrections and core-valence effects. The resulting (ATY2013) line list should be valid from 0 to 9000 cm^{-1} and for temperature up to 2000 K. ATY2013 with cut off intensity of order 10^{-31} $cm^{-1}/(molecule \times cm^{-2})$ contains $\sim 36 \times 10^6$ transitions at 2000 K.

In addition, the pure rotational transition frequencies of H_2S in natural abundance in its ground and first excited vibrational states have been recorded at room temperature at 0.005 cm^{-1} resolution in the region 45 to 360 cm^{-1} with a globar continuum source at SOLEIL synchrotron. 2400 rotational transitions are assigned to ground vibrational state of the four isotopologues $H_2{}^{32}S$, $H_2{}^{33}S$, $H_2{}^{34}S$ and $H_2{}^{36}S$ where 65% of them are new. 91 rotational transitions of $H_2{}^{36}S$ were identified for the first time, as well as 406 rotational lines of $H_2{}^{32}S$ and $H_2{}^{34}S$ in their first excited bending vibrational state were recorded and analysed for the first time.

Contents

List of Figures

Chapter 1

Introduction

1.1 General background

Hydrogen sulphide (H_2S) also known as sewer gas, is colourless, flammable, poisonous, with a characteristic odour of rotten eggs [pubchem.ncbi.nlm.nih.gov]. It is a light, nonrigid, triatomic molecule with bent shape of C_{2v} symmetry at its equilibrium, with bond lengths (r_e) H-S of 1.3356 Å, and a bond angle (θ_e) H-S-H of 92.11° [Edwards et al. [1967]]. It is similar in its molecular shape to the water molecule (H_2O) and hydrogen selenide molecule (H_2Se), but H_2S is a near oblate asymmetric top rotor with Ray's asymmetry parameter (κ = (2B - A - C)/(A - C)) = 0.52. As it is clear from its molecular formula, this molecule contains two hydrogen atoms with one electron each ($1s^1$), and one sulphur atom with 16 electrons ($1s^2 2s^2 2p^6 3s^2 3p^4$). Four sulphur isotopes are stable: ^{32}S, ^{33}S, ^{34}S, and ^{36}S with natural abundances of 95.02%, 0.75%, 4.21% and 0.02%, respectively.

H_2S is produced naturally in volcanoes [Hoshyaripour et al. [2012]] and is a byproduct of human activity such as water treatment processes [L. Colomer et al. [2012]]; it is therefore a trace species in the Earth's atmosphere. It is known to be more abundant in the atmospheres of solar system gas giants [Visscher et al. [2006]] and it is thought to be important for the sulphur chemistry of extra-solar planets [Zahnle et al. [2009]]. Indeed it is also found in the atmospheres of cool stars and is the dominant sulphur-bearing gas-phase species in sub-stellar objects such as brown dwarfs [Visscher et al. [2006]]. H_2S has long been known to be

present in interstellar clouds in our galaxy [Thaddeus et al. [1972b]] and has been also observed in star-burst galaxies [Aladro et al. [2011]]. Its role in shocks and star formation regions is thought to be of particular importance [Wakelam et al. [2004]]. Modern astronomical telescopes such as Herschel, SOFIA and ALMA have allowed astronomers to observe species such as H_2S at THz frequencies for the first time [Justtanont et al. [2012]], thus opening a window on higher-lying rotational levels for this species.

1.2 ExoMol

$H_2{}^{32}S$ was studied as part of the ExoMol project to produce a database of synthetic molecular line lists [www.exomol.com]. ExoMol aims to provide the information needed to understand the physics and chemistry of astronomical bodies cool enough to form molecules in their atmospheres such as cool stars, extrasolar planets and planetary disks. The list of molecules in this database are selected mainly on the basis of their importance for modelling spectra of extrasolar planets. The idea of probability for detecting life outside our planet became promising especially after very many confirmed detections of exoplanets. EChO 'the Exoplanet Characterisation Observatory' is a space mission specifically geared for this purpose of detecting and investigating exoplanetary atmospheres and to address the suitability of planets for the presence of life. EChO will simultaneously observe a broad spectral region (from the visible to the mid-infrared) to constrain the temperature structure of the atmosphere, the abundances of the molecular species and magnetospheric signatures, see Tinetti et al. [2012].

ExoMol's list of molecules contains diatomic molecules such as: LiH, OH, CN, NO, HCl, KCl, NaCl, NaH, SiH, SiO, VO, YO, NiH, CrH, SH, SO, TiH, TiO, AlH, AlO, FeH, CaH, CH, CO, BeH, MgH, triatomic molecules such as: H_2O, H_2S, SO_2, CO_2, O_3, C_3, HCN/HNC, HDO, and larger molecules such as: PH_3, NH_3, SO_3, CH_4, HOOH, H_2CO, C_2H_2, C_2H_4, C_2H_6, C_2H_8. This list of molecules also contains some ions such as: HeH^+, $H_3{}^+$, H_2D^+ [Tennyson and Yurchenko [2012]]. Comprehensive and very large rotation-vibration and rotation-vibration-electronic (rovibronic) line lists for this list of molecules will be computed using mixture of first principles and empirically-tuned quantum mechanical methods.

A water line list (BT2) was produced using Dvr3d program suite [Tennyson et al. [1995]] (the same program used for calculating H_2S line list). BT2 comprises over 500 million transitions (65 % more than any other list) and it is also the most accurate (over 90 % of all known experimental energy levels are within 0.3 cm^{-1} of the BT2 values). Its accuracy has been confirmed by extensive testing against astronomical and laboratory data. BT2 has been used to identify individual water lines in a variety of objects including comets, sunspots, a brown dwarf and the nova-like object V838 Mon, where water abundances and temperatures were derived for these objects, see Barber et al. [2006] for more details. Importantly, BT2 was also instrumental in the detection of water in exoplanet HD189733b [[Tinetti et al. [2007]].

Hot line list for BeH, MgH and CaH in their ground electronic states were calculated up to 2000 K as part of ExoMol by Yadin et al. [2012]. Line lists for SO_3 and PH_3 at room temperature were calculated by Underwood et al. [2013] and Sousa-Silva et al. [2013], respectively, as part of ExoMol as well, and the calculations for producing hot line lists for these two molecules are in progress.

1.3 Sulphur chemistry in space

The investigation of the sulphur chemistry in space is a subject of the active research [Aladro et al. [2011]; Hu et al. [2013]; Russell and Kivelson [2001]; Visscher et al. [2006]; Zahnle et al. [2009]]. Hu et al. [2013] studied the atmospheric composition and the spectra of terrestrial exoplanets with sulphur compounds (i.e., H_2S and SO_2) emitted from their surfaces using one-dimensional photochemistry model and radiative transfer model to investigate the sulphur chemistry in atmospheres ranging from reducing to oxidising. Visscher et al. [2006] used thermochemical equilibrium and kinetic calculations to model sulphur chemistry in giant planets, brown dwarfs, and extrasolar giant planets, and according to them, hydrogen sulphide is the dominant S-bearing gas throughout substellar atmospheres and approximately represents the atmospheric sulphur inventory. Therefore, observations of H_2S in these objects should provide a good estimate of their atmospheric sulphur content.

Aladro et al. [2011] detected H_2S for the first time in M82 galaxy, where they studied the chemical complexity towards the central parts of the starburst galaxy, and investigated the role of certain molecules as tracers of the physical processes in the galaxy circumnuclear region. Evidence for sulphur dioxide, sulphur monoxide, and hydrogen sulphide in the Io exosphere were found by Russell and Kivelson [2001]. For Venus, the H_2S composition of the atmosphere below 100 km altitude was studied by Zahn and Moroz [1985] and de Bergh et al. [2006]. Determination of the abundances of gases such as CO, SO_2, OCS, S_2 or H_2S near the surface is important to constrain the oxidation state of the lower atmosphere and surface, and determine the stability of various minerals. Also, measurements at higher altitudes of, for example, SO_3, SO or elemental sulphur, are needed to better understand the sulphur cycle and the chemistry at work below the cloud base.

An accurate and complete line list for H_2S is very important for astrophysics applications especially for modelling [Barber et al. [2006]; Tennyson and Yurchenko [2012]]. Although, the experimentally measured transitions are more accurate than their counterpart *ab initio* calculated transitions as will be shown below, the experimentally measured data are incomplete for two reasons: first, different parts of the spectrum are measured separately and sometimes by different people. As a result, some gaps can be found along the spectrum, see as an example the region 14 500 – 15 500 cm^{-1} in Fig. 1.2. Second, the effective Hamiltonians used to fit some molecular rotational constants predict transitions very well up to certain extent in terms of the rotational quantum number J, but these Hamiltonians perform very badly for the transitions with high values of J and K_a and can be not reliable. Because of this a very high extrapolation for the experimentally measured transitions is not recommended. At least because of these two reasons, the variational calculations are considered more complete than the data available in spectroscopic databases such as HITRAN for instant, see Chapter 5 for more detail about the completeness of the variational calculations.

1.4 Previous studies

Numerous experimental and theoretical studies have been performed on the absorption spectrum of this molecule. This section summarises the previous studies

for $H_2{}^{32}S$ absorption spectra (up to our knowledge) on the basis of experimental and theoretical works.

1.4.1 Experimental studies

The general experimental procedures for detecting and analysing spectra are: (1) recording spectra, (2) assigning recorded transitions, (3) fitting the parameters of a chosen theoretical model to the recorded transitions, and (4) making predictions (extrapolation). The accuracy of the predicted transitions depends on the accuracy of the theoretical model used. Chapter 6 in this thesis provides an example of experimental work that includes recording, assigning, fitting and predicting spectra. Fig. 1.1 shows some assigned experimentally measured transitions for H_2S in natural abundance.

Known experimental absorption spectra of H_2S molecule cover the region from the microwave region up to 16 500 cm^{-1} and include transitions belonging to 59 vibrational bands from 14 polyad regions, covering its rotational, fundamental, overtone, hot, and combination bands [Polovtseva et al. [2012]]. The polyad number is defined as $v = v_1 + v_2/2 + v_3$, where v_i are the vibrational quantum numbers.

The ground vibrational (rotational) band has received attention from many experimentalists, such as Burenin et al. [1985]; Burrus et al. [1953]; Cupp et al. [1968]; Flaud et al. [1983]; Helminger et al. [1972]; Huiszoon [1971]; Huiszoon and Dymanus [1966]; Miller et al. [1969]; Yamada and Klee [1994] and Belov et al. [1995]. The first bending vibrational band (ν_2) at 1183 cm^{-1} was studied by Lane et al. [1982]; Strow [1983] and Ulenikov et al. [1996a]. The two fundamental stretching; symmetric (ν_1) and asymmetric (ν_3) lying at 2615 and 2626 cm^{-1}, respectively, are not isolated but overlapped with strong Coriolis and Fermi resonance interactions. The first triad region ($2\nu_2, \nu_1$, and ν_3) was studied by Gillis and Edwards [1981], while the second triad region ($3\nu_2, \nu_1 + \nu_2$, and $\nu_2 + \nu_3$) was studied by Snyder and Edwards [1969] and Ulenikov et al. [1996b]. Brown et al. [1998] studied these two triad regions together recently. The spectral region 4500 – 5600 was investigated by Brown et al. [1997]. Brown et al. [2004] and Ulenikov et al. [2005] recorded and analysed the transitions in the

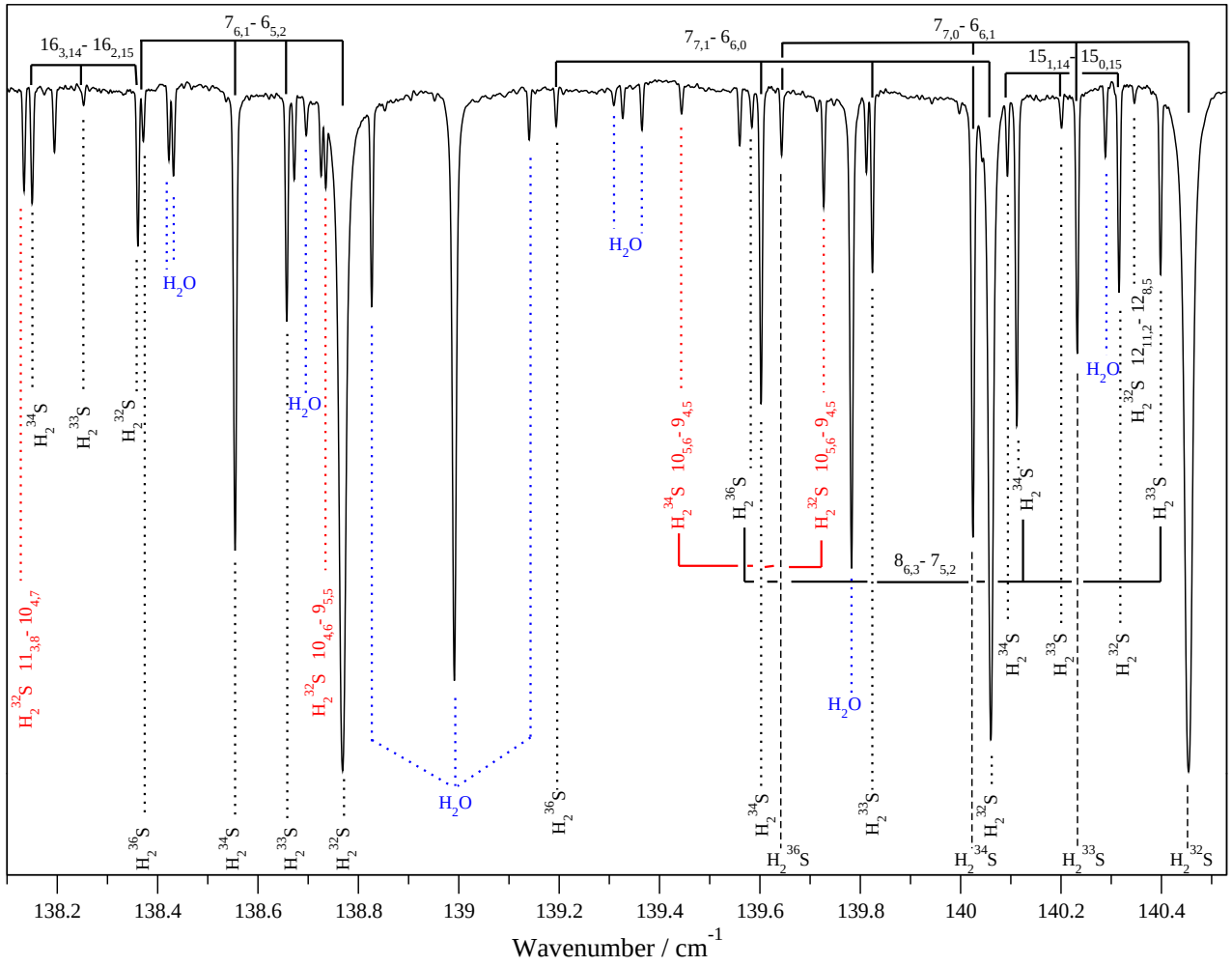

Figure 1.1: A portion of the absorption spectrum of H_2S recorded at SOLEIL synchrotron, showing some pure rotational transitions in both ground and bending vibrational states $v_2 = 1$. The pure rotational transitions within $v_2 = 1$ are illustrated in red. see Chapter 6 for detail.

region 5700 – 6600 cm^{-1}. In the region 7300 – 7900 cm^{-1}, more than 1550 transitions up to $J = 14$ were recorded and analysed by Ulenikov et al. [2004] as well. The absorption spectrum in the region 8400 – 8900 cm^{-1} has been recorded by Brown et al. [2004]. Many other regions have been studied, namely, 9540 – 10 000 cm^{-1} by Ding et al. [2003], 10 780 – 11 330 cm^{-1} by Naumenko and Campargue [2001b], 11 930 – 12 300 cm^{-1} by Großkloß et al. [1994] and Flaud et al. [1995], 12 270 – 12 670 cm^{-1} by Vaittinen et al. [1997], near 13 200 cm^{-1} by Campargue and Flaud [1999], 14 100 – 14 400 cm^{-1} by Flaud et al. [1998], and 16 180 – 16 440 cm^{-1} by Naumenko and Campargue [2001a], see Fig. 1.2. As one can see, the detection and analysis of the absorption spectrum of H_2S molecule up to 16 500 cm^{-1} needed more than 50 years. Different groups of experimentalists had employ different types of experimental setups for different spectral regions, e.g. the Fourier transform spectrophotometer, tunable diode laser, and interactivity laser absorption spectrometer. The accuracy of these measurements for the transition positions can be summarised as follows: 10^{-6} – 10^{-5} cm^{-1} in the microwave region, 0.0008 – 0.002 cm^{-1} up to 9000 cm^{-1}, and 0.005 – 0.02 cm^{-1} up to 16 500 cm^{-1}. The highest recorded value of the rotational quantum number J is 22 in the rotational band region, and the highest predicted value is 27 in the same region. Now, around 10 000 ro-vibrational (for rotational vibrational) energy levels are known experimentally.

The spectroscopic data for the H_2S molecule from some of these publications can be found in different databases. Table 1.1 summarises the data given in HITRAN 2008 [Rothman et al. [2005, 2009]], GEISA [Jacquinet-Husson et al. [2011]], IAO LMS Spectra [spectra.iao.ru], W@DIS [Polovtseva et al. [2012]], CDMS [Müller et al. [2001, 2005]], and JPL [Pickett et al. [1998]] databases. All these databases contain data resulting from fitted effective Hamiltonians, apart from W@DIS which contains only measured transitions without intensities (i.e. transition positions with their full assignments). In the new release of HITRAN 2012, apart from our contribution for the rotational band of H_2S spectrum (see Chapter 6), the added data to the database for this molecule is the same data published in IAO LMS Spectra.

Table 1.1: Summary for the H_2S spectral data available in different databases.

Database	isotopologue	Bands #	Transitions #	Wavenumber_{min} (cm^{-1})	Wavenumber_{max} (cm^{-1})
HITRAN 2008	$H_2{}^{32}S$	14	12330	2.9853	4256.54681
	$H_2{}^{33}S$	8	3564	5.6009	4098.23423
	$H_2{}^{34}S$	8	4894	5.6146	4171.17585
GEISA	$H_2{}^{32}S$	14	12330	2.9853	4256.54681
	$H_2{}^{33}S$	8	3564	5.6009	4098.23423
	$H_2{}^{34}S$	8	4894	5.6146	4171.17585
IAO LMS Spectra	$H_2{}^{32}S$	35	21905	4471.77211	11329.77986
	$H_2{}^{33}S$	11	1814	4790.94190	11071.42137
	$H_2{}^{34}S$	16	5273	4692.08729	11226.58655
W@DIS	$H_2{}^{32}S$	59	34148	1.168413	16436.572
CDMS	$H_2{}^{32}S$	1	1501	1.168413	554.490418
	$H_2{}^{33}S$	1	4759	1.096896	402.391663
	$H_2{}^{34}S$	1	990	1.030569	444.369071
JPL	$H_2{}^{32}S$	1	1525	1.168413	332.866807

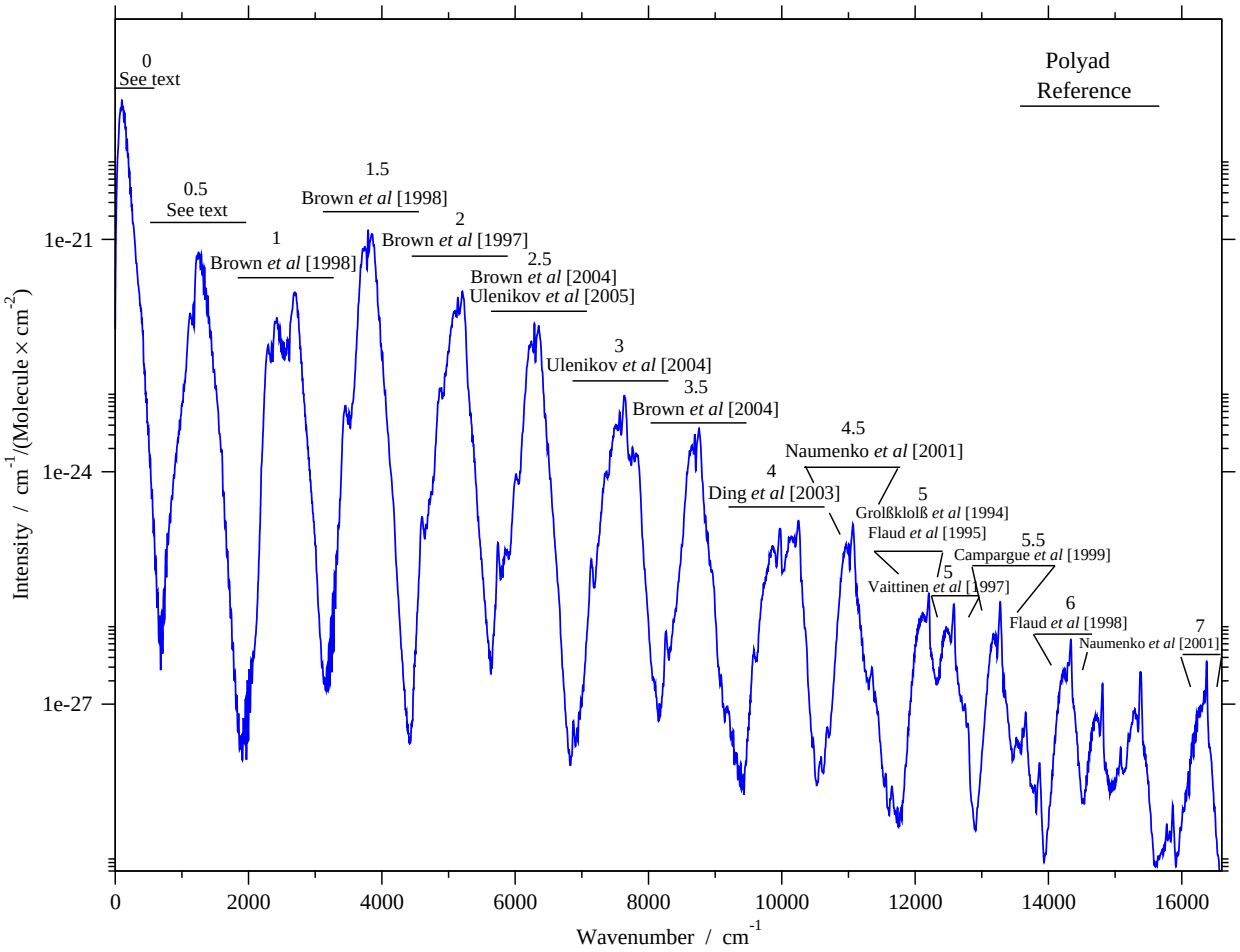

Figure 1.2: Summary for the experimental work on the H_2S absorption spectrum. Note: The spectrum in this plot is calculated at T = 296 K, see Chapter 5 for more details. For the polyad definition see the text.

1.4.2 Theoretical studies

In general, theoretically, the spectrum of a molecule can be calculated from theoretical principles, where transition positions and intensities can be calculated for different spectral regions at the same time. The major part of this thesis describes this kind of work in detail.

The ro-vibrational spectrum of H_2S was calculated by Senekowitsch et al. [1989]; Tarczay et al. [2001a] and Tyuterev et al. [2004]. In the work of Senekowitsch et al. [1989], the room temperature absorption ro-vibrational spectrum of H_2S was calculated variationally for the pure rotational and ν_2, $2\nu_2$, ν_1, and ν_3 transitions from $J = 0$ to 13, where the full account of the anharmonicity effects and ro-vibration couplings were considered. Senekowitsch et al. [1989] calculated the vibrational band origins of the fundamental transitions with accuracy better than 10 cm^{-1}, and the ro-vibrational transitions to within a few tenths of a cm^{-1} for low J's and up to a few cm^{-1} for high J's. The anomalies in the spectral intensity for this molecule were obtained qualitatively and the different kinds of the anomalies in the spectrum are discussed in details in Chapter 4. Tarczay et al. [2001a] calculated the vibrational band origins of $H_2{}^{32}S$ with accuracy of 29 cm^{-1} up to 14 300 cm^{-1}, and the rotational transitions of the ground vibrational state for $J = 17$ with deviations from the experimental values from 2 to 10 cm^{-1}, where the nuclear motion calculations were performed using the Dvr3d program of Tennyson et al. [1995]. Tyuterev et al. [2004] calculated the spectrum for this molecule for the interval 0 – 8000 cm^{-1}, up to J_{max} and $K_{a\ max} = 18$ with intensity cut-off $\leq$ 10^{-27} $cm^{-1}/(molecule \times cm^{-2})$. Tyuterev et al. [2004] reported that the convergence of their calculated transitions to be better than 0.01 cm^{-1} for the line positions in the wavenumber range considered and 1-3% in the intensities for the strong and medium lines and to $\sim$10% for the weak lines for room temperature conditions. The general methodology of calculating a line list for triatomic molecules is discussed in Chapter 2.

1.5 Thesis structure

This work presents a detailed study of theoretical $H_2{}^{32}S$ spectra up to 2000 K and experimental rotational spectrum for this molecule recorded at room temperature.

Chapter 2 introduces the main theoretical framework of the molecular spectroscopy, where the Schrödinger equation is solved in two steps using the Born-Oppenheimer approximation: (1) motion of electrons and (2) motion of nuclei.

Chapter 3 presents tests for some potential energy surfaces (PESs), where the PESs labelled as PES-Y, PES-Y0125 and PES-Y0-6 where constructed and fitted by S. Yurchenko. In this chapter, the convergence tests for the ro-vibrational energy levels in order to obtain the optimum values for some computational parameters are presented as well.

Chapter 4 discusses a study for construction of an accurate dipole moment surface (DMS) important to describe the known anomalies in the transition intensities of H_2S spectrum quantitatively. During the work presented in this chapter some very useful advices were given directly from L. Lodi who constructed previously an accurate DMS for the water molecule.

Chapter 5 examines the accuracy of the calculated line list by comparing the transition positions and intensities with the available experimental data at room temperature. The hot spectra and calculations of the partition functions are presented in this chapter as well.

Finally, Chapter 6 describes new experimental measurements of the rotational absorption spectrum of H_2S at room temperature, where a comprehensive analysis of the spectrum as well as comparison with previous studies were performed . The author of this thesis had the opportunity to do this experiment at the SOLEIL synchrotron in Paris with the team from the AILES beamline; M.-A. Martin-Drumel and O. Pirali.

Chapter 2

Theory

Theoretical spectroscopy from *ab initio* (from first principles) is a very important field in chemical physics research for its applications in many scientific domains including atmospheric physics and astrophysics. Different spectroscopic parameters such as transition positions and intensities can be calculated with high accuracy (some times with an accuracy close to the experimental accuracy) by employing the established theories underlying molecular spectroscopy since the first quarter of the 20th century. One should note that one of the major factors of the achieved accuracy is not just these theories, but also the available numerical computational methods and the computational resources (such as high performance computing systems) which made this high accuracy accessible theoretically, and this is because of the many-body problem which one cannot solve analytically. In quantum chemistry, the calculation of energy and the wavefunction of a system of nuclei and electrons is not an easy task without employing the Born-Oppenheimer (BO) approximation. Using this approximation the problem can be solved in two major consecutive steps. This approximation was proposed in 1927 by Max Born and J. Robert Oppenheimer and is still applicable in quantum chemistry. This chapter summarises this approximation and its two major steps.

2.1 Born-Oppenheimer approximation

The BO approximation is considered as a central approximation in molecular spectroscopy, since it allows one to separate the electronic and nuclear (rotation and vibration) motions. There are two approaches for this approximation: the perturbation theory approach, and the variation theory approach, see the book by Bunker and Jensen [2000] for details. In basic terms, this approximation breaks the wavefunction of a molecule into its electronic and nuclear components.

$$\Psi_{molecule} = \psi_{electrons}(\mathbf{r};\mathbf{R}) \times \psi_{nuclei}(\mathbf{R}), \tag{2.1}$$

where $\mathbf{r}$ and $\mathbf{R}$ are the set of electronic and nuclear coordinates, respectively. In making this approximation we assume that the motions of the electrons are unaffected by the motions of the nuclei and only depend on the nuclear positions. The high ratio between the nuclear and electronic masses makes this approximation applicable. The Coulombic forces acting on the nuclei and on the electrons are similar in magnitude, but the electrons are much lighter. The electrons therefore move much faster than the nuclei and, as a consequence, the electronic motion can be separated from the nuclear motion. For more details about BO approximation see the book by Jensen and Bunker [1998].

The exact non-relativistic molecular (rovibronic; rotational, vibrational and electronic motion) Hamiltonian operator with the axis system origin at the nuclear centre of mass with an arbitrary space-fixed orientation is written as

$$\hat{H} = \hat{K}_N + \hat{K}_e + V(\mathbf{R},\mathbf{r}), \tag{2.2}$$

where $\hat{K}_N$ and $\hat{K}_e$ are the kinetic energy operators for nuclei and electrons, respectively. $V(\mathbf{R},\mathbf{r})$ is the potential for the system under study. Using the BO approximation the wavefunctions $\psi_{electrons}$ and energies $E_{electrons}$ that describe the electronic motion are obtained from the Schrödinger equation that results after neglecting the nuclear kinetic energy term $\hat{K}_N$ (clamped-nuclei) from Eq. (2.2). As a result, the electronic Schrödinger equation can be written as

$$\hat{H}_{electrons}(\mathbf{r};\mathbf{R})\psi_{electrons}(\mathbf{r};\mathbf{R}) = E_{electrons}(\mathbf{R})\psi_{electrons}(\mathbf{r};\mathbf{R}). \tag{2.3}$$

The eigenvalue $E_{electrons}(R)$ as a function of the nuclear geometry plays the role of a potential energy for the motion of the nuclei in the second step of the solution, where the nuclear Schrödinger equation is

$$\left[\hat{K}_N + E_{electrons}(R)\right] \psi_{nuclei}(R) = E\psi_{nuclei}(R). \tag{2.4}$$

2.2 Electronic motion problem

Ab initio construction of a potential and dipole moment hypersurfaces involves

1. choice of an accurate electron correlation methodology,
2. application of a basis set, and
3. design of a suitable geometrical grid for the calculations.

Independent of the choices made for the basis set and the electron correlation technique, the accuracy of the computational results can vary significantly with varying internuclear separation [Császár et al. [2000]]. For the electronic structure calculations in this work, the MOLPRO software package [Werner et al. [2012]] was used.

The following subsections describe the *ab initio* quantum chemistry methods and the basis sets which are used in the electronic structure calculations in general.

2.2.1 *Ab initio* quantum chemistry methods

Fig. 2.1 shows a hierarchy of methods of electronic structure theory. As one can see from this figure, to achieve results close to the non-relativistic limit 'exact solution', the extension of both the atomic basis sets (one-particle wavefunction) and the method (many-electron wavefunction) is needed. Therefore, there are two approximations to be made: (i) truncation of the bases set and (ii) truncation of the method. The usefulness, quality, and reliability of any given approximation must be assessed from a large number of tests, where one should take into account the desirable accuracy (depending on the studied physical property) and the

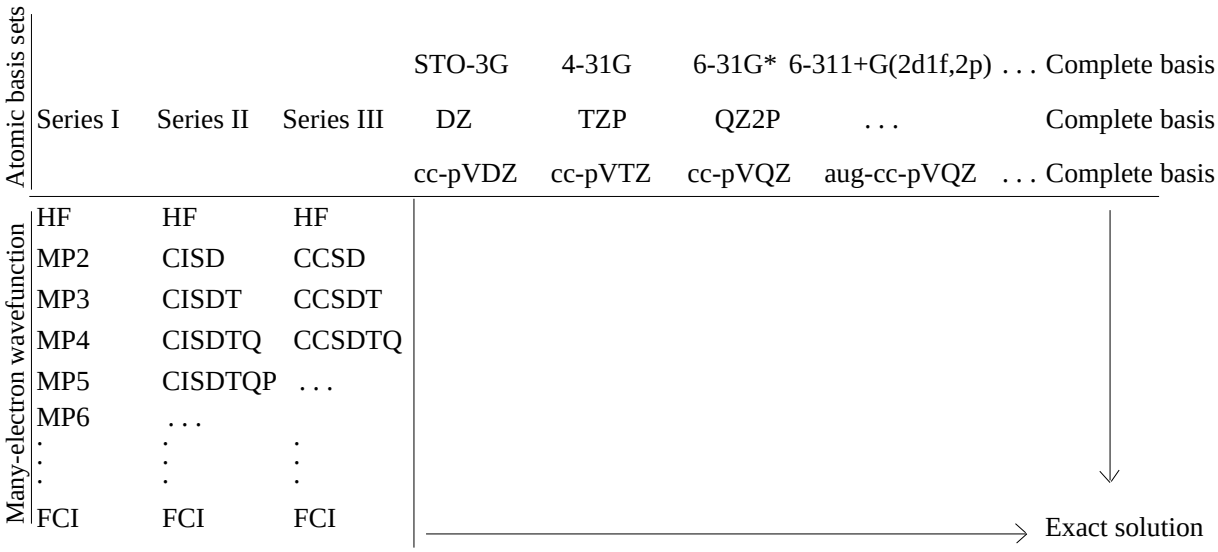

Figure 2.1: Computational matrix of *ab initio* electronic structure theory indicating quality of the basis sets versus quality of the computational method (as plotted in Császár et al. [2000].

available computational resources. One should note that, to approach the exact solution using *ab initio* methods, the computational cost should be paid, where this often takes enormous amounts of computer time, memory, and disk space.

Many *ab initio* electronic structure methods are available, and which one to use for a specific problem is usually chosen by comparing the results against known experimental data. The most popular classes for these methods are: Hartree-Fock methods and Post-Hartree-Fock methods. In the following subsections, these two classes of methods are described from a very general point of view. For more details, see for example Jensen [2006] and Jensen and Bunker [2000]

2.2.1.1 Hartree-Fock methods

Hartree-Fock (HF), also called the self-consistent field method (SCF), is used for closed-shell systems with all orbitals doubly occupied. The solution of this method is the central starting point for most methods that describe the many-electron system more accurately. The HF model considers the molecular orbitals (MO) as one-electron functions describing movement of an electron in an average (effective) field of all other electrons. Using this method, the exact n-electron

wavefunction $\psi_{electrons}$ can be approximated by a single Slater determinant of n spin-orbitals (ansatz):

$$\psi_{electrons} \approx \psi_{HF} = \begin{vmatrix} \phi_1(\mathbf{r_1})\alpha(\sigma_1) & \phi_1(\mathbf{r_1})\beta(\sigma_1) & \phi_2(\mathbf{r_1})\alpha(\sigma_1) & \cdots & \phi_n(\mathbf{r_1})\beta(\sigma_1) \\ \phi_1(\mathbf{r_2})\alpha(\sigma_2) & \phi_1(\mathbf{r_2})\beta(\sigma_2) & \phi_2(\mathbf{r_2})\alpha(\sigma_2) & \cdots & \phi_n(\mathbf{r_2})\beta(\sigma_2) \\ \vdots & \vdots & \vdots & \ddots & \vdots \\ \phi_1(\mathbf{r_n})\alpha(\sigma_n) & \phi_1(\mathbf{r_n})\beta(\sigma_n) & \phi_2(\mathbf{r_n})\alpha(\sigma_n) & \cdots & \phi_n(\mathbf{r_n})\beta(\sigma_n) \end{vmatrix}, \quad (2.5)$$

where ϕ is typically a linear combination of atomic orbitals (LCAO), and α and β are the two possible spin functions for an electron which can be written as $\left|\frac{1}{2}, \frac{1}{2}\right\rangle$ and $\left|\frac{1}{2}, -\frac{1}{2}\right\rangle$, respectively, and σ_i is the spin coordinate of the electron i. In the spin-restricted HF method (RHF), pairs of electrons occupy the same spatial orbital.

For the open-shell systems where some of the electrons are not paired, the restricted open-shell HF (ROHF) method is used, where electrons that are paired with each other are restricted to occupy the same spatial orbital as in the RHF method. Also, for these systems the spin-unrestricted HF (UHF) method can be used, where spin-orbitals are still restricted to be of a product form, but α and β electrons are allowed to occupy different spatial functions.

HF methods do not account for the electrons correlation energy E_{corr}, which is defined as

$$E_{corr} = E - E_{HF}, \quad (2.6)$$

where E is the exact non-relativistic electronic energy of the system. In other words, E_{corr} is the residual energy not accounted for by the HF solution.

2.2.1.2 Post-Hartree-Fock methods

The HF method determines the energetically best one-determinant trial wavefunction (within the given basis set). A generic multi-determinant trial wavefunction can be written as

$$\psi_{electrons} = a_0\psi_{HF} + \sum_{i=1} a_i\psi_i. \quad (2.7)$$

Post-Hartree-Fock methods (electron correlation methods) differ in how they calculate the coefficients in front of the other determinants, with a_0 being determined by the normalisation condition. The multi-determinant wavefunction $\psi_{electrons}$ can be considered as describing the total wavefunction in a 'coordinate' system of Slater determinants, where the number of determinants included determines the size of the many-electron basis. The ψ_i determinants may be generated by replacing MOs that are occupied in the HF determinant by MOs that are unoccupied (virtual). This replacement process produces Slater determinants for excited states. Limiting the number of determinants to only those that can be generated by exciting the valence electrons is known as the frozen-core approximation.

There are three main methods for calculating the electron correlation:

1. configuration interaction (CI),
2. many-body perturbation theory (MBPT), and
3. coupled cluster (CC).

CI is the oldest method and is based on the variational principle, analogous to the HF method. The trial wavefunction of this method is written as

$$\psi_{CI} = a_0\psi_{HF} + \sum_S a_S\psi_S + \sum_D a_D\psi_D + \sum_T a_T\psi_T + ... = \sum_{i=1} a_i\psi_i, \qquad (2.8)$$

where the subscripts S, D, T, etc., indicate determinants that are Singly, Doubly, Triply, etc., excited relative to the HF configuration. The expansion coefficients in this equation are determined by requiring that the energy should be minimal under the constraint that the total CI wavefunction is normalised. The MOs used for building the excited Slater determinants are taken from a HF calculation and held fixed. In another method called 'Multi-Configuration Self-Consistent Field' (MCSCF), not only the coefficients in front of the determinants are optimised by the variational principle, but the MOs used for constructing the determinants are also optimised. In the CI method, all the excited determinants are generated from a single determinant (ψ_{HF}). In another method called 'Multi-Reference Configuration Interaction' (MRCI), which uses many reference configurations to generate CI, it is usual to choose an MCSCF wavefunction as the reference.

CC theory constructs multi-electron wavefunctions using the exponential cluster operator to account for electron correlation. The fundamental equation of CC theory is

$$|\psi\rangle_{CC} = e^{\hat{T}} |\psi_0\rangle \,, \tag{2.9}$$

where $|\psi\rangle_{CC}$ is the correlated molecular electronic wavefunction ansatz and $|\psi_0\rangle$ is the reference wavefunction (a Slater determinant constructed from HF molecular orbitals). The exponential operator $e^{\hat{T}}$ may be expanded as

$$e^{\hat{T}} = 1 + \hat{T} + \frac{\hat{T}^2}{2} + ..., \tag{2.10}$$

and the cluster operator has the form

$$\hat{T} = \hat{T}_1 + \hat{T}_2 + \hat{T}_3 + \hat{T}_4 + ..., \tag{2.11}$$

where $\hat{T}_1$ is the operator for all single excitations, $\hat{T}_2$ is the operator of all double excitations and so on. There are different types of CC methods, depending on the number of excitations considered, where CCS is the CC with single excitations, CCSD for single and double excitations, CCSDT for single double and triple excitations and CCSDTQ for the quadruple excitations included in the treatment as well. As an example, the $\hat{T}$ operator in CCSDT has the form

$$\hat{T} = \hat{T}_1 + \hat{T}_2 + \hat{T}_3. \tag{2.12}$$

Some methods of CC theory are available with an approximate treatment of triples excitations, CCSD-T, CCSD(T) and CCSD[T]. Including all levels of excitation fully treated gives the exact correlation energy for the given basis set. However, as the number of excitations included increases the computational time increases dramatically.

2.2.2 Basis sets

A basis set in theoretical chemistry is a set of functions (called basis functions) which are combined in linear combinations to create molecular orbitals (MO). Typically, these functions are atomic orbitals centred on atoms, but also can be

any function. An exact molecular orbital can be thought of as a function in the infinite coordinate system spanned by the complete basis set (an infinite number of functions). The accuracy of the MO used in the calculations is affected by:

1. when a finite basis set is used, only the components of the MO along those coordinate axes corresponding to the selected basis functions can be represented. The smaller the basis set, the poorer the representation, and

2. the type of basis functions used also influence the accuracy. The better a single basis function is able to reproduce the MO, the fewer basis functions are necessary for achieving a given level of accuracy.

The expansion of the MOs during the calculations leads to integrals of quantum mechanical operators over basis functions, and the ease with which these integrals can be calculated depends on the type of the basis function used.

In electronic structure calculations there are two common types of basis functions (atomic orbitals (AO); note, these AOs are not solutions of any atomic Schrödinger equation): Slater type orbitals (STO) and Gaussian type orbitals (GTO). These two types are identified as

$$\chi_{\zeta,n,l,m}(r,\theta,\phi) = NY_{l,m}(\theta,\phi)r^{n-1}e^{-\zeta r} \quad , \quad (STO) \tag{2.13}$$

$$\chi_{\zeta,n,l,m}(r,\theta,\phi) = NY_{l,m}(\theta,\phi)r^{2n-2-l}e^{-\zeta r^2} \quad , \quad (GTO) \tag{2.14}$$

where N is a normalisation constant and $Y_{l,m}$ are spherical harmonic functions. Both STOs and GTOs can be chosen to form a complete basis, but more GTOs are necessary for achieving a certain level of accuracy compared with STOs (in general with ratio 3 GTOs to 1 STO). This is compensated by the ease with which of integrals can be computed in the case of GTOs.

For a certain molecular geometry (certain nuclei positions), after specifying the function type (STO/GTO), the most important factor for the accuracy of the calculations is the number of functions to be used. The smallest number of functions possible is called a minimum basis set, where only enough functions are employed to contain all the electrons of neutral atoms. This means the following:

1. for hydrogen and helium atoms a single s-function is used,

2. for the atoms in the first row of the periodic table, two s-functions ($1s$ and $2s$) and one set of p-functions ($2p_x$, $2p_y$ and $2p_z$) are used, and

3. for the atoms in the second row of the periodic table, three s-functions ($1s$, $2s$ and $3s$) and two sets of p-functions ($2p$ and $3p$) are used.

The next step for improving the basis set is a doubling of all basis functions, producing a double zeta (DZ) type basis (the term zeta for the exponent used in the mathematical form of the basis functions denoted by the Greek letter ζ). When the doubling is just for the valence basis, the term VDS (for valence double zeta) is used. When the basis set contains three times as many functions as the minimum basis, it is called valance triple zeta (VTZ). Basis sets with quadruple zeta (VQZ) and pentuple zeta (V5Z) can be used for more accurate calculations. Higher angular momentum functions are also important, and these are denoted as polarisation functions, where p-orbitals can be used for polarising s-orbitals, d-orbitals for polarising p-orbitals, f-orbitals for polarising d-orbitals, etc. Higher angular momentum functions are essential for methods including electron correlation (electron correlation describes the energy lowering by the electrons avoiding each other, beyond the average effect taken into account by Hartree-Fock methods).

After deciding on the number of the basis functions used, the next step is to determine the values of the exponents in the basis functions. This is typically done by performing variational calculations for the wavefunctions of atoms, using the exponents as variational parameters, where the exponent values that give the lowest energy are the best. The process of specifying the values of the exponents based on minimising the energy of a wavefunction is called 'basis set optimisation'. Another step for constructing certain basis sets is called 'basis set contraction', where a full set of basis functions, known as the primitive GTOs/STOs (PGTOs/PSTOs), are combined into a smaller set of functions by forming fixed linear combinations

$$\chi(CTGO) = \sum_{i}^{k} a_i \chi_i(PGTO). \tag{2.15}$$

Contraction is especially useful for orbitals describing the inner (core) electrons, since they require a relatively large number of functions for representing the wavefunction cusp near the nucleus, and furthermore are largely independent of the environment. Contracting a basis set will always increase the energy, since it is a restriction of the number of variational parameters, and makes the basis set less flexible, but it will also reduce the computational cost significantly. So, contracted basis sets are useful in the calculations for the chemical properties which are affected by the accuracy of the outer electrons distribution representation rather than the inner electrons. For the contracted basis sets, the previously introduced acronyms DZ, TZ, etc., refer to the number of contracted basis functions, while the degree of contraction is the number of PGTOs entering the CGTO.

Correlation consistent basis sets are geared towards recovering the correlation energy of the valence electrons. These basis sets are defined with the acronym (cc). The name correlation consistent refers to the fact that the basis sets are designed such that functions that contribute similar amounts of correlation energy are included at the same stage, independent of the function type. For example, the first d-function provides a large energy lowering, but the contribution from a second d-function is similar to that from the first f-function.The energy lowering from a third d-function is similar to that from the second f-function and the first g-function. The addition of polarisation functions should therefore be done in the order: $1d$, $2d1f$ and $3d2f1g$.

Dunning and co-workers produced several different sizes of cc basis sets: cc-pVDZ, cc-pVTZ, cc-pVQZ, cc-pV5Z and cc-pV6Z Woon and Dunning [1993]; correlation consistent polarised Valence Double/Triple/Quadruple/ Quintuple/Sextuple Zeta). These basis sets can be augmented with diffuse functions (indicated by adding the prefix aug- to the acronym). The augmentation consists of adding one extra function with a smaller exponent for each angular momentum, i.e. the aug-cc-pVDZ has additionally one s-, one p- and one d-function, the cc-pVTZ has $1s1p1d1f$ extra for non-hydrogens and so on. The cc-basis sets may also be augmented with additional tight functions (large exponents) if the interest is in recovering core-core and core-valence electron correlation, producing the acronyms cc-pCVXZ (X = D, T, Q, 5). The cc-pCVDZ has additionally one tight s- and one p-function, the cc-pCVTZ has $2s2p1d$ tight functions, the cc-pCVQZ has

$3s3p2d1f$ and the cc-pCV5Z has $4s4p3d2f1g$ for non-hydrogens.

For second row systems it has been found that the performance is significantly improved by adding an extra tight d-function [Dunning et al. [2001]] (indicated by adding +d; pV(D+d)Z, pV(Q+d)Z, pV(5+d)Z, etc.). Such basis sets are tested below.

2.3 Relativistic effects

A relativistic effect is defined as the difference in an observable property that arises from the true velocity of light as opposed to the assumed infinite velocity in traditional treatments of quantum chemistry. Relativistic effects in chemistry can be considered to be perturbations, or small corrections, to the non-relativistic theory of chemistry, which is developed from the solutions of the Schrödinger equation. These corrections have differential effects on the electrons in various atomic orbitals within the atom, according to the speed of these electrons relative to the speed of light.

The effects due to relativity can be described as follows:

1. differences in the dynamics due to the velocity-dependent mass of the electron. This alters the size of the orbitals: s- and p-orbitals are contracted while d- and f-orbitals are expanded,

2. new (magnetic) interactions in the Hamiltonian operator due to the electron spin. The spin-orbit coupling, for example, destroys the picture of an orbital having a definite spin,

3. introduction of 'negative' energy (positron) states. The coupling between the electronic and positronic states introduces a 'small' component in the electronic wavefunction. This leads to a change in the shape of the orbitals 'relativistic orbitals', and

4. modification of the potential operator due to the finite speed of light.

Results from fully relativistic calculations are rare, and there is no clear consensus on which effects are the most important. Working with a full four-component wavefunction and the Dirac-Fock operator is very complicated and

computationally is not feasible. Therefore, various approximative methods have been developed such as the Douglas-Kroll transformations.

The relativistic effects can be neglected when the Schrödinger equation is used instead of the Dirac equation. For some phenomena, such as spin-orbit coupling, there is no classical counterpart and only a relativistic treatment can provide an understanding. The relativistic effects include in the calculations as a one component(mass-velocity and Darwin terms), two components (spin-orbit) or full four component method. For the details about the relativistic effects in the electronic energies calculations, see the book by Hess and Marian [2000].

With MOLPRO one can perform calculations within the second-order scalar-relativistic Douglas-Kroll-Hess (DKH2) theory [Reiher and Wolf [2004a,b]]. In this approach the relativistic effects for mass-velocity and Darwin terms are included in an approximate way at the onset by a modification of the Schrödinger equation.

2.4 Nuclear motion problem

Theoretical calculations of ro-vibrational energy levels of polyatomic molecules is a topic with a long history. The following section focuses exclusively on the development of the DVR3D program suite, since it is the program used in this study.

2.5 DVR3D

Ro-vibrational Hamiltonians for different sets of body-fixed axes with different embeddings were reviewed by Tennyson [1986]. Sutcliffe and Tennyson [1986] formulated a generalised coordinate system for triatomic molecules, which includes both Jacobi and Radue coordinates. The discrete variable representation (DVR) methods developed by Bačić and Light [1989] for calculating vibrational wavefunctions in one or more coordinates were implemented in the DVR3D program to yield an efficient method of calculating high-lying ro-vibrational levels of triatomic systems by Tennyson and Henderson [1989]. The DVR3D suite of

programs was developed by Tennyson et al. [1995], and has been subject to subsequent improvements [Tennyson et al. [2004]].

2.5.1 The internal coordinates

Several coordinate systems have been used in the calculations of the ro-vibrational energy levels, two of them are implemented in the DVR3D suite:

1. Jacobi, or scattering coordinates, r_1, r_2 and θ: for a triatomic molecule A_1 - A_2A_3, r_1 is the bond length of the diatomic A_2A_3, r_2 is the length between atom A_1 and the baricenter of the diatomic A_2A_3, and θ is the angle between the vectors r_1 and r_2. This coordinate system in general is suitable for systems formed by a strong bond diatomic molecule (A_2A_3) and a weak bond atom (A_1), and

2. Radau coordinates: The two radial coordinates r_1 and r_2 measure the distance of the two light atoms from the so-called canonical point, which lies very close to the centre of the heavy atom in the light-heavy-light systems (e.g. H_2S), in this coordinate θ represents the angle between the vectors r_1 and r_2.

In DVR3D the internal coordinates are specified by two parameters g_1 and g_2 [Tennyson et al. [2004]], see Fig. 2.2, where

$$g_1 = \frac{A_3 - P}{A_3 - A_2} \quad , \quad g_2 = \frac{A_3 - R}{A_3 - A_1}, \tag{2.16}$$

where for scattering coordinates

$$g_1 = \frac{m_2}{m_2 + m_3} \quad , \quad g_2 = 0, \tag{2.17}$$

and for Radau coordinates

$$g_1 = 1 - \frac{A}{A + B - AB} \quad , \quad g_2 = 1 - \frac{A}{1 - B + AB}, \tag{2.18}$$

and

$$A = \left(\frac{m_3}{m_1 + m_2 + m_3}\right)^{1/2} \quad , \quad B = \frac{m_2}{m_1 + m_2}, \tag{2.19}$$

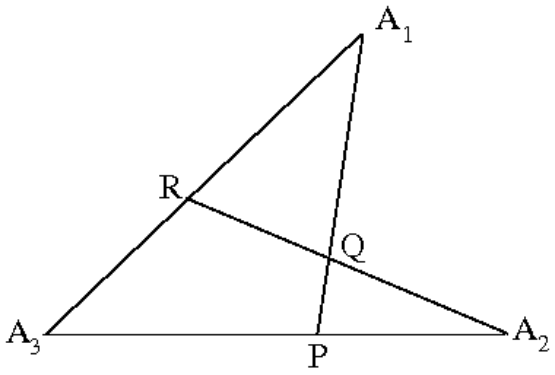

Figure 2.2: Internal coordinate system of Tennyson et al. [2004]. A_1, A_2, and A_3 are three atoms.

In case of H_2S (using Radau coordinates), where $m_1 = m_2$, we get $B = 1/2$, $A = (m_3/(2m_1 + m_3))^{1/2}$, $g_1 = g_2 = 1 - 2A/(1 + A)$.

2.5.2 Reference frames

The nuclear Hamiltonian of a triatomic system in Cartesian coordinates is

$$H = K + V = -\frac{\nabla_1^2}{2m_1} - \frac{\nabla_2^2}{2m_2} - \frac{\nabla_3^2}{2m_3} + V(\mathbf{R_1}, \mathbf{R_2}, \mathbf{R_3}), \tag{2.20}$$

where $\mathbf{R} = \mathbf{X}\hat{\mathbf{i}} + \mathbf{Y}\hat{\mathbf{j}} + \mathbf{Z}\hat{\mathbf{k}}$ is the nuclei coordinates, m_i are the nuclear (or atomic) masses and V is the potential energy surface of the molecule. The first step to solve the Schrödinger equation with Hamiltonian 2.20 is to specify the reference frame. In general we can define three frames of reference as follows:

1. laboratory-fixed frame. It is a reference frame fixed in the laboratory, in this frame the Hamiltonian can be written in its simplest form given by Eq. (2.20),

2. space-fixed frame. It is a frame where the axes are parallel to the laboratory-

fixed frame and the centre-of-mass of the molecule in the origin. This means that the translational motion of the molecule is removed in this frame of reference, and

3. body-fixed or molecule-fixed frame. This frame can be obtained by rotating the space fixed frame to make one of the axes; z axis as an example, embedded (the process of orienting the molecule) in a certain way with respect to the plane of the molecule.

For a molecule of N atoms, in the laboratory-fixed frame there are 3N degrees of freedom: we can refer to the position of each atom by specifying three coordinates (e.g. the x, y, and z Cartesian coordinates). Using the body-fixed frame, the number of internal degrees of the freedom can be minimised to 3N-6 for nonlinear molecules; i.e. the translational motion uses three of the 3N degrees of freedom leaving 3N-3, and three degrees of rotational freedom are required in case of the nonlinear molecule leaving 3N-6 degrees of freedom (in case of the linear molecule, there are two rotational degrees of freedom leaving 3N-5 internal modes). H_2S is a nonlinear molecule with three atoms, so the number of the degrees of vibrational freedom is three.

2.5.3 Orientation of the molecule in the body-fixed frame

The next step to solve the Schrödinger equation for a ro-vibrational Hamiltonian is to fix the coordinate axes to the molecule. Calculations showed there is no unique way of fixing the coordinate axes. In other words a good choice of the coordinates depends on the particular molecule considered, and that there is no single coordinate system that would be satisfactory for all triatomics [Tennyson [2000]].

The orientation of the body-fixed axes with respect to the space-fixed axes is important in the Dvr3d suite, since it speeds up solving the problems with rotational excitation. The software allows the following four possible choices for orienting the molecule in combination with Jacobi or Radau internal coordinates:

1. r_1 embedding: z axis is parallel to r_1, and the x axis in the plane of the molecule,

2. r_2 embedding: z axis is parallel to r_2, and the x axis in the plane of the molecule,

3. bisector embedding: the x axis bisects the angle θ between r_1 and r_2, and the z axis in the plane of the molecule, and

4. perpendicular embedding: the x axis bisects the angle θ, and the z axis perpendicular to the plane of the molecule.

The bisector embedding is appropriate for the AB_2 class of triatomics such as H_2S.

2.5.4 Method

The general Hamiltonian for the nuclear motion within the Born-Oppenheimer approximation is:

$$\hat{H} = \hat{K}_V + \hat{K}_{VR} + V, \tag{2.21}$$

where $\hat{K}_V$ is the vibrational kinetic energy operator, $\hat{K}_{VR}$ is the vibration-rotation kinetic energy operator, and V is the potential energy function. Dvr3d solves this equation in two steps. The first module 'Dvr3drjz' solves the zero rotational Hamiltonian matrix ($J = 0$), where the vibration-rotation kinetic energy operator ($\hat{K}_{VR}$) is null, using the finite basis representation (FBR). For the triatomic problem in the (r_1, r_2, θ) coordinates a basis set representation of the ith state is:

$$|i\rangle = \sum_{j,m,n} c^i_{j,m,n} P_j(\theta) Q_m(r_1) R_n(r_2), \tag{2.22}$$

where Dvr3d expands the bending motion in terms of Legendre polynomials, and the stretching motion in terms of Morse oscillator-like functions which is expressed in terms of Laguerre polynomials. The Morse oscillator-like functions are defined as:

$$H_n(r) = \beta^{1/2} N_{n\alpha} \exp\left(-\frac{y}{2}\right) y^{(\alpha+1)/2} L^\alpha_n(y), \tag{2.23}$$

where

$$y = A \exp\left[-\beta\left(r - r_e\right)\right], \tag{2.24}$$

and $N_{n\alpha}L_n^{\alpha}(y)$ are normalised associated Laguerre polynomials. Because the potential in Eq. (2.21) has the Morse form

$$V(r) = D_e\left(1 - \exp\left[-\beta\left(r - r_e\right)\right]\right)^2 - D_e, \tag{2.25}$$

then it is possible to write the scaling parameters in Eq. (2.24) in terms of the dissociation energy D_e and the energy of the fundamental vibration ω_e,

$$A = 4D_e/\omega_e \qquad , \qquad \beta = \omega_e\left(\frac{\mu}{2D_e}\right)^{1/2}, \tag{2.26}$$

where r_e, ω_e, and D_e are considered as variational parameters, and these parameters should be adjusted for each molecule to give an optimal basis set expansion. The process of adjusting these parameters for H_2S is discussed in Chapter 3. As a result the rotationless Hamiltonian matrix can be written as

$$\hat{H}^{J=0}_{jj'mm'nn'} = \left\langle P_j Q_m R_n | \hat{K}_V + V | P_{j'} Q_{m'} R_{n'} \right\rangle. \tag{2.27}$$

The discrete variable representation (DVR) is obtained as a transformation from a corresponding FBR. The DVR transformation T in one dimension for either of r_1, r_2, or θ is defined in terms of the Gaussian quadrature points η and weights ω_η of the basis functions used in the expansion for that dimension

$$T^{\alpha}_j = \sqrt{\omega_\alpha} P_j(\alpha) \qquad , \qquad T^{\beta}_m = \sqrt{\omega_\beta} Q_m(\beta) \qquad , \qquad T^{\gamma}_n = \sqrt{\omega_\gamma} R_n(\gamma), \tag{2.28}$$

where α, β, and γ are defined as the zeroes of the M^{th}, N^{th}, and L^{th} order functions P_M, Q_N, and R_L, respectively. The three-dimensional DVR is obtained by applying the transformation

$$T = T^{\alpha}_j T^{\beta}_m T^{\gamma}_n, \tag{2.29}$$

to the corresponding FBR

$$\hat{H}^{J=0}_{\alpha\alpha'\beta\beta'\gamma\gamma'} = \sum_{j,m,n} \sum_{j',m',n'} T^{\alpha}_j T^{\beta}_m T^{\gamma}_n \hat{H}_{J=0} T^{\alpha'}_{j'} T^{\beta'}_{m'} T^{\gamma'}_{n'}. \tag{2.30}$$

After diagonalising this matrix the vibrational energy levels are obtained. One of the DVR method's advantage is that no integration is required at all over the potential, where the potential energy function is diagonal in the quadrature representation, and hence is easily evaluated [Tennyson et al. [2004]]. In order to calculate the rotationally excited states ($J > 0$), a similar Hamiltonian matrix to that in Eq. (2.27) is used with extra terms to produce $H^{J,k}$ where k is the projection of J onto the body-fixed axis. These additional terms differ depending on the selected axis embedding. The angular basis functions are based on either associated Legendre polynomials or Jacobi polynomials depending also on the embedding. After diagonalising, the lowest energy solutions of these calculations are used as a basis in the second step in order to calculate the full problem, where the module 'ROTLEV3B' should be used, see Tennyson and Sutcliffe [1992]. The wavefunctions from the output of DVR3DRJZ or ROTLEV3B are used as input for the module DIPOLE3. This module calculates the transition dipole integral of the dipole moment on the wavefunctions as the sum over the grid points. Then the line strength $S(f-i)$ for every allowed transition is calculated as

$$S(f-i) = \sum_{A=X,Y,Z} |\langle i|\mu_A|f\rangle|^2, \tag{2.31}$$

for a transition between initial ($\langle i|$) and final ($|f\rangle$) wave functions. In this equation μ_A is the component of the molecular dipole moment operator along the A axis ($A = X, Y$ or Z); the (X, Y, Z) axis system having the origin at the molecular center of mass and space fixed orientation [Jensen and Bunker [1998]]. The Einstein A-coefficient of spontaneous emission can be defined in terms of the linestrength as

$$A_{if} = \frac{64\pi^4}{3c^3h}\omega_{if}^3 \frac{S(f-i)g_i}{2J'+1}, \tag{2.32}$$

where c is the speed of light, h is Planck's constant, ω is the transition frequency, g_i is the nuclear spin degeneracy, and $J^{'}$ is the upper state of the transition. Einstein A-coefficient of spontaneous emission gives the rate of the process for spontaneous emission by which an electron 'spontaneously' (i.e. without any outside influence) decays from a higher energy level to a lower one. On another had, stimulated emission (also known as induced emission) is the process by which

an electron is induced to jump from a higher energy level to a lower one by the presence of electromagnetic radiation at the frequency of the transition, and this process is known as Einstein B-coefficient of stimulated emission. The process by which an electron transfare from lower energy level to a higher one by absorping a photone is described by the Einstein B-coefficient of stimulated absorption.

The integrated absorption coefficients can be calculated using the formula

$$I(\omega_{if}) = \frac{4.162034 \times 10^{19} \omega_{if} g_i [\exp(-E''/kT) - \exp(-E'/kT)]}{Q(T)} S(f-i), \quad (2.33)$$

where k is the Boltzmann constant, E'' and E' are the energies of the upper and lower state, respectively, T is the temperature, and $Q(T)$ is the partition function of the system [Tennyson et al. [2004]].

2.6 Dvr3d modules and the symmetry block

There are four modules in the Dvr3d suite:

1. Dvr3drjz calculates the vibrational wavefunctions which represents the first of the two successive steps in the computation of the full ro-vibrational wavefunctions. Each run of this module computes the wavefunctions for certain rotational quantum number J value and one vibrational symmetry q (where $q = 0$ (even) and 1 (odd)). This run needs optimal values for some computational parameters, see Section 3.1.1, and an accurate potential energy function, where a subroutine containing the potential energy function should be supplied to the program, see Section 3.2 as well.

2. Rotlev3z performs the rotational part of the computation as a second step after calculating the vibrational wavefunctions described above (with exception for $J = 0$); it takes the wavefunctions computed by Dvr3drjz as its input. Its output contains the full ro-vibrational wavefunctions and eigenvalues for certain J. Each Rotlev3z run is for a single q value and computes values for both rotational parities ($p = 0$ (even) and 1 (odd)). Optimal values of some computational parameters are needed to be specified for this run, see Section 3.1.2.

Table 2.1: Symmetry blocks. the vibrational symmetry (q) and the rotational parity (p) are labelled as either symmetric (e) or anti-symmetric (o) states. O/P are for *ortho*/*para* coupling.

	J even				J odd			
q	e	e	o	o	e	e	o	o
p	e	o	e	o	e	o	e	o
O/P	P	O	O	P	O	P	P	O

3. DIPOLE3 takes the output of two ROTLEV3Z runs and calculates Einstein A-coefficients for every allowed dipole transition (see Table 2.1), where a subroutine containing the dipole moment function that must be given to the program, see Chapter 4. The results of the total run of DIPOLE3 for all allowed transitions and all J values is the molecule line list (in our case an H_2S line list), see Chapter 5.

4. SPECTRA takes as an input the line list and calculates the temperature dependent spectrum, where the value of the partition function at certain temperature must be given to the program, see Chapter 5.

The DVR3D suite of programs generates four ro-vibrational symmetry blocks in case of H_2S molecule, which are labelled *ee*, *eo*, *oe*, *oo*. In these labels the first term is the vibrational symmetry q and the second term is the rotational parity quantum number p. The nuclear permutation operation in which the two identical protons (hydrogen nuclei) are interchanged gives two nuclear spin states of the molecule. The nuclear spins may couple symmetrically or anti-symmetrically. The anti-symmetric coupling gives the *ortho* (O) state which is triply degenerate, while the symmetric coupling gives the *para* (P) state which is non-degenerate. Table 2.1 summarises the selection rules which govern the allowed ro-vibrational transitions of H_2S molecule, which obey $\Delta J = 0, \pm 1$, O$\leftrightarrow$O and P$\leftrightarrow$P.

DVR3D gives exact quantum numbers for the total angular momentum, wavefunctions symmetry, wavefunctions parity, *ortho* state and *para* state. But it produces approximate quantum numbers for the vibrational stats (v_1, v_2, v_3) as well as the two components of the total angular momentum (K_a, K_c), and this is because of the used basis functions for the bending mode and the stretching modes

in DVR3D which give approximate quantum numbers far from integer numbers where they can not be rounded. So, no assignments for the calculated transitions are given for the quantum numbers (v_1, v_2, v_3) and (K_a, K_c).

Chapter 3

Convergence tests and PESs

3.1 Convergence tests

As mentioned in Chapter 2, some computational parameters should be adjusted in order to have converged energy levels. Some of these computational parameters should be included in the input file at the first step of the calculations using the Dvr3drjz module, where the vibrational bands energy levels should converge up to a certain level of accuracy. Some other parameters are included in the input file for the second step of calculations using the Rotlev3b module, where the ro-vibrational energy levels should show convergence up to a certain level of accuracy. In the following subsections, the process of optimising these parameters for both Dvr3drjz and Rotlev3b modules are described.

3.1.1 Vibrational bands convergence test

The first step in calculating a line list for triatomic molecules, using the Dvr3d suite, is to define the effective Morse oscillator-like parameters, which are the equilibrium bond length (r_e), the harmonic frequency (ω_e), and the dissociation energy (D_e) of the molecule under study, into the first module of the Dvr3d suite 'Dvr3drjz'. However, these effective parameters differ from the physical parameters and must be empirically determined by testing the convergence of the pure vibrational energy levels. As an initial guess for the values of these parameters, the water parameters were used [Barber et al. [2006]], where $r_e = 2.6$,

ω_e = 0.01 and D_e = 0.4 all in atomic unites (a.u.) (note: atomic mass unit is converted as 1 $a.u.$ = 1822.8883 m_e, the conversion factor for energy is 1 E_h = 219 474.624 $cm^{-1}$and 1 a.u. = 2.5417662 D for dipole). Then these parameters were changed gradually in a systematic way until the set of the calculated pure vibrational states showed convergence. This test was done using $J = 0$ and $q = 0$, where J is the rotational quantum number and $q = 0$ is the even vibrational symmetry. Radau coordinates were selected in our calculations, which are defined on a grid of the radial coordinates, r_1 and r_2, each with n_r points, and an angular coordinate, θ, with n_{th} points. The accuracy of the calculations is affected by the number of the grid points. Increasing the number of grid points gives more accurate results but also increases the computation time.

The numbers of the grid points were chosen to be $n_r = 70$ and $n_{th} = 48$. Then the following criteria were used to test the convergence of the energy levels up to 25 000 cm^{-1}:

1. the values of the energy levels are insensitive for the value of D_e [Tennyson et al. [2004]], so this value was kept constant during the test,

2. the high values of the grid points make the run time relatively long but help to make the values of the energy levels more stable,

3. the energy levels are very sensitive to the values of r_e and ω_e, so the values of these parameters were changed gradually, and

4. the sum of the first 16, 40, 100, 164, 200, 300, 357 energy levels were calculated and tabulated. Table 3.1 is an extract from our convergence test table.

During the test we noticed that for a certain value of r_e, choosing very small ω_e caused some of the radial points to be placed at negative values or r, which is indicated in the table by the letter N. On the other hand, choosing very large ω_e caused the values of the energy levels to suddenly increase to very high values which is indicated in the table by three dots. As a result of this test, the following values of the Morse-like parameters were selected: r_e = 3.8, ω_e = 0.005 and D_e = 0.4 (all in a.u.). Then by doing the test for the value of the radial basis

set, we found that the values of the energy levels converge very well by selecting $n_r = 40$ and $n_\theta = 48$. The nuclear masses were adopted for all calculations: $m(H) = 1.007825$ and $m(^{32}S) = 31.972071$ both in atomic mass units.

To give an idea about the time needed: in general the time needed to do the calculations using these selected parameters is dominated by the final 3D matrix diagonalisation. As mentioned in Chapter 5.2, the calculations were performed using 16 processors on machine Amun (see Section 5.2 for Amun's specifications). As an example, for $J = 0$ for one run, the calculations needs less than 30 minutes using 3 processors run in parallel.

3.1.2 Rotational energy levels convergence test

The second step in the line list calculations is to find the optimum size of the Hamiltonian (the value of $IBASS$) in the rotational module 'Rotlev3b'. $IBASS$ depends on J ($IBASS = n(J+1-p)$), where n is the value to be found during the convergence test of the rotational energy levels, and p is the rotational parity which has the values 0 (even) or 1 (odd). The value of n was found by convergence tests at $J = 20$ and 50. Our test showed that using $n = 1400$, the maximum convergence error is 0.26 cm^{-1} for just one energy level from 4270 energy levels for $J = 20$, see Table 3.2. For $J = 50$, 20 energy levels from 835 energy levels have errors of convergence between 0.2 and 0.8 cm^{-1}.

Also to give an idea about the time needed during these tests: for one run with $J = 20$ and $n = 1400$ using 8 processors, around two weeks of real time were needed, while for one run with $J = 50$ and $n = 1400$ using the same number of processors two months of real time were needed. Execution time of Rotlev3b is dominated by two processes, building the Hamiltonian matrix and diagonalisation. In fact, building the Hamiltonian matrix step needs much more time than the diagonalisation. For instance, for $J = 20$, in the example mentioned above, diagonalisation needs a couple of hours. Rotlev3b builds the Hamiltonian matrix as independent, separate, blocks ($(J + 1)$ blocks). These blocks are calculated successively using the BLAS rank-one routine 'dger' (which does the vector-vector multiplication) within an algorithm calling this routine very many times. Every block here results from multiplying the coefficients of two effective

Table 3.1: An extract from the vibrational energy levels convergence test log. The lines in every block represent the sum of the first 16, 40, 100, 164, 200, 300 and 357 energy levels (cm^{-1}), respectively.

	$\omega_e(Hartree)$					
$r_e(Bohr)$	**0.005**	**0.006**	**0.008**	**0.010**	**0.020**	**0.030**
2.6	N	N	N	72099.32	72099.32	72099.32
				294838.09	294838.09	294838.11
				1118591.18	1118591.18	1118611.74
				2248932.12	2248933.82	2249625.32
				2964719.46	2964746.62	2967096.45
				5183585.44	5184672.81	5198595.59
				6569521.56	6573824.28	6600697.58
2.8	N	N	N	72099.32	72099.32	72099.32
				294838.09	294838.09	294838.09
				1118591.18	1118591.18	1118591.55
				2248932.12	2248932.15	2248976.21
				2964719.46	2964720.37	2965049.65
				5183584.50	5183844.31	5187463.36
				6569427.88	6571099.40	6580838.92
3.0	N	N	72099.32	72099.32	72099.32	72099.32
			294838.09	294838.09	294838.09	294838.09
			1118591.18	1118591.18	1118591.18	1118591.19
			2248932.12	2248932.12	2248932.12	2248933.47
			2964719.46	2964719.46	2964719.48	2964740.64
			5183584.29	5183584.65	5183634.62	5184569.38
			6569313.25	6569385.87	6570213.06	6573337.18
3.2	N	N	72099.32	72099.32	72099.32	72099.62
			294838.09	294838.09	294838.09	294842.54
			1118591.18	1118591.18	1118591.18	1118645.56
			2248932.12	2248932.12	2248932.12	2249138.73
			2964719.46	2964719.46	2964719.47	2965087.76
			5183584.29	5183584.29	5183593.97	5184847.74
			6569301.22	6569332.84	6569807.63	6572480.93
3.4	N	72099.32	72099.32	72099.32	72099.32	...
		294838.09	294838.09	294838.09	294838.09	...
		1118591.18	1118591.18	1118591.18	1118591.19	...
		2248932.12	2248932.12	2248932.12	2248932.16	...
		2964719.46	2964719.46	2964719.46	2964719.54	...
		5183584.29	5183584.29	5183584.29	5183586.67	...
		6569295.77	6569297.20	6569308.82	6569571.73	...
3.6	N	72099.32	72099.32	...	...	...
		294838.09	294838.09	...	...	...
		1118591.18	1118591.18	...	...	...
		2248932.12	2248932.12	...	...	...
		2964719.46	2964719.46	...	...	...
		5183584.30	5183584.29	...	...	...
		6569295.76	6569296.08	...	...	...
3.8	72099.32	72099.32	72099.32	...	...	...
	294838.09	294838.09	294838.09	...	...	...
	1118591.18	1118591.18	1118591.18	...	...	...
	2248932.12	2248932.12	2248932.12	...	...	...
	2964719.46	2964719.46	2964719.46	...	...	...
	5183584.30	5183584.30	5183584.29	...	...	...
	6569295.77	6569295.76	6569295.81	...	...	...

vibrational wavefunctions which differ in k, which result from first step calculations using module DVR3DRJZ. These are used to transform the Coriolis-coupling matrix elements which are off-diagonal in k, see Tennyson and Sutcliffe [1992]. In general mathematical form, every non-zero block which is off-diagonal in k, $\mathbf{G}$, results from multiplying the three matrices as follows:

$$\mathbf{G} = \mathbf{C}^T\mathbf{B}\mathbf{C}' \tag{3.1}$$

where $\mathbf{C}$ and $\mathbf{C}'$ are the coefficients of the vibrational wavefunctions (coef1 and coef2 in DVR3DRJZ module) and $\mathbf{B}$ is the general off-diagonal k matrix. During the calculations, ROTLEV3B does not save the calculated blocks on the desk, and because of this and because of the very long time needed to do the computations, our calculations were at risk all the time because of any unexpected problems such as sudden power shut down. In fact we faced problems with the power shut down twice during our tests for $J = 50$. Because of that, the subroutine which builds the Hamiltonian matrix in ROTLEV3B was rewritten, so the separate blocks could be calculated on different machines and could be saved to be gathered later for the diagonalisation step.

However, another idea for computing $\mathbf{G}$ was used, in which the three matrices multiplications are carried out into two successive steps as follows:

$$\mathbf{D} = \mathbf{B}\mathbf{C}' \tag{3.2}$$

$$\mathbf{G} = \mathbf{C}^T\mathbf{D} \tag{3.3}$$

where the 'dger' routine was replaced by the BLAS rank-two routine 'dgemm' (which does the matrix-matrix multiplication). This requires extra storage because of the construction of the intermediate matrix $\mathbf{D}$, but this replacement made the Hamiltonian building step very much faster. For the same example above with $J = 20$, the new algorithm builds the Hamiltonian matrix in less than two minutes. This greatly improved the program and made the calculations significantly less expensive during the hot line list calculations (see Chapter 5), where the calculations up to $J = 40$ required less than 35 days compared to more than seven months for calculating a cold line list up to $J = 30$ before the

Table 3.2: Results of the rotational energy levels convergence test for $J = 20$. Each row represents the maximum absolute value of the convergence error and the number of the energy levels with convergence error greater than 0.2 cm^{-1} for two sets of energy levels calculated using n_2 and n_1 values. $IBASS = n_i(J + 1 - p)$, where $i = 1, 2$.

n_2 - n_1	Max. convergence error (cm^{-1})	Number of energy levels convergence error > 0.2 cm^{-1}
650-690	4.04	1132
710-750	2.66	832
750-800	3.33	750
800-850	2.13	592
850-900	1.43	391
900-950	1.80	311
950-1000	0.81	191
1100-1150	0.44	46
1150-1200	0.42	27
1200-1250	0.51	8
1250-1300	0.36	3
1300-1350	0.34	1
1350-1400	0.26	1

implementation of the new algorithm.

3.2 PESs

In this work, four PESs were tested. The first one is a semi-empirical PES constructed by S. Yurchenko using the CCSD(T)/aug-cc-pV(Q+d)Z level of theory as implemented in the Molpro software package [Werner et al. [2012]]. This surface was constructed using 1200 geometries covering the energy range up to 40 000 cm^{-1} above equilibrium. Then this surface was refined by fitting it to the available experimental values of H_2S for $J \leq 6$ covering the energy range up to 16 500 cm^{-1} with a root-mean-square (rms) error of 0.03 cm^{-1} for the fitting. We will call this surface PES-Y. This surface was tested by calculating the energy levels for $J = 0$, 1, 2, 5 and 10, and comparing the results with experimental energy levels. Fig. 3.1 shows the errors in the calculated ro-vibrational energy levels using this surface.

Another PES was tested and compared to PES-Y. This surface has been constructed by Tyuterev et al. [2001], where the data set of experimentally determined H_2S energy levels have been used to fit a ground state PES. This surface was obtained by the simultaneous fit of a very large sample of high-resolution ro-vibrational data, using an extensive set of more than 12 000 experimental ro-vibrational transitions for 7 isotopologues of H_2S. As far as we know, this surface was the most accurate available PES empirically determined. PES-T will be used to label this surface during this discussion. However, using the parameters of PES-T published in the same work and calculating the ro-vibrational energy levels, we found some problems which can be summarised as following: Tyuterev *et al.* used Dvr3d to confirm the convergence of the basis set used in their work for high vibrational states, using $r_e = 2.75$, $D_e = 0.1$, $\omega_e = 0.01$ (all in a.u.), $n_r = 35$ and $n_{th} = 98$. First, calculating the vibrational energy levels using PES-T with the parameters suggested for Dvr3d by Tyuterev *et al.*, and then by comparing these calculated energy values with the experimental vibrational energy levels (these experimental energy levels were taken from Tyuterev et al. [2001]), we do not reproduce the values for the vibrational energy levels as published by Tyuterev *et al.*. Column 4 in Table 3.3 shows the residuals published by Tyuterev et al. [2001], and column 5 in the same table shows the results we obtained using the same surface. Second, testing PES-T for convergence shows that by increasing the number of the radial points n_r, some of the energy levels become negative. Our investigations showed a deficiency in this surface, see Fig. 3.2. This problem was solved by considering the coefficients up to the quadratic order and ignoring the coefficients with the higher orders in the refining function for the energies above 50 000 cm^{-1}. The modified PES-T was used to calculate the vibrational energy levels again. We also noticed that Tyuterev *et al.*'s vibrational basis set is not converged above 9000 cm^{-1}, see Fig. 3.3.

PES-T was further refined by S. Yurchenko. Up-to-date experimental energy level values up to 17 000 cm^{-1} were used to fit 71 parameters in two different refinements: (1) using experimental energy levels with $J = 0$, 1, 2 and 5; (2) using experimental energy levels with $J \leq 6$. The resulted two new PESs will be referred to as PES-Y0125 and PES-Y0-6, respectively. Convergence tests were performed also for these new refined surfaces by calculating ro-vibrational energy levels for

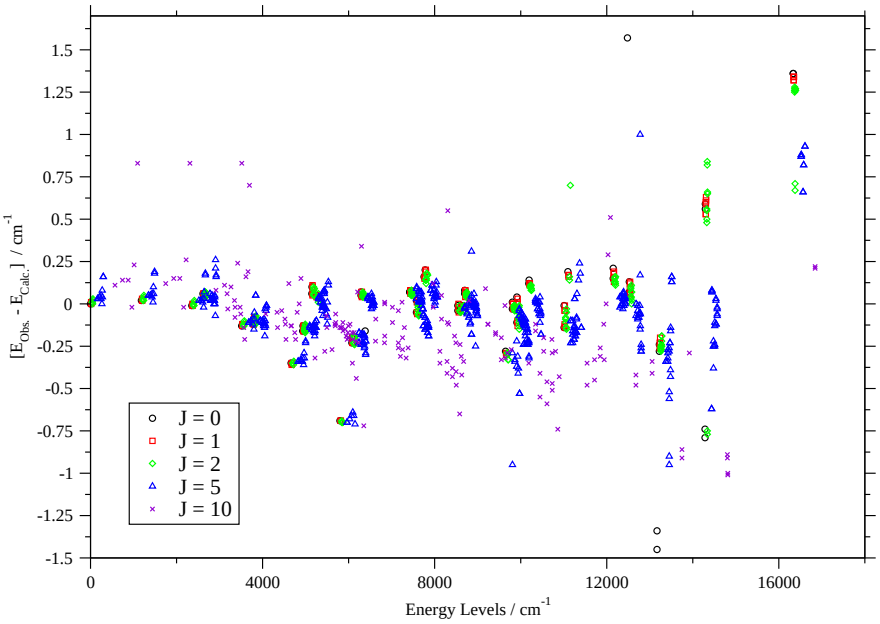

Figure 3.1: Residuals of the calculated energy levels from the observed values for $J = 0$, 1, 2, 5 and 10 using PES-Y.

$J = 0$, 1, 2, 5 and 10, and comparing the calculated values with the available experimental data. Fig. 3.4 and Fig. 3.5 illustrate the residuals of the calculated ro-vibrational energy levels using PES-Y0125 and PES-Y0-6, respectively. As can be seen from these plots, PES-Y0125 shows better results than PES-Y0-6.

Results show that PES-Y0125 predicts experimentally known energy levels with $J \leq 10$ with a standard deviation of 0.11 cm^{-1} compared to 0.23 cm^{-1} using PES-T (using our parameters for Dvr3d). Tyuterev *et al.* claimed that their PES predicts experimentally known levels with $J \leq 10$ with a standard deviation of 0.10 cm^{-1}. Table 3.4 shows the standard deviations for the calculated ro-vibrational energy levels up to 17 000 cm^{-1} using PES-T and PES-Y0125 for $J = 0$, 1, 2, 5 and 10. Also, calculations show that using PES-Y0125, around 7.3% of the ro-vibrational energy level values have errors more than 0.25 cm^{-1} for J from 0 to 5 when compared to the experimental values. All of these levels lie above 12 450 cm^{-1}. While 26% of the values have this error for $J = 10$, all of them above 8600 cm^{-1}. PES-Y0125 is used for the remainder of the thesis.

As used by Tyuterev et al. [2001], our potential energy function has the ana-

Table 3.3: Comparison between the experimental and the calculated vibrational levels. Col.3: Observed vibrational bands origins. Col.4: residuals of the vibrational bands origins published by Tyuterev et al. [2001]. Col.5: residuals of the vibrational bands origins using PES-T with the parameters for DVR3D suggested by Tyuterev et al. [2001]. Col.6: residuals of the vibrational bands origins using PES-Y0125 with our parameters for DVR3D.

Normal	Local	Obs.	Obs.-Calc. Tyuterev et al. [2001]	Obs.-Calc. This calculations	Obs.-Calc. This calculations
$(\nu_1\nu_2\nu_3)$	$[n_1\ n_3^{\pm},b]$	cm^{-1}	cm^{-1}	cm^{-1}	cm^{-1}
1	2	3	4	5	6
(010)	[00^+,1]	1182.58	-0.01	-0.01	0.02
(020)	[00^+,2]	2353.96	0.00	-0.01	-0.02
(100)	[10^+,0]	2614.41	-0.02	-0.01	0.06
(030)	[00^+,3]	3513.79	0.00	0.00	-0.13
(110)	[10^+,1]	3779.17	0.00	0.00	-0.11
(040)	[00^+,4]	4661.68	-0.01	0.00	-0.35
(120)	[10^+,2]	4932.70	0.01	0.01	-0.16
(200)	[20^+,0]	5144.99	-0.01	0.02	0.07
(002)	[11^+,0]	5243.10	-0.02	-0.01	0.05
(050)	[00^+,5]	5797.24	0.01	0.01	-0.69
(130)	[10^+,3]	6074.58	-0.04	-0.04	-0.23
(210)	[20^+,1]	6288.15	0.04	0.07	0.05
(102)	[30^+,0]	7576.38	-0.03	0.04	0.02
(300)	[21^+,0]	7752.26	-0.01	0.02	0.15
(112)	[30^+,1]	8697.14	-0.01	0.06	0.08
(202)	[40^+,0]	9911.02	0.00	0.18	0.04
(400)	[31^+,0]	10188.30	-0.01	0.06	0.12
(212)	[40^+,1]	11008.68	-0.05	0.13	-0.02
(302)	[50^+,0]	12149.46	0.04	0.40	0.21
(104)	[41^+,0]	12524.63	0.01	0.19	0.07
(312)	[50^+,1]	13222.77	0.05	0.42	-0.22
(322)	[50^+,2]	14284.71	0.02	0.42	-0.74
(402)	[60^+,0]	14291.12	0.03	0.66	0.58

Table 3.4: Standard deviation values of the ro-vibrational energy levels up to 17 000 cm^{-1} for J = 0, 1, 2, 5 and 10.

	Standard deviation (cm^{-1})	
J	PES-Y0125	PES-T
0	0.19	0.24
1	0.06	0.21
2	0.07	0.21
5	0.07	0.23
10	0.19	0.24

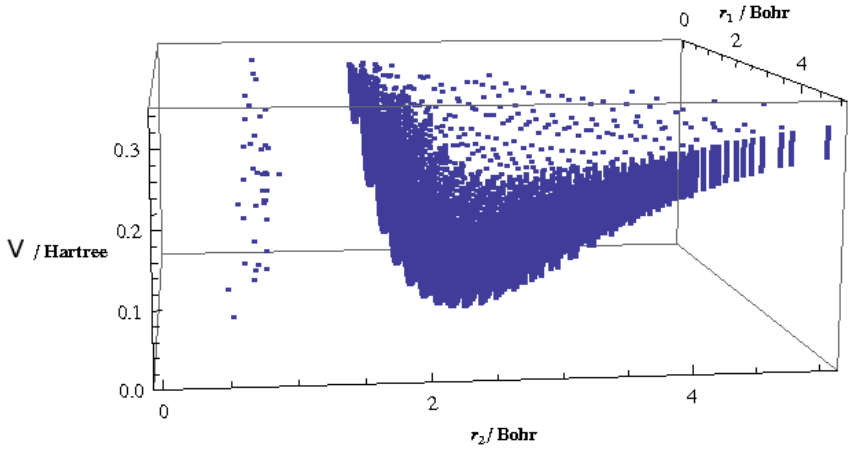

Figure 3.2: PES-T. V is shown as a function of the internuclear distances r_1 and r_2.

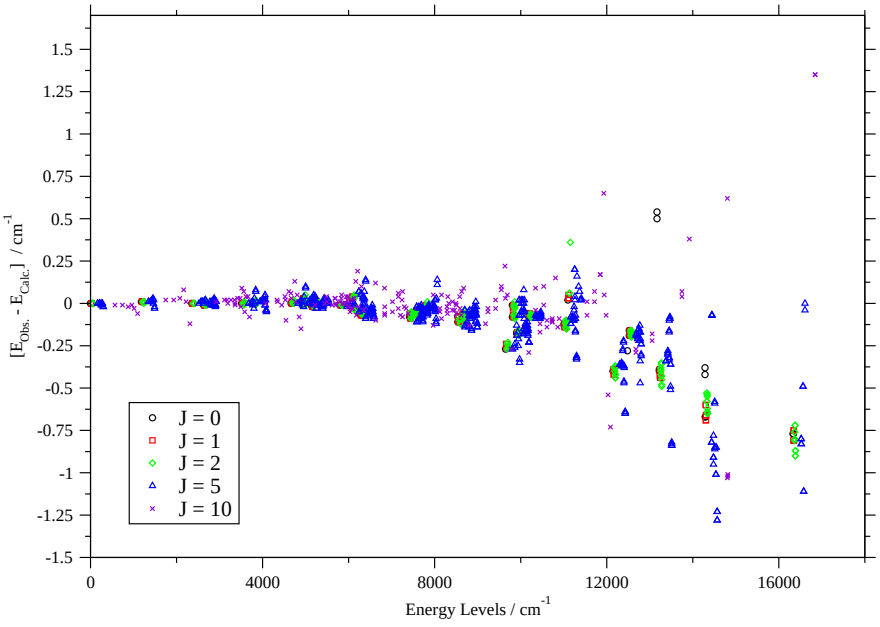

Figure 3.3: Residuals of the calculated energy levels from the observed values for $J = 0$, 1, 2, 5 and 10 using PES-T.

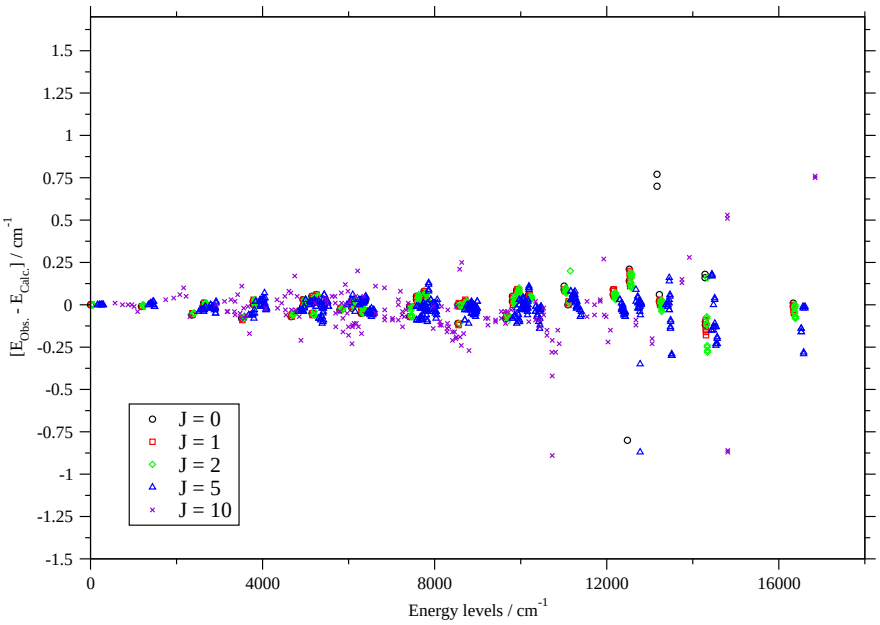

Figure 3.4: Residuals of the calculated energy levels from the observed values for $J = 0$, 1, 2, 5 and 10 using PES-Y0125.

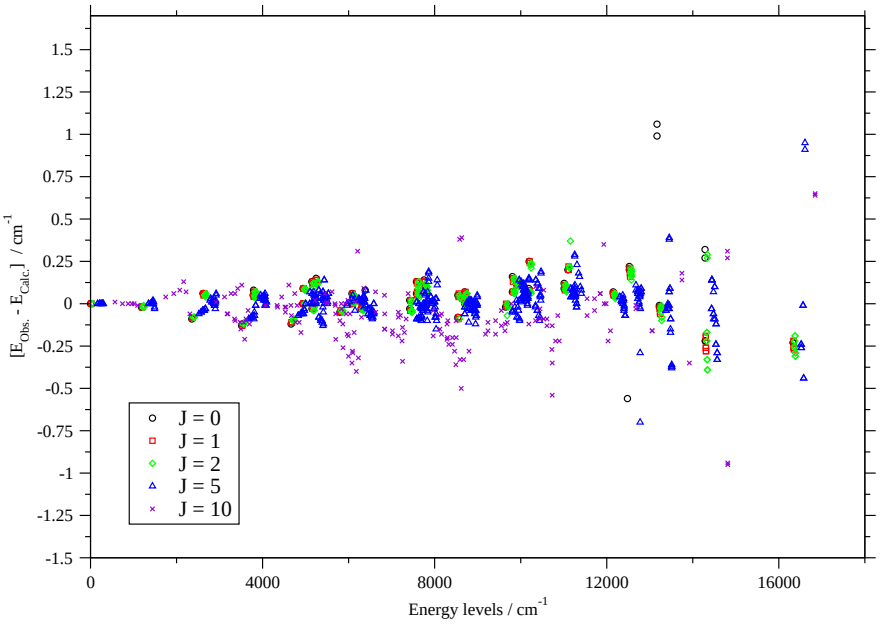

Figure 3.5: The error in the calculated energy levels comparing to observed values for $J = 0$, 1, 2, 5 and 10 using PES-Y0-6.

lytical form:

$$V = V_{HH} + V', \tag{3.4}$$

here V_{HH} is the H $\leftrightarrow$ H repulsion at short distances, with the form:

$$V_{HH} = \sum_{i}^{2} B_i \exp(-g_i r_{HH}) \tag{3.5}$$

where r_{HH} is the distance between the two hydrogen nuclei, B and g are constants given in Table 1 in Appendix A. V' in Eq.(3.4) is an expansion of the stretching variables r_1, r_2 and the cosine of the instantaneous value of the bond angle supplement ρ ($\rho = \pi - \theta$) which has the form:

$$V'(r_1, r_2, \rho) = \sum_{skm} \chi_{skm} y_1^s h^k y_2^m \qquad , \qquad (m \leq s); \tag{3.6}$$

where Eq.(3.6) is symmetrized under $y_1 \leftrightarrow y_2$, and

$$y_i = 1 - \exp(-b\Delta r_i) \qquad , \qquad h = cos(\rho_e) - cos(\rho) \tag{3.7}$$

where b is a molecular constant, Δr_i with $i = 1$ or 2, is defined as the displacement from the equilibrium. The χ_{skm} expansion coefficients were determined from the fit to the experimental data, and these parameters are presented in Table 1 in Appendix A.

Chapter 4

Dipole moment surface

4.1 Introduction

The interesting anomalies in the ro-vibrational intensity distributions of H_2S have different types:

1. Unusual behaviour of band intensities in a number of vibrational bands:

   (a) the observed intensities of H_2S fundamental bands (ν_1 and ν_3) are much weaker than those of combination bands ($\nu_1 + \nu_2$, $\nu_2 + \nu_3$ and $\nu_1 + \nu_3$). The second triad combination bands were found to be several times stronger than the first triad fundamentals [Brown et al. [1998]]. The fundamental band ν_3 is particularly weak; for example this band is weaker than the $2\nu_2$ band, see Fig. 4.1 for comparison, and

   (b) the ν_1 and ν_2 fundamental bands of H_2S are two orders of magnitude weaker than in similar triatomics such as H_2O and H_2Se, while the ν_3 band is three orders of magnitude weaker, see Fig. 4.1 for comparison.

2. The fundamental bands have rotational anomalies in their intensity distributions:

   (a) the P-branch ($\Delta J = -1$) regions of the ν_1, ν_2 and ν_3 are much less intense than the R-branch ($\Delta J = 1$) regions [Brown et al. [1998]; Gillis and Edwards [1981]; Strow [1983]], and

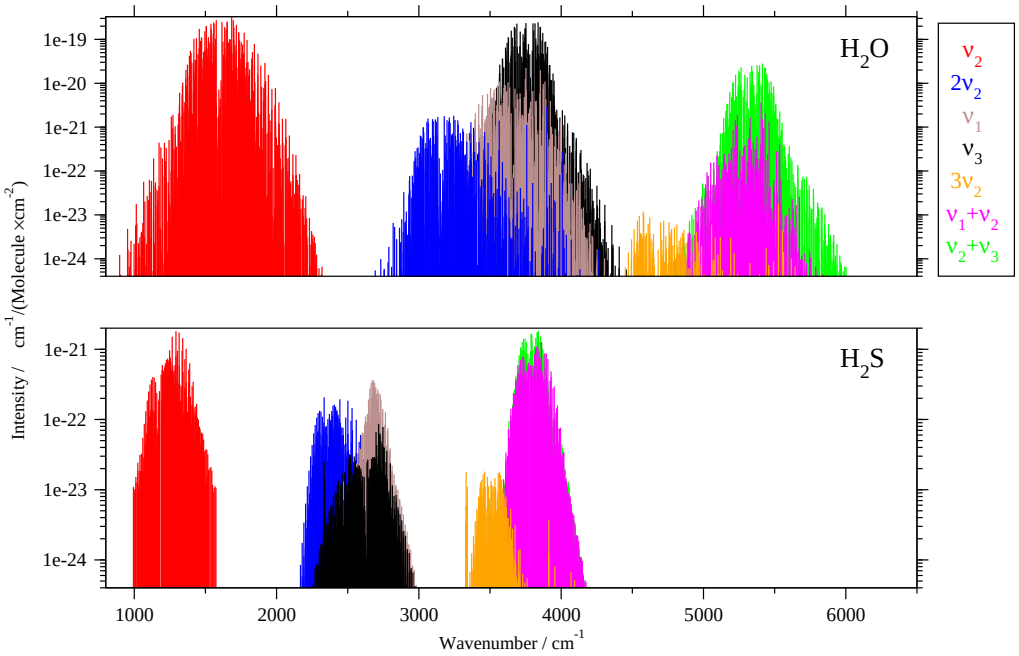

Figure 4.1: General comparison between H_2S and H_2O spectra for the fundamental, overtone, and combination bands. These data are from the HITRAN 2008 database.

(b) in ν_3 band in the same branch regions, some 'forbidden' $\Delta K_a = 2$ transitions are more intense than corresponding 'allowed' $\Delta K_a = 0$ transitions [Brown et al. [1998]].

The mean first derivatives of the dipole moment function with respect to internal coordinates were found experimentally to be extremely small (symmetric stretch +0.0265 D/Å, bending -0.0755 D and asymmetric stretch -0.00923 D/Å) [Camy-Peyret and Fiaud [1985]], as stated by Senekowitsch et al. [1989].

Reproducing the intensity features mentioned above using an *ab initio* electric DMS represents a challenge for the theoretical spectroscopy and H_2S is therefore an important benchmark system [Carter et al. [1989]; Cours et al. [2002]; Le Sueur et al. [1992]]. *Ab initio* dipole moment surfaces of H_2S have been calculated by Senekowitsch et al. [1989], Cours et al. [2000, 2002], and Henon et al. [2003]. In Senekowitsch *et al.*'s work a Gaussian basis set used in the calculations as follows:

1. The 18s and 13p basis of Partridge [1987] for sulphur was augmented by:

(a) one s diffuse function with an exponent of 0.048 a_0^{-2},

(b) a set of four d functions; expt.: 2.7, 1.1, 0.4, and 0.15 a_0^{-2}, and

(c) one f function; expt.: 0.4 a_0^{-2}.

2. For the hydrogen atom the $7s$ of Huzinaga [1965] basis was augmented by:

(a) one s function; expt.: 0.03 a_0^{-2},

(b) three p functions; expt.: 1.8, 0.6, 0.2 a_0^{-2}, and

(c) one d function; expt.: 0.7 a_0^{-2}.

The basis was contracted only in the core region: $6s$ and $5p$ on S and $3s$ on H. The dipole moment was calculated as the energy derivative with respect to an external electric field with a strength of $\pm 0.001 E_h/ea_0$ along the symmetric and the asymmetric axes. In Senekowitsch *et al.*'s work, although the resulting intensities in the ro-vibrational spectrum showed the anomalies in the H_2S spectrum qualitatively, there was large discrepancy between the calculated and the experimental intensities of the fundamental bands. Senekowitsch et al. [1989] concluded that accurate calculations for the changes of the dipole moment function along the symmetric stretch and asymmetric stretch displacement coordinates and the corresponding line intensities were very difficult by purely *ab initio* methods because of the very small first derivatives.

Cours et al. [2000] presented a much-improved DMS, and they confirmed their results again [Cours et al. [2002]]. This surface was the most accurate available dipole moment surface for H_2S to our knowledge. The DMS published by Cours et al. [2000] was based on the (frozen-core, non-relativistic) coupled-cluster singles, doubles and perturbative triples (CCSD[T]) method and a basis set derived from Dunning's cc-pV5Z [Dunning [1989]] (similar in size to aug-cc-pVQZ). The basis set was restricted to the s, p, d and f orbitals for sulphur atom, and to s, p and d for the hydrogen atoms. some diffuse functions were used to augment the basis set. These functions are given as follows:

1. The $20s$, $12p$, $4d$ and $3f$ basis for sulphur atom was augmented by:

(a) two diffuse s functions, 0.04 a_0^{-2} and 0.015 a_0^{-2},

(b) two diffuse p functions, 0.031 a_0^{-2} and 0.012 a_0^{-2}, and

(c) one diffuse d function, 0.08 a_0^{-2}.

2. The $8s$, $4p$ and $3d$ basis for hydrogen atom was augmented by:

(a) one s diffuse function, 0.025 a_0^{-2}, and

(b) one p diffuse function, 0.1 a_0^{-2}.

Cours *et al.*'s surface was calculated using the energy derivatives with respect to an external electric field with a finite field of $\pm 0.005 E_h/ea_0$ along the symmetric and the asymmetric axes. They claimed that their *ab initio* dipole moment function was an accurate function which could simulate all observed anomalies in intensity distribution of ro-vibrational lines in fundamental absorption bands and their surface could provide experimental absolute intensities [Cours et al. [2000]]. But as we will show, this DMS overestimates the intensities of the ν_1 and ν_2 fundamental bands by about 40 % and 30 %, respectively, as well as of the $\nu_1 + \nu_2 - \nu_2$ hot band. Our calculations show that these bands as well as the ν_3 fundamental band are particularly sensitive to the treatment of DMS, in contrast to the other bands lying below 4000 cm^{-1}. The difficulty of representing the unusual features of H_2S spectrum was described by Cours et al. [2000] where they noted that the calculations of the ro-vibrational intensities are extremely sensitive to small errors in a DMS calculations because of the unusual features in this spectrum. Cours et al. [2002] considered a study of intensity anomalies in infrared absorption spectra of the H_2S molecule as a particularly interesting and challenging problem which may be considered as a benchmark for theoretical dipole moment calculations.

The electronic structure computations reported here were performed with the quantum chemistry package Molpro [Werner et al. [2012]]. The ro-vibrational line intensities have been calculated using the Dvr3d. Unless otherwise stated, the ro-vibration calculations were done for states with rotational quantum number up to $J = 5$ and were based on PES-Y0125; see Section 3.2 for more information about this surface.

The aim of the present study is to produce systematically improved DMS for H_2S along the lines of recent studies on the water molecule [Lodi et al. [2008,

2011]; Schwenke and Partridge [2000]], see Lodi and Tennyson [2010] for a general discussion. These studies have resulted in DMS, LTP2011 [Lodi et al. [2011]], which has been shown to be capable of predicting transition intensities with an uncertainty close to 1 % [Grechko et al. [2012]; Lodi et al. [2011]; Polyansky et al. [2012]]. This has resulted in transition intensities computed using this DMS being extensively used to replace measured data in standard compilations [Lodi and Tennyson [2012]; Rothman et al. [2013]].

The computed *ab initio* DMSs of this study are evaluated both with respect to the stability and consistency of the *ab initio* treatment employed and are judged through comparison of *ab initio* transition intensities with their empirical counterparts available in the HITRAN 2008 database [Rothman et al. [2005, 2009]]. As will be discussed below, it transpires that our best *ab initio* results are in much better agreement with directly-measured line intensities than with line intensities calculated from effective Hamiltonian models. All the DMSs points were computed using a distributed memory computing cluster, Legion, located at UCL which has 5728 cores, each with 2-4 GB RAM.

4.2 Dipole moment calculations

The electronically averaged dipole moments $\bar{\mu}$ were calculated as numerical energy derivatives. This method is thought to be more accurate than computing dipoles as an expectation value [Lodi and Tennyson [2010]] and has the further advantage of allowing corrections to the dipoles due to terms in the Hamiltonian to be treated by first-order perturbation theory for the energy, e.g. relativistic corrections. In this method the dipole components $\bar{\mu}_\alpha$ ($\alpha = x, y$) are obtained as $\bar{\mu}_\alpha = (E_{+\lambda_\alpha} - E_{-\lambda_\alpha})/2\lambda_\alpha$, where $\lambda_\alpha = 7.5 \times 10^{-4}$ a.u. is an external, weak, static and uniform electric field along the α direction.

The disadvantage of using the numerical energy derivatives compared to expectation values is that the total energy of the system must be computed four times at each geometry. Our calculations used an electric field strength of which was found to give stable results but required the use of enhanced convergence parameters in Molpro. This caused issues with some calculations as will be discussed below.

4.2.1 Construction of DMS - First stage

Three dipole moment surfaces were constructed by S. Yurchenko. These surfaces were constructed using CCSD(T)/aug-cc-pVQZ, CCSD(T)-F12/cc-pVQZ, and CCSD(T)-F12/aug-cc-pV5Z methods as implemented in MOLPRO. About 8000 geometries covering the energy range up to 40 000 cm^{-1} above equilibrium were used to fit the surfaces. Fig. 4.2 shows the axes and the coordinates used to make the *ab initio* calculations. The *pq*-frame is used to represent the dipole moment vector $\bar{\mu}$ of H_2S; this is the same frame used by Jørgensen and Jensen [1993] and Cours et al. [2000]. In this representation the dipole vector is projected onto the two axes **q** and **p** attached to the instantaneous nuclear configuration of the molecule as follows:

1. the origin is in the nuclear centre of mass,
2. the **q** axis bisects the bond angle θ (HSH), and
3. the **p** axis is perpendicular to **q**, and r_1 is in the first quarter of the coordinate system, see Fig. 4.2.

The corresponding two q and p dipole moment components $\bar{\mu}^{(q)}$ and $\bar{\mu}^{(p)}$ are then represented by the MORBID-like expansion of Jørgensen and Jensen [1993] used by Cours et al. [2000] and by Cours et al. [2002] to represent their *ab initio* H_2S DMS. In this representation, $\bar{\mu}^{(q)}$ and $\bar{\mu}^{(p)}$ are given as following expansions in terms of the coordinate displacements $\Delta r_1 = r_1 - r_e$, $\Delta r_2 = r_2 - r_e$, and $\cos\rho_e - \cos\bar{\rho}$, where $\bar{\rho} = \pi - \theta$ is the apex angle, θ is the bond angle, and r_1 and r_2 are the bond lengths:

$$\begin{aligned}\mu^{(q)}(\Delta r_1, \Delta r_2, \Delta\bar{\rho}) = \sin\bar{\rho}\Bigg[&\mu_0^{(q)}(\bar{\rho}) + \sum_j \mu_j^{(q)}(\bar{\rho})\Delta r_j + \sum_{j\le k}\mu_{jk}^{(q)}(\bar{\rho})\Delta r_j\Delta r_k \\ &+ \sum_{j\le k\le m}\mu_{jkm}^{(q)}(\bar{\rho})\Delta r_j\Delta r_k\Delta r_m \\ &+ \sum_{j\le k\le m\le n}\mu_{jkmn}^{(q)}(\bar{\rho})\Delta r_j\Delta r_k\Delta r_m\Delta r_n + \ldots\Bigg],\end{aligned} \tag{4.1}$$

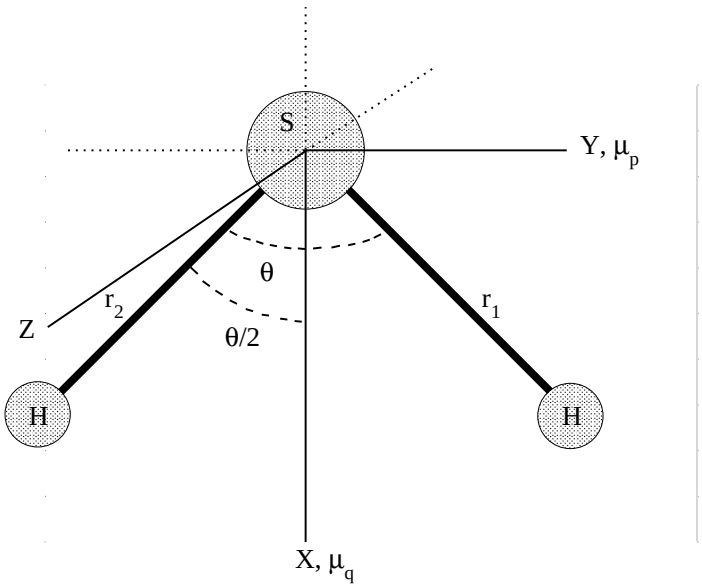

Figure 4.2: Molecule orientation with respect to the pq-coordinates system.

$$\mu^{(p)}(\Delta r_1, \Delta r_2, \Delta\bar{\rho}) = \mu_0^{(p)}(\bar{\rho}) + \sum_j^{(p)} \mu_j^{(p)}(\bar{\rho})\Delta r_j + \sum_{j\le k} \mu_{jk}^{(p)}(\bar{\rho})\Delta r_j \Delta r_k$$
$$+ \sum_{j\le k\le m} \mu_{jkm}^{(p)}(\bar{\rho})\Delta r_j \Delta r_k \Delta r_m$$
$$+ \sum_{j\le k\le m\le n} \mu_{jkmn}^{(p)}(\bar{\rho})\Delta r_j \Delta r_k \Delta r_m \Delta r_n + \ldots, \tag{4.2}$$

where all indices j, k, m, and n assume the values 1 or 2,

$$\mu_{jk\ldots}^{(q)}(\bar{\rho}) = \sum_{l=0}^{N} Q_{jk\ldots}^{(l)} (\cos\rho_e - \cos\bar{\rho})^l, \tag{4.3}$$

$$\mu_{jk\ldots}^{(p)}(\bar{\rho}) = \sum_{l=0}^{N} P_{jk\ldots}^{(l)} (\cos\rho_e - \cos\bar{\rho})^l, \tag{4.4}$$

and the $Q_{jk\ldots}^{(l)}$ and $P_{jk\ldots}^{(l)}$ are molecular dipole parameters. The expansion coefficients in Eqs. (4.3, 4.4) are subject to the conditions that the functions $\mu^{(q)}$ are unchanged under the interchange of the identical protons, whereas the function $\mu^{(p)}$ is antisymmetric under this operation.

These surfaces were tested by calculating the intensity ratio ($I_{Calc.}/I_{Obs.}$) for some of the most intense lines in selected vibrational bands. The results of these tests are presented in Table 4.1, where $I_{Calc.}$ is the line intensities calculated from *ab initio* and $I_{Obs.}$ is the published, empirical line intensities. In Fig. 4.3 the intensity ratio ($I_{Calc.}/I_{HITRAN}$) versus HITRAN's line intensities are plotted. This figure contains lines with rotational quantum numbers up to $J = 5$ for 14 vibrational bands. As can be seen from Table 4.1 and Fig. 4.3, although the dipole moment surface of Cours et al. [2002] represents ν_3 correctly, this surface over estimates the intensities of the ν_1 and ν_2 fundamental bands and the $\nu_1 + \nu_2 - \nu_2$ combination band. On the other hand, none of the three dipole moment surfaces calculated so far in this work are better than Cours *et al.*'s surface. Furthermore, our calculations showed that the fundamental bands and the $\nu_1 + \nu_2 - \nu_2$ band are the most sensitive to the method used to calculate the dipole moments. The overtone, combination, and the other hot bands are not as sensitive to the level of treatment as these bands, and are generally in good agreement with the observations. As a result, in order to track the method which best represents the H_2S spectrum quantitatively and keeping in mind:

1. the overtone, combination, and hot (except $\nu_1 + \nu_2 - \nu_2$) bands are not as sensitive as the fundamental bands to the method of calculations of the dipole moment surface, and

2. the ν_2 band is much more intense than ν_1 and ν_3 bands.

the ν_2 band was selected to be our guide in our tests, so the dipole moment surface which produces ν_2 band intensity closer to the experimental results will be considered as improved surface.

4.2.2 Construction of DMS - Second stage

Since the problem of constructing the DMS which represents the spectral intensity of the H_2S quantitatively was not solved so far, the following systematic strategy was developed. First, we tested the effect of the core and relativistic corrections on the dipole moment values. Second, we performed a systematic comparative

Quantum numbers		ν	Intensity	$\text{Intensity}_{Calc.}/\text{Intensity}_{Obs.}$														Reference
Vibrational	Rotational	cm^{-1}	$cm^{-1}/(molecule \times cm^{-2})$	1	2	3	4	5	6	7	8	9	10	11	12	13	14	
				ALYT2013	DMS-8	DMS-9	DMS-1	DMS-4	Cours	DMS-7		DMS-2	DMS-3	DMS-6			DMS-5	
																		Flaud et al. [1983]
000-000	$4_{4,1}$-$3_{3,0}$	78.27	9.64(-20)	1.00	1.00	0.99	0.99	1.03	0.98	1.04	1.03	1.03	1.07	1.04	1.02	1.08	1.08	
000-000	$5_{5,0}$-$4_{4,1}$	101.02	1.34(-19)	1.00	1.01	1.00	0.99	1.03	0.98	1.04	1.03	1.03	1.07	1.04	1.02	1.08	1.08	
																		Strow [1983]
010-000	$4_{1,4}$-$5_{0,5}$	1130.52	4.17(-22)	1.24	1.25	1.27	1.30	1.34	1.43	1.45	1.47	1.50	1.54	1.57	1.58	1.77	1.79	
010-000	$3_{0,3}$-$4_{1,4}$	1140.09	4.17(-22)	1.24	1.25	1.28	1.31	1.34	1.43	1.45	1.47	1.51	1.55	1.57	1.59	1.78	1.79	
010-000	$2_{1,2}$-$3_{0,3}$	1149.77	3.70(-22)	1.23	1.23	1.26	1.30	1.32	1.42	1.43	1.45	1.49	1.52	1.55	1.57	1.75	1.77	
010-000	$1_{0,1}$-$2_{1,2}$	1158.17	2.62(-22)	1.23	1.24	1.27	1.30	1.33	1.43	1.44	1.46	1.50	1.53	1.56	1.59	1.77	1.79	
010-000	$3_{1,2}$-$2_{2,1}$	1224.28	3.20(-22)	1.26	1.26	1.29	1.31	1.34	1.39	1.42	1.44	1.47	1.50	1.51	1.53	1.67	1.69	
010-000	$4_{1,4}$-$3_{0,3}$	1225.44	7.81(-22)	1.29	1.29	1.32	1.35	1.37	1.45	1.47	1.49	1.53	1.55	1.58	1.60	1.76	1.77	
																		Brown et al. [1998]
020-000	$4_{1,4}$-$5_{0,5}$	2302.12	1.42(-22)	1.04	1.02	1.04	1.06	1.02	0.90	1.02	1.06	1.04	1.01	1.15	1.07	1.18	1.14	
020-000	$3_{0,3}$-$4_{1,4}$	2311.80	1.37(-22)	1.05	1.03	1.04	1.07	1.02	0.90	1.02	1.06	1.05	1.02	1.15	1.07	1.19	1.15	
020-000	$4_{1,4}$-$3_{0,3}$	2397.03	1.62(-22)	1.06	1.04	1.05	1.08	1.04	0.92	1.05	1.08	1.06	1.04	1.18	1.09	1.22	1.18	
020-000	$3_{3,0}$-$2_{2,1}$	2423.63	1.44(-22)	1.06	1.05	1.05	1.08	1.05	0.95	1.06	1.09	1.07	1.06	1.16	1.09	1.20	1.17	
020-000	$4_{4,1}$-$3_{3,0}$	2444.90	2.03(-22)	1.07	1.06	1.06	1.09	1.06	0.96	1.07	1.10	1.08	1.07	1.17	1.10	1.21	1.19	
																		Brown et al. [1998]
100-000	$2_{1,1}$-$2_{2,0}$	2606.44	2.77(-23)	1.06	0.84	1.43	1.69	0.43	1.31	0.28	0.61	0.82	0.07	0.50	1.12	0.14	0.11	
100-000	$1_{0,1}$-$1_{1,0}$	2608.58	6.78(-23)	1.11	0.88	1.51	1.79	0.45	1.38	0.30	0.65	0.88	0.08	0.53	1.19	0.15	0.11	
100-000	$3_{0,3}$-$2_{1,2}$	2646.48	1.99(-22)	1.10	0.94	1.38	1.57	0.61	1.28	0.48	0.77	0.94	0.26	0.68	1.17	0.35	0.30	
100-000	$3_{3,0}$-$2_{2,1}$	2675.06	1.69(-22)	1.07	0.96	1.26	1.39	0.69	1.23	0.58	0.80	0.91	0.37	0.73	1.08	0.44	0.40	
100-000	$4_{4,1}$-$3_{3,0}$	2688.95	2.87(-22)	1.11	0.94	1.40	1.58	0.70	1.19	0.59	0.89	1.10	0.40	0.81	1.31	0.52	0.48	
																		Brown et al. [1998]
001-000	$4_{2,2}$-$5_{4,1}$	2519.43	3.17(-23)	0.94	1.06	0.73	0.66	1.14	0.99	1.22	0.95	0.78	1.30	0.99	0.68	1.13	1.14	
001-000	$4_{1,3}$-$4_{3,2}$	2600.65	1.33(-23)	0.81	1.13	0.36	0.23	1.35	0.97	1.57	0.82	0.44	1.83	0.94	0.26	1.29	1.34	
001-000	$5_{4,2}$-$4_{4,1}$	2699.26	6.84(-23)	1.11	0.89	1.60	1.84	0.69	1.06	0.57	1.02	1.38	0.42	0.92	1.67	0.64	0.60	
001-000	$5_{4,1}$-$4_{4,0}$	2704.36	4.61(-23)	1.09	0.90	1.46	1.66	0.71	1.09	0.60	0.96	1.24	0.45	0.89	1.47	0.63	0.59	
																		Brown et al. [1998]
030-000	$3_{1,2}$-$3_{2,1}$	3507.39	1.41(-23)	0.88	0.87	0.87	0.93	0.90	0.88	0.92	0.96	0.93	0.95	0.90	0.85	1.01	0.96	
030-000	$1_{0,1}$-$1_{1,0}$	3508.64	1.27(-23)	0.87	0.87	0.87	0.93	0.89	0.88	0.92	0.96	0.93	0.95	0.90	0.84	1.00	0.95	
030-000	$1_{1,0}$-$1_{0,1}$	3521.26	1.22(-23)	0.84	0.84	0.84	0.90	0.86	0.85	0.89	0.93	0.90	0.92	0.87	0.81	0.97	0.92	
030-000	$2_{1,2}$-$1_{0,1}$	3539.45	1.15(-23)	0.86	0.86	0.86	0.92	0.89	0.88	0.91	0.95	0.92	0.94	0.89	0.83	0.99	0.94	
																		Brown et al. [1998]
110-000	$5_{3,2}$-$5_{4,1}$	3767.81	5.88(-22)	1.03	1.03	1.02	1.01	1.03	0.94	1.02	1.02	1.00	1.02	1.03	1.01	1.02	1.02	
110-000	$3_{2,1}$-$3_{3,0}$	3770.17	6.78(-22)	1.03	1.03	1.02	1.01	1.03	0.95	1.03	1.02	1.00	1.02	1.03	1.01	1.02	1.02	
110-000	$4_{1,4}$-$3_{0,3}$	3820.32	1.09(-21)	1.04	1.05	1.03	1.02	1.04	0.96	1.04	1.03	1.01	1.03	1.05	1.03	1.04	1.04	
110-000	$4_{4,1}$-$3_{3,0}$	3861.00	1.33(-21)	1.03	1.04	1.02	1.02	1.03	0.96	1.03	1.02	1.01	1.03	1.04	1.02	1.03	1.03	
																		Brown et al. [1998]
011-000	$3_{2,2}$-$4_{2,3}$	3737.74	1.05(-21)	1.03	1.03	1.03	1.02	1.03	0.96	1.04	1.03	1.03	1.04	1.03	1.02	1.05	1.04	
011-000	$3_{3,1}$-$3_{3,0}$	3788.56	1.76(-21)	1.02	1.03	1.03	1.02	1.03	0.96	1.03	1.03	1.03	1.04	1.03	1.01	1.05	1.04	
011-000	$4_{4,0}$-$4_{4,1}$	3792.90	1.72(-21)	1.02	1.03	1.03	1.02	1.03	0.96	1.03	1.03	1.02	1.03	1.03	1.01	1.04	1.04	
011-000	$4_{0,4}$-$3_{0,3}$	3830.71	1.86(-21)	1.03	1.03	1.03	1.02	1.03	0.96	1.04	1.03	1.03	1.04	1.04	1.02	1.05	1.04	

Table 4.1: Comparisons between the calculated transition intensities and the transition intensities available in the literature for the most intense transitions in some vibrational bands using all the constructed DMSs in this study (powers of ten in parenthesis).

1 CCSD(T)/aug-cc-pV(6+d)Z, added corrections
2 CCSD(T)-F12b/aug-cc-pV(Q+d)Z, added corrections
3 CCSD[T]/aug-cc-pV(6+d)Z, added corrections
4 CCSD[T]/aug-cc-pCV5Z-DK, with corrections
5 CCSD(T)-F12b/cc-pVQZ, added corrections
6 Cours et al. [2002]'s parameters
7 CCSD(T)-F12b/aug-cc-pV(Q+d)Z, without corrections
8 CCSD(T)-F12/aug-cc-pV5Z, First stage
9 CCSD[T]/aug-cc-pCV5Z-DK, without corrections
10 CCSD(T)-F12b/cc-pVQZ, without corrections
11 CCSD(T)-F12c/cc-pVQZ, added corrections
12 CCSD(T)/aug-cc-pVQZ, First stage
13 CCSD(T)-F12/cc-pVQZ, First stage
14 CCSD(T)-F12c/cc-pVQZ, without corrections

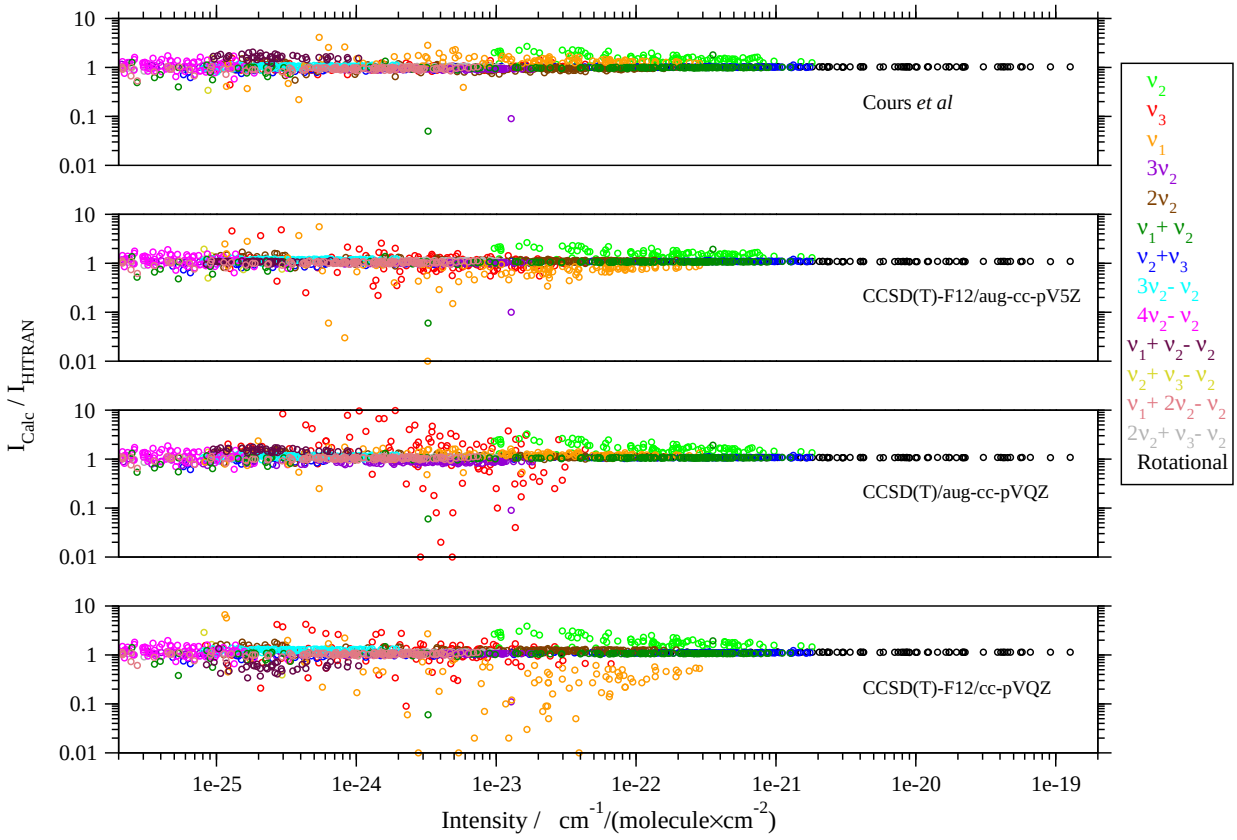

Figure 4.3: Intensities ratio using the dipole moment surfaces constructed in the first stage.

investigations of various approaches of the electronic structure calculations. These two steps are described below in details.

4.2.2.1 Core-correlation and relativistic corrections

Core-correlation and relativistic corrections are known to be essential for the calculation of accurate *ab initio* PESs [Barletta et al. [2002]; Tarczay et al. [2001b]]. Their effect on DMSs was shown to be small but relevant for the water molecule [Lodi et al. [2008, 2011]]. We investigated the magnitudes of these effects for the H_2S DMS for the first time.

In a preliminary test, dipole moments were computed using the CCSD[T] method on a grid of 200 geometries using four, increasingly-sophisticated levels of theory:

1. frozen-core, non-relativistic, using the basis set aug-cc-pV5Z [Dunning [1989]],
2. frozen-core, relativistic, using the basis set aug-cc-pV5Z-DK [Peterson and Dunning [2002]],
3. core-correlated, non-relativistic, using the basis set aug-cc-pCV5Z [Woon and Dunning [1993]], and
4. core-correlated, relativistic, using the basis set aug-cc-pCV5Z-DK [Peterson and Dunning [2002]].

The relativistic calculations were generated using the second-order Douglas-Kroll Hamiltonian as implemented in MOLPRO while in the core-correlation calculations the $1s$ orbital of the sulphur atom was kept frozen.

Results are shown in Fig. 4.4. These results can be summarised as follows:

1. the effect of the core-correlation on the dipole moment values is
   (a) very small, its value is not more than 0.005 D for the selected geometries up to energy values of 13 000 cm^{-1} and up to 0.010 D for energies up to 25 000 cm^{-1}, and
   (b) decreasing the dipole moment values.

2. the effect of the relativistic corrections on the dipole moment values is

   (a) large enough not to be ignored; its value is not less than 0.017 D for the selected geometries up to energy values 13 000 cm^{-1} and 0.012 - 0.017 D for energies up to 25 000 cm^{-1}, and

   (b) decreasing the dipole moment values.

3. dipoles computed by the combined relativistic/core-correlation calculations (point 4 above) give an overall correction which is nearly identical (within 0.0005 D) to the sum of the corrections calculated one-by-one; in other words following these tests, the relativity and core-correlation can be processed independently, and

4. both relativistic and core-correlation effects tend to reduce the magnitude of the dipole moment, so that mutual cancellation does not generally happen. Partial exception to this behaviour occurs for energies up to 5000 cm^{-1} for the (small) asymmetric component of the dipole moment (perpendicular to the bond-angle bisector); in this particular case the two corrections have similar magnitude (about 0.001 D) and opposite signs, so that they do cancel each other out to a large extent. However, for the same geometries no cancellation occurs for the correction to the (large) symmetric component of the dipoles (along the bond-angle bisector). This situation is quite different to the one found in water [Lodi et al. [2008]], where the core-correlation and relativistic corrections to the dipole moment have the same magnitude and, furthermore, were found to cancel each other out to a large extent.

It is not possible to directly infer the effect of the corrections on computed rovibrational line intensities, as this depends in a complicated way on the derivatives of the DMS, rather than on its absolute value. In fact, as discussed below, even though these two corrections affect the value of dipoles by only about 2 % their effect on line intensities is much larger, up to a factor 10 or even more (see below). Both relativistic and core-correlations corrections were therefore included in our calculations.

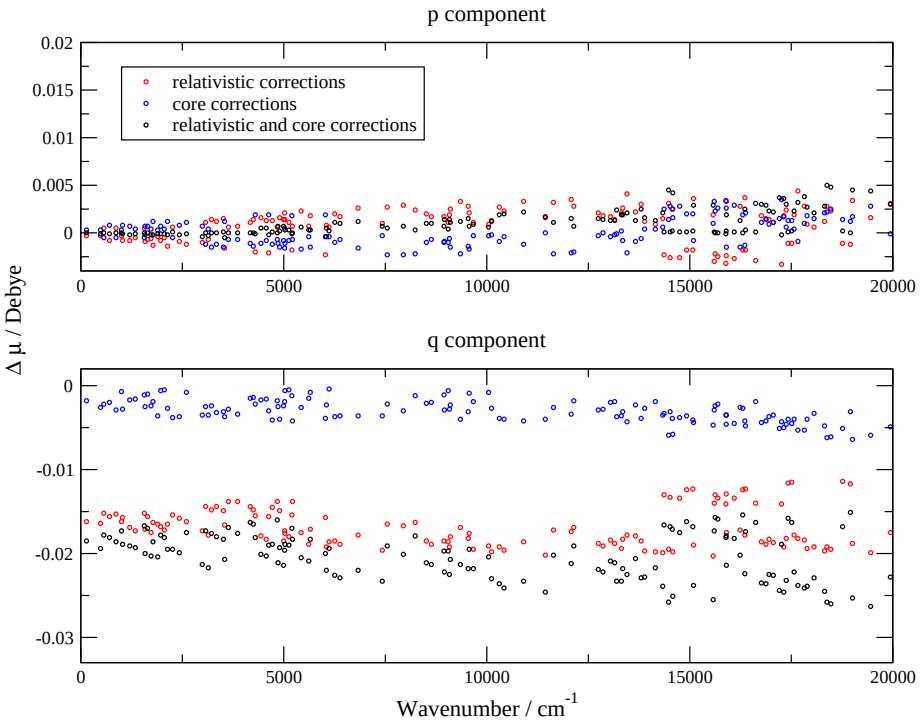

Figure 4.4: Effect of relativity and core correlation on the dipole moments for 200 selected geometries using CCSD[T]. $\Delta\mu = \mu_{with\ \ correction} - \mu_{without\ \ correction}$.

4.2.2.2 Equilibrium dipole

Our second step was to test the effects of different levels of the *ab initio* theory on the equilibrium dipole moment of H_2S. To gain a general idea about the effect of different methods and different basis sets on the dipole moment values, and also to estimate the computational resources needed to perform these calculations, the dipole moments were calculated using a large number of different methods and different bases sets. These tests were performed at experimental equilibrium geometry of $r_e = 1.3356$ Å, $\theta_e = 92.11°$ [Edwards et al. [1967]] and compared to the accurately-known experimental value $\mu_e = 0.978325(10)$ D [Viswanathan and Dyke [1984]]. The permanent dipole moment values and the CPU time are summarised in Table 4.2. Comparing the results from this table with the experimental permanent dipole moment value, we notice the following:

1. the values of the calculated dipole moment using the highest level of theory (in our table) , namely, using aug-cc-pCV5Z-DK basis set with corrections, deviate from the experimental value by 0.0078, 0.0084 and 0.0087 D for CCSD-T, CCSD(T) and CCSD[T], respectively, and

2. by extracting the core and the relativistic corrections ($\mu_{with\ corrections} - \mu_{without\ corrections}$) from the calculated values using the aug-cc-pCV5Z-DK basis set and adding these corrections to the values calculated using the aug-cc-pV(6+d)Z basis set, the dipole moment values will deviate from the experimental value by 0.0075, 0.0082 and 0.0084 D for CCSD-T, CCSD(T) and CCSD[T], respectively.

In another extra test the H_2S dipole moment computed at the experimental equilibrium geometry of $r_e = 1.3356$ Å, $\theta_e = 92.11°$ [Edwards et al. [1967]] using ALYT2013 surface was compared to the experimental value $\mu_e = 0.978325(10)$ D [Viswanathan and Dyke [1984]], as reported in Table 4.3. In this table a vibrational-averaging correction was added by performing nuclear motion calculations using the Dvr3d program suite [Tennyson et al. [2004]]. Our final value for the permanent dipole moment of H_2S is 0.0079 D or 0.8 % larger than the experimental value. If relativistic and core-correlation effects were discarded the discrepancy with experiment would increase to 1.1 %.

Table 4.2: Permanent dipole moment values (in Debye) at the equilibrium geometry using different levels of theory and associated with the computer time, where 'with': with corrections, 'without': without corrections, s: second, m: minute, h: hour.
The experimental permanent dipole moment value is 0.978325(10) D [Viswanathan and Dyke [1984]].

	Basis set	CCSD	Time	CCSD-T	Time	CCSD(T)	Time	CCSD[T]	Time	CCSD(T)-F12a	Time	CCSD(T)-F12b	Time	CCSD(T)-F12c	Time
without	cc-pVQZ	1.0496	37 s	1.0450	1 m	1.0445	1 m	1.0438	1 m	1.0335	1 m	1.0307	1 m	1.0311	2 m
	cc-pV5Z	1.0418	5 m	1.0363	9 m	1.0358	8 m	1.0351	8 m	1.0260	11 m	1.0236	11 m	1.0236	14 m
	cc-pV6Z	1.0245	35 m	1.0178	50 m	1.0173	50 m	1.0166	50 m						
	aug-cc-pVQZ	1.0013	3 m	0.9913	4 m	0.9907	4 m	0.9899	4 m	0.9934	6 m	0.9912	6 m	0.9918	7 m
	aug-cc-pV5Z	0.9986	22 m	0.9891	32 m	0.9886	33 m	0.9878	32 m	0.9920	41 m	0.9900	41 m	0.9901	50 m
	aug-cc-pV6Z	0.9989	2 h	0.9896	3 h	0.9891	3 h	0.9883	3 h						
	aug-cc-pV(Q+d)Z	0.9928	3 m	0.9830	5 m	0.9824	5 m	0.9816	5 m						
	aug-cc-pV(5+d)Z	0.9969	24 m	0.9875	34 m	0.9870	35 m	0.9862	35 m						
	aug-cc-pV(6+d)Z	0.9984	2 h	0.9892	3 h	0.9886	3 h	0.9879	3 h						
	cc-pVQZ-F12	—		—		—		—		1.0113	5 m	1.0093	5 m	1.0099	6 m
	**	—		—		—		—		0.9941	21 m	0.9922	21 m		
with	cc-pVQZ	1.0320	2 m	1.0269	4 m	1.0264	4 m	1.0258	5 m						
	cc-pV5Z	1.0264	13 m	1.0196	31 m	1.0191	33 m	1.0186	33 m						
	cc-pV6Z	1.0081	1 h	0.9998	3 h	0.9992	3 h	0.9988	3 h						
	aug-cc-pVQZ	0.9838	7 m	0.9731	17 m	0.9726	17 m	0.9717	17 m						
	aug-cc-pV5Z	0.9833	48 m	0.9724	2 h	0.9718	2 h	0.9712	2 h						
	aug-cc-pV6Z	0.9825	5 h	0.9714	11 h	0.9709	12 h	0.9704	12 h						
	aug-cc-pV(Q+d)Z	0.9737	8 m	0.9629	19 m	0.9624	19 m	0.9617	19 m						
	aug-cc-pV(5+d)Z	0.9850	51 m	0.9738	2 h	0.9733	2 h	0.9727	2 h						
	aug-cc-pV(6+d)Z	0.9860	5 h	0.9747	12 h	0.9742	12 h	0.9737	12 h						
without	cc-pCVQZ-DK	1.0431	3 m	1.0388	6 m	1.0383	6 m	1.0378	6 m						
	cc-pCV5Z-DK	1.0407	26 m	1.0352	1 h	1.0347	45 m	1.0341	44 m						
	aug-cc-pCVQZ-DK	0.9940	12 m	0.9843	17 m	0.9838	14 m	0.9830	14 m						
	aug-cc-pCV5Z-DK	0.9983	2 h	0.9889	2 h	0.9884	2 h	0.9876	2 h						
with	cc-pCVQZ-DK	1.0256	9 m	1.0193	29 m	1.0188	29 m	1.0184	30 m						
	cc-pCV5Z-DK	1.0243	1 h	1.0166	3 h	1.0161	3 h	1.0158	3 h						
	aug-cc-pCVQZ-DK	0.9768	32 m	0.9648	1 h	0.9643	1 h	0.9638	1 h						
	aug-cc-pCV5Z-DK	0.9822	4 h	0.9705	9 h	0.9699	9 h	0.9696	9 h						

** Using H=aug-cc-pVQZ,S=aug-cc-pV(Q+d)Z with Auxiliary RI (OptRI) matched to the aug-cc-pV(n+d)Z Quadruple-ζ basis set of S [Yousaf and Peterson [2009]].

Table 4.3: Permanent dipole at the equilibrium geometry $r_e = 1.3356$ Å and $\theta_e = 92.11°$ as a function of theoretical model.

	Method	$\bar{\mu}$ (D)
1	CCSD(T)/aug-cc-pV(6+d)Z	0.9886
2	CCSD[T]/aug-cc-pCV5Z-DK with corrections	0.9696
3	CCSD[T]/aug-cc-pCV5Z-DK without corrections	0.9876
4	Correction = row 1 − row 2	-0.0180
5	Row 1 plus row 4 ($\bar{\mu}_0$)	0.9706
6	Vibrational averaging	-0.0002
7	Calculated permanent dipole moment (μ_e)	0.9704
	Experimental value [Viswanathan and Dyke [1984]]	0.978325(10)

4.2.2.3 DMSs

Since the best available up-to-date dipole moment surface (DMS) was calculated using the CCSD[T] method by Cours et al. [2002], we also decided to test this method in conjunction with Peterson and Dunning [2002]'s basis set aug-cc-pCV5Z-DK after including the core and the relativistic corrections in the electronic Hamiltonian. This DMS was computed using a large grid of 7000 symmetry-independent geometries. These geometries cover the bond lengths from 2.00 to 2.86 a_0 and bond angles from 60° to 125° (the extension of these geometry ranges is discussed below), see Fig. 4.5. The grid was designed to be denser in the vicinity of the equilibrium geometry and to cover energies up to 20 000 cm^{-1} above the ground state. The two components of this surface were plotted versus the energy (above the ground state), see Fig. 4.6. We will refer to this surface hereafter as DMS-1.

The transition intensities calculated using DMS-1 were tested by comparing their values to the experimental values in the same way we tested the three previously constructed DMSs presented above, see Section 4.2.1. See Table 4.1 for some qualitative comparisons and Fig. 4.7 for general overview.

Comparing the results using DMS-1 with the results using Cours *et al.*'s surface we notice that:

1. the ν_2 band is better reproduced than using Cours *et al.*'s surface,

2. the ν_1 band has a larger error than the error resulted from using Cours *et*

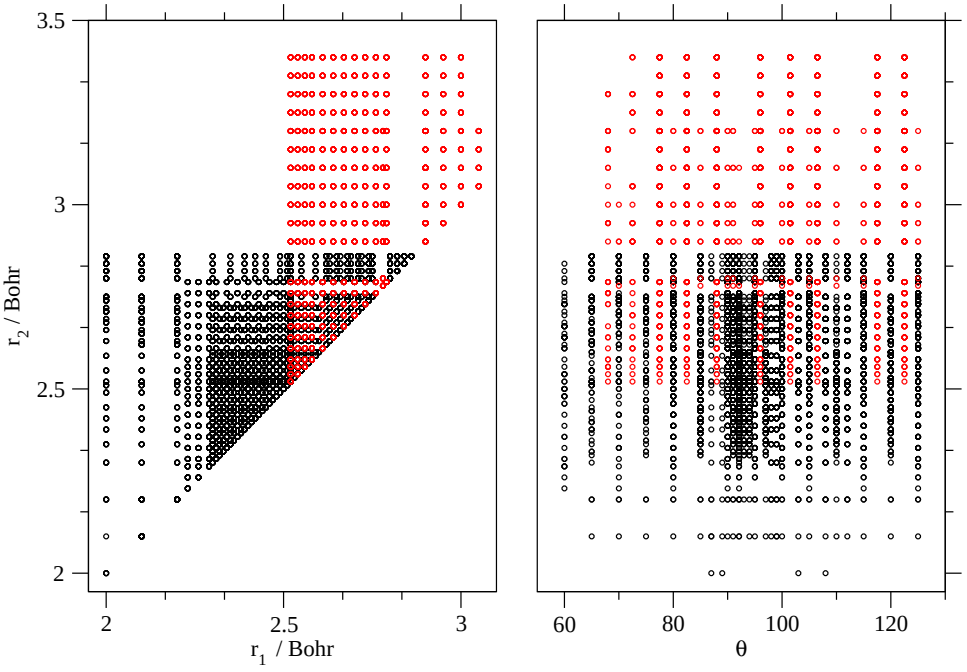

Figure 4.5: Grid points for r_1 and r_2 and θ used in the *ab initio* dipole moment calculations in the second stage of this study. The red points are extra *ab initio* points which were added later to extend the range of the DMS, see Chapter 5.

al.'s surface,

3. the ν_3 band is very badly reproduced, while the calculations resulted using Cours *et al.*'s surface were very good, and

4. the higher vibrational bands are reproduced very well, which agrees with Cours *et al.*'s calculations.

Another DMS was constructed using the same method and the same basis set used for DMS-1 but without the core and the relativistic corrections in order to compare the intensities results calculated using this surface with the results using Cours *et al.*'s surface. Besides, the including of the core and the relativistic corrections in the calculations are very time demanding (see Table 4.2), we can extract these corrections from the calculations and add them later to any surface calculated without them using ($\mu_{with\ \ corrections} - \mu_{without\ \ corrections}$), here $\mu_{with\ \ corrections}$ and $\mu_{without\ \ corrections}$ are calculated at the same molecular geometry. DMS obtained in this way will be called DMS-2. The extracted corrections of the two components of the dipole moment are plotted versus the energy in Fig. 4.8.

The transition intensities were also calculated using DMS-2. The intensity ratio ($I_{Calc.}/I_{Obs.}$) was calculated for the same transitions used before and presented in Table 4.1. Also, the ratios ($I_{Calc.}/I_{HITRAN}$) versus HITRAN's line intensities were calculated and plotted, see Fig. 4.7. Comparing the intensities results using DMS-1 and DMS-2, one can notice the effect of the core and relativistic corrections in the calculations from the improvement of the ν_2 intensity calculations. However, the results are still not satisfactory so more dipole moment surfaces were calculated. The extracted core and relativistic corrections were added to these calculated surfaces as mentioned above.

Different methods were used to construct different dipole moment surfaces; CCSD(T), CCSD(T)-F12b, CCSD(T)-F12c, and MRCI+Q. These methods were used in conjunction with different basis sets; cc-pVQZ and aug-cc-pV5Z [Woon and Dunning [1993]], aug-cc-pV(Q+d)Z with Auxiliary RI (OptRI) basis set [Yousaf and Peterson [2009]], and aug-cc-pV(6+d)Z [Dunning et al. [2001]]. Fig. 4.9 shows the q component for all of these surfaces after adding the extracted corrections. The resulting surfaces were fitted and used in the transition intensities

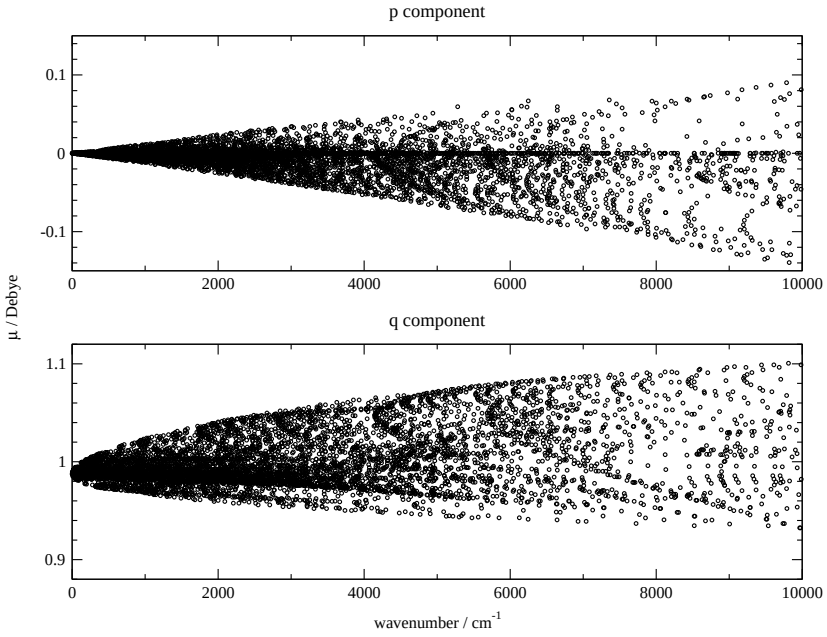

Figure 4.6: *Ab initio* values of the two components of the dipole moment surface of H_2S using CCSD[T]/aug-cc-pCV5Z-DK.

calculations, see Table 4.4 for a summary of the fits and Figs. 4.10 and 4.11 for general idea about the fitting residues at different energies. The coefficients $Q^{(l)}_{ij\ldots}$ and $P^{(l)}_{ij\ldots}$ of all the constructed MDSs are provided in Appendix A.

Typically 48 terms were used for the q component and 33 for p components. For all the electronic-structure methods investigated, the fitted surfaces reproduced the *ab initio* data with a root-mean-square deviation less than 5×10^{-5} D. There was, however, two exceptions to this. Fits to the MRCI+Q results gave much higher standard deviations of up to 0.003 D for the q component, while the p component had errors up to 0.06 D. And fits to CCSD[T]/aug-cc-pV(6+d)Z) had some high residues as well. All the other surfaces have fitting errors less than 0.0006 and 0.0004 D for the p and q components respectively for energies below 20 000 cm^{-1}. It is clear that the MRCI+Q calculations have problems. To do the finite field calculations it was necessary to significantly increase the convergence thresholds in all calculations. It transpires that in many cases the MRCI+Q calculations struggled to meet these thresholds and the results were therefore very noisy. For this reason more tests should be done for using the MRCI+Q approach,

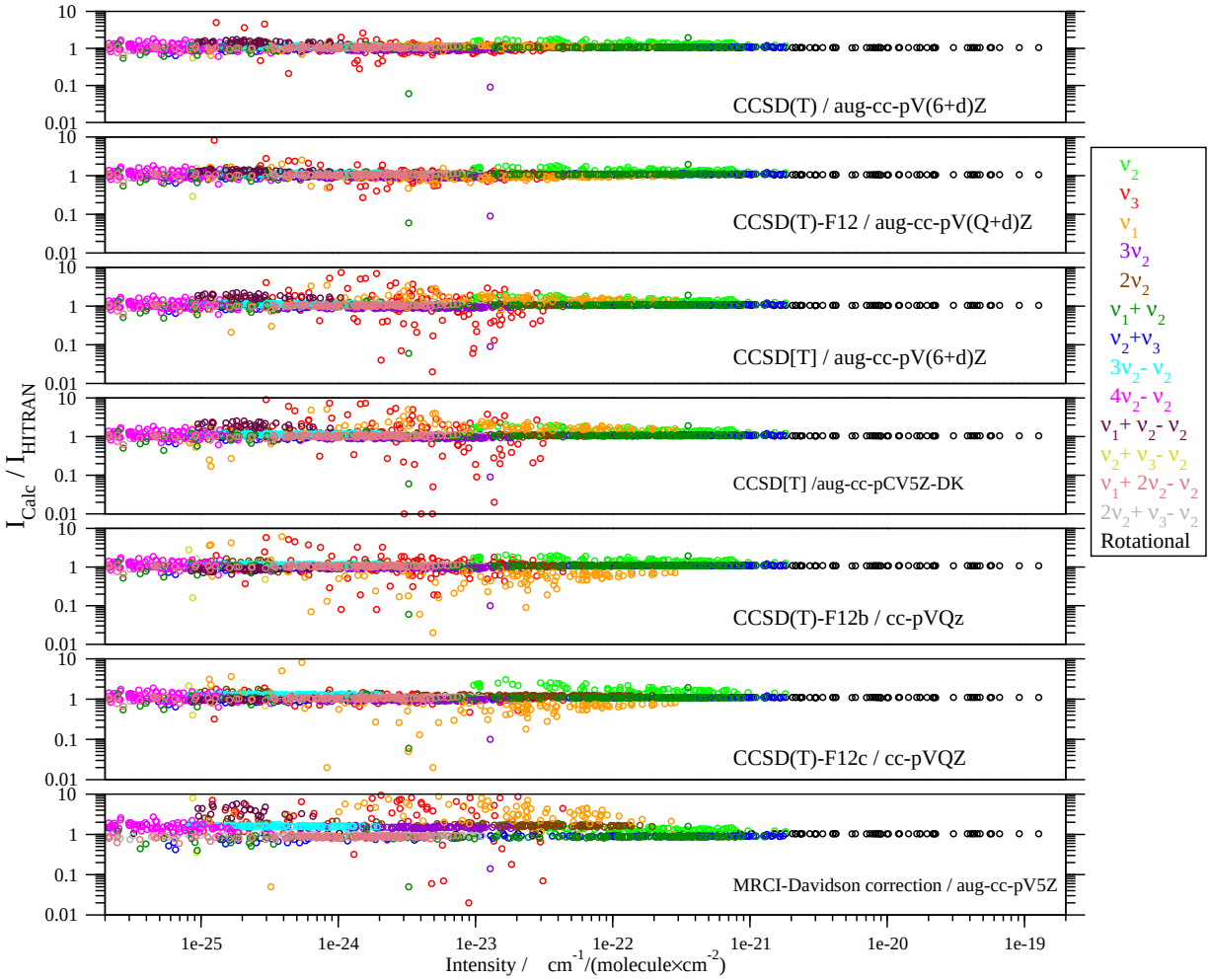

Figure 4.7: Intensity ratio ($I_{Calc.}/I_{HITRAN}$) versus HITRAN's lines intensities using different methods and different bases sets after adding the extracted core and relativistic corrections to the calculated dipole moment surfaces. This plot is based on the lines with J values up to 5 for 14 vibrational bands.

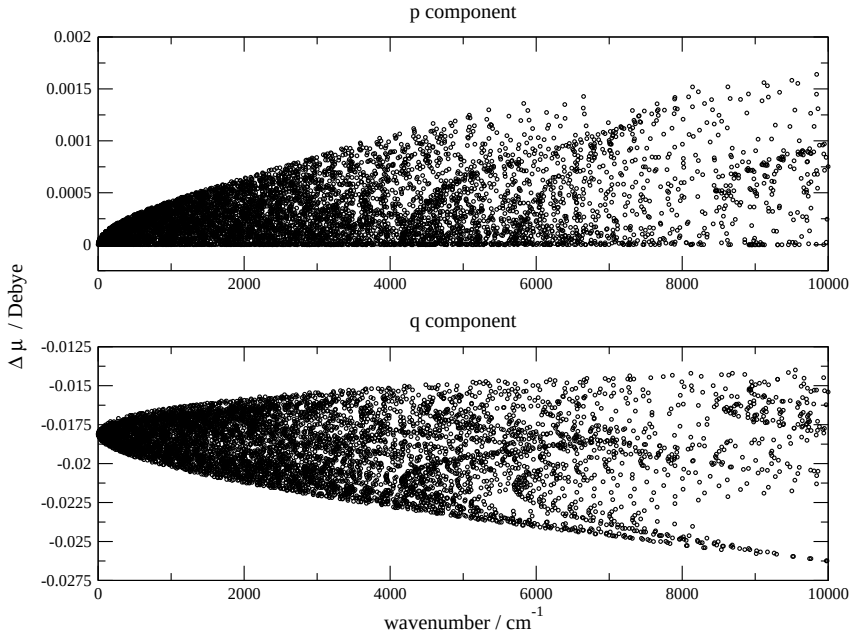

Figure 4.8: The core and relativistic corrections added to the dipole moment surfaces.

but these were not pursued. For CCSD[T]/aug-cc-pV(6+d)Z, we think the high residues were occur in places of big gaps of the *ab initio* points.

As before, the most intense transitions from the same selected vibrational bands were computed to test the accuracy of each calculated dipole moment surface, see Table 4.1. Also, see Fig. 4.7 for the ratios ($I_{Calc.}/I_{HITRAN}$) versus HITRAN's transition intensities comparisons. As can be seen from this table and this figure, our best surface (which we will call ALYT2013), computed at the CCSD(T)/aug-cc-pV(6+d)Z level with the added corrections computed using CCSD[T]/aug-cc-pCV5Z-DK, shows significantly improved behaviour compared to the other methods used in our study. To summarise, ALYT2013 surface:

1. represents the ν_1 and ν_3 bands very well,

2. overestimates the intensity of the ν_2 transitions by about 20 %, and

3. represents all the overtone, combination, and hot bands very well including the $\nu_1 + \nu_2 - \nu_2$ band.

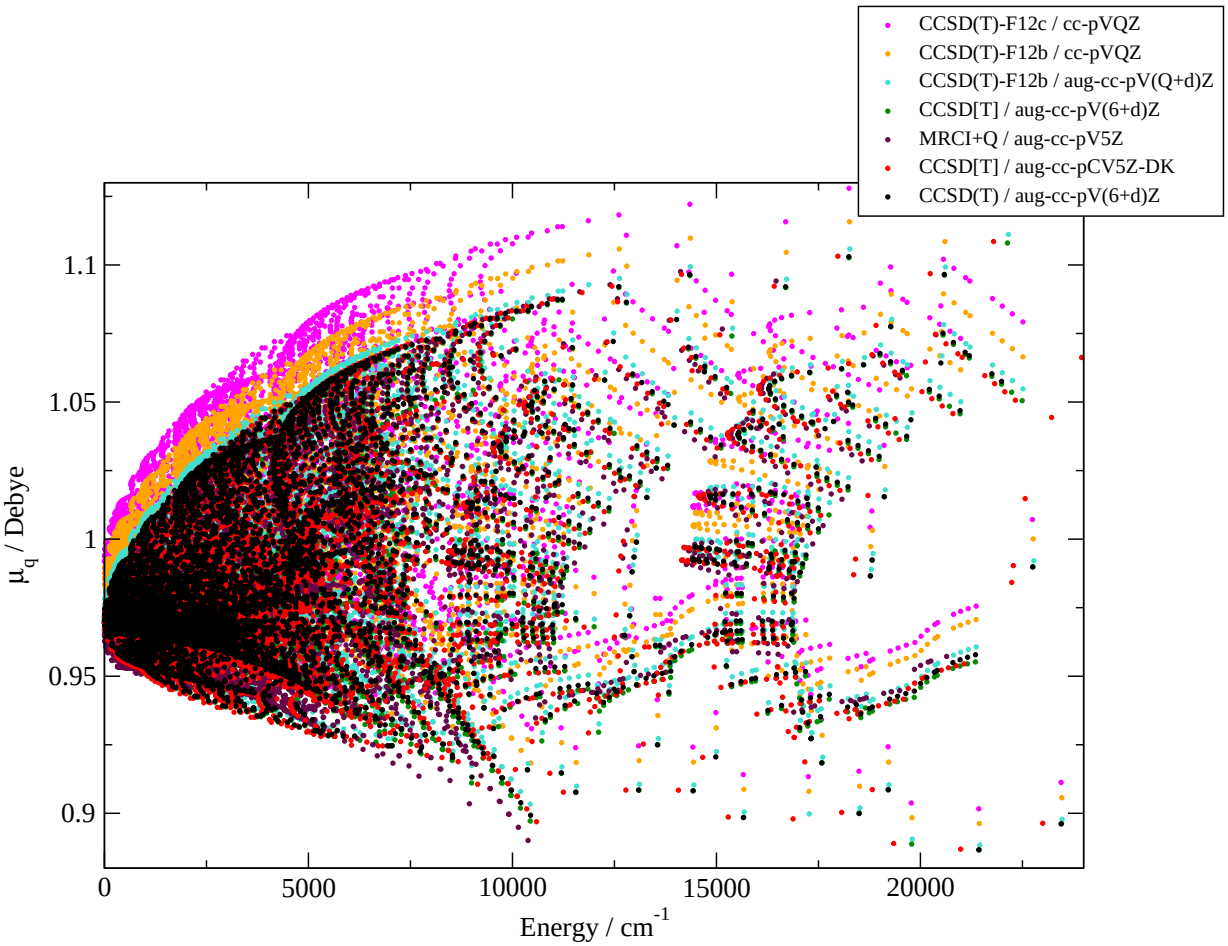

Figure 4.9: μ_q component of different *Ab initio* dipole moment surfaces with the added corrections.

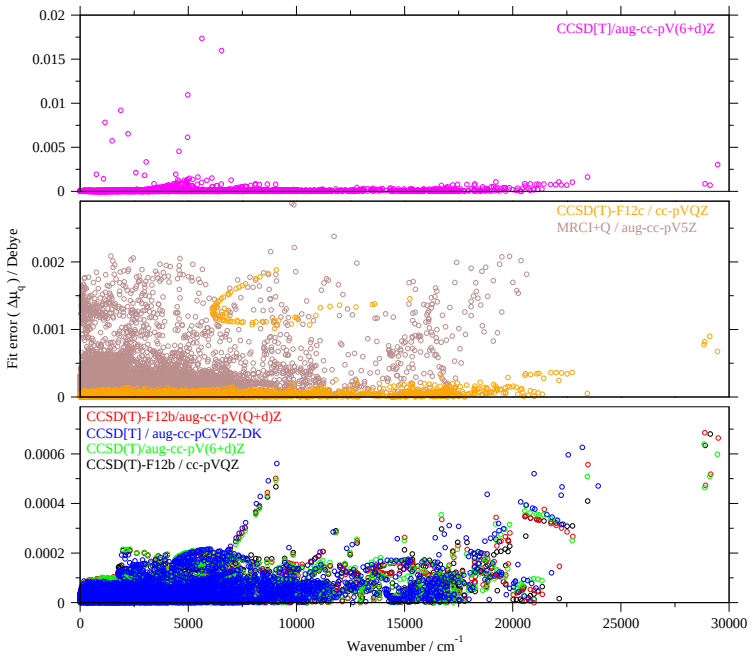

Figure 4.10: Residues in the fits for μ_q with respect to energy for the dipole moment surfaces calculated with corrections.

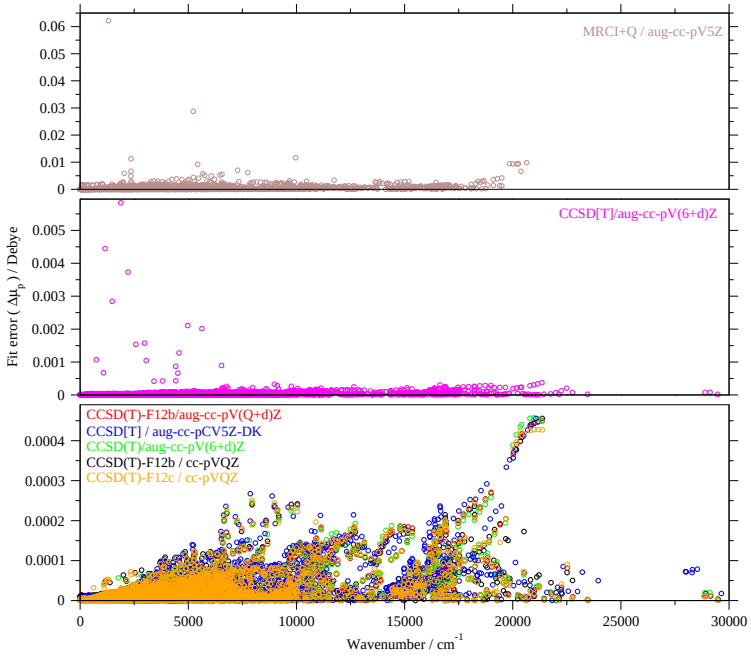

Figure 4.11: Residues of the fits for μ_p with respect to energy for the dipole moment surfaces calculated with corrections.

In the following the constructed DMSs will be referenced to as defined in Table 4.1.

4.3 Discussion

During this study we learnt that taking into account the core and relativistic corrections in the calculations of H_2S dipole moments not only alter significantly the values of the calculated dipole moments, but also improve the calculated intensities of the spectrum, see Fig. 4.12. Also, Table 4.1 shows the effect of including these corrections for the intensity calculations, which can be seen by comparing the ν_2 values from surfaces constructed with and without these corrections. For example, compare column 14 with column 11, column 10 with 5, and column 9 with 4 (for ν_2 band). These corrections are particularly important for the ν_2 bending mode. For water, these corrections in the PES were also found to be important for reproducing the ν_2 bending mode frequencies but to essentially cancel each other in the DMS [Lodi et al. [2008]].

With all the methods used in this study including MRCI+Q method, we could describe the H_2S spectrum qualitatively well. The general intensity envelopes of the fundamental bands could be reproduced very well and the anomalies in these bands as well, regardless of the used method, see Figs. 4.13 and 4.14. The real problem is the construction of a dipole moment surface which reproduces the intensities quantitatively.

By comparing the surfaces constructed in this work with Cours *et al.*'s surface we noticed that: although the dipole moment values for the q component around the equilibrium geometry have significant differences (around 0.03 D), the p component of all of these surfaces (apart from MRCI+Q surface) showed much less differences (of order 10^{-4} D). This reflects how much the asymmetric component is sensitive even to the very small differences in the calculations. These comparisons showed that good results could be obtained only by using basis sets of (n+d)Z quality with a large n value. The use of the F12 method did not significantly improve the predictions.

Our calculations show that the intensities of the transitions within the fundamental bands are very sensitive to changes in the treatment used to compute

Table 4.4: Summary of the fits for the q and p components of the dipole moment surfaces. (powers of ten in parenthesis).

	q-component					p-component				
	Num. Parameters	Num. Points	Standard deviation	rms	Stability	Num. Parameters	Num. Points	Standard deviation	rms	Stability
1 - CCSD(T)/aug-cc-pV(6+d)Z[b]	48	7051	0.47609(-4)	0.53394(-4)	0.213(-13)	33	7051	0.25019(-4)	0.32601(-4)	0.339(-14)
2 - CCSD(T)-F12b/aug-cc-pV(Q+d)Z[b]	48	7241	0.47825(-4)	0.54002(-4)	0.720(-13)	33	7241	0.25571(-4)	0.33042(-4)	0.782(-14)
3 - CCSD[T]/aug-cc-pV(6+d)Z[b]	43	6993	0.39877(-3)	0.39651(-3)	0.122(-14)	33	6993	0.12337(-3)	0.12279(-3)	0.330(-14)
4 - CCSD[T]/aug-cc-pCV5Z-DK[c]	50	7393	0.50066(-4)	0.65680(-4)	0.585(-12)	34	7393	0.28718(-4)	0.35820(-4)	0.212(-14)
5 - CCSD(T)-F12b/cc-pVQZ[b]	49	7260	0.48196(-4)	0.55213(-4)	0.650(-13)	34	7260	0.26306(-4)	0.33804(-4)	0.322(-14)
6 - CCSD(T)-F12b/aug-cc-pV(Q+d)Z[a]	49	7527	0.45810(-4)	0.53191(-4)	0.510(-13)	33	7527	0.24037(-4)	0.32060(-4)	0.634(-14)
7 - CCSD[T]/aug-cc-pCV5Z-DK[a]	48	7427	0.48685(-4)	0.75052(-4)	0.209(-13)	33	7427	0.26407(-4)	0.35997(-4)	0.103(-14)
8 - CCSD(T)-F12b/cc-pVQZ[a]	48	7545	0.46098(-4)	0.57678(-4)	0.123(-13)	34	7545	0.25362(-4)	0.33575(-4)	0.334(-14)
9 - CCSD(T)-F12c/cc-pVQZ[b]	48	7282	0.49633(-4)	0.55923(-4)	0.806(-14)	33	7282	0.26374(-4)	0.33572(-4)	0.257(-14)
10- CCSD(T)-F12c/cc-pVQZ[a]	49	7281	0.46977(-4)	0.50952(-4)	0.113(-13)	33	7281	0.24741(-4)	0.31684(-4)	0.931(-14)

[a] Without the corrections
[b] After adding the corrections
[c] With the corrections

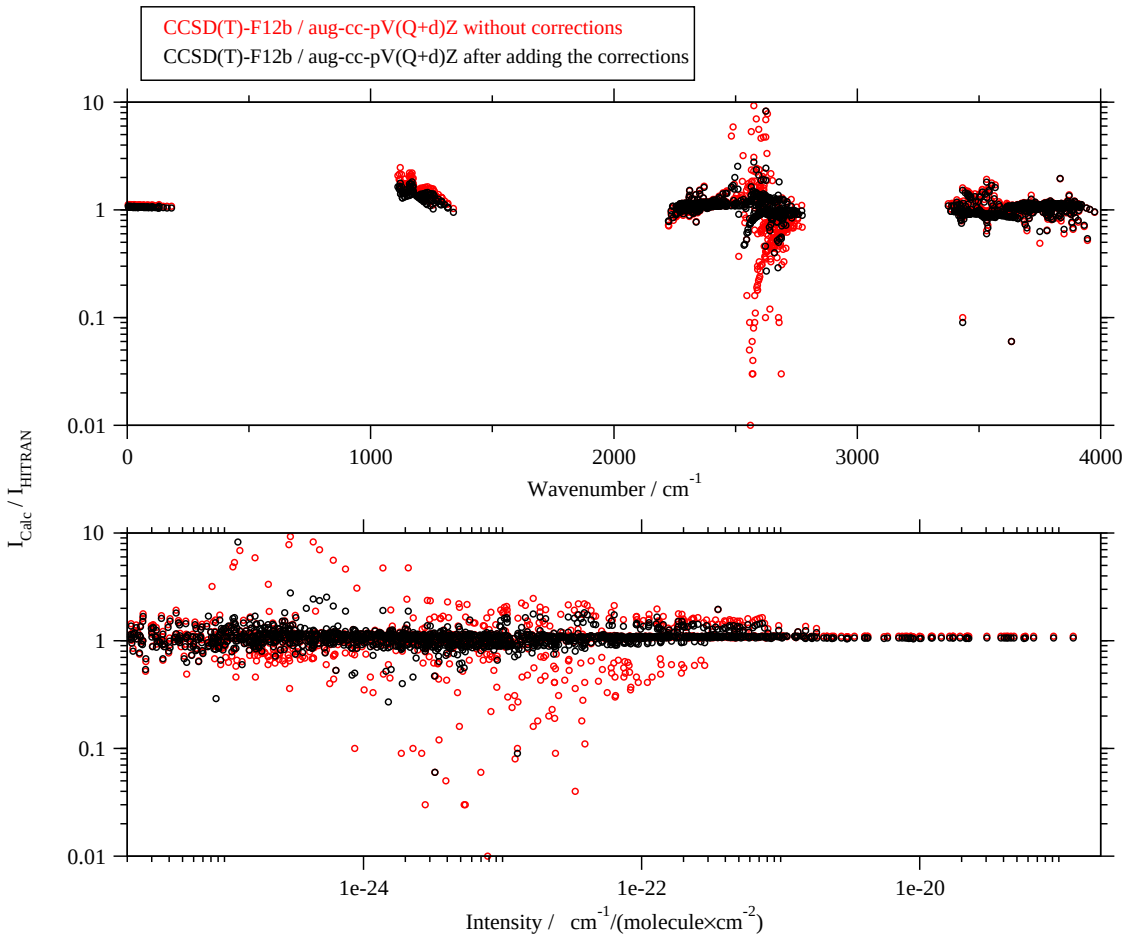

Figure 4.12: Effect of adding the corrections on the intensities using CCSD(T)-F12b/aug-cc-pV(Q+d)Z.

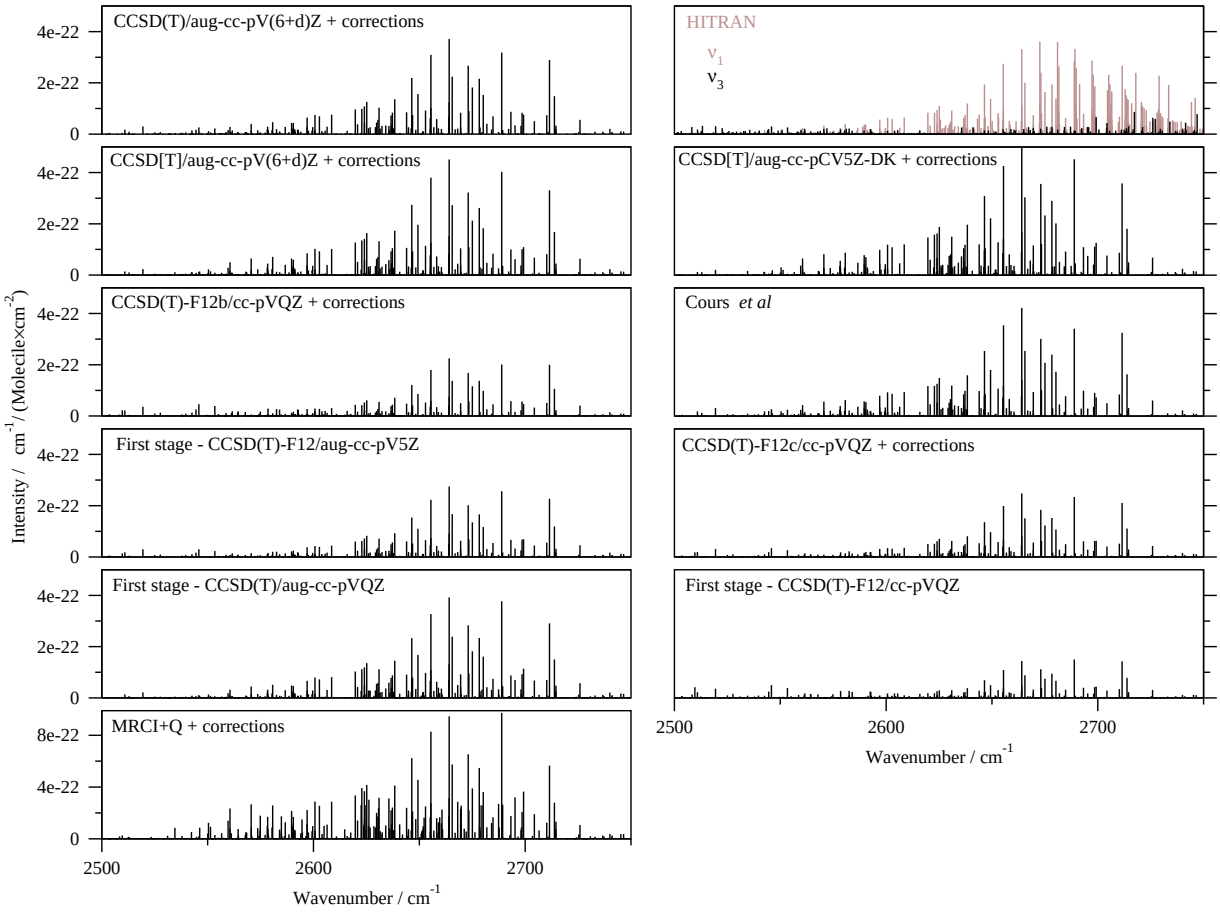

Figure 4.13: ν_1 and ν_3 bands calculated using the different methods with the corrections up to $J = 5$. Note: HITRAN spectrum contains lines with higher values of J.

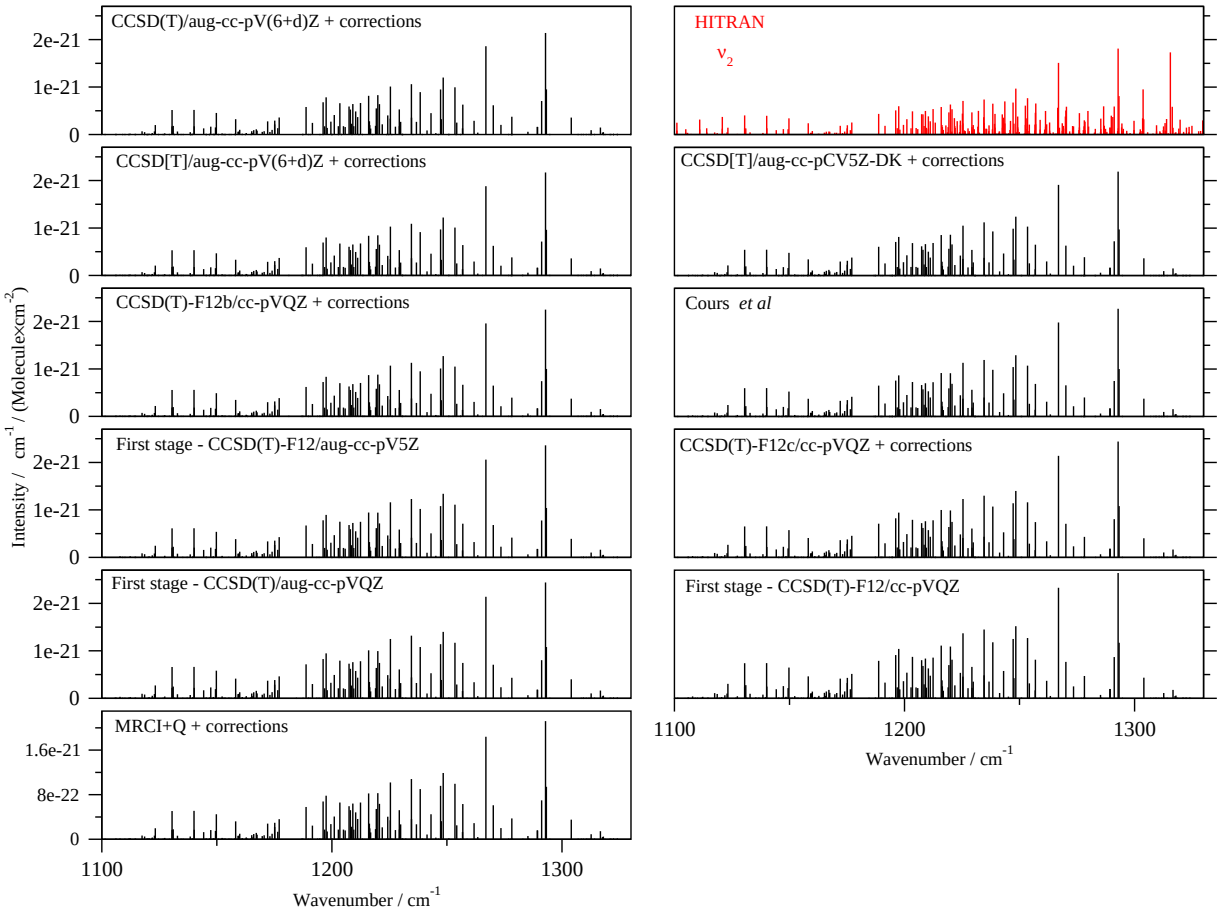

Figure 4.14: The ν_2 band calculated using the different methods with corrections up to $J = 5$. HITRAN spectrum contains lines with higher values of J.

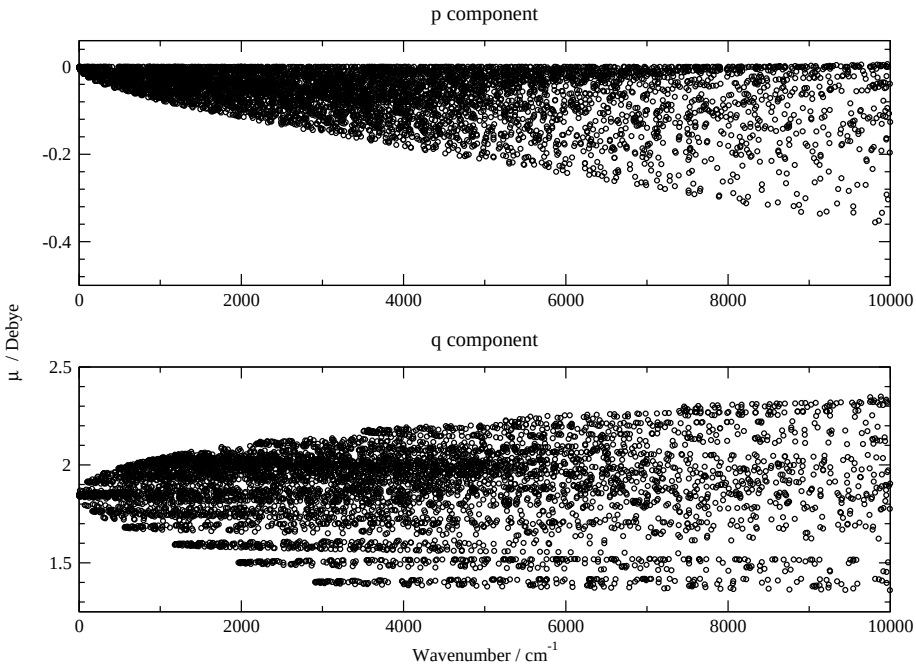

Figure 4.15: *Ab initio* dipole moment components of water.

the dipole moment components. Conversely the intensity of transitions within other bands, with the exception of the $\nu_1 + \nu_2 - \nu_2$ combination band, are well reproduced for the whole range of treatments we tested.

The H_2S DMS has a rather unusual topology. In particular the $\mu^{(p)}$ component changes very slowly in the vicinity of the equilibrium geometry and undergoes a sign change in this region. This causes the transition dipoles to be very small after $\mu^{(p)}$ is averaged over the vibrational wavefunctions. This behaviour contrasts with that of the H_2O and H_2Se molecules, where the sign-change for the asymmetric component happens for geometries with energies above 4000 cm^{-1} for H_2Se and around 10 000 cm^{-1} for H_2O, compare Figs. 4.15 and 4.16 with Fig. 4.6.

In various comparisons made using the HITRAN 2008 intensity data, we noticed that some lines in hot and combination bands have systematically lower/higher intensities in all calculations by about 50 % for all the method used in our study, this can be seen in Fig. 4.17. Further investigation showed that such disagreements could probably be linked to problems in the line intensities in the HITRAN 2008 database associated with extrapolations using effective Hamiltonian

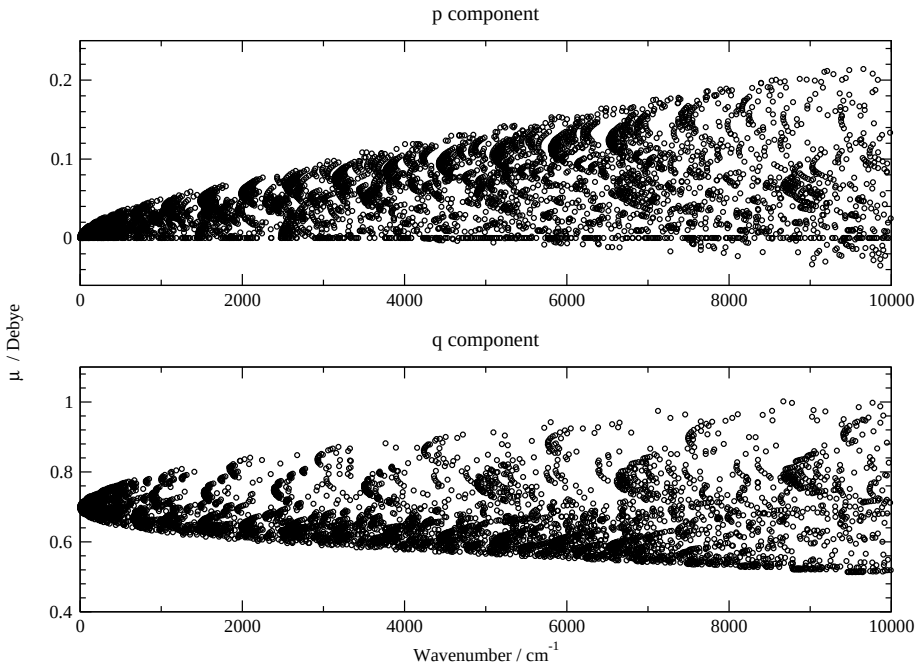

Figure 4.16: *Ab initio* dipole moment components of H_2Se.

fits.

We therefore decided to make a set of comparisons to distinguish between the actually measured intensities and those predicted on the basis of fits. This required collecting the measured lines directly from the original literature [Brown et al. [1998]]. New comparisons were made for the 2200 – 4000 cm^{-1} region. The following two bands were excluded from this analysis: (i) the rotational band, because of the very good agreement found with all HITRAN data, (ii) ν_2 band because we could not access the data from the original reference [Goldman and Gillis [1984]]. The results of our analysis are illustrated in Figs. 4.18 and 4.19. It is clear the disagreement is largest for cases associated with predicted intensities. Our calculations agree significantly better with the actual experimentally measured line intensities.

A possible source of the error in our calculations is in the variationally computed wavefunctions. It is therefore necessary to check if this disagreement is due to systematic errors introduced by these wavefunctions, for example due to an incomplete treatment of resonance interactions. To test the sensitivity of

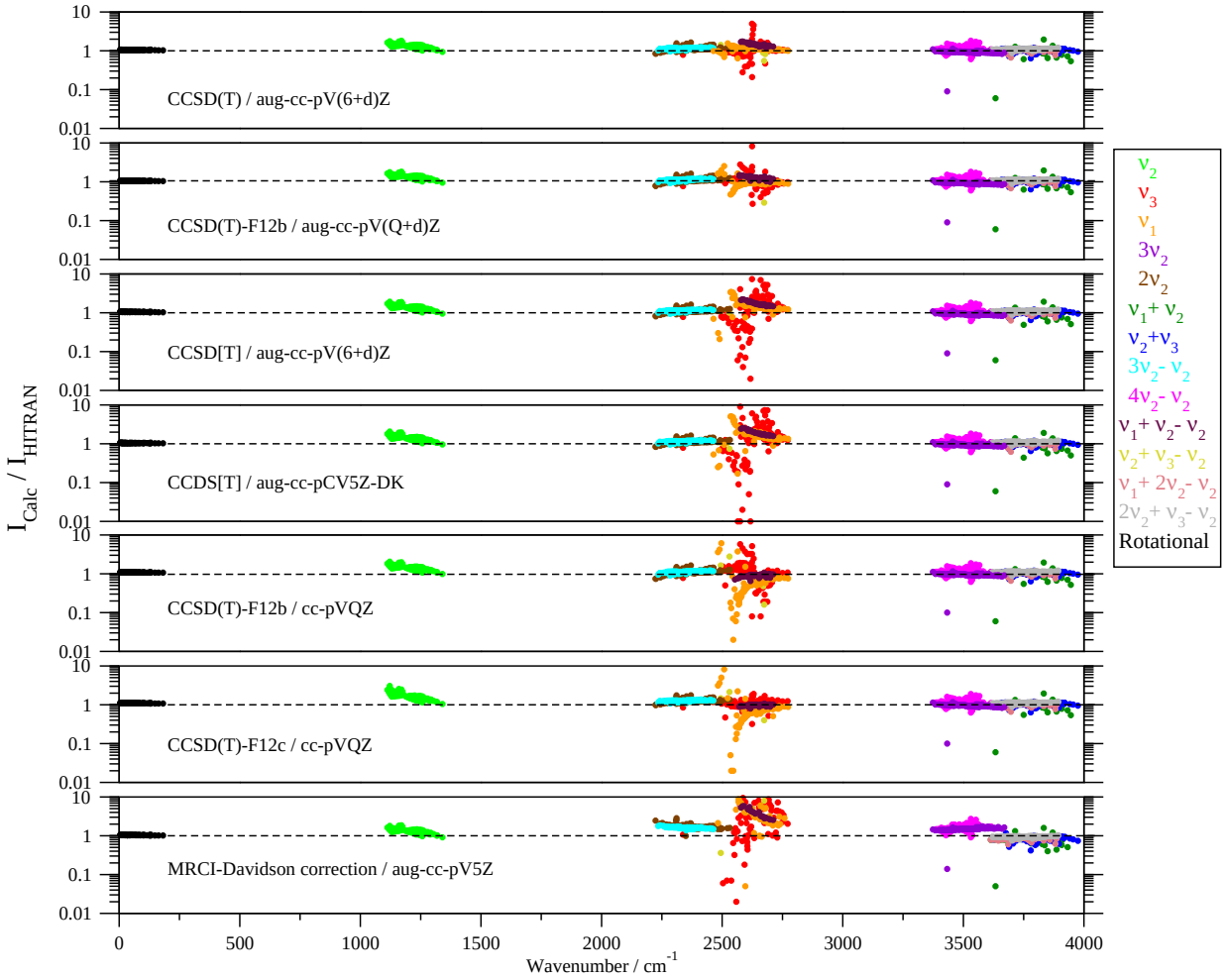

Figure 4.17: Intensity ratios calculated for different bands using different dipole moment surfaces (with corrections).

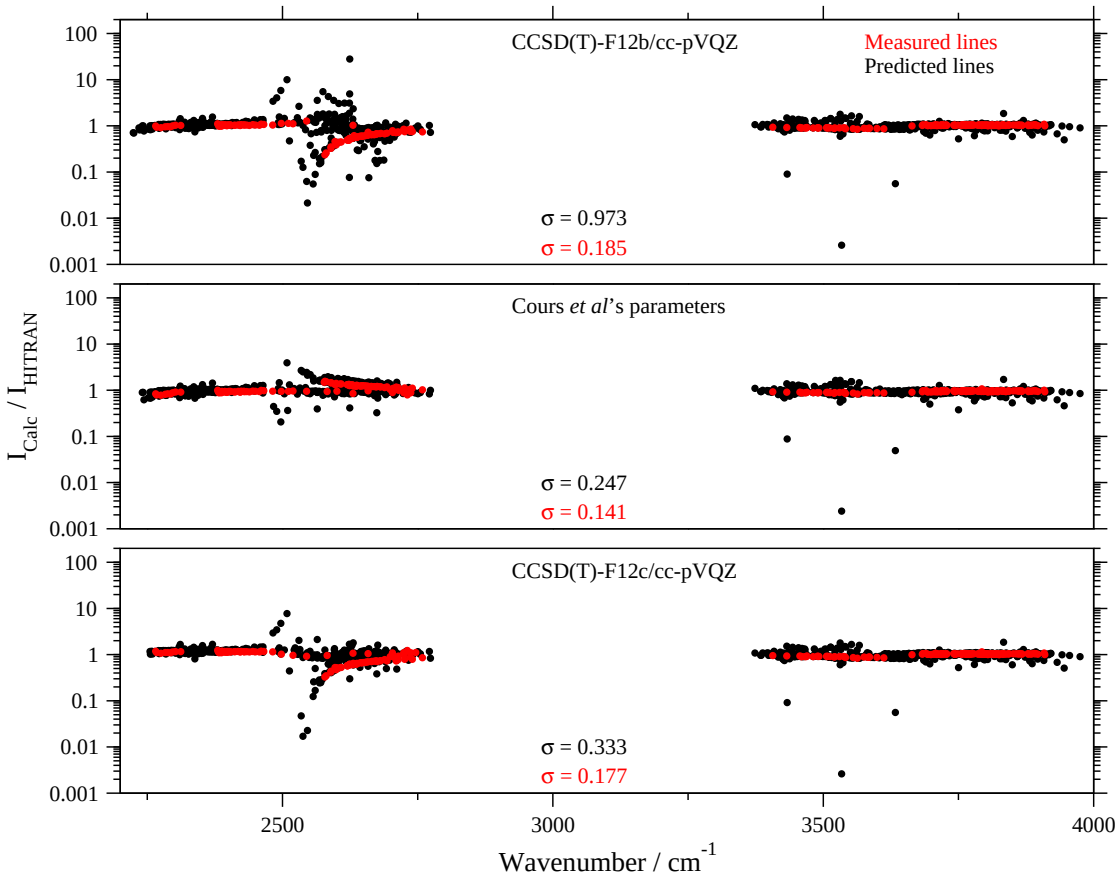

Figure 4.18: Errors in intensities for the predicted and measured lines using various dipole moment surfaces; our surfaces all include relativistic and core corrections. The standard deviation, σ, is given for the intensity ratios: upper value is for measured lines only, lower value is for predicted lines only.

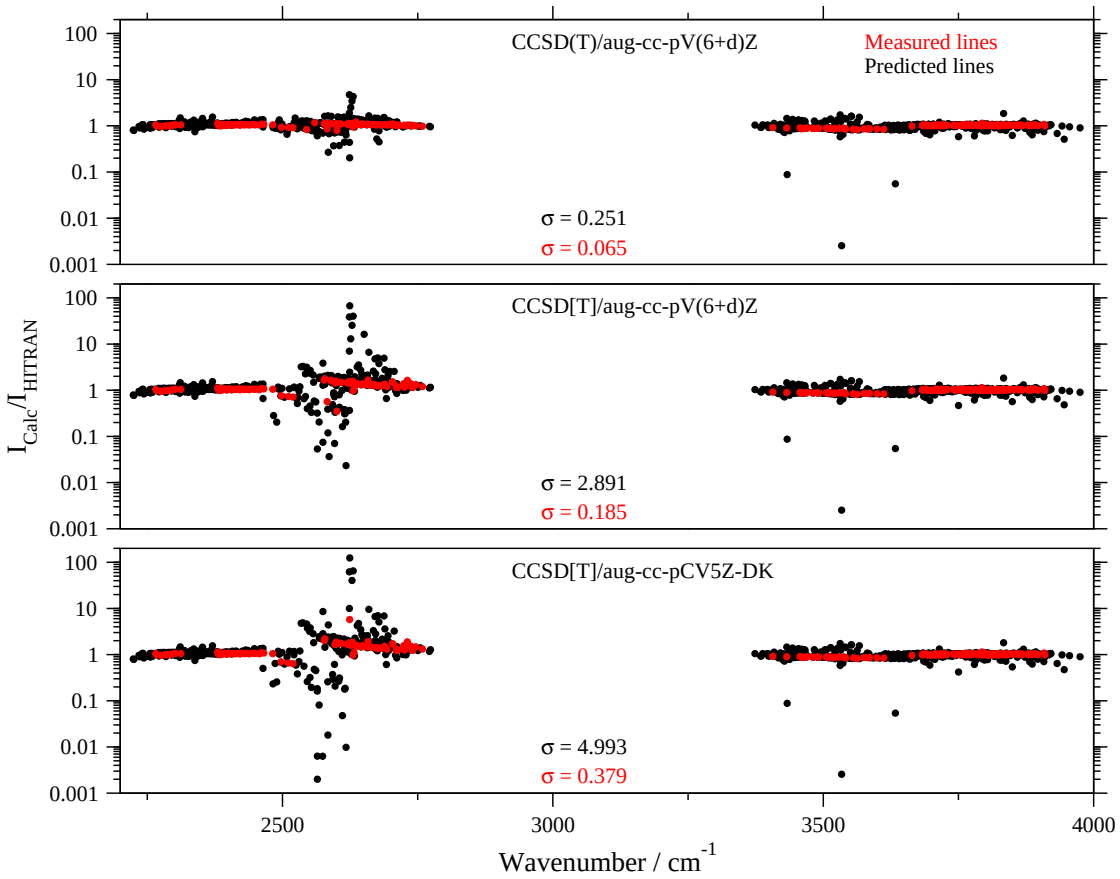

Figure 4.19: Errors in intensities for the predicted and measured lines using various dipole moment surfaces; our surfaces all include relativistic and core corrections. The standard deviation, σ, is given for the intensity ratios: upper value is for measured lines only, lower value is for predicted lines only.

Table 4.5: Samples for hot and combination band $H_2{}^{32}S$ lines with large differences in transition intensities between our calculations and HITRAN 2008 [Rothman et al. [2009]]. Columns give transition wavenumber, ν in cm^{-1} and intensities, I in $cm^{-1}/(molecule \times cm^{-2})$ (powers of ten in parentheses); Ab is for $H_2{}^{32}S$ abundance = 0.95, calculation A is CCSD[T]/agu-cc-pCV5Z-DK with corrections and B is CCSD(T)/agu-cc-pV(6+d)Z after adding corrections (ALYT2013).

HITRAN [Rothman et al. [2009]]			Transition		Calculations (this work)				
ν	$I = I_C/Ab$	Uncertainty Range	$v_1'v_2'v_3' - v_1''v_2''v_3''$	$J'_{K_a,K_c} - J''_{K_a,K_c}$	ν	I_A	I_B	I_A/I	I_B/I
3750.02	5.63(-26)	$\geq 2\%$ and $< 5\%$	1 1 0 - 0 0 0	$3_{3,0} - 4_{2,3}$	3750.03	2.36(-26)	1.46(-26)	0.42	0.58
3945.54	2.85(-26)	$\geq 2\%$ and $< 5\%$	1 1 0 - 0 0 0	$5_{4,1} - 4_{1,4}$	3945.58	1.35(-26)	3.27(-26)	0.47	0.51
3531.25	1.41(-25)	$\geq 5\%$ and $< 10\%$	0 4 0 - 0 1 0	$5_{0,5} - 4_{1,4}$	3531.21	8.23(-26)	8.18(-26)	0.58	0.58
3531.26	4.73(-26)	$\geq 5\%$ and $< 10\%$	0 4 0 - 0 1 0	$5_{1,5} - 4_{0,4}$	3531.21	8.23(-26)	8.18(-26)	1.74	1.73
3551.69	8.07(-26)	$\geq 5\%$ and $< 10\%$	0 4 0 - 0 1 0	$5_{1,4} - 4_{2,3}$	3551.65	1.32(-25)	1.31(-25)	1.63	1.62
3552.14	2.74(-26)	$\geq 5\%$ and $< 10\%$	0 4 0 - 0 1 0	$5_{2,4} - 4_{1,3}$	3552.11	4.44(-26)	4.40(-26)	1.62	1.61
3566.65	3.71(-26)	$\geq 5\%$ and $< 10\%$	0 4 0 - 0 1 0	$5_{2,3} - 4_{3,2}$	3566.61	5.76(-26)	5.72(-26)	1.55	1.54

the transition intensities to the calculated wavefunctions, we tested our intensities using a different PES, where a new *ab initio* PES was constructed using CCSD(T)/aug-cc-pV(6+d)Z with the core and relativistic corrections. using this PES, new eigenvalues and wavefunctions were obtained and used in transition intensities calculations together with ALYT2013 DMS. Fig. 4.20 shows that apart from very weak lines, our transition intensities are not sensitive to the calculated wavefunctions. Besides, these transitions have large differences in their positions comparing to the other transitions within the same bands, see Table 4.5 and Fig. 4.21 for a comparison. Table 4.6 presents a list of the most suspicious lines in HITRAN 2008 with $J \leq 5$. These lines all come originally from the publication by Brown et al. [1998].

To summarise, among all surfaces tested, the ALYT2013 DMS (constructed using CCSD(T)/aug-cc-pV(6+d)Z method with core and the relativistic corrections) gave the best transition intensities. The standard deviations of $(I_{Calc.}/I_{HITRAN})$ for lines involving J up to 5 are: 0.7 % for the rotational band, 16.8 % for the ν_2 band and 22.5 % for all the other bands. But for the measured lines the standard deviation is 6.5 %, while for the predicted lines it is 25 %. The standard deviations using Cours *et al.*'s surface are: 0.7 % for the rotational band, 30.1 % for the ν_2 band and 22.9 % for all the other bands. But for the measured lines the standard deviation is 14.1 %, while for the predicted lines it is 24.7 %.

These results suggest that the predictions are considerably less accurate than

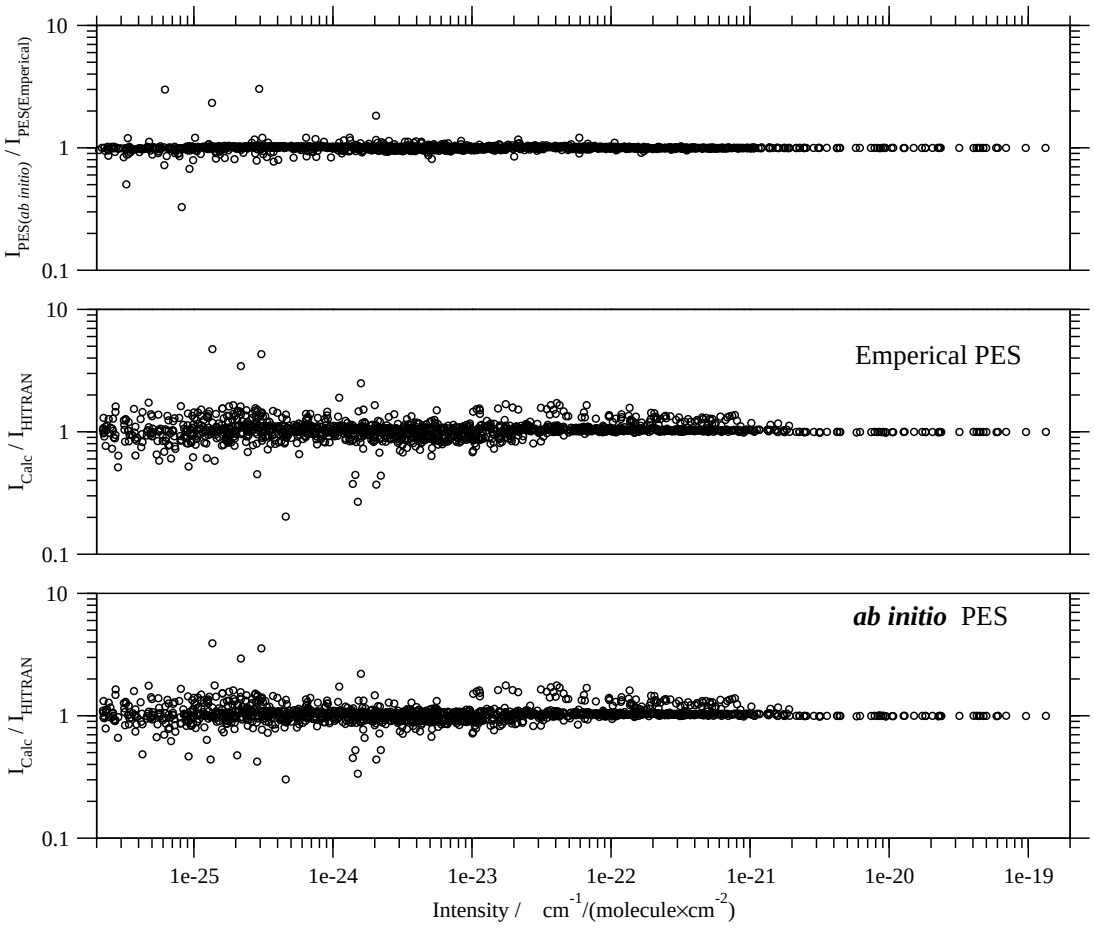

Figure 4.20: Results of the test of the lines transitions intensities sensitivity to the calculated wavefunctions.

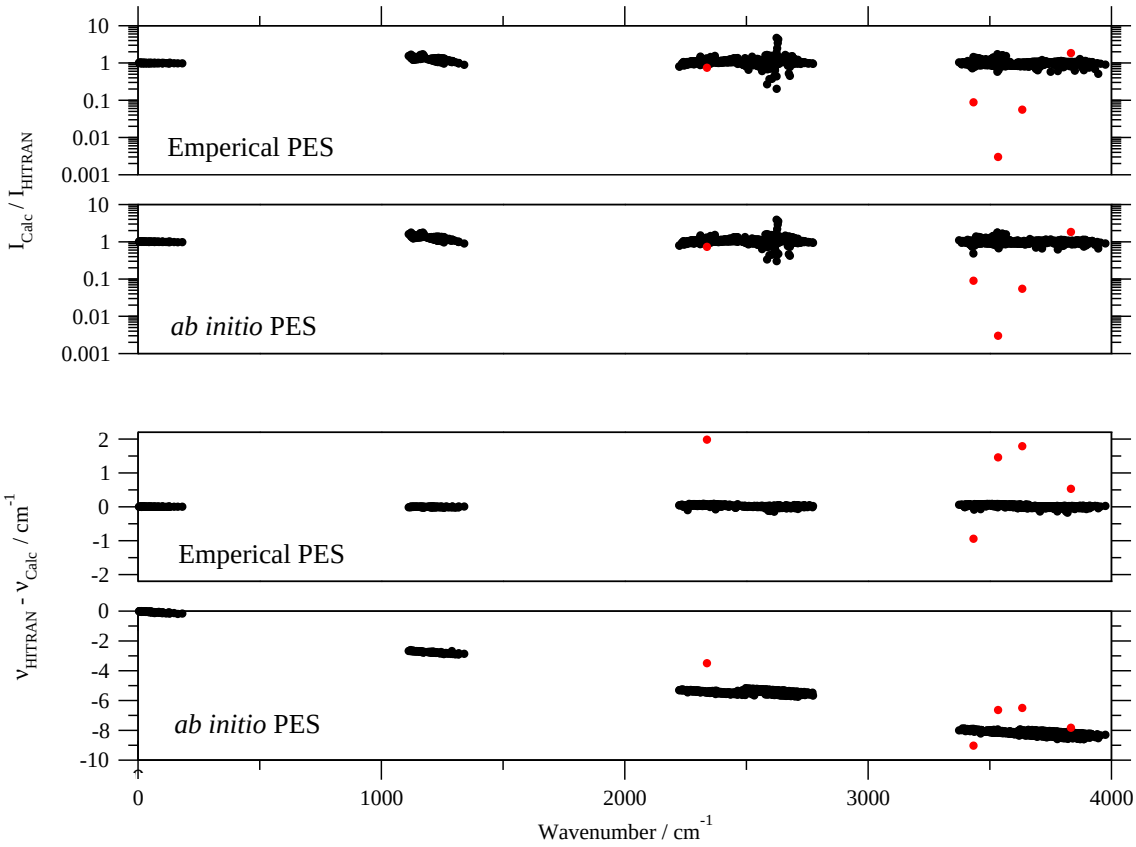

Figure 4.21: Lines in HITRAN 2008 with problems are given in red.

Table 4.6: Problematic $H_2{}^{32}S$ transitions in HITRAN 2008 [Rothman et al. [2009]]. Columns give transition wavenumber, ν in cm^{-1} and intensities, I in $cm^{-1}/(molecule \times cm^{-2})$ (powers of ten in parenthesis); calculation are performed using ALYT2013.

		HITRAN		Calculated			
$v_1^{'}v_2^{'}v_3^{'} - v_1^{''}v_2^{''}v_3^{''}$	$J^{'}_{K_a,K_c} - J^{''}_{K_a,K_c}$	ν	I	ν	I	$\Delta\nu$	I_{Calc}/I_{HITRAN}
0 0 1 - 0 0 0	$4_{1,3} - 5_{5,0}$	2337.94	5.58(-25)	2335.96	4.16(-25)	1.99	0.745
0 3 0 - 0 0 0	$3_{3,0} - 4_{4,1}$	3433.15	1.35(-23)	3434.09	1.19(-24)	-0.95	0.088
0 3 0 - 0 0 0	$3_{0,3} - 2_{1,2}$	3533.91	1.54(-23)	3532.45	3.90(-26)	1.46	0.003
1 1 0 - 0 0 0	$4_{0,4} - 5_{3,3}$	3633.33	3.43(-24)	3631.54	1.91(-25)	1.79	0.056
1 1 0 - 0 0 0	$4_{3,2} - 3_{2,1}$	3833.31	3.73(-22)	3832.78	6.89(-22)	0.53	1.850

the actual measurements in HITRAN 2008 for H_2S. Our results represent a significant improvement over calculations by Cours et al. [2000] which reproduces the rotational intensities with the same accuracy as the ALYT2013 DMS but gives a larger ($\sim$2 times) errors for the intensities in the ν_2 band as well as for the measured lines in the other bands. Fig. 4.22 shows some cuts for ALYT2013 DMS, while Fig. 4.23 shows the contour plot for the differences between ALYT2013 DMS and Cours *et al.*'s DMS.

A plot for the *ab initio* dipole moment points in terms of the energy versus the molecular geometries (bond lengths r_1 and r_2 and bond angle θ) shows that our calculated DMS is not complete up to 10 000 cm^{-1}, see Fig. 4.24. So, more *ab initio* dipole moment points were added to the surface (the red points in the plot are the new data while the black points are the old data). This process should improve our DMS.

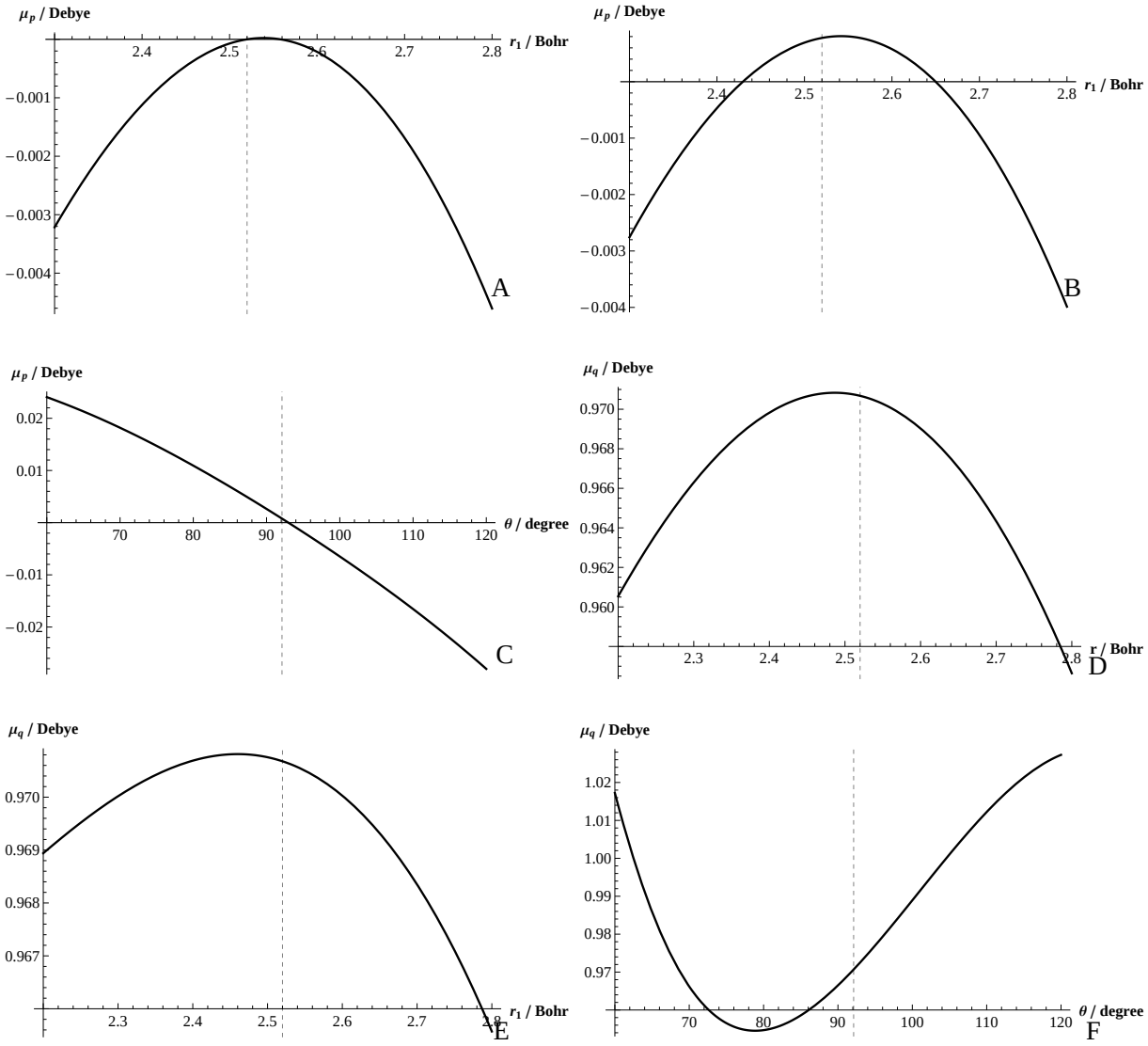

Figure 4.22: A) μ_p at $\theta = \theta_e = 92.11°$ and $r_2 = r_e = 2.52$ Bohr. B) μ_p at $\theta = \theta_e = 92.11°$ and $r_2 = 2.65$ Bohr. C) μ_p at $r_1 = r_e = 2.52$ Bohr and $r_1 = 2.65$ Bohr. D) μ_q at $\theta = \theta_e = 92.11°$ and $r_1 = r_2$. E) μ_q at $\theta = \theta_e = 92.11°$ and $r_2 = r_e = 2.52$ Bohr. F) μ_q at $r_1 = r_2 = r_e = 2.52$ Bohr.

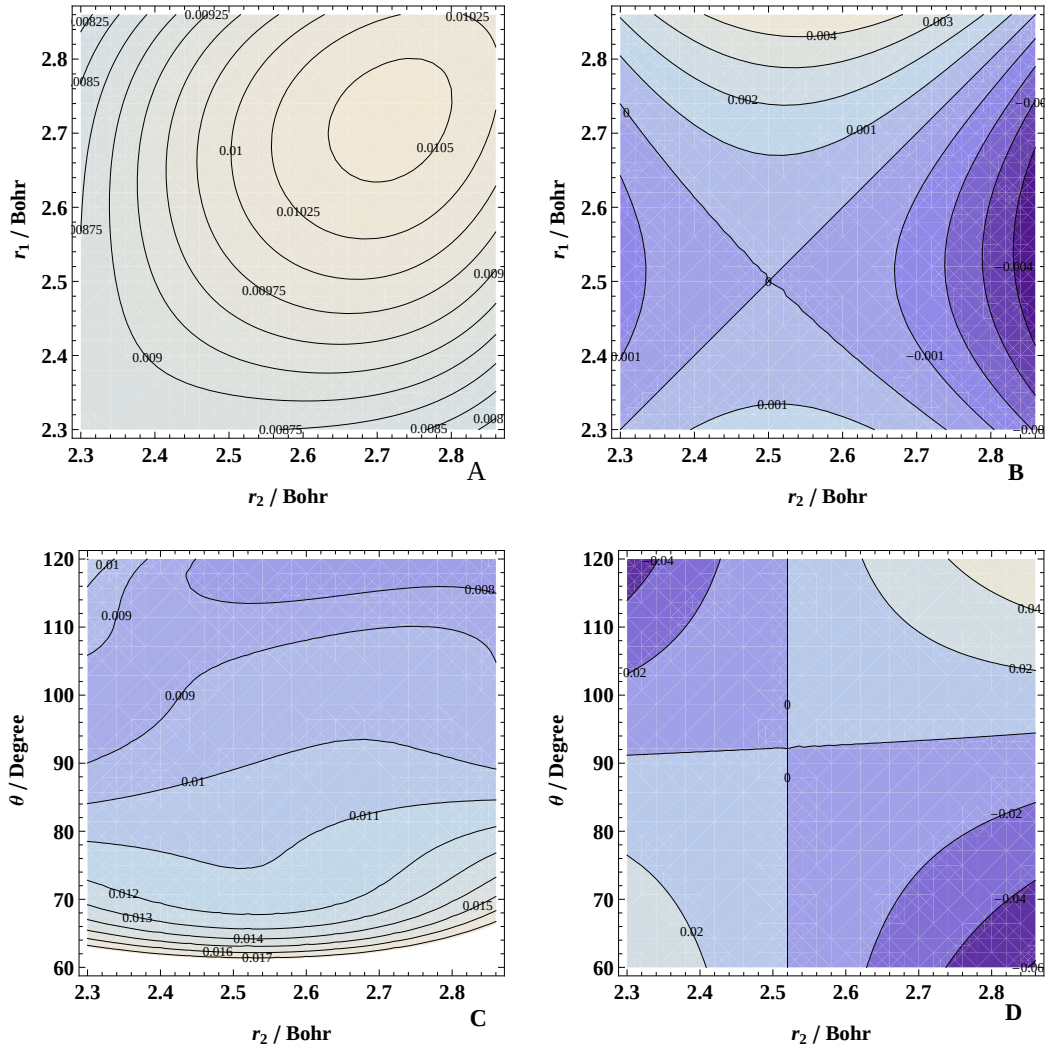

Figure 4.23: Contour plots of $\mathrm{DMS}_{Our\ best}$ – $\mathrm{DMS}_{Cours\ etal.}$ in Debye. A) μ_q at $\theta = \theta_e = 92.11°$. B) μ_p at $\theta = \theta_e = 92.11°$. C) μ_q at $\mathrm{r}_1 = \mathrm{r}_e = 2.52$ Bohr. D) μ_p at $\mathrm{r}_1 = \mathrm{r}_e = 2.52$ Bohr.

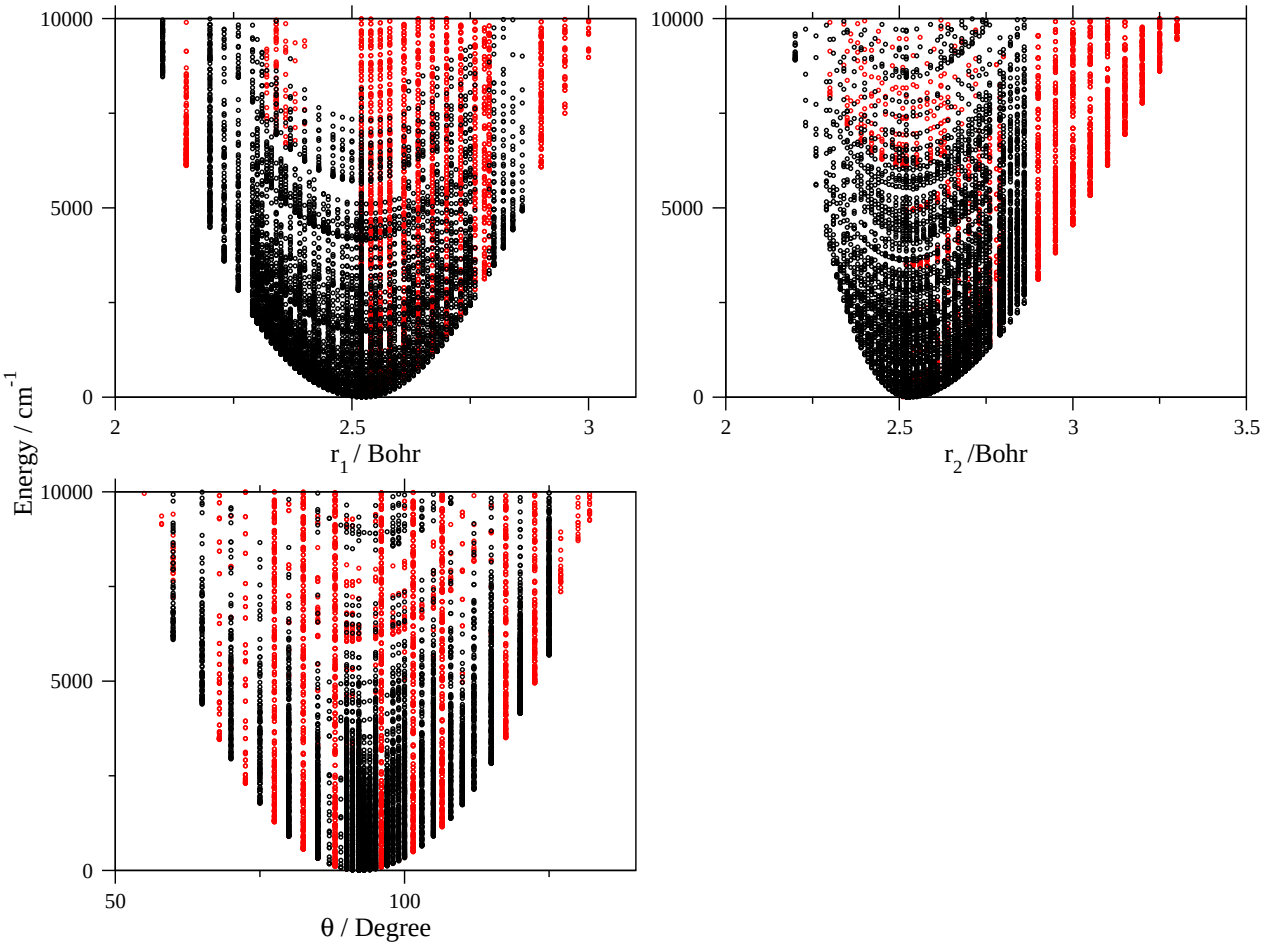

Figure 4.24: Total energy for the *ab initio* points of ALYT2013 surface versus bond lengths r_1 and r_2 and bond angle θ. Red points in this plot are the added *ab initio* points to fill the empty areas in ALYT2013 surface.

Chapter 5

Line list

5.1 Introduction

Now all ingredients are ready for our final calculations of a line list. The parameters for Dvr3d were determined and tested for convergence in Chapter 3. Our best potential energy surface (PES-Y0125) showed reliable agreement when tested against experimental ro-vibrational energy levels up to 15 000 cm^{-1} and J up to 10, see Chapter 3. Also, our best dipole moment surface (ALYT2013) gave good results for the transition intensities when compared to 14 vibrational bands spanning the spectrum up to 4000 cm^{-1} for J up to 5. The intensity tests showed good agreements especially for the actual measured data, while some problems were pointed out with the predicted data, as discussed in Chapter 4.

In this chapter, our final line list is presented. This line list is calculated up to energy levels of value 20 000 cm^{-1} and spans J values up to 40. As will be shown in this chapter, we think our calculated line list is reliable in transition positions up to 9000 cm^{-1}. In the following sections, the calculation procedures are described. The accuracy of the calculated line list at room temperature is tested by comparison to the data available in the HITRAN 2008 [Rothman et al. [2005, 2009]] and IAO LMS Spectra [spectra.iao.ru] databases. The partition function values were calculated up to 2000 K and compared to the available values from different sources. Finally, the calculated line list at high temperatures is presented. Our calculated line list is referenced to as ATY2013.

5.2 Line list calculations

The calculations for the ATY2013 was performed using 16 processors on the machine Amun which are Intel(R) Xeon(R) CPU E7340 @ 2.40GHz, in three major steps.

In the first step, as mentioned in Chapter 2, every run for each J value was done twice using Dvr3drjz; one time for $q = 0$ (even symmetry) and another time for $q = 1$ (odd symmetry). Then for each symmetry, the calculations for the ro-vibrational energy levels were performed using Rotlev3z. As a result, four runs for each J value were performed. During these calculations, one should be very careful to use the right parameters in the input files for every J value, since the input files are not the same and depend on J value, see Tennyson et al. [1995]. Because of this, a FORTRAN program was written to do the following tasks:

1. prepare all the input files for Dvr3drjz and Rotlev3z up to certain J,
2. run Dvr3drjz calculations up to certain J, and copy the vibrational wavefunctions output file (fort.26) to another name so we do not overwrite the file during the next run, and
3. run Rotlev3z up to certain J, then copy the transformed eigenvector with even parity output file (fort.8) and the transformed eigenvector with odd parity output file (fort.9) to other names for the reason mentioned in the previous point.

In the second step, another program was written to do the following tasks:

1. prepare four different input files for the Dipole3 calculations for every allowed transition for each J value, and
2. run Dipole3 after copying the fort.8 and fort.9 files correctly to fort.11 and fort.12 depending on the selection rules as summarised in Table 2.1 in Chapter 2. In order to speed up the calculation we do not compute transitions for which the lowest energy level is higher than a certain threshold (the energy threshold in our case is 10 000cm^{-1}); such transitions will

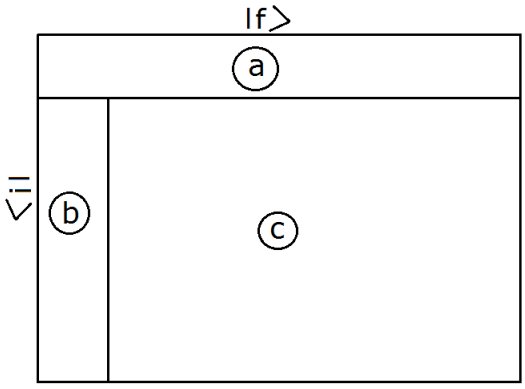

Figure 5.1: Sketch for illustrating the two steps for calculating the transitions using DIPOLE3 module, where $|i\rangle$ and $|f\rangle$ are the initial and the final wavefunctions of the transition.

result in very small intensities due to the $e^{-E_{\text{low}}/kT}$ Boltzmann factor in formula 2.33. DIPOLE3 provides the option for computing transition intensities in two steps using two different input files for the same transition, where every input file specify the number of the bra and ket eigenfunctions to be considered and the number of the bra or ket to be skipped (bra and ket are the wavefunctions of the stats where the transition take place). As an example, for the matrix sketch illustrated in Fig. 5.1, one of the input files for DIPOLE3 will calculate block a, while the second input files will calculate block b, and all the transitions in the block c are skipped.

The last step in the line list calculations is to run the module SPECTRA. In this step, a line list for the molecule under study can be generated, Table 5.1 is an extract from the calculated H_2S line list log. In the input file for SPECTRA, one should specify the temperature and the partition function value (Q) at this temperature, along with some other parameters.

5.2.1 Room temperature line list accuracy

The accuracy of the calculated spectrum can be checked by comparing the transition positions and intensities with their counterparts in the literature and the databases. The only available experimental data for H_2S spectrum is at room temperature ($T = 296$ K), so we judge the accuracy of our calculations using the

Table 5.1: Extract from the ATY2013 log. ipar is for *para*/*ortho* with 0/1, J is the rotational quantum number, P is the parity with 0 (even) and 1 (odd), I is energy levels counting number for given J and symmetry block, E is the ro-vibrational energy level in cm^{-1}, S(f-i) is the line strength in D^2, $I(\nu)$ is the transition intensity in $\mathrm{cm}^{-1}/(\mathrm{molecule}\times\mathrm{cm}^{-2})$, and A(if) is the Einstein A-coefficient in s^{-1}.

ipar	J'	P'	I'	J''	P''	I''	E'	E''	ν	S(f-i)	Absolute $I(\nu)$	Relative $I(\nu)$	A(if)
1	3	0	1	2	0	1	71.424760	38.297961	33.126799	0.22541023E+01	0.228817E-19	0.160961E+00	0.367127E-02
1	2	1	1	1	1	1	55.161460	19.375563	35.785896	0.14125348E+01	0.182304E-19	0.128241E+00	0.406038E-02
0	4	0	1	3	0	1	114.173085	71.465653	42.707432	0.32127932E+01	0.150351E-19	0.105764E+00	0.872072E-02
1	4	0	1	3	0	1	114.178495	71.424760	42.753735	0.32147216E+01	0.452343E-19	0.318200E+00	0.875437E-02
1	5	0	1	4	0	1	166.344887	114.178495	52.166393	0.41589721E+01	0.692371E-19	0.487047E+00	0.168332E-01
0	5	0	1	4	0	1	166.345606	114.173085	52.172521	0.41591920E+01	0.230860E-19	0.162398E+00	0.168401E-01
1	4	1	1	3	1	1	148.418470	95.056267	53.362204	0.22322630E+01	0.425542E-19	0.299347E+00	0.118197E-01
0	3	0	2	2	0	2	115.340038	58.368621	56.971416	0.20066523E+01	0.172267E-19	0.121181E+00	0.166244E-01
0	6	0	1	5	0	1	227.947026	166.345606	61.601421	0.51027005E+01	0.299784E-19	0.210882E+00	0.287760E-01
1	6	0	1	5	0	1	227.947126	166.344887	61.602239	0.51027286E+01	0.899381E-19	0.632667E+00	0.287773E-01
1	5	1	1	4	1	1	210.217731	148.418470	61.799260	0.31250511E+01	0.604528E-19	0.425254E+00	0.210289E-01

spectrum calculated at this temperature. But one should note this is not an easy task for two reasons. First, in order to compare a calculated transition with its counterpart in the literature and the databases, the full assignment for the transition for its quantum numbers (vibrational ($v_1v_2v_3$) and rotational (JK_aK_c)) is needed and this is not the case for the calculated transitions using Dvr3d, see Table 5.1, this also was discussed in Section 2.6. Second, our experience with this kind of comparisons showed that the agreement of our calculations with the experimentally measured transitions is much better than the predicted transitions, as shown in Chapter 4. As a result, during the comparison, we distinguish between the experimental and predicted transitions. However, this distinction is not available in databases in general (at least in HITRAN 2008, IAO LMS Spectra and GEISA), where one cannot know which transitions are fitted and which transitions are predicted. So, the experimental data needs to be collected from the original sources. In order to overcome these difficulties, different strategies were adopted for testing the accuracy of calculations in the different regions of the spectrum (see below).

As a preliminary comparison, Fig. 5.2 gives a general idea about the number of transitions available in HITRAN 2008 and IAO LMS Spectra databases compared to the number of transitions calculated in this work at room temperature. Also, Figs. 5.3 – 5.7 give a general idea about the accuracy of our calculated line list (ATY2013) compared to the data in these databases; more detailed comparisons are presented in the following subsections. Also, Fig. 5.8 shows the general envelope of our calculated spectrum compared to these databases. The following subsections present comprehensive comparisons with the data available in HITRAN 2008 and IAO LMS Spectra databases, respectively.

5.2.1.1 HITRAN 2008 database

The data available in HITRAN 2008 covers the frequency region up to 4000 cm^{-1} , J value up to 27 and cut off intensity of the order of 10^{-26} $cm^{-1}/(molecule \times cm^{-2})$ containing around 12 330 transitions. For the purpose of comparisons between our calculations and the databases, a FORTRAN program was written. But, because of the assignments problem mentioned above, this program had to match

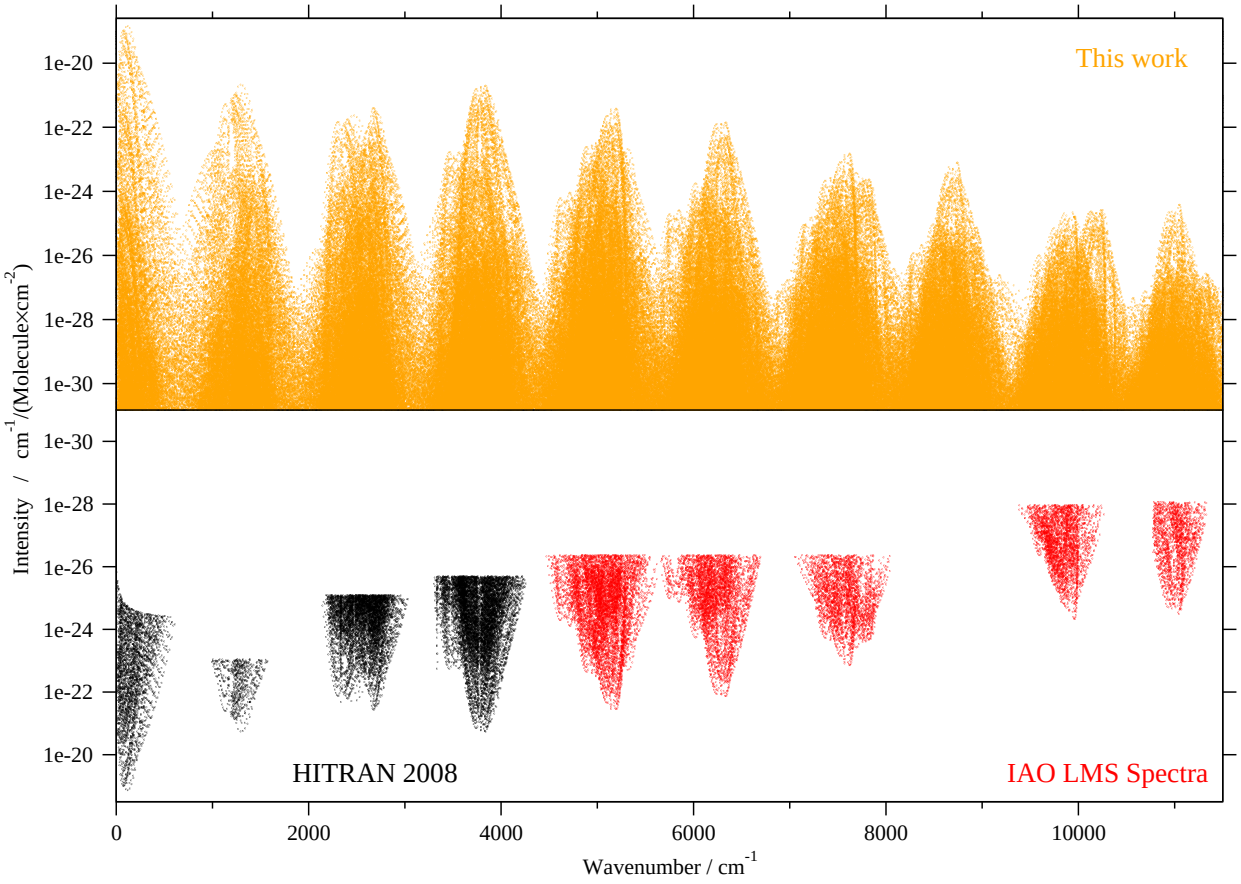

Figure 5.2: Our calculated spectrum compared to all available data in HITRAN 2008 [Rothman et al. [2005, 2009]] and IAO LMS Spectra [spectra.iao.ru] databases.

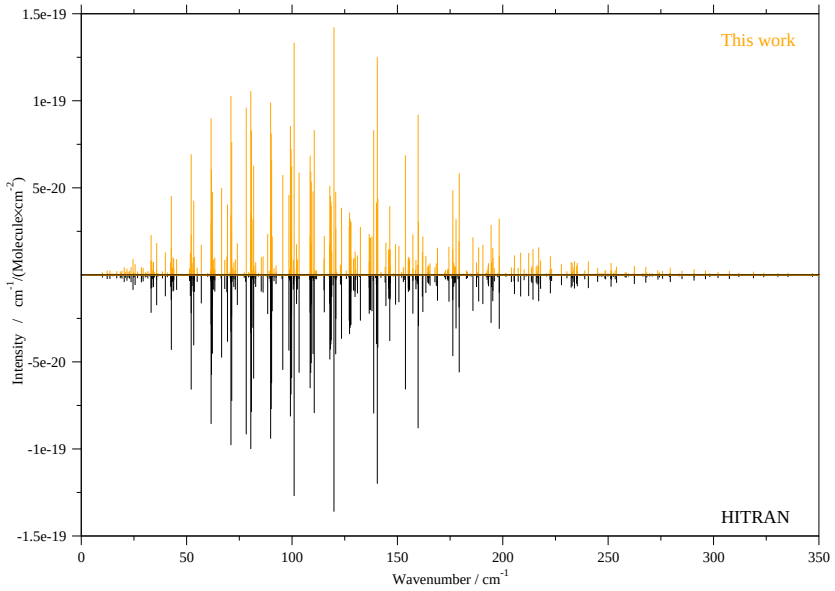

Figure 5.3: A calculated rotational band compared to that from the HITRAN 2008 database at $T = 296$ K.

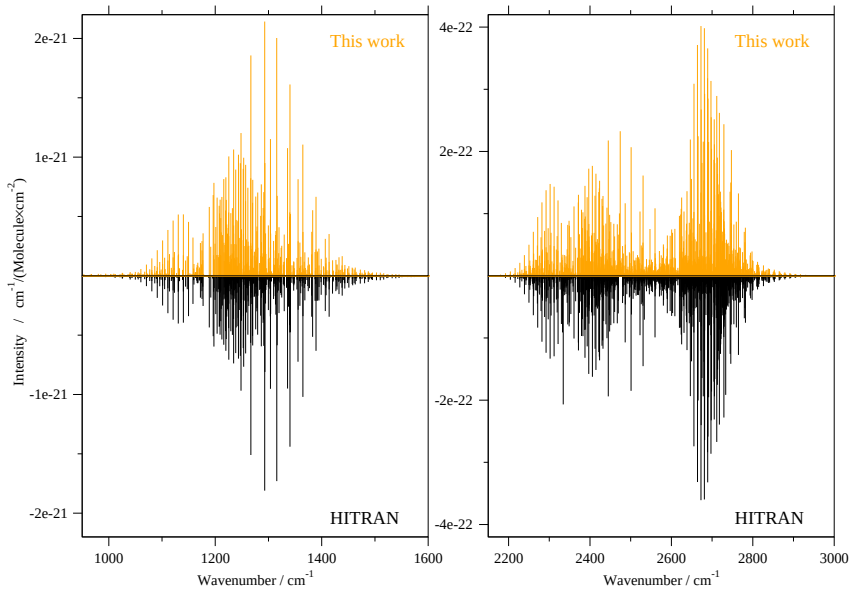

Figure 5.4: Calculated spectrum compared to that from the HITRAN 2008 database for the polyads 0.5 (left) and 1 (right) at $T = 296$ K.

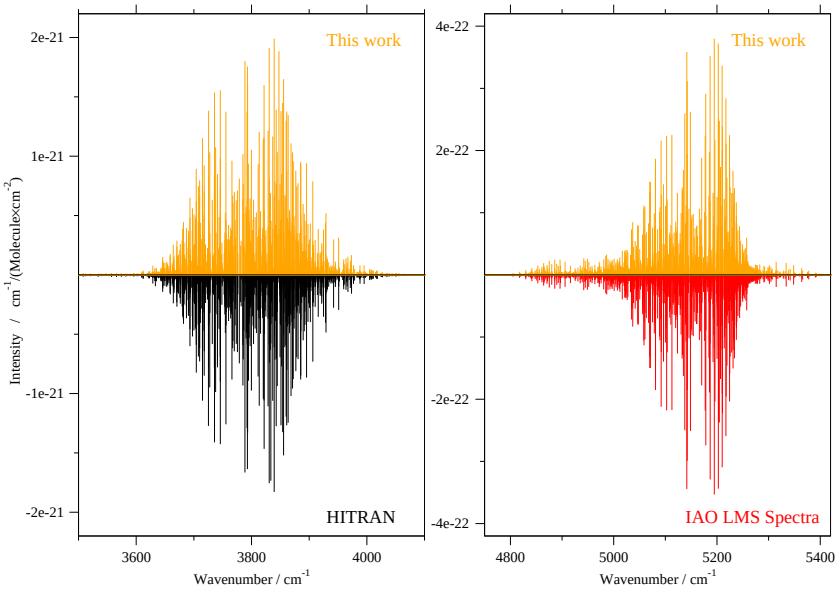

Figure 5.5: Calculated spectrum compared to that from the HITRAN 2008 database for the polyads 1.5 (left) and 2 (right) at $T = 296$ K.

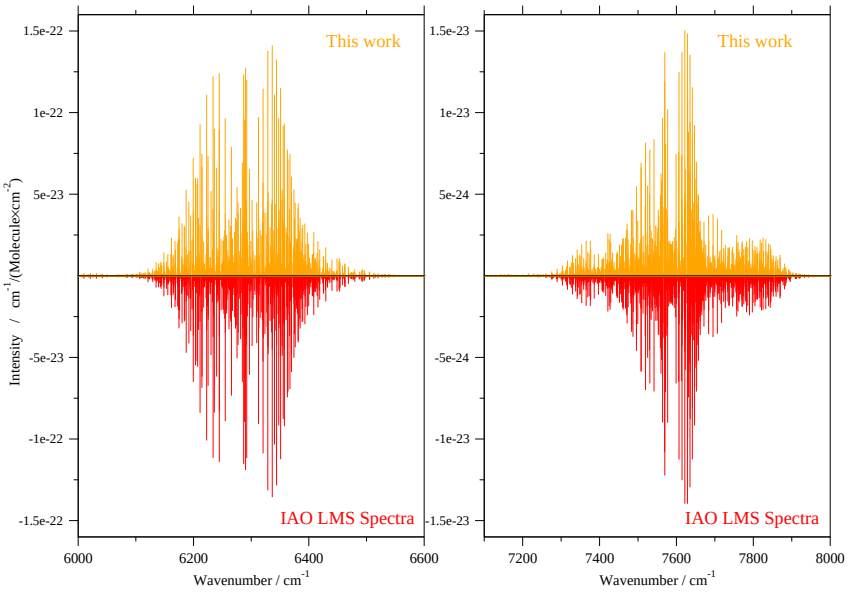

Figure 5.6: Calculated spectrum compared to that from the IAO LMS Spectra database for the polyads 2.5 (left) and 3 (right) at $T = 296$ K.

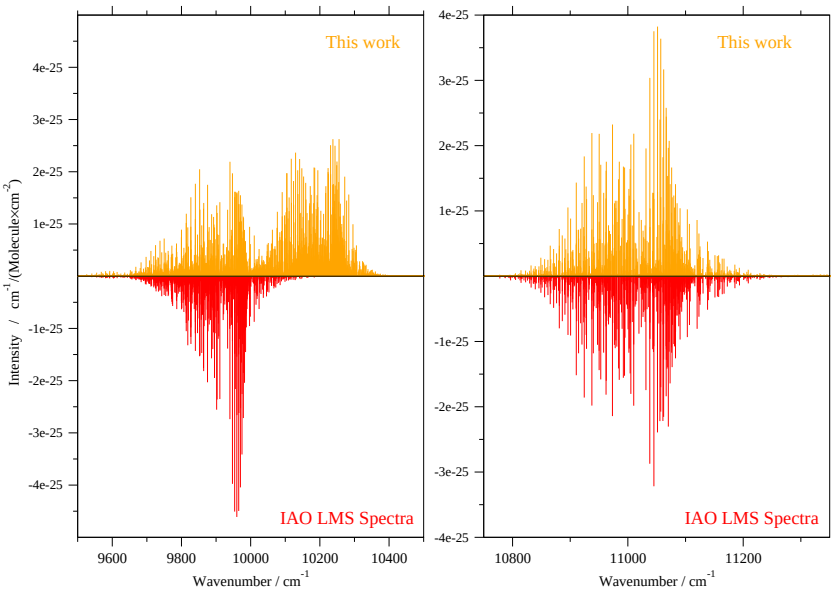

Figure 5.7: Calculated spectrum compared to that from the IAO LMS Spectra database for the polyads 4 (left) and 4.5 (right) at $T = 296$ K.

the transitions (in our calculations and the database) using J values as certain value for the matching. Then using the transition positions and intensities to select the best matches between our calculations and the database (within certain estimated interval of error for the transition positions). The matching results using this program were also checked manually for randomly selected transitions in different regions of the spectrum. Comparison with the published experimental transitions were performed manually. Figs. 5.9 and 5.10 show the errors of ATY2013 in this region of the spectrum when compared to this database for transition frequencies and intensities, respectively. A summary for the analysis of the comparison between our calculations and the data in this database for every polyad region is presented in Tables 5.2 and 5.3.

For the rotational region (polyad 0), the standard deviation for the absolute values of the errors of the calculated transition positions compared to the measured transition positions published by Flaud et al. [1983] up to $J = 22$ is of order 10^{-3} cm^{-1} with maximum absolute error of 0.08 cm^{-1}. In the case of the predicted transitions (these transitions span J values up to 27), the standard deviation is of order 10^{-2} cm^{-1} and the maximum absolute error in this case is

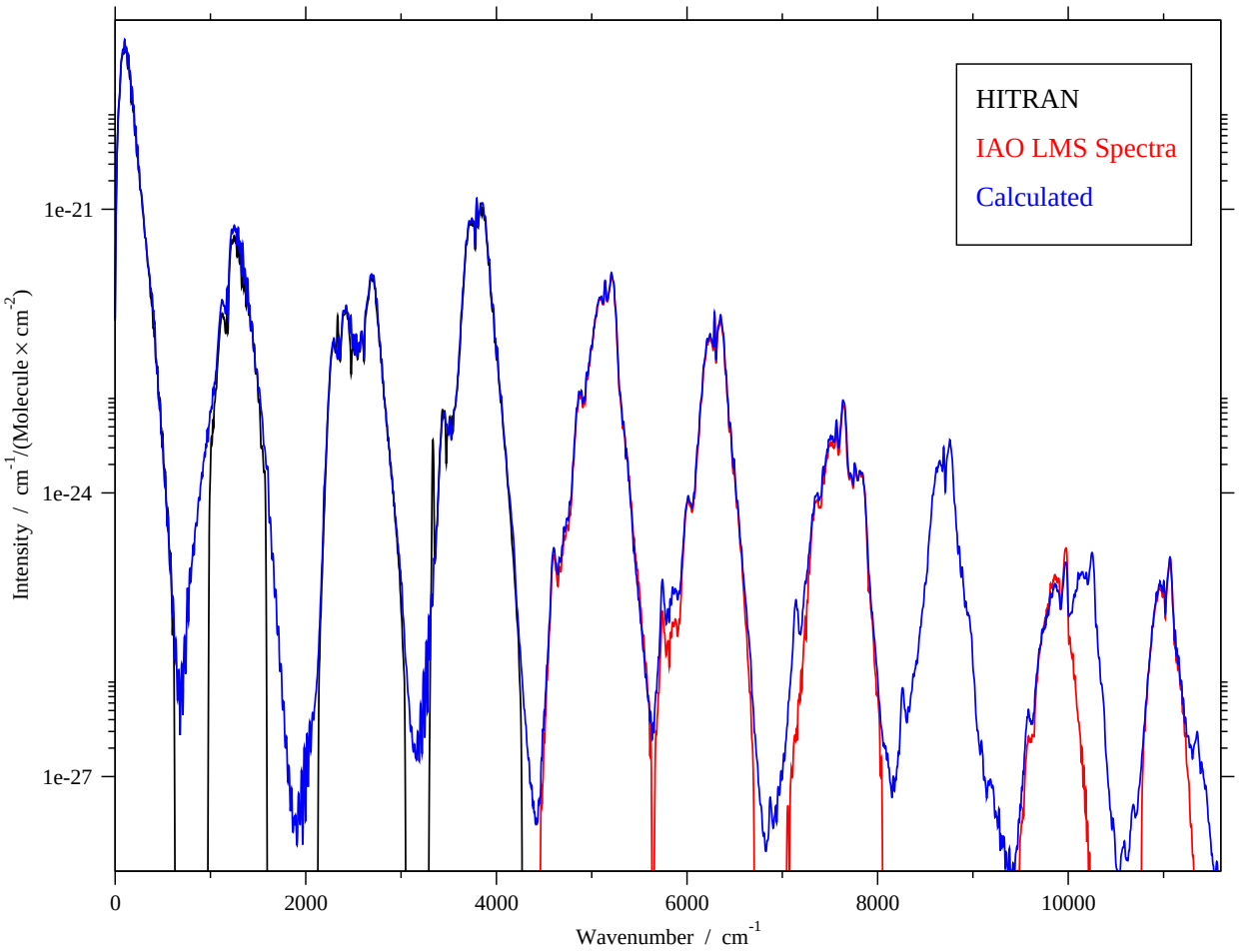

Figure 5.8: Spectrum envelope compared to that from the HITRAN 2008 and IAO LMS Spectra databases at $T = 296$ K.

0.27 cm^{-1}, where 17 out of 1121 transitions have absolute error values more than 0.1 cm^{-1} in their positions. In case of the transition intensities in this region of the spectrum, the intensity ratio between the calculated transitions and the measured transitions is in the range 0.92 – 1.05 (the error ∼5%). Fig. 5.10 shows how the intensities of the predicted transitions is increasing systematically comparing to our calculations beyond the region of the measured transitions, may be this reflects some how a systematic problem in the intensities of the predicted transitions in this region.

For polyad 0.5 region, as mentioned in Chapter 4, the original work by Goldman and Gillis [1984] could not be found. Therefore, our comparison does not include any distinction for the measured transitions in this region. The standard deviation for the absolute values of the errors in the transition positions is 0.03 cm^{-1}. 15 transitions out of 551 from this polyad have absolute error values in the range 0.1 – 0.3 cm^{-1}. On average, the calculated band is around 25% more intense than the band from the database. This is in agreement with our tests up to $J = 5$ for the calculated intensities explained in Chapter 4.

For polyad 1 and 1.5 regions, the comparison with the transitions published by Brown et al. [1998] showed some huge problems for some predicted transitions. As one can see from Figs. 5.9 and 5.10, our calculations agree very well with all measured transitions and the majority of the predicted transitions. But, 148 and 100 predicted transitions that belong to the polyad regions 1 and 1.5, respectively, showed huge disagreements with our calculations, unlike the majority of the transitions in these two regions (∼ 8400 measured and predicted transitions). We noticed that some of these transitions have disagreements with our calculations in their positions, some in their intensities, and some in both (positions and intensities). This also appeared in our tests of the dipole moments in Chapter 4. In the polyad region 1, 43 predicted transitions have absolute differences between our calculations and their positions in the range 0.3 – 4.1 cm^{-1}. The intensity ratios ($I_{Calc.}/I_{HITRAN}$) for 68 transitions are in the ranges 0.001 – 0.5 and 2 – 6. 37 transitions have problems in their positions and intensities as well. In polyad region 1.5, 25 predicted transitions have problems in their positions. The absolute differences between our calculations and their predicted positions are in the range 0.3 – 1.9 cm^{-1}. The biggest disagreements in the intensity were for 57

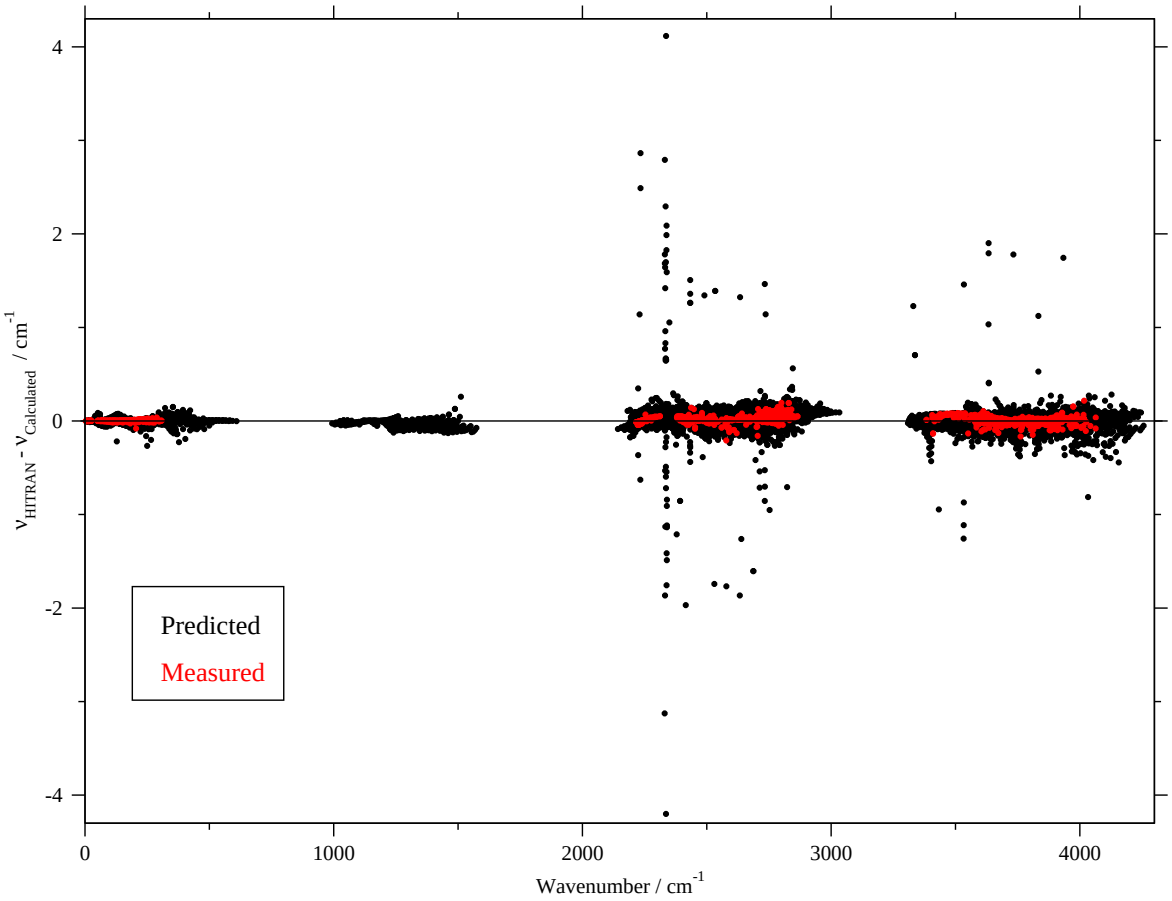

Figure 5.9: Errors in the line positions comparing to all HITRAN 2008's available data. The measured and predicted lines in this database are considered separately.

transitions with ratio ($I_{Calc.}/I_{HITRAN}$) in the range 0.000 1 – 0.5, two transitions of them with ratios 2.3 and 3.6. 17 transitions have problems both with their positions and intensities. All these lines with their quantum numbers are presented in tables in Appendix B. The analysis results in Table 5.3 does not include these lines in these two polyad regions.

5.2.1.2 IAO LMS Spectra database

This database contains 21 893 transitions spanning J values up to 20 with cut off intensity of the order 10^{-29} cm^{-1}/(molecule×cm^{-2}) in the spectral range 4400 – 11 300 cm^{-1}.

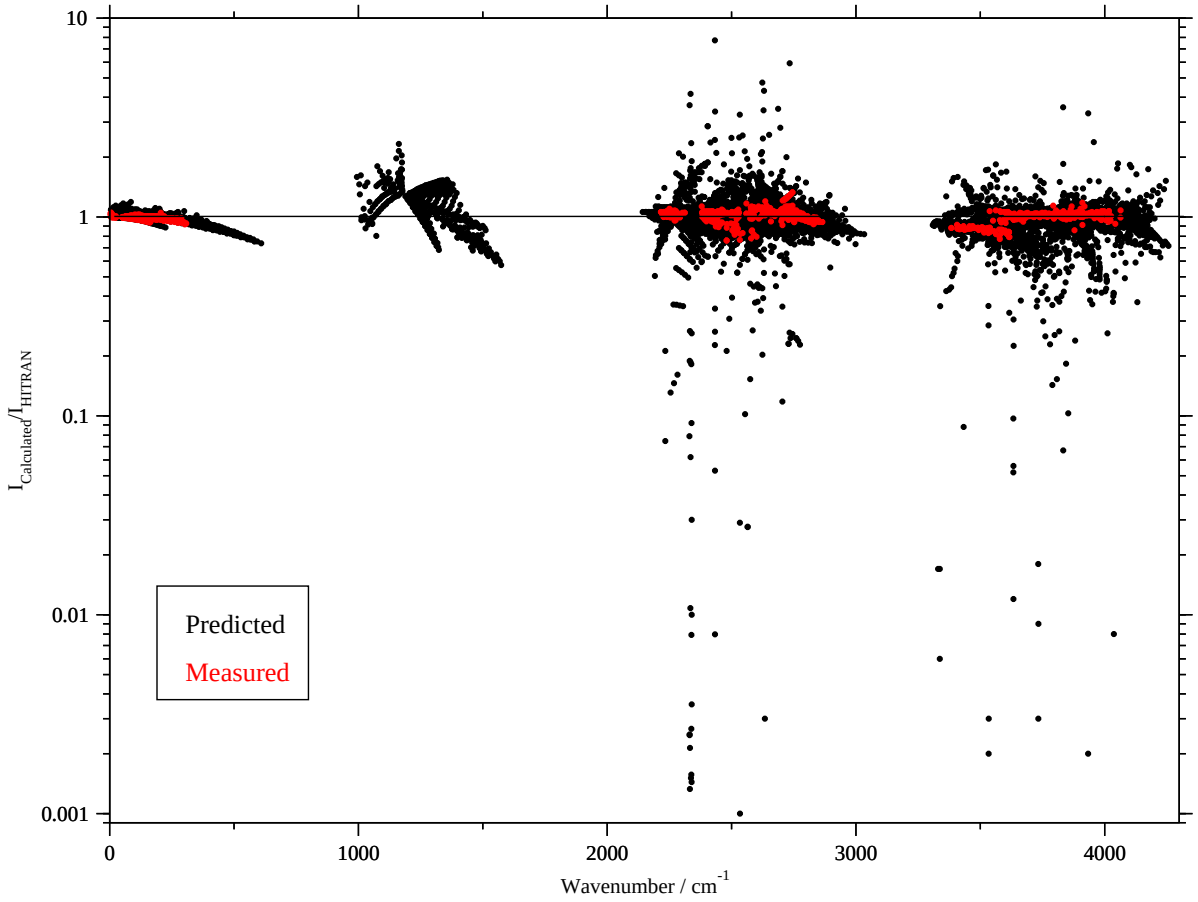

Figure 5.10: Errors in the transition intensities comparing to all HITRAN 2008's available data. The measured and predicted lines in this database are considered separately.

Table 5.2: Comparison between the calculated transitions in this thesis and the data available in HITRAN 2008 for the polyad regions 0 and 0.5. σ is the standard deviation. The average error, σ, maximum error and minimum error are in cm^{-1} in case of the frequency comparisons, and in $cm^{-1}/(molecule \times cm^{-2})$ in case of the intensity comparisons, (powers of ten in parenthesis). Note: the frequency errors are absolute errors.

	Frequency				Intensity			
Polyad			Measured	Predicted			Measured	Predicted
0	J range		1 – 22	2 – 27				
	Range		3 – 308	5 – 610	Range		3.4(-26) – 1.43(-19)	1.53(-26) – 9.91(-20)
	Average error		0.0042	0.0174	Average error		0.99	0.99
	σ		0.0068	0.0272	σ		0.02	0.07
	Max. error		0.0795	0.2656	Max. error		1.05	1.19
	Min. error		0.0001	0.0001	Min. error		0.92	0.74
	# lines with error	$< 0.001^a$	130	121	# lines with error	$< 0.8^b$	0	16
		$< 0.01^a$	363	690		$< 0.9^b$	0	133
		$< 0.1^a$	419	1104		$< 1.1^b$	419	1100
	Total # lines		419	1121		$< 1.5^b$	419	1121
0.5	J range			0 – 16				
	Range			994 – 1573	Range			9.58(-24) – 1.91(-21)
	Average error			0.0376	Average error			1.15
	σ			0.0312	σ			0.27
	Max. error			0.2587	Max. error			2.32
	Min. error			0.0001	Min. error			0.57
	# lines with error	$< 0.001^a$		12	# lines with error	$< 0.8^b$		59
		$< 0.01^a$		123		$< 0.9^b$		111
		$< 0.1^a$		528		$< 1.1^b$		245
	Total # lines			551		$< 1.5^b$		512

[a] $\nu_{Experimental} - \nu_{Calculated}$ in cm^{-1} .
[b] $(I_{Calculated}/I_{HITRAN})$.

Table 5.3: Comparison between the calculated transitions in this thesis and the data available in HITRAN 2008 for the polyad regions 1 and 1.5. σ is the standard deviation. The average error, σ, maximum error and minimum error are in cm^{-1} in case of the frequency comparisons, and in $cm^{-1}/(molecule \times cm^{-2})$ in case of the intensity comparisons, (powers of ten in parenthesis). Note: the frequency errors are absolute errors.

	Frequency				Intensity			
Polyad			Measured	Predicted			Measured	Predicted
1	J range		0 – 19	0 – 20				
	Range		2216 – 2864	2143 – 3034	Range		9.55(-26) – 2.99(-22)	8.49(-26) – 3.8(-22)
	Average error		0.0433	0.0624	Average error		1.02	1.02
	σ		0.0327	0.0452	σ		0.07	0.17
	Max. error		0.2080	0.2461	Max. error		1.33	1.96
	Min. error		0.0002	0.0000	Min. error		0.76	0.50
	# lines with error	$< 0.001^a$	6	25	# lines with error	$< 0.8^b$	5	163
		$< 0.01^a$	45	260		$< 0.9^b$	21	729
		$< 0.1^a$	514	2883		$< 1.1^b$	509	2769
	Total # lines		547	3525		$< 1.5^b$	547	3466
1.5	J range		0 – 16	0 – 20				
	Range		3384 – 4064	3309 – 4257	Range		2.86(-26) – 1.85(-21)	2.12(-26) – 1.54(-21)
	Average error		0.0337	0.0552	Average error		1.00	0.96
	σ		0.0289	0.0948	σ		0.10	0.18
	Max. error		0.2168	1.9016	Max. error		2.61	3.56
	Min. error		0.0000	0.0000	Min. error		0.24	0.00
	# lines with error	$< 0.001^a$	20	87	# lines with error	$< 0.8^b$	4	434
		$< 0.01^a$	94	656		$< 0.9^b$	76	967
		$< 0.1^a$	491	3352		$< 1.1^b$	497	3530
	Total # lines		503	3812		$< 1.5^b$	502	3784

[a] $\nu_{Experimental} - \nu_{Calculated}$ in cm^{-1} .
[b] $(I_{Calculated}/I_{HITRAN})$.

It is clear from Figs. 5.11 and 5.12 that our calculated spectrum loses accuracy in the polyad region 4 (around 10 000 cm^{-1}) and above. Besides, the comparison with the experimental transitions in the polyad region 3.5 could not be done because: (1) the experimental transitions in this region are not available in the IAO LMS Spectra database (nor any other databases as well), (2) the original publication [Brown et al. [2004]] contains derived experimental energy levels only (not transitions). So, our comparisons with this database cover the spectrum region up to 8000 cm^{-1} only.

Since the measured transitions in the region of the polyad numbers 2, 2.5 and 3 could not be collected (the publications contain only the energy levels [Brown et al. [1997, 2004]; Ulenikov et al. [2004, 2005]]), the comparison was performed without any distinction between the measured and predicted transitions. Our program could match around 11 000 transitions from 16 000 transitions available in the IAO LMS Spectra database (in the region 4400 – 8000 cm^{-1}). Table 5.4 summarises the results of the analysis. As one can see from Table 5.4 and Figs. 5.11 and 5.12, our calculations agrees very well with the transition positions where the maximum absolute error is around 0.25 cm^{-1} for all but 6 transitions. In case of the transition intensities, the ratio shows errors sometimes up to two orders of magnitudes. After adding more *ab initio* points to ALYT2013, the resulted improved surface should give better agreement for the transition intensities in the regions of the polyad numbers 2, 2.5 and 3 but not for other polyads.

Our calculated spectrum at room temperature contains around 5×10^5 transitions up to $J = 40$ with cut off intensity of the order 10^{-31} $cm^{-1}/(molecule \times cm^{-2})$ comparing to 2.8×10^4 experimentally available transitions up to 9000 cm^{-1}. This spectrum has a standard deviation of the absolute errors in the transition positions of about 0.066 cm^{-1} from an average of 0.060 cm^{-1}, where 82 % of the transitions have the absolute errors in their positions less than 0.1 cm^{-1}. The standard deviation of the ratios of the calculated intensities to the transition intensities available in the databases is 1.08 with an average ratio of 1.02, where 83 % of the transition intensities have errors within 20 %.

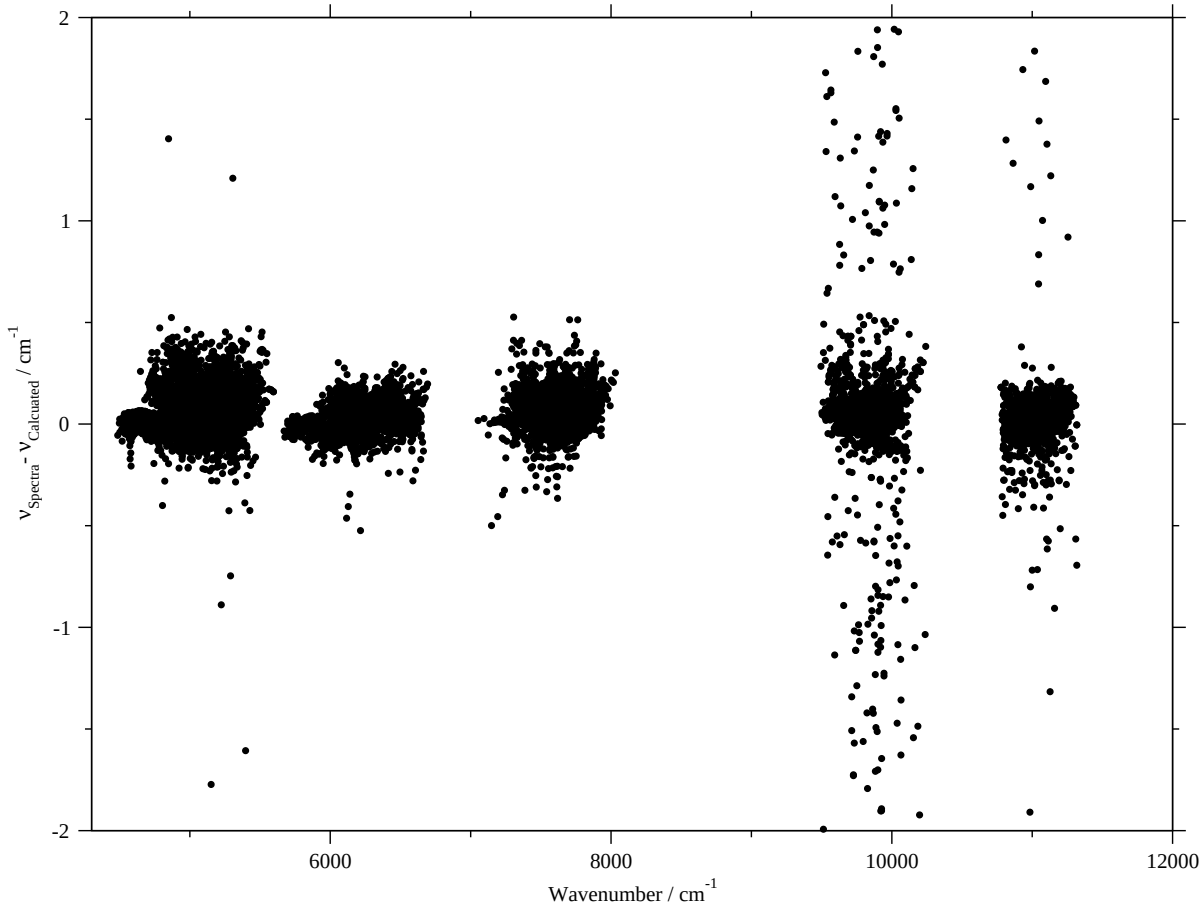

Figure 5.11: Errors in line positions comparing to all IAO LMS Spectra's available data.

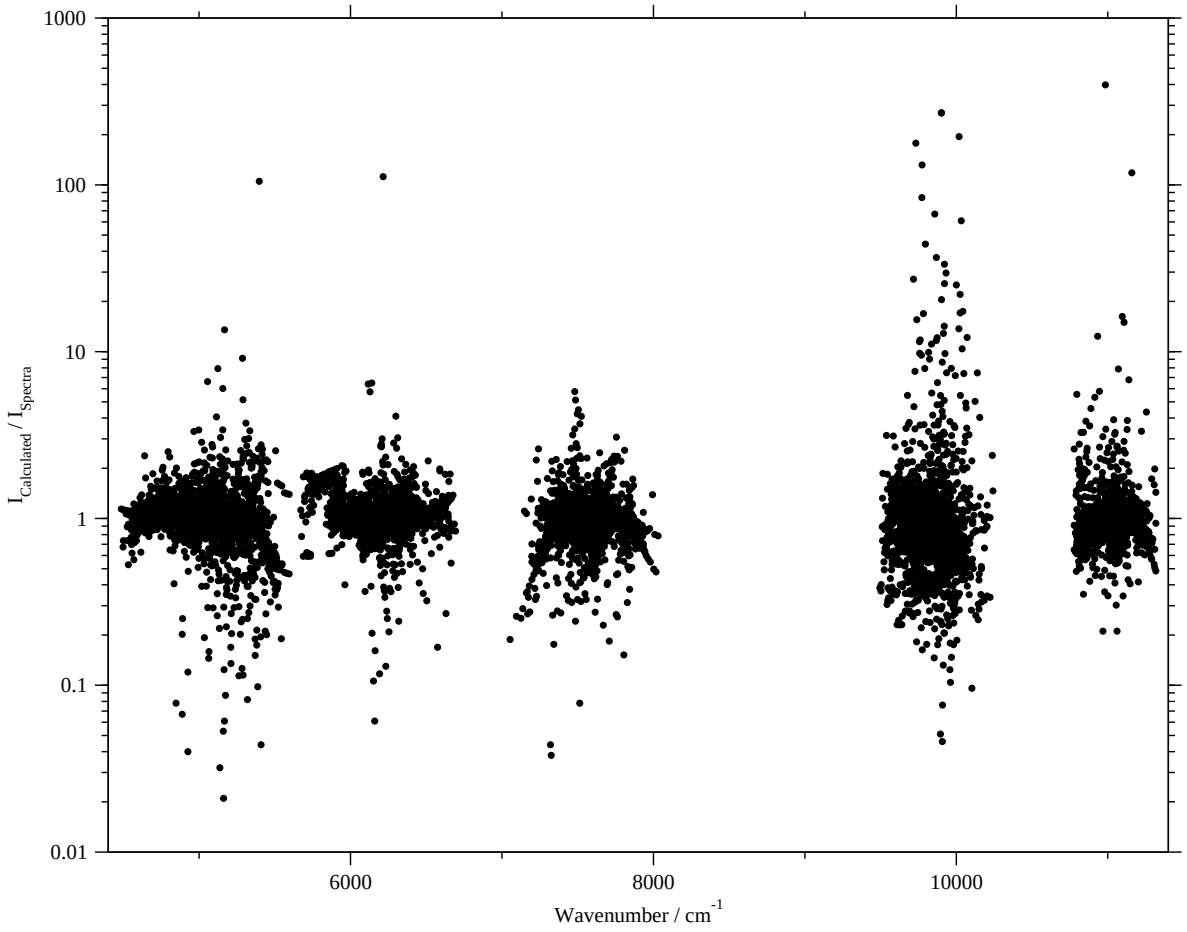

Figure 5.12: Errors in transition intensities comparing to all IAO LMS Spectra's available data.

Table 5.4: Comparison between the calculated transitions in this study and the data available in IAO LMS Spectra database for polyad regions 2, 2.5 and 3. σ is the standard deviation. The average error, σ, maximum error and minimum error are in cm^{-1} in case of the frequency comparisons, and in $cm^{-1}/(molecule \times cm^{-2})$ in case of the intensity comparisons, (powers of ten in parenthesis). Note: the frequency errors are absolute errors.

Frequency			Intensity		
J range		0 – 20			
Range		8031 – 4486	Range		4.47(-27)-3.63(-22)
Average error		0.0735	Average error		1.05
σ		0.0794	σ		1.50
Max. error		1.7730	Max. error		111.95
Min. error		0.0000	Min. error		0.02
# lines with error	$< 0.001^a$	116	# lines with error	$< 0.8^b$	1041
	$< 0.01^a$	1152		$< 0.9^b$	2135
	$< 0.1^a$	8101		$< 1.1^b$	8439
Total # lines		10758		$< 1.5^b$	10294

[a] $\nu_{Experimental} - \nu_{Calculated}$ in cm^{-1} .
[b] $(I_{Calculated}/I_{HITRAN})$.

5.3 Partition function

The partition function value (Q) of a molecule in the singlet electronic state at certain temperature (T) is given by

$$Q(T) = \sum_J \sum_i g_i(2J+1) exp\left(-\frac{c_2 E_i^{(J)}}{T}\right), \tag{5.1}$$

where g is the nuclear statistical weight which is 1/3 for *para*/*ortho* states for $H_2{}^{32}S$, $E_i^{(J)}$ is the ro-vibrational energy level for a certain J value, and c_2 is the second radiation constant. The summation in this equation should be performed for all ro-vibrational energy levels with all nuclear symmetry and all J values until the value Q converges. Fig. 5.13 shows how Q converges with J at different temperatures up to 2000 K. Table 5.5 presents Q values at different temperatures in comparison with the values from the HITRAN 2008, the JPL [Pickett et al. [1998]], and the CDMS databases and the values calculated as result from the experiment summarised in Chapter 6.

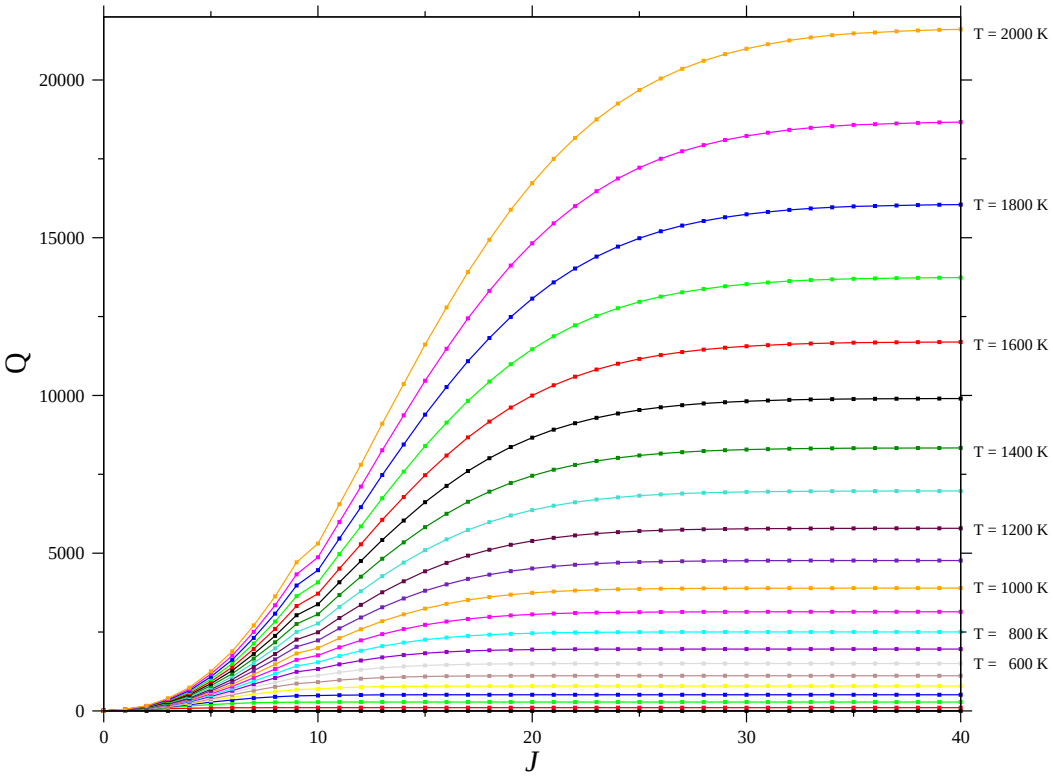

Figure 5.13: Partition functions convergence curves.

Table 5.5: Partition function values at different temperatures from different sources.

T	This work[1]	HITRAN 2008[2]	JPL[3]	CDMS[4]	This work[5]
2.725	1.007834			1.0077	
5.000	1.245873			1.2458	
9.375	2.910636		2.9106	2.9106	2.9106
18.750	8.699775		8.6996	8.6996	8.6996
37.500	23.86561		23.8654	23.8653	23.8654
75.000	65.52686	65.48540	65.5265	65.5265	65.5265
100.000	100.1494	99.97209			
150.000	182.5641	182.2696	182.7622	182.7622	182.7622
200.000	279.4633	279.6049			
225.000	332.5639	333.3219	334.5222	334.5222	334.5222
296.000	498.7866	503.07[a]			504.2091
300.000	508.8194	513.3829	514.4470	514.4498	514.4498
400.000	783.8200	797.6368			
500.000	1110.268	1136.460			
600.000	1497.257	1537.079			
700.000	1955.422	2009.062			
800.000	2496.703	2563.217			
900.000	3134.386	3211.929			
1000.000	3882.981	3968.802			
1100.000	4758.150	4848.387			
1200.000	5777.080	5866.361			
1300.000	6958.012	7039.470			
1400.000	8320.399	8385.471			
1500.000	9885.331	9923.019			
1600.000	11675.20	11672.66			
1700.000	13713.62	13655.08			
1800.000	16025.78	15893.10			
1900.000	18636.33	18409.06			
2000.000	21575.47	21229.28			

[1] Calculated using Eq. (5.1) and the variationally calculated ro-vibrational energy levels .
[2] As calculated using the HITRAN's FORTRAN programs for partition functions sums from the HITRAN 2008 compilation. The calculations using these programs consider the temperature range 70 – 3000 K.
[3] As published on the JPL's website.
[4] As published on the CDMS's website.
[5] Calculated using CALPGM program [Pickett [1991]] as a result of the experiment discussed in Chapter 6.
[a] From Šimečková et al. [2006]

5.4 Hot spectra

The ATY2013 line list contains 95 million lines which cover all transitions with $J \leq 40$ and a lower energy below 10 000 cm^{-1} and upper energy below 20 000 cm^{-1}. Fig. 5.14 shows the calculated spectra at different temperatures. This figure shows how the weak transitions at low temperatures become stronger at higher temperatures. The spectrum at 2000 K contains 36×10^6 transitions up to 9000 cm^{-1}, up to $J = 40$ with cut off intensity of order 10^{-31} $cm^{-1}/(molecule \times cm^{-2})$. Transition positions do no change at different temperatures unlike transition intensities which are temperature dependent due to the $e^{-E_{low}/kT}$ Boltzmann factor in formula 2.33.

No data could be found to compare our calculations with, neither experimental nor theoretical with temperature higher than the room temperature. This made our line list as the first available source of data for $H_2{}^{32}S$ spectrum at temperatures higher than the room temperature, thus, opening the door for probability of identifying $H_2{}^{32}S$ transitions in exoplanet and brown dwarfs atmospheres as well as the sun spots. Also, this line list can be used in the high temperature laboratory spectra analysis, such as the emission spectra described in Chapter 6.

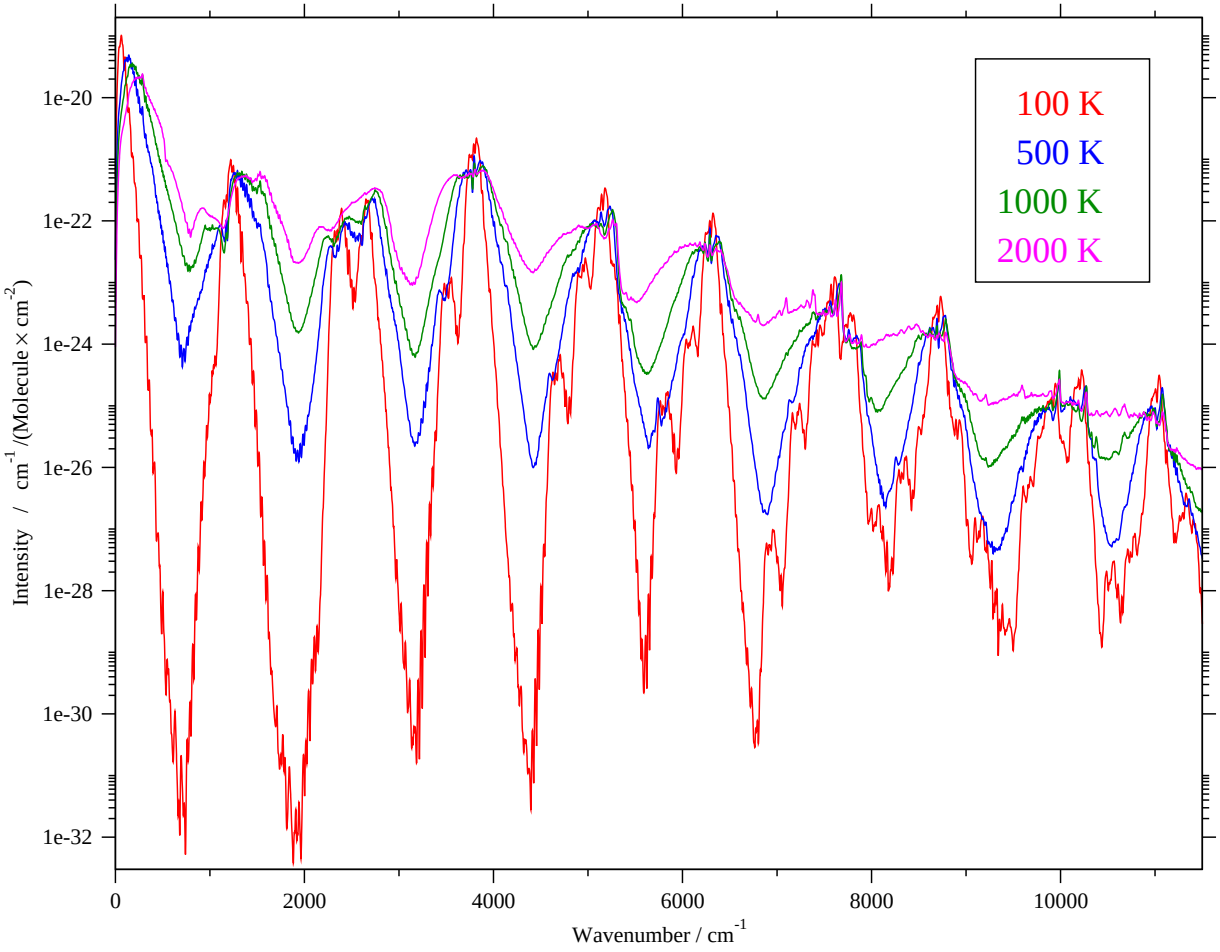

Figure 5.14: Spectra generated from the line list (ATY2013) at different temperatures.

Chapter 6

Measurement and analysis of the pure rotational band

This work is based on publication by Azzam et al. [2013]. In this chapter we present new experimental measurements of the spectrum of hydrogen sulphide in the region 1.4 – 10.5 THz (45 – 360 cm^{-1}). This work is a byproduct of our work on the hot line list calculations. As mentioned in Chapter 2, new experimental energy levels are very important for the *ab initio* PESs refinement process. So, the author of this thesis had the opportunity to arrange for experimental work in order to record an emission spectrum of H_2S at high temperatures in collaboration with the team work in the AILES beamline at the SOLEIL synchrotron [Brubach et al. [2010]]. As far as we know, no experimental emission spectrum of H_2S has been published. As will be described in Section 6.2, this experiment failed, but another successful experiment for absorption spectrum detection at room temperature was performed and analysed. In this more than 2400 rotational lines were detected, belonging to the ground vibrational state transitions of the four isotopologues $H_2{}^{32}S$, $H_2{}^{33}S$, $H_2{}^{34}S$, and $H_2{}^{36}S$ observed in natural abundance, and 320 pure rotational transitions of $H_2{}^{32}S$ in its first excited bending vibrational state. The results presented in this chapter have been submitted for inclusion in the 2012 update of the HITRAN database [Rothman et al. [2013]].

6.1 Introduction

Since the work of Burrus et al. [1953], numerous studies have been performed on H_2S absorption rotational transitions in the ground vibrational state in the region up to about 9.3 THz (310 cm^{-1}). In the microwave region, 82 lines have been detected for the main isotopologue ($H_2{}^{32}S$) by Burenin et al. [1985]; Burrus et al. [1953]; Cupp et al. [1968]; Helminger et al. [1972]; Huiszoon [1971]; Huiszoon and Dymanus [1966] and Belov et al. [1995], 40 transitions for $H_2{}^{34}S$ by Burrus et al. [1953]; Huiszoon [1971]; Huiszoon and Dymanus [1966] and Saleck et al. [1995], 155 transitions for $H_2{}^{33}S$ with hyperfine splitting due to ^{33}S nucleus by Burrus et al. [1953] and Saleck et al. [1995], and 3 experimental transitions for $H_2{}^{36}S$ as well by Saleck et al. [1995]. In the far infrared (FIR), 443 observed absorption transitions have been reported for $H_2{}^{32}S$ by Flaud et al. [1983]; Miller et al. [1969]; Yamada and Klee [1994] and Belov et al. [1995], 71 transitions for $H_2{}^{33}S$ by Flaud et al. [1983], and 173 transitions for $H_2{}^{34}S$ by Flaud et al. [1983].

Particularly important for this work are the measurements by Flaud et al. [1983], who probed the region below 9.3 THz, and by Yamada and Klee [1994], who made measurements in the same region. Effective Hamiltonian fits using frequencies from these two works in addition to the available experimental microwave data, provided the rotational spectra used in HITRAN 2008 [Rothman et al. [2005, 2009]] and JPL [Pickett et al. [1998]] databases, respectively. However rotational frequencies beyond 10 THz were estimated by extrapolations using these fitted effective Hamiltonians. In the CDMS database [Müller et al. [2001, 2005]], the pure rotational transitions have been calculated using all the available measured transitions in the microwave and (FIR) region. We note that the higher rotational states of H_2S are also of interest theoretically [Kozin and Jensen [1994]].

Many other studies have been performed in order to detect the absorption transitions of H_2S molecule and its isotopologues ($H_2{}^{33}S$ and $H_2{}^{34}S$) in its fundamental, hot, and combination vibrational bands covering the spectrum range up to 16 500 cm^{-1}, as showed in Chapter 1. The most important for this chapter are the transitions in the fundamental bending mode (ν_2) [Lane et al. [1982, 1985]; Strow [1983]; Ulenikov et al. [1996a]]. Among these studies, Ulenikov et al.

[1996a] reported the most accurate experimental upper state energy levels in ν_2 band for $H_2{}^{32}S$, $H_2{}^{33}S$, and $H_2{}^{34}S$. See Table 6.1 for the summary.

The following section gives experimental details. Section 6.3 gives general overview about the theoretical part, Section 6.4 presents the analysis of the new spectrum. In Section 6.5 a comprehensive comparison with the previous measurements is presented.

6.2 Experiment

The two experiments were performed using two different setups. In the following two subsections, these two experiments are described in detail.

6.2.1 Emission spectrum experiment

For this experiment a new cell was built. The H_2S gas in natural abundance was allowed to flow in a Pyrex cell of length 1.5 m at pressure 7.36 mbar. A discharge was made into the gas to excite the molecules to high energy levels, see Fig. 6.1. Then the emitted light was recorded in the far infrared region (45 to 350 cm^{-1}). During this experiment we only obtained 54 successful scans because of the following problems:

1. free sulphur molecules recombined and produced solid sulphur which coated the inner side of the cell. This coating prevented the magnetic field from flowing inside the cell and killed the plasma. Because of this we needed to clean the cell by discharging air into the cell, see Fig. 6.1,

2. the solid sulphur filled the exit point where the discharged gas should flow out of the cell. Because of this the pressure inside the cell went out of control, see Fig. 6.2, and

3. the acidic nature of this gas destroyed the gas regulator, and that caused some leakage into the environment.

Fig. 6.3 shows the emission spectrum which was detected with a resolution of 0.01 cm^{-1}. Unfortunately, as a result of the above problem, the team decided to

Table 6.1: Summary of the fits for the four isotopologues of H_2S in the ground and first bending vibrational states with a comparison with the previous works for the same molecule.

Reference	Used method	Vib. state	ISO	MW lines		IR lines		parameters	RMS		σ^c
				Previous	Recorded	Previous	Recorded		MW(MHz)	IR(cm^{-1})	cm^{-1}
Flaud et al. [1983]	A-I^r	000	$H_2{}^{32}S$	39 [Burrus et al., 1953; Helminger et al., 1972] [Huiszoon, 1971; Huiszoon and Dymanus, 1966]	—	—	387	29	0.25	0.00035	0.0008
			$H_2{}^{33}S$	1 [Burrus et al., 1953; Huiszoon, 1971]	—	—	71	8	—	0.00031	0.0008
			$H_2{}^{34}S$	2 [Burrus et al., 1953; Huiszoon, 1971]	—	—	173	15	—	0.00025	0.0010
Yamada and Klee [1994]	S-I^r	000	$H_2{}^{32}S$	40 [Burenin et al., 1985; Helminger et al., 1972]	—	—	376	30	82	0.000213	0.0007
Belov et al. [1995]	Padé-I^r	000	$H_2{}^{32}S$	29 [Burenin et al., 1985; Helminger et al., 1972]	64	376 [Yamada and Klee, 1994]	30	24	366	0.000265	0.0003
Saleck et al. [1995]	A-I^r	000	$H_2{}^{33}S$	—	155	71 [Flaud et al., 1983]	—	37[a]			
			$H_2{}^{34}S$	2 [Huiszoon, 1971]	38	173 [Flaud et al., 1983]	—	28			
This work	S-I^r	000	$H_2{}^{32}S$	82 [Belov et al., 1995; Helminger et al., 1972]	—	380 [Belov et al., 1995] [Yamada and Klee, 1994]	926	44	0.339	0.00046	
			$H_2{}^{33}S$	155 [Saleck et al., 1995]	—	—	433	34[a]	0.258	0.00046	
			$H_2{}^{34}S$	40 [Huiszoon and Dymanus, 1965; Saleck et al., 1995]	—	—	576	41	0.063	0.00047	
			$H_2{}^{36}S$	1 [Saleck et al., 1995]	—	—	91	24	0.002	0.00051	
		010	$H_2{}^{32}S$	—	—	743[b]	320	42	—	0.00038	
			$H_2{}^{34}S$	—	—	240[b]	86	23	—	0.00043	

[a] Including hyperfine constants.

[b] Calculated from experimental energy levels given by Ulenikov et al. [1996a].

[c] Standard deviation between our measurements and the recorded transitions for each work.

stop the experiment. As can be seen in Fig. 6.3 some transitions were recorded. So, a trial for calibrating this spectrum was done using the residual water transitions and the accurate transition frequencies from Matsushima et al. [1995] and Horneman et al. [2005]. Fig. 6.4 shows the dispersion of the water transitions before and after the calibration. As can be seen from this figure, the calibration was not perfect for this spectrum.

Since our planned experiment failed, the team decided to record the absorption spectrum of H_2S at room temperature using the facilities available at SOLEIL. This decision was made just to test what kind of spectrum could be seen. The following subsection describes this experiment.

6.2.2 Absorption spectrum experiment

The Fourier transform FIR absorption spectrum of gas phase H_2S in natural abundance was recorded using a globar source available on the Bruker IFS125 interferometer. A resolution of 0.005 cm^{-1} was used to record the spectrum in the spectral range 45 – 360 cm^{-1}. A pressure of 0.16 mbar of H_2S was injected in a room-temperature White-type cell aligned for an optical path length of 150 m. The interferometer was pumped to a pressure below 10^{-4} mbar using a turbomolecular pump; two polypropylene windows were used to separate the interferometer from the absorption cell. The resulting spectrum is the co-addition of 1020 scans (about 12 hours of acquisition time). Fig. 6.5 shows an overview of the recorded spectrum. Fig. 1.1 in Chapter 1 gives an illustrative region containing newly observed lines.

Spectral calibration was performed using the residual water transitions as mentioned above for the emission spectrum. A calibration curve was prepared to facilitate the correction of the recorded frequencies for H_2S. Fig. 6.6 shows the dispersion of the water transitions before and after the calibration. The accuracy of the line position is thus estimated to be 0.0005 cm^{-1}.

An initial analysis of this spectrum (by comparing to the available data from spectroscopic databases, as will be detailed below) showed inaccurate positions of some transitions published in the databases in this region of the spectrum for the main isotopologue of this molecule. Also, this preliminary analysis showed

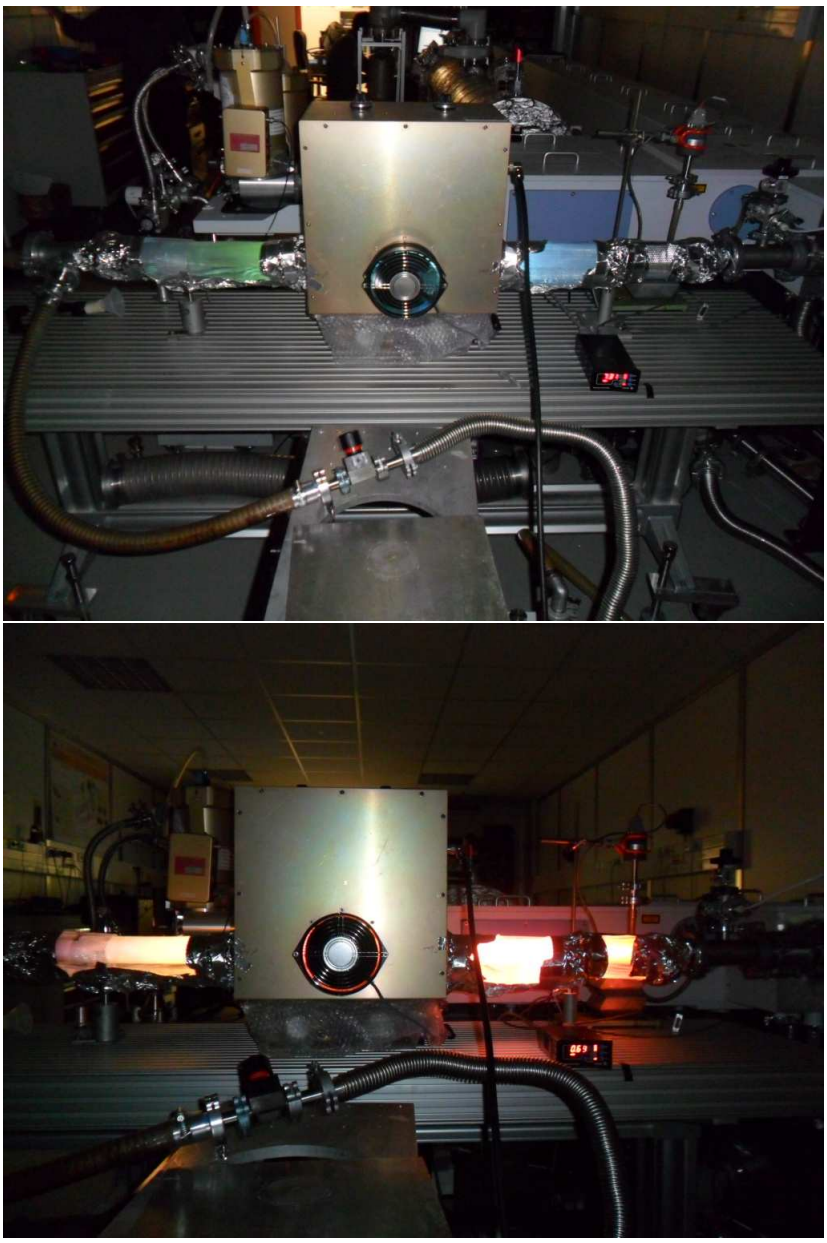

Figure 6.1: Emission experiment setup. H_2S discharging (top), where the solid sulphur (appears in yellow colour) coating the left tube from inside. Air discharging for cleaning the tube from solid sulphur (bottom).

Figure 6.2: Sulphur deposition in the valves and on the inner side of the pyrex cell.

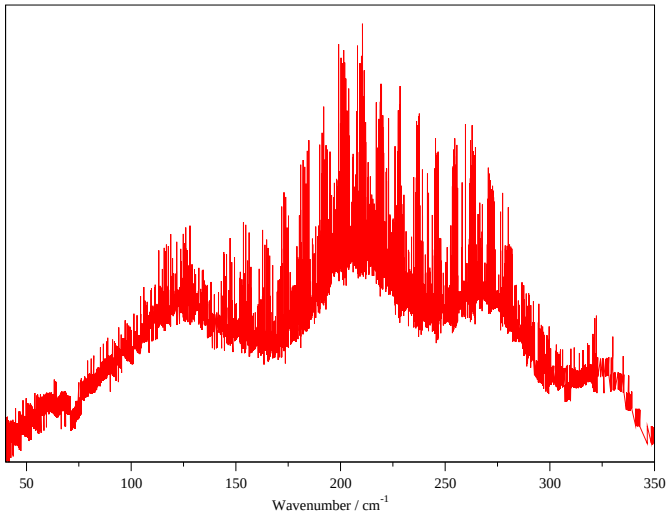

Figure 6.3: Emission spectrum obtained from the experiment in SOLEIL.

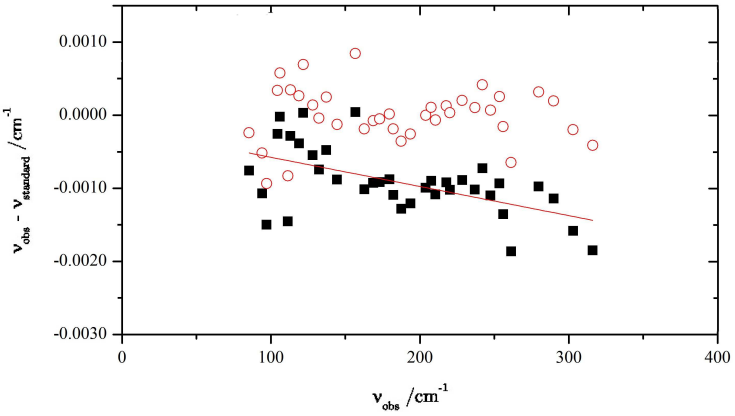

Figure 6.4: Calibration of the emission spectrum recorded in this work. Water line positions before calibration (■) and after calibration (○) based in the accurate water line positions of Matsushima et al. [1995] and Horneman et al. [2005]. The line equation in cm^{-1} is $d = -3.99(99) \times 10^{-6}\nu - 1.76(19) \times 10^{-4}$, where d is the dispersion and ν is the transition frequency. The standard deviation after calibration is 0.95×10^{-3} cm^{-1}.

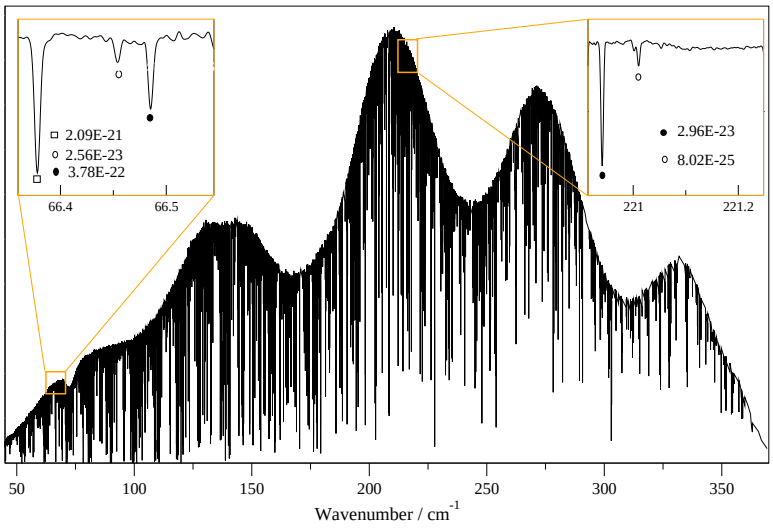

Figure 6.5: Room temperature absorption spectrum of H_2S recorded at the AILES beamline. The insets illustrate detection of different line intensities for two sample regions of the spectrum. The numbers next to the symbols give the intensities of the lines in $cm^{-1}/(molecule \times cm^{-2})$ according to HITRAN 2008 [Rothman et al. [2009]].

the possibility of identifying new transitions. So, this spectrum was analysed and comprehensive comparisons were performed with the previously published experiments, as well as with the data available in different databases. The following sections summarise this work.

6.3 Theory

According to the spectroscopic convention the moments of inertia are arranged as:

$$I_A \leq I_B \leq I_C, \tag{6.1}$$

where

$$I_A = \frac{h^2}{8\pi^2 A},\ I_B = \frac{h^2}{8\pi^2 B},\ I_C = \frac{h^2}{8\pi^2 C}, \tag{6.2}$$

where A, B, and C are the rotational constants of the molecule in Hz. Ray's asymmetry parameter, $\kappa = (2B - A - C)/(A - C)$, is often used to characterise

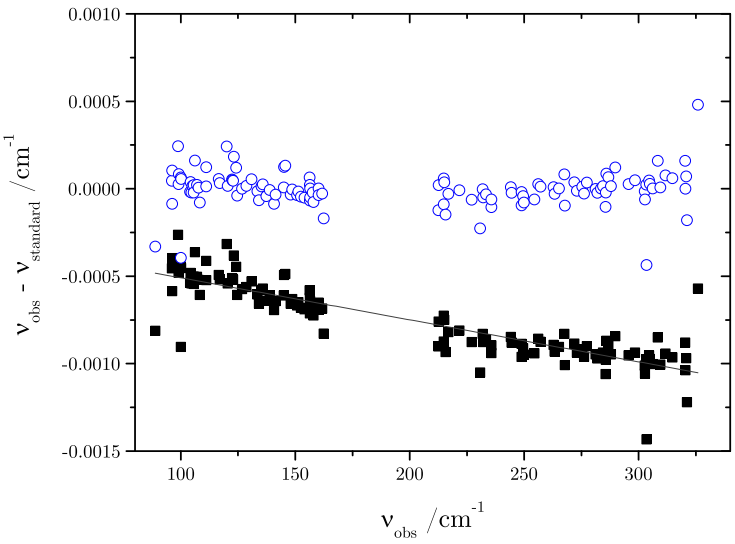

Figure 6.6: Calibration of the FIR Fourier transform spectrum recorded in this work. Water line positions before calibration (■) and after calibration (○) based in the accurate water line positions of Matsushima et al. [1995] and Horneman et al. [2005]. The line equation in cm^{-1} is $d = -2.40(12)\times10^{-6}\nu - 2.69(26)\times10^{-4}$, where d is the dispersion and ν is the transition frequency. The standard deviation after calibration is 1.05×10^{-4} cm^{-1}.

the degree of asymmetry for the molecule. when $A \approx B$, κ approaches $+1$ for the oblate case and when $B \approx C$, κ approaches -1 for the prolate case. For H_2S, $\kappa = 0.52$, so it is a near oblate top.

The recorded and assigned transitions can be used to fit the parameters of an effective Hamiltonian using a least-squares fit. These fitted parameters can then be used to predict more transitions. The accuracy of the predicted lines depends on the efficiency of the effective Hamiltonian employed and the quality of the fit which is also affected by the number of the experimental transitions used in the fit. The predicted transitions are useful for identifying more transitions and for assigning them. Watson's reduced Hamiltonian [Watson [1977]] is one of the widely used models for H_2S spectrum. This Hamiltonian has two reduced forms A and S. These two forms are used with different representations given by the orientation of the molecular axes with respect to the Cartesian axes. Conventionally, either the I^r $(x, y, z \rightarrow b, c, a)$ or I^l $(x, y, z \rightarrow c, b, a)$ representations is used for a prolate asymmetric top $(-1 < \kappa < 0)$, and the III^r $(x, y, z \rightarrow a, b, c)$ or III^l $(x, y, z \rightarrow b, a, c)$ representations for an oblate asymmetric top $(0 < \kappa < 1)$. The representation is usually chosen in this way because as $\kappa \rightarrow -1$ the off-diagonal matrix elements of the rigid-rotor Hamiltonian become very small in the I^r representation, while as $\kappa \rightarrow +1$ they become very small in the III^r representation. As demonstrated by Strow [1983] and Yamada and Klee [1994], the III^r representation converges slowly and fits to experimental data poorly. As a result, many studies for H_2S spectrum have been performed using I^r representation.

The quality of the fit is characterised by the root mean square error (σ)

$$\sigma = \sqrt{\frac{1}{N-P}\sum_{i=1}^{N}\left(\frac{\nu_i^{exp} - \nu_i^{calc}}{\delta_i}\right)^2}, \tag{6.3}$$

where N is the number of detected lines, P is the number of the effective Hamiltonian parameters, ν^{exp} is the measured transition frequency with precision δ, and ν^{calc} is the theoretical analog of ν^{exp} resulted from the used effective Hamiltonian. A correct treatment should have $\sigma \lesssim 1$.

6.4 Spectral analysis

Lines for H_2S molecule with intensities above 10^{-25} cm^{-1}/(molecule×cm^{-2}) were detected for the region above 80 cm^{-1}. In the region below 50 cm^{-1} only lines with intensity above about 10^{-23} cm^{-1}/(molecule×cm^{-2}) were detected as a consequence of the nature of the spectrum obtained from the blackbody radiator: the low intensity of the light leads to a limited signal-to-noise ratio which fast decreases below 50 cm^{-1} as seen in Fig. 6.5. Examples of line detections with different intensities in the different regions of the spectrum are given in the same figure.

The absorption spectrum was analysed manually by matching lines with the available data in the HITRAN 2008 database [Rothman et al. [2009]] and the CDMS database [Müller et al. [2001, 2005]] for the main isotopologue for the vibrational ground state transitions. For $H_2{}^{33}S$ and $H_2{}^{34}S$ in their vibrational ground state, the HITRAN 2008 database was used. For the $H_2{}^{36}S$ isotopologue, many transitions were identified and assigned manually by extrapolating the line positions of the three other isotopologues for given quantum numbers, see Fig. 1.1. The pure rotational transitions of the vibrational state $v_2 = 1$ of $H_2{}^{32}S$ were initially assigned using the variational line list presented in Chapter 5. Experimental upper energy levels belonging to the ν_2 band given by Ulenikov et al. [1996a] were used to calculate the pure rotational transitions in the $v_2 = 1$ state for $H_2{}^{32}S$ and $H_2{}^{34}S$. These calculated transitions were used to confirm the assignments for $H_2{}^{32}S$ and to identify pure rotational transitions for $H_2{}^{34}S$.

Pickett's program CALPGM [Pickett [1991]] was used to fit the observed spectra for each of the four isotopologues in both states of this molecule studied in this work. Table 6.1 summarises the number of the fitted parameters and the number of the spectral lines used in the fit for each isotopologues in both vibrational states. For $H_2{}^{32}S$ in the ground vibrational state, the 926 newly-recorded lines were combined with 462 lines of Belov et al. [1995]; Helminger et al. [1972] and Yamada and Klee [1994]. The resulting fit parameters were used to predict 2919 transitions for $H_2{}^{32}S$ in the ground vibrational state up to $J = 30$ and $K_a = 20$. For $H_2{}^{34}S$, 576 of our measured lines were combined with 40 lines from Saleck et al. [1995] and Huiszoon and Dymanus [1965] to

fit 41 parameters. Using the fitted parameters, a pure rotational spectrum was predicted up to around 600 cm^{-1}. This predicted spectrum contains 2554 lines with J up to 28 and K_a up to 19. For $H_2{}^{32}S$, 320 newly-recorded pure rotational transitions belonging to the vibrational state $v_2 = 1$ were used in the fits together with 743 pure rotational transitions calculated from the ν_2 experimental energy levels of Ulenikov et al. [1996a]. For $H_2{}^{34}S$, the 86 newly-recorded transitions were combined with 240 pure rotational transitions calculated from the ν_2 experimental energy levels from the same paper, see Table 6.2. For $H_2{}^{33}S$, 433 of our measured lines were used together with 155 microwave lines measured by Saleck et al. [1995] to fit 31 rotational constants and 3 electric quadrupole hyperfine constants for the ^{33}S nucleus. The predicted spectrum was calculated using the fitted rotational constants only, *i.e.* neglecting the hyperfine structure. This spectrum contains 2471 lines with J up to 32 and K_a up to 20. Because of the lower abundance of the isotopologue $H_2{}^{36}S$, we were able to detect only 91 transitions, with highest J and K_a values of 15 and 11, respectively. These transitions were combined with a single microwave line published by Saleck et al. [1995] to fit 24 rotational parameters.

The presence of the H_2S *ortho – para* doublets with the 3 to 1 intensity ratio was taken into account in the line assignment process. A value for the permanent dipole moment of $\mu = 0.9783$ D [Viswanathan and Dyke [1984]] was used in our intensity calculations. This value was used even for transitions within the ν_2 bending mode because no observed value is available for the dipole associated with this state. Our *ab initio* calculations imply that in practice the ν_2 dipole should be about 1 % bigger than that for the ground state. For $H_2{}^{32}S$, $H_2{}^{33}S$ and $H_2{}^{34}S$, the 296 K partition function values 503.07, 503.725 and 504.35 [Šimečková et al. [2006]], respectively, were used in our calculations. For $H_2{}^{36}S$, the partition function $Q = 506.51$ was calculated by the CALPGM program. For the intensities of the pure rotational transitions of $H_2{}^{32}S$ and $H_2{}^{34}S$ within their first excited vibrational states $v_2 = 1$, the vibrational band origins from Ulenikov et al. [1996a] were used in order to correct the intensity produced by the CALPGM program as given by:

$$I = aI_{\mathrm{CALPGM}} e^{-c_2 E_{\mathrm{BO}}/T}, \tag{6.4}$$

where a is the isotopologue abundance, E_{BO} is the band origin in cm^{-1}, c_2 is the second radiation constant and T is the temperature in K.

The constants obtained from the fits are presented in Tables 6.3 and 6.4. The measured and predicted transitions of $H_2{}^{32}S$ and $H_2{}^{34}S$ in their ground and $v_2 = 1$ vibrational states, as well as these for $H_2{}^{33}S$ and $H_2{}^{36}S$ in their ground vibrational states, are given in the supplementary material in our publication [Azzam et al. [2013]].

6.5 Results and discussion

In this work, more than 2400 lines are recorded for the four isotopologues of H_2S in the ground vibrational state, and for $H_2{}^{32}S$ and $H_2{}^{34}S$ in the first excited bending state. Table 6.1 summarises the measurements of the H_2S pure rotational spectra from this work and from previous studies. Detailed results for the pure rotational transitions of $H_2{}^{32}S$ and $H_2{}^{34}S$ in their ground and first excited bending state, as well as $H_2{}^{33}S$ and $H_2{}^{36}S$ in their ground states are given in the supplementary material in our publication [Azzam et al. [2013]]. After a description of the available data used for comparison with this work, results will be detailed.

6.5.1 Available data

The line positions of the rotational band spectrum collected in HITRAN 2008 were originally obtained by Flaud et al. [1983], who recorded a hydrogen sulphide spectrum between 50 and 310 cm^{-1} with a Fourier transform spectrometer at a resolution of 0.005 cm^{-1}. In this experiment the three isotopic species $H_2{}^{32}S$, $H_2{}^{33}S$, $H_2{}^{34}S$ were observed in natural abundance. Flaud et al. [1983] measured 631 lines in this region and combined them with 42 previously published microwave transitions in a least squares fit. Rotational constants for each isotopologue were calculated using the A-I^r representation of the Watson Hamiltonian. These constants were used to predict the positions of the absorption of the natural abundance hydrogen sulphide in the FIR region and intensities using $\mu = 0.974$ D for the permanent dipole moment [Huiszoon and Dymanus [1966]].

Table 6.2: Summary of the available data for H_2S pure rotational transitions.

Vib. state	Data source		Number of lines				Max. J		Max. K_a		σ^b
			Total	M	M	P	M	P	M	P	cm^{-1}
				Microwave	Infrared						
000	HITRAN 2008 Flaud et al. [1983]	$H_2{}^{32}S$	1540	39 [Burrus et al., 1953; Helminger et al., 1972] [Huiszoon, 1971; Huiszoon and Dymanus, 1966]	387 [Flaud et al., 1983]	1114	22	27	15	19	0.0062
		$H_2{}^{33}S$	808	1 [Burrus et al., 1953; Huiszoon, 1971]	73 [Flaud et al., 1983]	734	15	22	10	13	0.0008
		$H_2{}^{34}S$	1048	2 [Burrus et al., 1953; Huiszoon, 1971]	173 [Flaud et al., 1983]	873	18	24	12	15	0.0019
	CDMS Müller et al. [2001, 2005]	$H_2{}^{32}S$	1501	82 [Cupp et al., 1968; Huiszoon, 1971] [Belov et al., 1995; Helminger et al., 1972]	441 [Flaud et al., 1983; Yamada and Klee, 1994] [Belov et al., 1995]	978	22	25	15	19	0.0037
		$H_2{}^{33}S$	4759[a]	155 [Saleck et al., 1995]	73 [Flaud et al., 1983]	4531	15	22	10	15	—
		$H_2{}^{34}S$	990	40 [Huiszoon, 1971; Saleck et al., 1995]	173 [Flaud et al., 1983]	777	18	24	12	16	0.0009
	JPL Pickett et al. [1998]	$H_2{}^{32}S$	1525	82 [Helminger et al., 1972, 1973] [Belov et al., 1995]	379 [Belov et al., 1995; Yamada and Klee, 1994]	1064	16	21	13	18	0.0168
	This work	$H_2{}^{32}S$	2919	82 [Cupp et al., 1968; Huiszoon, 1971] [Belov et al., 1995; Helminger et al., 1972]	1306	1531	26	30	17	20	
		$H_2{}^{33}S$	2471	155 [Saleck et al., 1995]	433	2038	21	32	14	20	
		$H_2{}^{34}S$	2554	40 [Huiszoon, 1971; Saleck et al., 1995]	576	1938	24	28	16	19	
		$H_2{}^{36}S$	1004	1 [Saleck et al., 1995]	91	912	15	17	11	13	
010	This work	$H_2{}^{32}S$	1801		1064	737	22	23	13	16	
		$H_2{}^{34}S$	1083		326	757	14	20	10	12	

[a] Including hyperfine structure.

[b] The standard deviation is calculated using the frequencies measured in this work relative to the results of fits, denoted P for Predicted in each database. M for measured.

Table 6.3: Parameters in MHz for the (000) vibrational state of $H_2{}^{32}S$, $H_2{}^{33}S$, $H_2{}^{34}S$ and $H_2{}^{36}S$.

	[a]	Parameter		$H_2{}^{32}S$	$H_2{}^{33}S$	$H_2{}^{34}S$	$H_2{}^{36}S$
1	10000	A		310583.5798(106)	310025.7737(197)	309502.3997(103)	308559.20(34)
2	20000	B		270367.6824(121)	270367.1693(224)	270366.9368(98)	270354.74(174)
3	30000	C		141820.0415(69)	141702.4070(174)	141591.8242(93)	141395.80(93)
4	200	Δ_J		20.861771(261)	20.87749(84)	20.90496(56)	20.6197(151)
5	1100	Δ_{JK}		-76.23237(64)	-76.33674(232)	-76.48005(180)	-73.937(98)
6	2000	Δ_K		117.72636(68)	117.58223(196)	117.49020(147)	115.559(126)
7	40100	δ_J		8.865995(99)	8.863831(281)	8.866950(141)	8.5716(195)
8	50000	δ_K		-0.641960(33)	-0.654477(112)	-0.666993(74)	-0.7067(38)
9	300	H_J		0.01022690(312)	0.0100421(84)	0.0102278(111)	
10	1200	H_{JJK}		-0.0903531(127)	-0.089668(58)	-0.091210(55)	
11	2100	H_{JKK}		0.155866(35)	0.154950(126)	0.157519(49)	0.0576(33)
12	3000	H_K		-0.0338364(300)	-0.033831(117)	-0.035149(42)	
13	40200	h_J	10^{-03}	2.88144(151)	2.8209(39)	2.8646(35)	-3.639(194)
14	50100	h_{JK}	10^{-03}	-0.96339(71)	-0.97261(229)	-0.98017(188)	-1.1850(286)
15	60000	h_K	10^{-03}	1.24685(33)	1.25103(125)	1.26596(65)	1.1179(110)
16	400	L_J	10^{-03}	-0.0056700(186)	-0.0040663(291)	-0.005551(71)	0.10398(288)
17	1300	L_{JJJK}	10^{-03}	0.072865(181)	0.058824(298)	0.07417(49)	-0.9742(215)
18	2200	L_{JJKK}	10^{-03}	-0.22325(78)	-0.18567(146)	-0.20564(95)	1.173(42)
19	3100	L_{JKKK}	10^{-03}	0.27447(96)	0.23823(310)	0.23350(146)	-0.5454(194)
20	4000	L_K	10^{-03}	-0.16145(53)	-0.14806(233)	-0.13911(68)	
21	40300	l_J	10^{-06}	-1.0205(81)	-0.6487(138)	-1.0517(280)	57.95(177)
22	50200	l_{JJK}	10^{-06}	-0.2743(37)	-0.2523(93)	-0.2579(98)	
23	60100	l_{JKK}	10^{-06}	-1.7256(50)	-1.5518(71)	-1.6312(56)	
24	70000	l_K	10^{-06}	0.39780(137)	0.4483(58)	0.4605(37)	
25	500	M_J	10^{-06}	0.004801(60)		0.003712(147)	-0.3644(167)
26	1400	M_{JJJJK}	10^{-06}	-0.06825(128)		-0.04173(149)	3.847(148)
27	2300	M_{JJJKK}	10^{-06}	0.2466(58)			-3.981(205)
28	3200	M_{JJKKK}	10^{-06}	-0.4541(77)	-0.0936(105)		1.756(130)
29	4100	M_{JKKKK}	10^{-06}	0.4151(40)	0.1808(240)	0.2908(127)	
30	5000	M_K	10^{-06}	-0.09827(255)	-0.0538(151)	-0.1882(95)	
31	40400	m_J	10^{-09}	0.8269(141)		0.941(64)	-187.8(86)
32	60200	m_{JJKK}	10^{-09}	0.7954(275)			
33	70100	m_{JKKK}	10^{-09}	-0.6732(104)	-0.7882(203)	-1.0281(192)	4.074(302)
34	80000	m_K	10^{-09}	0.33763(256)	0.3172(123)	0.2162(38)	
35	600	N_J	10^{-09}	-0.003664(90)			
36	1500	N_{JJJJJK}	10^{-09}	0.07339(253)		-0.02754(260)	-2.857(188)
37	2400	N_{JJJJKK}	10^{-09}	-0.2464(111)		0.3880(168)	
38	3300	N_{JJJKKK}	10^{-09}	0.2604(134)		-0.954(39)	
39	5100	N_{JKKKKK}	10^{-09}	-0.1150(63)		0.2930(165)	
40	50400	n_{JJJJK}	10^{-12}	0.9302(190)	0.5108(216)	0.571(60)	
41	60300	n_{JJJKK}	10^{-12}	-0.509(48)		1.175(57)	
42	70200	n_{JJKKK}	10^{-12}	0.2140(203)		0.7967(281)	
43	80100	n_{JKKKK}	10^{-12}	-0.4382(77)	-0.549(34)		
44	90000	n_K	10^{-12}	0.02109(147)		0.0954(46)	
45	3400	$O_{JJJJKKK}$	10^{-12}			1.205(70)	
46	3500	$P_{JJJJJKKK}$	10^{-15}			-1.633(65)	
	110010000	X_{aa1}			-32.841(78)		
	110020000	X_{bb1}			-8.635(98)		
	10020000	C_{bb1}			0.0281(77)		
		$\sigma_{\rm rms}$		0.93487	0.93345	0.95080	1.01830

[a] Pickett's program CALPGM notations [Pickett [1991]]

Table 6.4: Parameters in MHz for the (010) vibrational state of $H_2{}^{32}S$ and $H_2{}^{34}S$.

	[a]	Parameter		$H_2{}^{32}S$	$H_2{}^{34}S$
1	10000	A		321437.64(67)	320320.21(128)
2	20000	B		276536.85(56)	276525.06(73)
3	30000	C		139967.83(42)	139744.39(52)
4	200	Δ_J		22.8142(110)	22.9556(119)
5	1100	Δ_{JK}		-84.0407(217)	-84.480(68)
6	2000	Δ_K		138.595(34)	138.641(87)
7	40100	δ_J		10.3334(42)	10.3734(56)
8	50000	δ_K		-0.15332(37)	-0.17489(136)
9	300	H_J		0.010084(124)	0.011547(83)
10	1200	H_{JJK}		-0.11031(36)	-0.10671(69)
11	2100	H_{JKK}		0.17914(93)	0.15188(261)
12	3000	H_K		-0.02510(49)	0.0212(37)
13	40200	h_J	10^{-03}	2.455(55)	3.161(56)
14	50100	h_{JK}	10^{-03}	-0.70401(264)	-0.6776(149)
15	60000	h_K	10^{-03}	1.7928(49)	1.7435(130)
16	400	L_J	10^{-03}	0.00930(62)	
17	1300	L_{JJJK}	10^{-03}	0.08994(193)	
18	2200	L_{JJKK}	10^{-03}		0.237(32)
19	3100	L_{JKKK}	10^{-03}	0.1985(210)	0.311(38)
20	4000	L_K	10^{-03}		-0.933(40)
21	40300	l_J	10^{-06}	9.518(290)	3.028(197)
22	60100	l_{JKK}	10^{-06}	-4.442(56)	-2.644(134)
23	500	M_J	10^{-06}	-0.03316(118)	
24	1400	M_{JJJJK}	10^{-06}		0.1670(141)
25	2300	M_{JJJKK}	10^{-06}	-2.201(34)	
26	3200	M_{JJKKK}	10^{-06}	1.698(71)	-6.545(265)
27	4100	M_{JKKKK}	10^{-06}	-4.188(278)	8.43(34)
28	5000	M_K	10^{-06}	-1.134(87)	
29	40400	m_J	10^{-06}	-0.02676(55)	
30	60200	m_{JJKK}	10^{-06}	0.011847(212)	
31	70100	m_{JKKK}	10^{-09}	3.0862(285)	
32	80000	m_K	10^{-09}	0.6733(224)	
33	2400	N_{JJJJKK}	10^{-09}	4.811(48)	
34	5100	N_{JKKKKK}	10^{-09}	41.08(156)	
35	6000	N_K	10^{-09}	2.80(36)	
36	700	O_J	10^{-12}	-0.11179(197)	
37	6100	$O_{JKKKKKK}$	10^{-12}	-203.3(45)	
38	60400	o_{JJJJKK}	10^{-12}	-0.09893(143)	
39	70300	o_{JJJKKK}	10^{-12}	-0.05405(49)	
40	80200	o_{JJKKKK}	10^{-15}	-8.75(33)	
41	90100	o_{JKKKKK}	10^{-15}	4.832(192)	
42	100000	o_K	10^{-15}	3.725(260)	
43	1700	$P_{JJJJJJJK}$	10^{-15}	2.979(53)	
44	3500	$P_{JJJJJKKK}$	10^{-15}	-42.39(39)	
45	7100	$P_{JKKKKKKK}$	10^{-15}	382.8(60)	
		σ_{rms}		0.76218	0.86440

[a] Pickett's program CALPGM notations [Pickett [1991]]

Yamada and Klee [1994] recorded a pure rotational spectrum for $H_2{}^{32}S$ in the FIR region using a Fourier transform infrared spectrometer. They detected more than 370 transitions in the region 30 to 260 cm^{-1} with a resolution of 0.0017 cm^{-1}. These lines were combined with the available 40 millimetre and sub-millimetre wave transition frequencies to test several forms of Watson's reduced Hamiltonian extended up to powers of J^{10}.

Ground state pure rotational transitions of $H_2{}^{32}S$ were studied by Belov et al. [1995]. They measured rotational transitions frequencies up to 36 cm^{-1} in Cologne and up to 85 cm^{-1} in Lille. The 84 measured lines were analysed together with the existing microwave and IR data recorded by Yamada and Klee [1994] to test a Watson-type Hamiltonian and a Hamiltonian with a Padé formulation [Polyansky [1985]].

Yamada and Klee [1994]'s measurements were subsequently combined with the measurements by Belov et al. [1995] and Helminger et al. [1972, 1973] to predict the $H_2{}^{32}S$ pure rotational lines which are in the JPL catalog [Pickett et al. [1998]] for J up to 21 using $\mu = 0.974$ D [Huiszoon and Dymanus [1966]]. The data published in CDMS catalog were predicted for $H_2{}^{32}S$ up to $J = 25$, $H_2{}^{33}S$ up to $J = 22$, and $H_2{}^{34}S$ up to $J = 24$ using the measurements from Cupp et al. [1968]; Flaud et al. [1983]; Helminger et al. [1972]; Huiszoon [1971]; Yamada and Klee [1994] and Belov et al. [1995] and the permanent dipole moment value $\mu = 0.9783$ D [Viswanathan and Dyke [1984]].

The most accurate study of lines positions in the ν_2 band of H_2S was performed by Ulenikov et al. [1996a]. They assigned lines to $H_2{}^{32}S$ and its isotopologues $H_2{}^{33}S$ and $H_2{}^{34}S$ with a resolution of 0.002 cm^{-1}. 226 upper state energy levels were obtained with $J \leq 17$ and $K_a \leq 13$ for $H_2{}^{32}S$. 181 of these energy levels up to $J \leq 17$ and $K_a \leq 10$ were fitted with a standard deviation of 9.96×10^{-5} cm^{-1}. For $H_2{}^{34}S$, 126 energy levels with $J \leq 14$ and $K_a \leq 10$ were obtained, 80 of them up to $J \leq 12$ and $K_a \leq 7$ were used to fit the constants for the $v_2 = 1$ vibrational state of this isotopologue. Ulenikov et al. [1996a] used the ground state energies for the three isotopologues from [Flaud et al. [1983]].

6.5.2 Rotational transitions in the ground vibrational state

As can be seen from Table 6.1, we were able to extend significantly the number of the experimental infrared lines for all of four isotopologues of H_2S considered. For instance, for the transitions within the ground vibrational state of $H_2{}^{32}S$, we recorded 926 lines, while only 387 lines in the same spectral region were reported by Flaud et al. [1983]. Our spectrum contains lines with J up to 26 and K_a up to 17, which also significantly extends the coverage of the energy levels probed, see Table 6.1. This table also shows standard deviations between our measured line positions and the previously measured line positions. Our analysis suggests that while we get very good agreement with the previous measurements, there are problems with the predicted line positions tabulated in the databases, see Table 6.2. Fig. 6.7 illustrates some of these errors in the prediction of the line positions in the HITRAN 2008 and CDMS databases; Table 6.5 summarises these problems. Figs. 6.8 and 6.9 give general idea about the accuracy of the line positions available in these databases and that from our fit.

Rotational transitions of the $H_2{}^{36}S$ isotopologue in its ground vibrational state are detected in this work up to $J = 15$ and $K_a = 11$. Over 50 lines were identified and assigned manually by the extrapolation method mentioned above. These first assignments were fitted and the predicted lines from the fit were used to identify and assign more rotational transitions for this isotopologue. As a result, 91 lines were assigned as $H_2{}^{36}S$ lines with a root mean square error of 0.00051 cm^{-1}. Table 6.6 shows examples of lines for the different isotopologues of H_2S recorded in this work with the same rotational quantum numbers in the ground vibrational state. Saleck et al. [1995] published three recorded microwave lines as $H_2{}^{36}S$ rotational transitions. From these lines, only the transition $2_{0,2} - 1_{1,1}$ at 686766.635 MHz could be added to our fit without destroying it. These three transitions are listed in Table 6.7 and compared to the predicted line positions resulting from our fit.

Table 6.5: Summary of the differences in the predicted line positions, in cm^{-1}, in different databases compared to the measured line positions of this work.

Vib. state transition	ISO	Data source	Max. absolute error	error > 0.001 cm^{-1}		Number of lines errors > 0.001 cm^{-1}
				Min. J	Min. K_a	
000-000	$H_2{}^{32}S$	HITRAN 2008	0.0687	3	1	213
		CDMS	0.0626	3	2	139
		JPL	0.2141	3	2	238
		This work	0.0025	4	0	105
		line list[a]	0.0848	3	3	780
	$H_2{}^{33}S$	HITRAN 2008	0.0056	2	0	124
		This work	0.0023	6	1	30
	$H_2{}^{34}S$	HITRAN 2008	0.0202	6	1	62
		CDMS	0.0087	6	1	40
		This work	0.0022	6	1	35
	$H_2{}^{36}S$	This work	0.0014	10	1	3
010-010	$H_2{}^{32}S$	This work	0.0023	9	2	18
		line list[a]	0.3695	2	1	203
	$H_2{}^{34}S$	This work	0.0024	7	3	10

[a] The variationally calculated line list in this study, see Chapter 5.

Table 6.6: Example of recorded pure rotational transitions involving the same quantum numbers for all isotopologues of H_2S. Wavenumbers are expressed in cm^{-1}. Tran. is for transmission. Relative intensities in arbitrary units of the experimental spectrum.

$J'_{K_a,K_c} - J''_{K_a,K_c}$	$H_2{}^{32}S$	Tran.	$H_2{}^{33}S$	Tran.	$H_2{}^{34}S$	Tran.	$H_2{}^{36}S$	Tran.
$6_{5,2} - 5_{2,3}$	144.54128	0.735	144.29279	0.291	144.06081	0.429	143.63731	0.051
$6_{5,2} - 5_{4,1}$	110.54568	0.446	110.13152	0.369	110.13152	0.369	109.75996	0.057
$6_{6,1} - 5_{5,0}$	119.89935	0.571	119.69107	0.386	119.49646	0.540	119.13770	0.111
$7_{5,2} - 6_{4,3}$	146.39028	0.517	146.41766	0.130	146.44235	0.557	146.49292	0.067
$7_{4,3} - 6_{3,4}$	162.08891	0.877	162.09509	0.065	162.10182	0.208	162.10861	0.087
$7_{6,2} - 6_{5,1}$	132.45696	0.739	132.20692	0.307	131.97096	0.485	131.53513	0.063
$7_{6,1} - 6_{5,2}$	138.76971	0.703	138.65730	0.389	138.55438	0.650	138.37194	0.109
$7_{7,1} - 6_{6,0}$	140.05996	0.738	139.82421	0.332	139.60245	0.497	139.19406	0.079
$7_{7,0} - 6_{6,1}$	140.45566	0.722	140.23227	0.437	140.02453	0.589	139.64322	0.137
$8_{2,7} - 7_{1,6}$	90.14059	0.351	90.06754	0.262	89.99708	0.336	89.86677	0.059
$8_{6,3} - 7_{5,2}$	140.70342	0.682	140.39834	0.328	140.11197	0.517	139.58412	0.088
$8_{7,1} - 7_{6,2}$	157.34204	0.641	157.17500	0.312	157.02155	0.399	156.74315	0.054
$8_{7,2} - 7_{6,1}$	153.81211	0.657	153.53890	0.335	153.28214	0.520	152.80716	0.094
$8_{8,1} - 7_{7,0}$	159.83409	0.574	159.56959	0.330	159.32037	0.481	158.86164	0.094
$8_{4,5} - 7_{1,6}$	205.52995	1.233	205.37989	0.474	205.23856	0.644	204.97733	0.072
$8_{4,5} - 7_{3,4}$	110.00203	0.437	109.88486	0.204	109.77541	0.335	109.57541	0.057
$8_{5,4} - 7_{4,3}$	123.48900	0.644	123.26161	0.288	123.04927	0.453	122.66113	0.094
$9_{0,9} - 8_{1,8}$	89.83722	0.337	89.76434	0.219	89.69433	0.327	89.56519	0.067
$9_{7,2} - 8_{6,3}$	177.81227	0.633	177.77345	0.258	177.74061	0.394	177.68369	0.056
$9_{7,2} - 8_{8,1}$	107.40658	0.213	107.90983	0.036	108.38541	0.085	109.28720	0.069
$9_{8,1} - 8_{7,2}$	176.29099	0.330	176.07297	0.270	175.86939	0.448	175.50004	0.067
$9_{9,0} - 8_{8,1}$	179.33075	0.670	179.04013	0.316	178.76731	0.470	178.26627	0.085
$10_{1,10} - 9_{0,9}$	99.22833	0.339	99.14430	0.233	99.06703	0.318	98.92457	0.065
$10_{3,8} - 9_{2,7}$	118.43834	0.543	118.34077	0.321	118.24802	0.408	118.07698	0.070
$10_{5,6} - 9_{4,5}$	137.92562	0.731	137.78550	0.263	137.65484	0.441	137.41588	0.054
$10_{6,5} - 9_{5,4}$	150.72537	0.707	150.46261	0.237	150.21826	0.392	149.77447	0.065
$10_{8,3} - 9_{7,2}$	185.83994	0.746	185.46602	0.281	185.11262	0.428	184.45735	0.062
$10_{9,2} - 9_{8,1}$	194.45476	0.967	194.15019	0.410	193.86381	0.563	193.33483	0.065
$10_{10,1} - 9_{9,0}$	198.31470	1.115	197.99054	0.441	197.68656	0.696	197.12716	0.098
$11_{0,11} - 10_{1,10}$	108.59757	0.423	108.50924	0.245	108.42474	0.373	108.26901	0.078
$11_{10,1} - 10_{9,2}$	214.34502	1.241	214.04423	0.445	213.76277	0.655	213.24863	0.063
$12_{1,12} - 11_{0,11}$	117.95711	0.340	117.85791	0.288	117.76632	0.436	117.59708	0.080
$13_{0,13} - 12_{1,12}$	127.29364	0.690	127.18866	0.307	127.08975	0.471	126.90695	0.070
$13_{1,12} - 12_{2,11}$	136.87308	0.730	136.76006	0.269	136.65361	0.438	136.45697	0.074
$14_{1,14} - 13_{0,13}$	136.61322	0.748	136.50046	0.274	136.39439	0.466	136.19867	0.073
$14_{2,13} - 13_{1,12}$	146.16518	0.848	146.04424	0.260	145.93067	0.361	145.71973	0.050
$14_{2,13} - 14_{1,14}$	130.79259	0.444	130.68577	0.105	130.58540	0.176	130.39491	0.050
$15_{0,15} - 14_{1,14}$	145.91185	0.734	145.79126	0.257	145.67828	0.400	145.46990	0.061

Table 6.7: Three $H_2{}^{36}S$ rotational transitions published by Saleck et al. [1995] and their counterparts calculated in this work. The numbers in parentheses next to Saleck *et al.* and This work transition values are the experimental uncertainty and the fitting estimated error, respectively. Δ is the difference between the transitions in the two works.

$J'_{K_a,K_c} - J''_{K_a,K_c}$	Saleck *et al.* (MHz)	This work (MHz)	Δ (MHz)
$3_{3,1} - 3_{2,2}$	559250.950(0.100)	559796(27)	-546
$4_{4,1} - 4_{3,2}$	636677.520(0.100)	637643(37)	-966
$2_{0,2} - 1_{1,1}$	686766.635(0.100)[a]	686772(24)	-6

[a] This line is included in our fit.

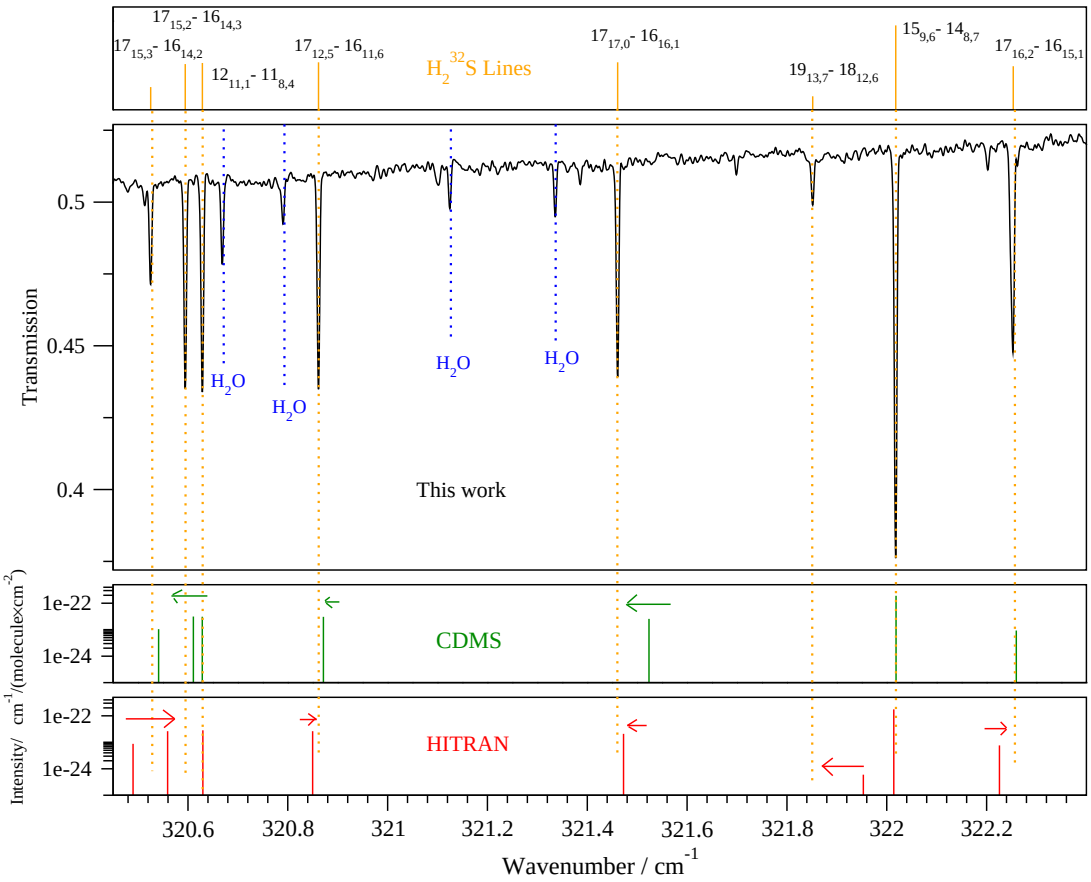

Figure 6.7: A portion of the absorption spectrum of H_2S recorded at SOLEIL, showing the errors in the line positions predicted in HITRAN 2008 [Rothman et al. [2009]] and CDMS [Müller et al. [2001]] databases.

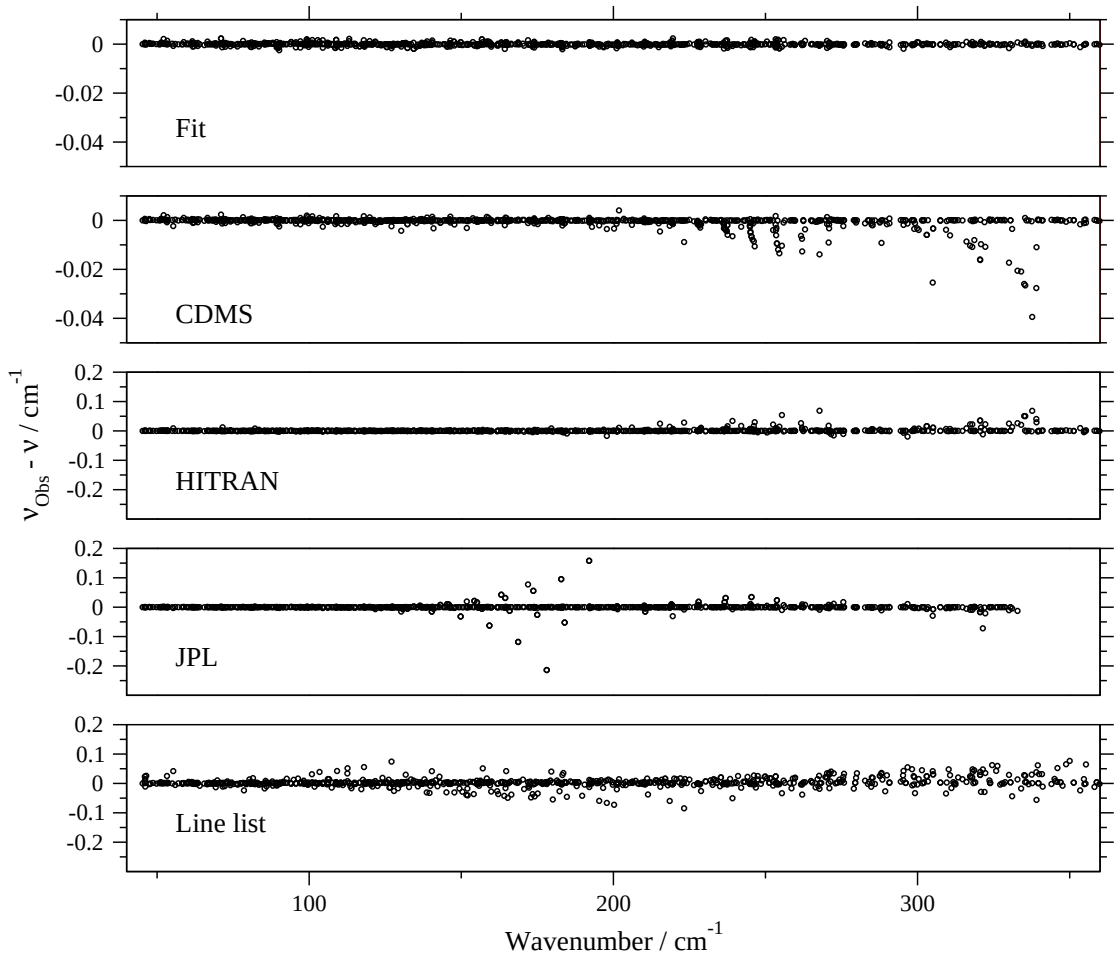

Figure 6.8: Accuracy of the ground vibrational state rotational transitions of $H_2{}^{32}S$ in different databases compared to our measurements. $\nu_{\mathrm{Obs}} - \nu$ represents the deviations of the line positions measured here from that of CDMS [Müller et al. [2001]], HITRAN 2008 [Rothman et al. [2009]], JPL [Pickett et al. [1998]] and variational calculations from Chapter 5. Note the magnified scale for our fit and CDMS.

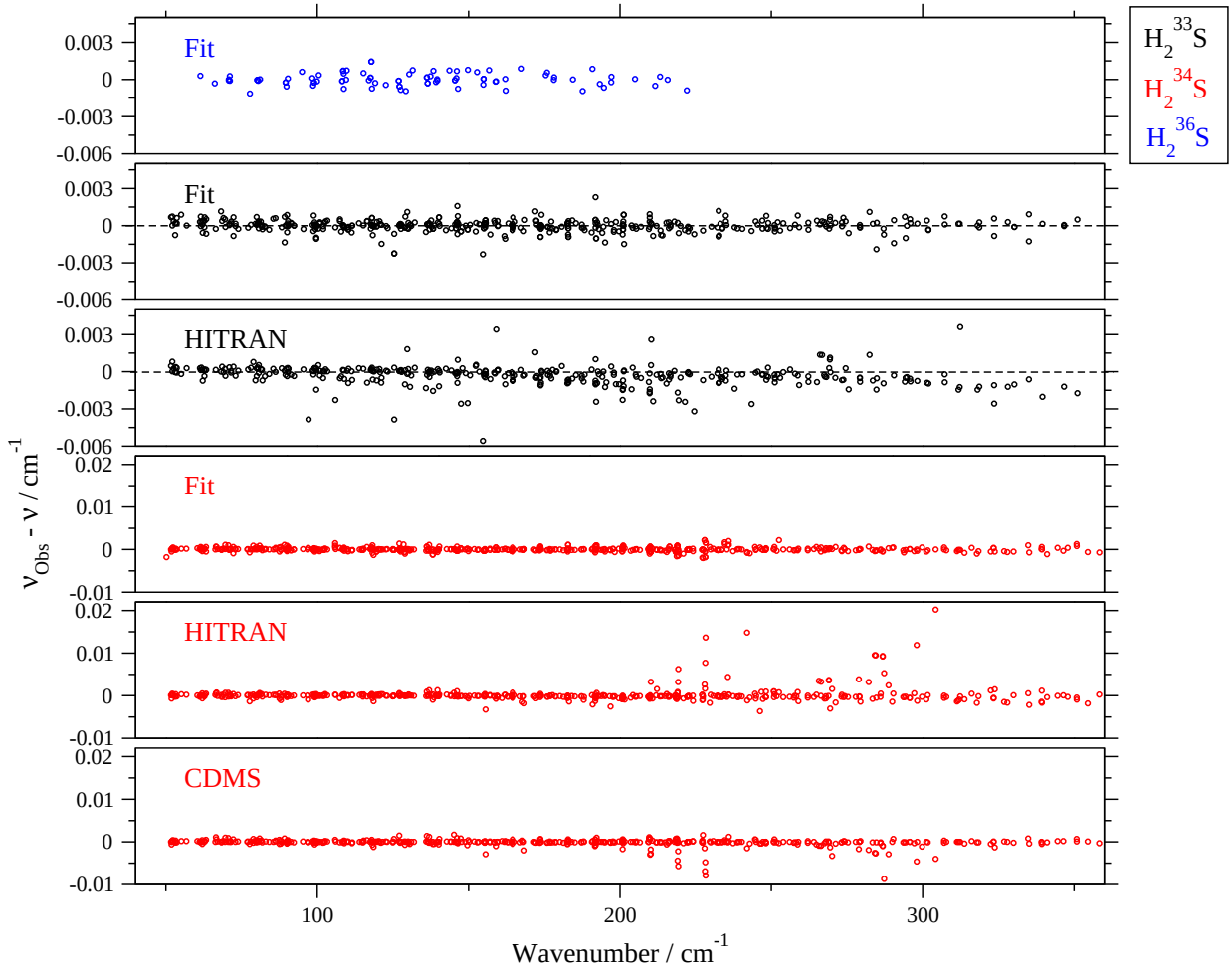

Figure 6.9: Accuracy of the ground vibrational state rotational transitions of $H_2{}^{33}S$ and $H_2{}^{34}S$ in our fit, HITRAN 2008 [Rothman et al. [2009]] and CDMS [Müller et al. [2001]] compared to our measurements. $\nu_{\mathrm{Obs}} - \nu$ are given as our observed frequency minus our fit, HITRAN 2008 and CDMS. Note the plots for $H_2{}^{34}S$ are on a different vertical scale.

6.5.3 Rotational transitions in the bending vibrational state $v_2 = 1$ of $H_2{}^{32}S$ and $H_2{}^{34}S$

We were able to initially assign 214 pure rotational transitions associated with the vibrational state $v_2 = 1$ of $H_2{}^{32}S$ covering energy levels up to $J = 20$ and $K_a = 14$ using the variationally calculated line list. Then 181 experimental energy levels up to $J \leq 17$ and $K_a \leq 10$ from Ulenikov et al. [1996a] were used to calculate 759 rotational transitions in the first excited bending state for $H_2{}^{32}S$. 559 of these calculated transitions are in the region 45 – 360 cm^{-1}. The calculations were performed using the combination differences method. As a result, 216 transitions could be matched to transitions in our spectrum with the standard deviation of 0.0004 cm^{-1}. Eight lines were found to have much higher errors in their calculated positions (all the values of these errors are close to 0.3 cm^{-1}). All of these lines belong to the energy levels $12_{2,11}$ and $12_{1,11}$, and all the calculated transitions involving these energy levels showed the same problem during the fit. We suspect this is a typographical problem in the corresponding table of Ulenikov et al. [1996a]. However these transitions were excluded from the fit; they are tabulated in Table 6.8. Our spectrum contains 104 transitions that cannot be calculated from Ulenikov *et al.*'s experimental energy levels. These new recorded transitions have quantum numbers up to $J = 22$ and $K_a = 13$ and these lines are given in Table 6.9. Fig. 6.10 shows the accuracy of the fit performed in this work for $H_2{}^{32}S$ rotational spectrum in the $v_2 = 1$ state as well as the calculated rotational transitions using the experimental energy levels of Ulenikov et al. [1996a] and the variationally calculated line list of Chapter 5.

For $H_2{}^{34}S$, 240 rotational transitions up to $J = 12$ and $K_a = 7$ were calculated using the 80 experimental energy levels published by Ulenikov et al. [1996a]. 177 lines of these calculated transitions are in the region 45 – 360 cm^{-1}. 42 lines could be assigned in our spectrum using these calculated transitions for $J \leq 10$ and $K_a \leq 6$. After fitting the effective Hamiltonian constants, 44 extra lines were assigned up to $J = 14$ and $K_a = 10$. These new transitions are listed in Table 6.10. Fig. 6.10 shows the accuracy of the fit for $H_2{}^{34}S$ pure rotational spectrum in the $v_2 = 1$ state and the calculated pure rotational transitions using the experimental energy levels of Ulenikov et al. [1996a].

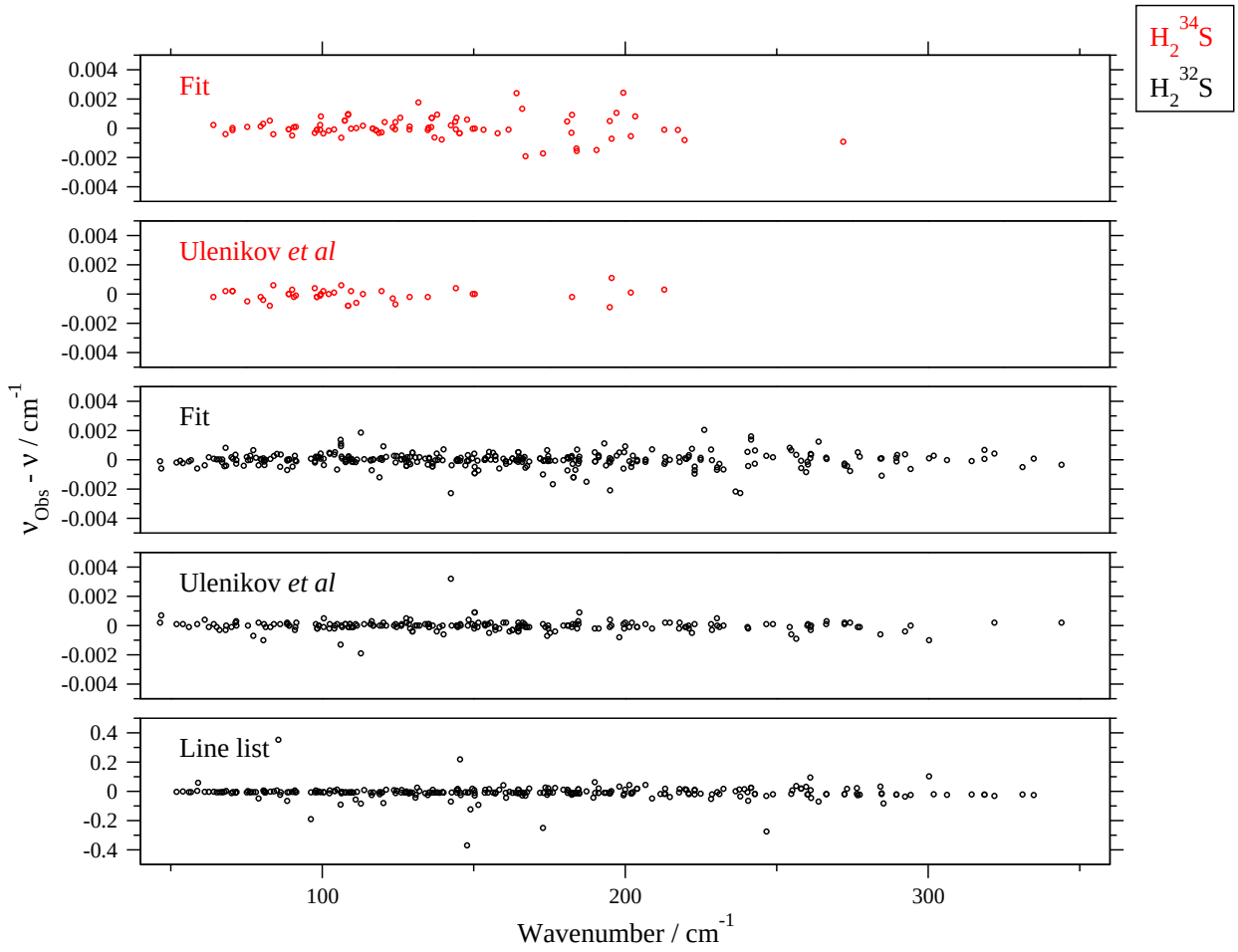

Figure 6.10: Accuracy of the first bending vibrational state pure rotational transitions of $H_2{}^{32}S$ and $H_2{}^{34}S$ in our fit, and the transitions calculated from the experimental energy levels published by Ulenikov et al. [1996a] compared to our measurements. Also the variational calculations from Chapter 5 compared to our measurements for $H_2{}^{32}S$. $\nu_{\mathrm{Obs}} - \nu$ given as our observed frequency minus our fit, Ulenikov *et al.*'s transitions, and the variational calculations. Note the reduced scale for the line list.

Table 6.8: Ulenikov et al. [1996a]'s transitions with high errors in their positions.

$J'_{K_a,K_c} - J''_{K_a,K_c}$	ν_{Exp}	ν_{Fit}	ν_{Ule}	$\Delta_{Exp-Fit}$	$\Delta_{Exp-Ule}$
$12_{2,10} - 12_{1,11}$	107.69932	107.69946	107.39941	-0.00014	0.29991
$12_{3,10} - 12_{2,11}$	107.69932	107.69948	107.39941	-0.00016	0.29991
$12_{1,11} - 12_{0,12}$	119.46226	119.46213	119.76208	0.00012	-0.29982
$12_{2,11} - 12_{1,12}$	119.46226	119.46213	119.76208	0.00012	-0.29982
$12_{1,11} - 11_{2,10}$	127.16366	127.16360	127.46338	0.00005	-0.29972
$12_{2,11} - 11_{1,10}$	127.16366	127.16360	127.46338	0.00005	-0.29972
$13_{1,12} - 12_{2,11}$	136.37118	136.37164	136.07178	-0.00046	0.29940
$13_{2,12} - 12_{1,11}$	136.37118	136.37164	136.07178	-0.00046	0.29940

Fig. 1.1 shows a portion of the assigned spectrum which includes transitions for the four isotopologues of H_2S with the same quantum numbers and some pure rotational $v_2 = 1$ transitions of $H_2{}^{32}S$ and $H_2{}^{34}S$. Also, Fig. 6.11 gives a good idea about the number of the transitions resulting from this work compared to the available data in HITRAN 2008 [Rothman et al. [2009]].

As a conclusion, a total of 11 830 transitions belong to the ground and the first vibrational states of $H_2{}^{32}S$ and $H_2{}^{34}S$ as well as transitions belong to the ground state of $H_2{}^{33}S$ and $H_2{}^{36}S$ were obtained as a result of this experiment. This number of transitions replaced 3400 transitions belonging to the ground vibrational states of $H_2{}^{32}S$, $H_2{}^{33}S$ and $H_2{}^{34}S$ which were in HITRAN 2008.

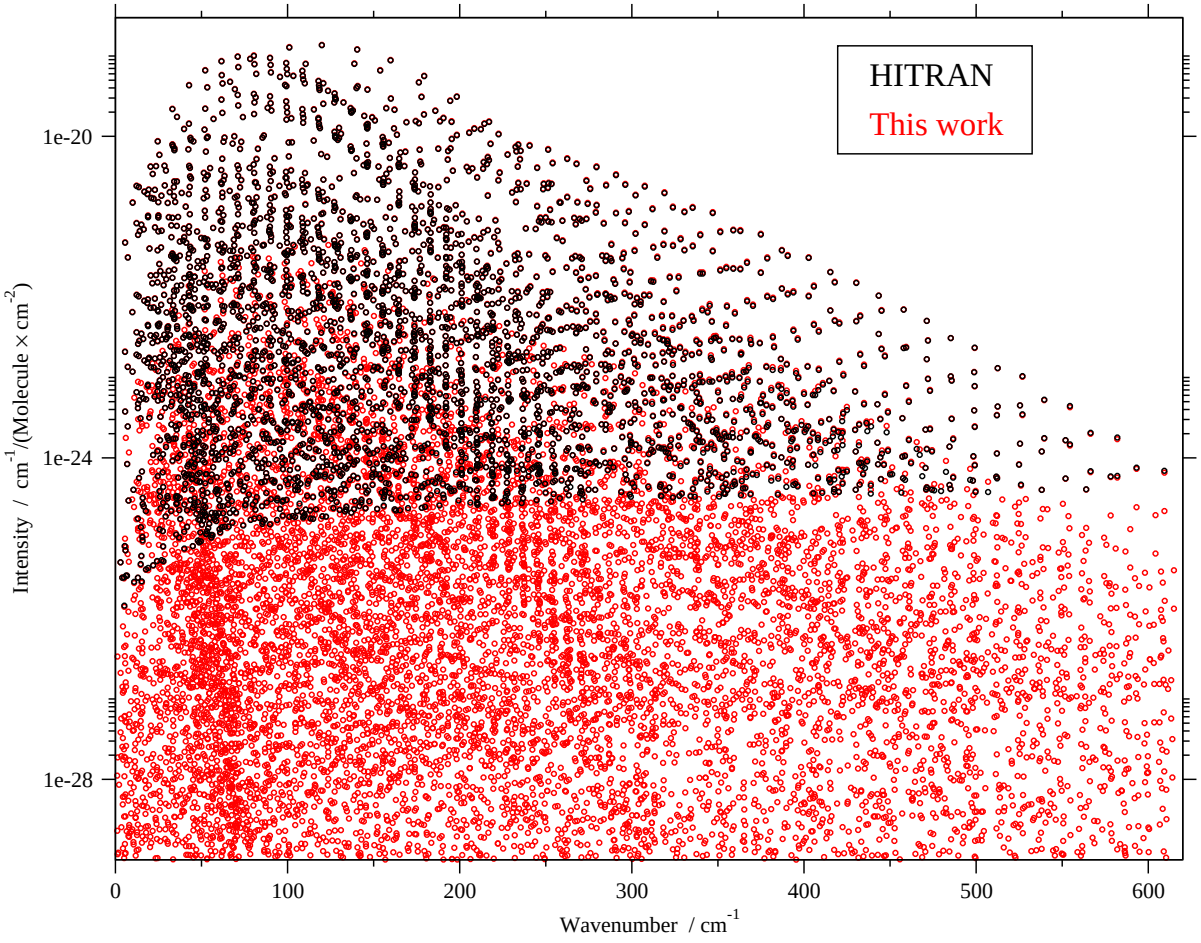

Figure 6.11: Results of this work compared to the data available in HITRAN 2008 [Rothman et al. [2009]] for the rotational region of H_2S spectrum.

Table 6.9: Observed pure rotational transitions for $H_2{}^{32}S$ within its first excited state which could not be calculated from the experimental energy levels given by Ulenikov et al. [1996a]. ν in cm^{-1} with experimental uncertainty 0.0005 cm^{-1}.

$J'_{K_a,K_c} - J''_{K_a,K_c}$	ν_{Exp}	$J'_{K_a,K_c} - J''_{K_a,K_c}$	ν_{Exp}	$J'_{K_a,K_c} - J''_{K_a,K_c}$	ν_{Exp}
$18_{13,5} - 18_{12,6}$	53.14814	$12_{3,10} - 11_{2,9}$	137.27563	$17_{4,13} - 16_{5,12}$	202.00327
$7_{2,5} - 7_{1,6}$	56.66191	$11_{3,8} - 10_{4,7}$	138.13373	$16_{6,11} - 15_{5,10}$	202.52251
$8_{2,6} - 8_{1,7}$	66.98295	$12_{4,9} - 11_{3,8}$	147.25325	$22_{2,20} - 22_{1,21}$	206.70169
$8_{3,6} - 8_{2,7}$	66.99451	$18_{13,5} - 18_{10,8}$	147.81527	$22_{3,20} - 22_{2,21}$	206.70169
$7_{2,6} - 7_{1,7}$	67.72515	$13_{3,10} - 12_{4,9}$	156.34953	$8_{3,5} - 7_{2,6}$	212.94106
$7_{0,7} - 6_{1,6}$	70.50716	$16_{1,15} - 16_{0,16}$	160.56175	$8_{4,5} - 7_{1,6}$	213.18393
$17_{9,8} - 17_{8,9}$	74.08741	$16_{2,15} - 16_{1,16}$	160.56175	$11_{11,1} - 10_{10,0}$	222.93073
$11_{4,7} - 11_{3,8}$	75.08725	$16_{1,15} - 15_{2,14}$	163.88423	$11_{11,0} - 10_{10,1}$	222.94486
$10_{3,7} - 10_{2,8}$	76.23482	$16_{2,15} - 15_{1,14}$	163.88423	$8_{2,6} - 7_{1,7}$	224.89184
$10_{4,7} - 10_{3,8}$	76.24727	$14_{4,11} - 13_{3,10}$	165.43067	$8_{3,6} - 7_{0,7}$	224.90367
$8_{2,7} - 8_{1,8}$	78.10829	$13_{5,9} - 12_{4,8}$	166.17447	$13_{9,5} - 12_{8,4}$	226.07196
$8_{0,8} - 7_{1,7}$	79.80092	$18_{0,18} - 17_{1,17}$	171.89444	$12_{10,2} - 11_{9,3}$	236.40391
$8_{1,8} - 7_{0,7}$	79.80092	$18_{1,18} - 17_{0,17}$	171.89444	$12_{9,3} - 11_{8,4}$	237.97054
$7_{1,6} - 6_{2,5}$	80.90541	$17_{1,16} - 16_{2,15}$	173.01350	$12_{12,1} - 11_{11,0}$	241.52392
$7_{2,6} - 6_{1,5}$	80.91698	$17_{2,16} - 16_{1,15}$	173.01350	$12_{12,0} - 11_{11,1}$	241.53067
$12_{5,8} - 12_{4,9}$	85.03784	$15_{3,12} - 14_{4,11}$	174.49161	$9_{3,6} - 8_{2,7}$	242.76797
$11_{3,8} - 11_{2,9}$	86.28734	$13_{6,8} - 12_{5,7}$	176.10799	$9_{4,6} - 8_{1,7}$	242.82469
$8_{2,7} - 7_{1,6}$	90.18470	$19_{0,19} - 18_{1,18}$	180.98948	$13_{12,2} - 12_{11,1}$	258.00707
$12_{4,9} - 12_{3,10}$	96.26502	$19_{1,19} - 18_{0,18}$	180.98948	$13_{12,1} - 12_{11,2}$	258.08982
$11_{2,9} - 11_{1,10}$	97.58732	$18_{1,17} - 17_{2,16}$	182.12004	$13_{13,0} - 12_{12,1}$	259.69516
$11_{3,9} - 11_{2,10}$	97.58732	$18_{2,17} - 17_{1,16}$	182.12004	$13_{9,4} - 12_{8,5}$	263.81547
$9_{1,8} - 8_{2,7}$	99.44812	$17_{2,15} - 16_{3,14}$	182.90597	$14_{12,3} - 13_{11,2}$	273.22297
$9_{2,8} - 8_{1,7}$	99.44812	$17_{3,15} - 16_{2,14}$	182.90597	$10_{3,8} - 9_{0,9}$	284.60560
$13_{3,10} - 13_{2,11}$	106.17405	$16_{3,13} - 15_{4,12}$	183.53117	$12_{8,5} - 11_{5,6}$	284.63071
$13_{4,10} - 13_{3,11}$	106.17405	$14_{5,9} - 13_{6,8}$	184.79970	$11_{4,7} - 10_{3,8}$	289.46793
$12_{2,10} - 12_{1,11}$	107.69932	$13_{7,7} - 12_{6,6}$	187.20577	$11_{5,7} - 10_{2,8}$	289.52163
$12_{3,10} - 12_{2,11}$	107.69932	$20_{0,20} - 19_{1,19}$	190.05844	$16_{7,10} - 17_{2,15}$	289.77205
$10_{3,8} - 9_{2,7}$	118.89904	$20_{1,20} - 19_{0,19}$	190.05844	$11_{3,8} - 10_{2,9}$	301.81395
$12_{1,11} - 12_{0,12}$	119.46226	$19_{1,18} - 18_{2,17}$	191.20186	$12_{6,7} - 11_{3,8}$	306.20219
$12_{2,11} - 12_{1,12}$	119.46226	$19_{2,18} - 18_{1,17}$	191.20186	$11_{2,9} - 10_{1,10}$	314.34565
$12_{1,11} - 11_{2,10}$	127.16366	$16_{5,12} - 15_{4,11}$	193.07653	$12_{4,8} - 11_{3,9}$	318.56487
$12_{2,11} - 11_{1,10}$	127.16366	$15_{5,10} - 14_{6,9}$	193.67254	$12_{5,8} - 11_{2,9}$	318.57811
$11_{2,9} - 10_{3,8}$	128.09393	$17_{13,4} - 16_{14,3}$	194.71717	$12_{4,9} - 11_{1,10}$	331.12752
$13_{1,12} - 12_{2,11}$	136.37118	$14_{7,8} - 13_{6,7}$	194.98412	$13_{5,8} - 12_{4,9}$	334.81627
$13_{2,12} - 12_{1,11}$	136.37118	$17_{13,5} - 17_{10,8}$	197.17199		

Table 6.10: Observed pure rotational transitions for $H_2{}^{34}S$ within its first excited state which could not be calculated from the experimental energy levels given by Ulenikov et al. [1996a]. ν in cm^{-1} with experimental uncertainty 0.0005 cm^{-1}.

$J'_{K_a,K_c} - J''_{K_a,K_c}$	ν_{Exp}	$J'_{K_a,K_c} - J''_{K_a,K_c}$	ν_{Exp}	$J'_{K_a,K_c} - J''_{K_a,K_c}$	ν_{Exp}
$11_{0,11} - 10_{1,10}$	107.43859	$13_{1,12} - 12_{2,11}$	136.15316	$8_{6,2} - 7_{5,3}$	165.98091
$11_{1,11} - 10_{0,10}$	107.43859	$13_{2,12} - 12_{1,11}$	136.15316	$7_{4,3} - 6_{3,4}$	167.07324
$12_{0,12} - 11_{1,11}$	116.66414	$12_{3,10} - 11_{2,9}$	137.05420	$10_{7,4} - 9_{6,3}$	172.85625
$12_{1,12} - 11_{0,11}$	116.66414	$11_{3,8} - 10_{4,7}$	137.91002	$9_{8,1} - 8_{7,2}$	180.83790
$11_{1,10} - 10_{2,9}$	117.74931	$10_{5,6} - 9_{4,5}$	139.44386	$9_{7,2} - 8_{6,3}$	182.23421
$11_{2,10} - 10_{1,9}$	117.74931	$7_{6,1} - 6_{5,2}$	142.46327	$9_{9,1} - 8_{8,0}$	183.90218
$10_{3,8} - 9_{2,7}$	118.70724	$7_{7,1} - 6_{6,0}$	143.92239	$9_{9,0} - 8_{8,1}$	183.98236
$7_{5,3} - 6_{4,2}$	120.59951	$7_{7,0} - 6_{6,1}$	144.32222	$10_{8,3} - 9_{7,2}$	190.51599
$6_{5,1} - 5_{4,2}$	124.05992	$14_{1,13} - 13_{2,12}$	145.32901	$11_{8,4} - 10_{7,3}$	197.12716
$8_{5,4} - 7_{4,3}$	125.74395	$14_{2,13} - 13_{1,12}$	145.32901	$10_{9,2} - 9_{8,1}$	199.38309
$10_{3,7} - 9_{4,6}$	128.78265	$11_{4,7} - 10_{5,6}$	147.81527	$10_{10,1} - 9_{9,0}$	203.31012
$9_{5,5} - 8_{4,4}$	131.72809	$10_{6,5} - 9_{5,4}$	153.24732	$11_{9,2} - 10_{8,3}$	217.39152
$14_{0,14} - 13_{1,13}$	135.06398	$8_{7,2} - 7_{6,1}$	157.88621	$11_{10,1} - 10_{9,2}$	219.59657
$14_{1,14} - 13_{0,13}$	135.06398	$8_{7,1} - 7_{6,2}$	161.47090	$10_{3,7} - 9_{2,8}$	271.96085
$7_{6,2} - 6_{5,1}$	135.98157	$8_{8,1} - 7_{7,0}$	164.12064		

Chapter 7

Conclusions

The ATY2013 line list for $H_2{}^{32}S$ was calculated covering the wavenumber region up to 9000 cm^{-1} and a temperature range up to 2000 K for the rotational quantum number up to $J = 40$ using DVR3D program suite [Tennyson et al. [1995]]. The computational parameters for DVR3D were optimised and the tests for energy levels convergence were performed up to the rotational quantum number $J = 50$. Four PESs were tested and the best surface among them (PES-Y0125) was refined from the previously published surface by Tyuterev et al. [2001]. This surface predicts experimentally known energy levels with $J \leq 10$ with a standard deviation of 0.11 cm^{-1} compared to 0.23 cm^{-1} using Tyuterev *et al.*'s surface for the same set of data. Calculations show that using PES-Y0125, around 7.3% of the ro-vibrational energy level values have errors more than 0.25 cm^{-1} for J from 0 to 5 when compared to the experimental values. All of these levels lie above 12 450 cm^{-1}. 26% of the values have this error for $J = 10$, all of them above 8600 cm^{-1}.

Several new *ab initio* dipole moment surfaces of H_2S were calculated using a variety of theoretical procedures as implemented in MOLPRO software package [Werner et al. [2012]]. The core and relativistic corrections give significant contributions to the calculations which, in contrast to the water molecule where they are found to approximately cancel out, cannot be neglected. Comparisons of calculated transition intensities with those available in HITRAN 2008 for 14 vibrational bands show that while the fundamental bands are all very sensitive to the method used in the calculations, the hot, overtone and combination bands

below 4000 cm^{-1} are not. Our best dipole moment surface (ALYT2013) was constructed using CCSD(T)/aug-cc-pV(6+d)Z with added core and the relativistic corrections. Using the ALYT2013 surface the ν_2 band is still 16 % too strong; this is in contrast to the DMS of water LTP2011, which has been shown to reproduce a variety of observed intensities to about 1 % [Grechko et al. [2012]; Lodi et al. [2011]]. This consideration bears testimony to the difficulties of accurately modelling H_2S line intensities. As mentioned in Chapter 4, ALYT2013 was found to be incomplete in the region 5000 – 10 000 cm^{-1}, we are working on the improvement.

At room temperature ATY2013 line list contains around 5×10^5 transitions up to $J = 40$ with cut off intensity of order 10^{-31} $cm^{-1}/(molecule \times cm^{-2})$ comparing to 2.8×10^4 transitions available in the databases up to 9000 cm^{-1}. Comprehensive comparisons were made to the experimental available data. The standard deviation of the absolute error for the transition positions is about 0.066 cm^{-1} from an average of 0.060 cm^{-1}, where 82 % of the transitions with absolute error in their positions $<$ 0.1 cm^{-1}. The standard deviation of the ratios of the calculated intensities to the transition intensities available in the databases is 1.08 from an average of 1.02, where 83 % of the transition intensities within 20 % of error. Our analysis suggested problems in some experimentally predicted transitions in the region below about 4500 cm^{-1}, some of them with problems in their predicted positions, some in their predicted intensities and some have problems in both. ATY2013 is expected to be reliable up to 2000 K, where it contains 36×10^6 transitions. ATY2013 is the first line list which gives predictions for hot spectra of $H_2{}^{32}S$ molecule up to 2000 K as far as we know. ATY2013 is expected to be useful for identifying H_2S in the space and for atmospheric modelling. ATY2013 can be useful also to be used for identifying H_2S in the lab, which already has been tested since ATY2013 was used to identify hot transitions for H_2S in the rotational band for experimental room temperature spectrum.

Pure rotational transitions of H_2S in its ground and first excited vibrational states were recorded at room temperature. The spectrum comprises an average of 1020 scans at 0.005 cm^{-1} resolution recorded in the region 45 to 360 cm^{-1} (1.4 to 10.5 THz) with a globar continuum source using a Fourier transform spectrometer located at the AILES beamline of the SOLEIL synchrotron. Over

2400 rotational lines have been detected belonging to ground vibrational state transitions of the four isotopologues $H_2{}^{32}S$, $H_2{}^{33}S$, $H_2{}^{34}S$, and $H_2{}^{36}S$ observed in natural abundance. 65% of these lines were recorded and assigned for the first time, sampling levels as high as $J = 26$ and $K_a = 17$ for $H_2{}^{32}S$. 320 pure rotational transitions of $H_2{}^{32}S$ in its first excited bending vibrational state were recorded and analysed for the first time and 86 transitions for $H_2{}^{34}S$, where some of these transitions belong to new experimental energy levels. The hot pure rotational transitions for $H_2{}^{32}S$ were identified initially using ATY2013 line list. Rotational constants were fitted for all of the isotopologues in both vibrational states using a standard effective Hamiltonian approach. Comprehensive comparisons were made with previously available data as well as the data available in HITRAN, CDMS, and JPL databases. The 91 transitions assigned to $H_2{}^{36}S$ give the first proper characterisation of its pure rotational spectrum. Our new data was submitted for inclusion in the 2012 update of the HITRAN database [Rothman et al. [2013]].

In different places in the space not more than one transition was used to identify the existence of H_2S. Here we give some examples and compare the used transitions for H_2S detection in space by the calculated transitions in our line list ATY2013. H_2S was observed in the ISM via the lowest frequency 1_{10}–1_{01} transition at 168.763 GHz (5.6293 cm^{-1}) by Thaddeus et al. [1972a]. Minh et al. [1989] detected interstellar hydrogen sulphide toward the cold, dark clouds L134N and TMC 1 by observing this transition. Also, the same transition was used for H_2S detection towards the central parts of the starburst galaxy M82 by Aladro et al. [2011]. In our calculation the transition 1_{10}–1_{01} has the frequency value 5.6292 cm^{-1}. Justtanont et al. [2012] detected a H_2S line in AFGL 5379 at 1196.010 GHz (39.8946 cm^{-1}), and this line was attributed to the 3_{12}–2_{21} transition. The calculated value for this transition in our line list is 39.8948 cm^{-1}. The 2_{20}–2_{11} transition at 217 GHz (7.2383 cm^{-1}) was detected during OVRO spectral survey of Orion A by Sutton et al. [1985], this transition has the value of 7.2285 cm^{-1} in our calculated line list.

For future work, the ATY2013 line list provides an important resource for atmospheric modelling of extrasolar planets and cool stars. this line list can be used for identifying H_2S transitions in the exoplanets and brown dwarfs atmospheres. for identifying new transitions in the laboratory spectra at high temperatures.

Also, it can be useful for analysing new unmeasured bands at room temperature. For instance, our calculations show some new features in the spectral regions 13 500 – 14 000 cm^{-1} and 14 500 – 16 000 cm^{-1}, see Fig. 1.2, as far as we know there are no measurements cover these two regions. Besides, extending the *ab initio* DMS calculations up to geometries covering the energy range above 10 000 cm^{-1} should be the next step for improving the ATY2013 line list.

The variationally calculated line list for H_2S at temperature (T) = 296 K and partition function (Q) = 503.07 with transition frequancies $\leq$ 9500 cm^{-1}, $J \leq 40$ and cut off intensity 10^{-30} cm^{-1}/(molecule *times* cm^{-2}) is available on ExoMole website (www.exomol.com). Also on the same website, files containing the experimantaly measured pure rotational transitions, the fitted constants and the correlation matrices for the four isotopologues of H_2S are available.

Appendix A

Table 1 contains the coefficients of the potential energy function (χ_{skm}) for Eq. (3.6), and the constants B_i and g_i in Eq. (3.5) for PES-Y0125. The following tables contain the coefficients $Q^{(l)}_{jk...}$ and $P^{(l)}_{jk...}$ of all the dipole moment surfaces presented in Chapter 4.

Table 1: Parameters of the potential energy surface for the ground electronic state of the hydrogen sulphide molecule, see Eq. (3.4). Note: powers of ten in parenthesis.

s	k	m	cm^{-1}	s	k	m	cm^{-1}
0	0	0	0.00000000000000(00)	2	2	2	-0.29736603824162(04)
0	0	1	0.25298724728304(01)	3	0	3	-0.39068887749886(04)
1	0	0	0.76001446034650(01)	3	1	2	0.22707809418082(04)
0	0	2	0.19119869561968(05)	3	2	1	0.23793551966211(05)
1	0	1	-0.26337942369521(04)	3	3	0	-0.34932314882947(04)
1	1	0	-0.34641383728936(03)	4	0	2	0.85923207392547(03)
2	0	0	0.37146640335080(05)	4	1	1	-0.11327987267957(05)
0	0	3	0.10372456946123(04)	4	2	0	0.37668571305335(03)
1	0	2	-0.48366811961179(04)	5	0	1	-0.15953549707091(05)
1	1	1	0.31178979423415(04)	5	1	0	0.14890386471456(04)
2	0	1	-0.12711176182111(04)	6	0	0	0.51484402685677(03)
2	1	0	-0.18726215609860(03)	0	0	7	-0.54617014746870(04)
3	0	0	-0.11796148983875(04)	1	0	6	-0.69943515992635(02)
0	0	4	0.47473763424544(04)	1	1	5	0.17427705522754(04)
1	0	3	-0.13610350468586(04)	2	0	5	0.29147560120520(03)
1	1	2	0.29144380025635(04)	2	1	4	-0.33646004327917(04)
2	0	2	-0.50653357937930(04)	2	2	3	-0.11202273117182(04)
2	1	1	-0.11097146714230(04)	3	0	4	-0.38323335633188(03)
2	2	0	0.10375282984635(03)	3	1	3	0.26441151817245(04)
3	0	1	0.48047328722297(04)	3	2	2	0.19366049577246(04)
3	1	0	-0.14060018110572(03)	3	3	1	0.38175718811604(04)
4	0	0	0.22425353263397(04)	4	0	3	0.30778367811357(04)
0	0	5	0.17914500029660(04)	4	1	2	-0.26353881747532(04)
1	0	4	-0.98184202293571(03)	4	2	1	0.83999500575225(04)
1	1	3	0.61294305063749(02)	4	3	0	-0.52450951528119(04)
2	0	3	-0.27151696719548(04)	5	0	2	-0.34729416630406(03)
2	1	2	0.26119013667838(04)	5	1	1	-0.50050684462558(04)
2	2	1	-0.61703073530707(04)	5	2	0	-0.28211904320344(04)
3	0	2	-0.48833736184025(04)	6	0	1	-0.10580696087439(05)
3	1	1	0.10049289144454(04)	6	1	0	0.53782996209764(04)
3	2	0	0.28708061338852(03)	7	0	0	-0.99734750908249(03)
4	0	1	0.67852017509792(04)	0	0	8	-0.74046834718425(03)
4	1	0	-0.10489708631647(04)				
5	0	0	0.74727382498639(03)	HH-repulsion parameters			
0	0	6	0.20496523413380(04)	B_1			0.80000000000000(06)
1	0	5	0.24807517966824(03)	B_2			0.80000000000000(05)
1	1	4	-0.19578362789532(04)	g_1			0.13000000000000(02)
2	0	4	0.70166633265091(02)	g_2			0.55000000000000(01)
2	1	3	0.51823676755422(04)	N(parameters) = 71			

Table 2: p component parameters of the dipole moment surfaces, see Eq. (4.2), where r_e = 1.336 Å, $\theta_e = 92.2°$.The headers 1-5 are as illustrated in Table 4.1.

Parameter	1	2	3	4	5
$P_{10}{}^0$	0.004578269904	0.007433592402	0.000526532338	-0.001925930245	0.009519116730
$P_{10}{}^1$	-0.767250625148	-0.768667723274	-0.768386694956	-0.766396250284	-0.770580163881
$P_{20}{}^0$	-0.220498682151	-0.219527538075	-0.230391938843	-0.234460221465	-0.223531705501
$P_{10}{}^2$	0.216934387437	0.215385824559	0.213297538855	0.214420315054	0.216454287488
$P_{20}{}^1$	0.377895393006	0.376012380853	0.373790341518	0.378140536274	0.376909978312
$P_{21}{}^0$	-0.210829920495	-0.211576114406	-0.190376667363	-0.213048720998	-0.207711123180
$P_{30}{}^0$	-0.154121993471	-0.152431099480	-0.170794528939	-0.179464069184	-0.157794108451
$P_{10}{}^3$	-0.146420213360	-0.147605112805	-0.141479869492	-0.147372056708	-0.144438139588
$P_{20}{}^2$	-0.204561208725	-0.204904968783	-0.218339697712	-0.210299249329	-0.204863865509
$P_{21}{}^1$	-0.304577220746	-0.307174486613	-0.299591224935	-0.295231567381	-0.302512213344
$P_{30}{}^1$	-0.220018751147	-0.222088746467	-0.196799905210	-0.217152558736	-0.215560102452
$P_{31}{}^0$	0.064026127420	0.052262190953	0.155422278083	0.072222669156	0.061384337357
$P_{40}{}^0$	-0.360859250102	-0.360979231916	-0.476372462276	-0.435786000657	-0.347863927238
$P_{10}{}^4$	0.361434193998	0.361657054586	0.363186164739	0.364973444724	0.365171599445
$P_{20}{}^3$	0.101002950622	0.104426685526	0.118715612103	0.110343416675	0.105249711585
$P_{21}{}^2$	0.684700565165	0.676742975144	0.697187659876	0.694247156016	0.684451155546
$P_{30}{}^2$	-0.705985386199	-0.705998936105	-0.680696788187	-0.714119553943	-0.720138869483
$P_{31}{}^1$	-0.392497397752	-0.426757316867	-0.415114730049	-0.390610117866	-0.406861943450
$P_{32}{}^0$	0.239511396023	0.174789659144	0.358404993516	0.245447816124	0.443315592647
$P_{40}{}^1$	0.878746629258	0.899030306193	0.921373992495	0.846890845477	0.877386213908
$P_{41}{}^0$	-0.363814953626	-0.371397443256	-1.115286069870	-0.449866618785	-0.314179068704
$P_{50}{}^0$	-0.370323836945	-0.336419533849	-0.775830307449	-0.346961707952	-0.437048645006
$P_{10}{}^5$	-0.150736260981	-0.147088406261	-0.153602290611	-0.140356758270	-0.149958296581
$P_{20}{}^4$	-0.071267724976	-0.066734516383	-0.070171416612	-0.061817531733	-0.066053034803
$P_{21}{}^3$	0.573182692983	0.568443206888	0.714894713180	0.641816924049	0.584079157960
$P_{30}{}^3$	0.096544240828	0.088507605684	0.116615384784	0.117782969058	0.078414001838
$P_{31}{}^2$	0.432205524393	0.396613306774	0.453103240876	0.254106806017	0.450100684278
$P_{32}{}^1$	1.379608305840	1.325735379730	1.616097941010	2.184712239710	1.512204987840
$P_{40}{}^2$	-0.495587621239	-0.483871215638	-0.177876234790	-0.514020092451	-0.479373469976
$P_{41}{}^1$	-0.676356743138	-0.736831752250	-1.025190099380	-0.283345651592	-0.650741629104
$P_{42}{}^0$	0.000000000000	0.000000000000	0.000000000000	-0.616578727672	0.944493788444
$P_{50}{}^1$	-0.461380514826	-0.375954928680	-0.811690618296	-0.549378572771	-0.431359240380
$P_{51}{}^0$	0.264408165952	0.280246703216	-3.002764840780	-0.391978427686	0.423488148248
$P_{60}{}^0$	-1.647078192360	-1.572047175510	-2.101393465620	-1.252506584760	-2.180313412490

Table 3: q component parameters of the dipole moment surfaces, see Eq. (4.1), where r_e = 1.336 Å, $\theta_e = 92.2°$.. The headers 1-5 are as illustrated in Table 4.1.

Parameter	1	2	3	4	5
Q_{00}^{0}	0.971531847649	0.975055721821	0.970756135422	0.970408532909	0.986667559156
Q_{00}^{1}	-0.154924057447	-0.155443296413	-0.155646392903	-0.156233228009	-0.159075528430
Q_{10}^{0}	-0.010746115800	-0.007905260831	-0.014333534644	-0.016536788916	-0.000761639684
Q_{00}^{2}	0.630054334271	0.631008178734	0.628286370822	0.628145314780	0.639231762179
Q_{02}^{0}	0.469436311118	0.470794684693	0.462628113556	0.464432957790	0.468408331410
Q_{10}^{1}	-0.204717886409	-0.204303229541	-0.201272197276	-0.200049152567	-0.204503637623
Q_{20}^{0}	-0.148894639324	-0.148684414382	-0.159818055377	-0.159905658489	-0.151681596837
Q_{00}^{3}	0.157773776711	0.156932560270	0.156491890880	0.154499330625	0.156575597282
Q_{02}^{1}	-0.192023371119	-0.191060274751	-0.192998355161	-0.195226963835	-0.191061905050
Q_{10}^{2}	0.241698144933	0.239879454729	0.232930344736	0.246274176326	0.240298795971
Q_{12}^{0}	0.061339870937	0.062199819928	0.058564330509	0.051496972269	0.067547268397
Q_{20}^{1}	0.099393055188	0.099268884625	0.067473252534	0.104302343557	0.080018410758
Q_{30}^{0}	-0.198562672978	-0.194499385660	-0.230535520660	-0.206532609785	-0.191606149382
Q_{00}^{4}	0.530695044883	0.530781825496	0.524132108773	0.528830355686	0.534177579985
Q_{02}^{2}	0.089452727051	0.090309837462	0.095657785572	0.086303930632	0.091630106735
Q_{04}^{0}	-0.084110286414	-0.085737046809	-0.077903893548	-0.098470230156	-0.087791116616
Q_{10}^{3}	-0.379106156732	-0.379275992299	-0.359318241245	-0.394373153307	-0.397033877155
Q_{12}^{1}	-0.088169075771	-0.088869902976	0.000000000000	-0.059073706372	-0.116576510337
Q_{20}^{2}	0.103838147731	0.108584596828	0.000000000000	-0.028974535906	0.039131015840
Q_{22}^{0}	0.368771107629	0.372663290293	0.520060704014	0.369582053106	0.376691422716
Q_{30}^{1}	-0.204126514863	-0.210597054048	-0.344783401022	-0.305064042794	-0.266662922842
Q_{40}^{0}	-0.192743514166	-0.198279646036	-0.244483462565	-0.229686616779	-0.217393278382
Q_{00}^{5}	0.390666116918	0.390917138517	0.393566072564	0.394612481405	0.394029538611
Q_{02}^{3}	-0.088613249928	-0.089972405678	-0.084020291633	-0.085262461213	-0.087038200104
Q_{04}^{1}	0.855852087534	0.854007356651	0.827404942399	0.885325544953	0.841355995066
Q_{10}^{4}	-0.160976219833	-0.157890712275	-0.224281790313	-0.157034140704	-0.158299530481
Q_{12}^{2}	0.504567644239	0.501293985058	0.324404175980	0.502337858176	0.526177658560
Q_{14}^{0}	0.091351006953	0.115706470272	0.795963041177	0.093282511558	0.123882733631
Q_{20}^{3}	-0.837472208543	-0.841431092015	-0.973743587792	-0.892726640130	-0.847142426715
Q_{22}^{1}	-0.467625582398	-0.472605838180	0.185959993249	-0.493842517741	-0.499576403666
Q_{30}^{2}	0.131813336067	0.123329490518	2.488744049350	0.229536190027	0.387795676185
Q_{32}^{0}	0.305372824875	0.299650354007	0.395431914077	0.281603571504	0.311738563355
Q_{40}^{1}	0.000000000000	0.000000000000	0.679508118389	-0.094831206461	0.179500731394
Q_{50}^{0}	-0.717517334833	-0.728411533283	-0.526376127927	-1.017354183600	-0.861232833465
Q_{00}^{6}	0.736416272840	0.738257209826	0.756103007614	0.743253844301	0.742180004692
Q_{02}^{4}	0.054943748635	0.055920208444	0.105576827990	0.065983437672	0.052781728682
Q_{04}^{2}	-0.444393932346	-0.445403067070	-0.514587861315	-0.390434868501	-0.468601124986
Q_{06}^{0}	-0.680765293000	-0.674687997928	-0.766245471377	-0.674966494735	-0.674512972679
Q_{10}^{5}	0.261431249073	0.260206669957	-0.819435644002	0.220403702866	0.358430573419
Q_{12}^{3}	1.366989575240	1.416411245460	1.009051407500	1.748932431430	1.508223560180
Q_{14}^{1}	0.000000000000	0.000000000000	-0.848301052347	-0.035856979684	0.000000000000
Q_{20}^{4}	-0.157405719775	-0.122667817217	0.000000000000	0.120246167524	-0.109704748370
Q_{22}^{2}	0.425285840963	0.489216046563	5.105679276420	0.695609185741	0.787117764828
Q_{24}^{0}	2.579929846380	2.702559254080	14.056905989200	3.463377414050	3.451674077030
Q_{30}^{3}	-1.132634292980	-1.117625288520	-1.572930795920	-1.171654572820	-1.101968104310
Q_{32}^{1}	-1.310145055780	-1.322922038000	0.000000000000	-1.723694094900	-1.195408139380
Q_{40}^{2}	0.601388202430	0.560196321238	7.229893836890	2.161200231980	1.632096470770
Q_{42}^{0}	1.183496320760	1.178718066410	0.000000000000	0.941570062184	1.031829517570
Q_{50}^{1}	-1.386575418790	-1.323263270870	0.000000000000	-0.468305477483	-0.392747758730
Q_{60}^{0}	-0.663330471654	-0.637705630411	0.000000000000	-1.312131592320	-1.196615445330

Table 4: p component parameters of the dipole moment surfaces, see Eq. (4.2), where r_e = 1.336 Å, $\theta_e = 92.2°$.. The headers 6-10 are as illustrated in Table 4.1.

Parameter	6	7	8	9	10
$P_{10}{}^0$	0.010322070573	0.000963988387	0.012408935397	0.005610131352	0.008503205534
$P_{10}{}^1$	-0.771205244271	-0.768928792510	-0.773114742746	-0.772417952385	-0.774980775672
$P_{20}{}^0$	-0.216900807975	-0.231857411828	-0.220887423994	-0.226251775182	-0.223606764901
$P_{10}{}^2$	0.219608018059	0.218705251641	0.220712177411	0.221449231993	0.225705495427
$P_{20}{}^1$	0.363064865684	0.364976532459	0.363892922864	0.378614470993	0.365586702982
$P_{21}{}^0$	-0.211575456098	-0.212937799692	-0.207814406096	-0.215325804858	-0.214780139720
$P_{30}{}^0$	-0.143562971635	-0.170735652375	-0.149030879564	-0.156404800114	-0.147851687361
$P_{10}{}^3$	-0.147908984502	-0.147309217255	-0.144694143663	-0.144464451988	-0.144044243808
$P_{20}{}^2$	-0.194777317378	-0.199698981650	-0.194419524548	-0.207452422606	-0.197582940883
$P_{21}{}^1$	-0.296277724400	-0.284284419132	-0.290197033960	-0.308982976802	-0.298618916077
$P_{30}{}^1$	-0.219285629465	-0.217923062007	-0.212571894902	-0.217433661873	-0.215734813505
$P_{31}{}^0$	0.038008059553	0.055531787449	0.046089084060	0.045519391309	0.036528198699
$P_{40}{}^0$	-0.348594357507	-0.423289281257	-0.337669002855	-0.370167565449	-0.360562013826
$P_{10}{}^4$	0.363123921327	0.366750351077	0.366606191773	0.367295204148	0.368891934783
$P_{20}{}^3$	0.087298185132	0.096710534137	0.088611524187	0.098915053142	0.084191627566
$P_{21}{}^2$	0.681121130108	0.693904478806	0.690933307113	0.692186467961	0.688325944079
$P_{30}{}^2$	-0.684441833908	-0.703001655016	-0.700384319165	-0.710394236754	-0.695546164732
$P_{31}{}^1$	-0.461254815142	-0.406956884402	-0.439481732713	-0.438526734081	-0.453006274921
$P_{32}{}^0$	0.194930803277	0.265610607474	0.467386670098	0.189630118761	0.211900923342
$P_{40}{}^1$	0.905119159471	0.851021273827	0.882735528203	0.904003326148	0.906831376916
$P_{41}{}^0$	-0.290197848696	-0.365639555994	-0.228774966356	-0.382575275090	-0.306116137475
$P_{50}{}^0$	-0.476980965450	-0.480298392868	-0.576807002926	-0.334219032312	-0.467466280230
$P_{10}{}^5$	-0.146912234197	-0.141249660006	-0.150149657325	-0.153297147208	-0.154964213947
$P_{20}{}^4$	-0.057797042701	-0.047965970687	-0.057549656682	-0.063967750311	-0.051155270410
$P_{21}{}^3$	0.576146079873	0.622747276503	0.583924111560	0.609703150927	0.606759726717
$P_{30}{}^3$	0.076450404047	0.103502772405	0.067420062851	0.073345907688	0.052330200994
$P_{31}{}^2$	0.327909249180	0.269939932062	0.399749383044	0.381439953963	0.344304090443
$P_{32}{}^1$	1.250534722860	2.088707059220	1.465390528400	1.372486800910	1.295302899200
$P_{40}{}^2$	-0.428765902767	-0.489528146655	-0.433213734771	-0.461571337022	-0.396624371478
$P_{41}{}^1$	-0.934734467816	-0.444625408903	-0.849740453898	-0.724105148203	-0.886640031665
$P_{42}{}^0$	0.000000000000	-0.545497004231	1.053743071510	0.000000000000	0.000000000000
$P_{50}{}^1$	-0.387691553648	-0.511626525794	-0.460279720565	-0.417002544646	-0.439401904554
$P_{51}{}^0$	0.627302772268	0.000000000000	0.811114952425	0.329283645204	0.603863685929
$P_{60}{}^0$	-1.962363412070	-1.637704840350	-2.547067791660	-1.761791290770	-2.103981356700

Table 5: q component parameters of the dipole moment surfaces, see Eq. (4.1), where r_e = 1.336 Å, $\theta_e = 92.2°$.. The headers 6-10 are as illustrated in Table 4.1.

Parameter	6	7	8	9	10
$Q_{00}{}^{0}$	0.993128676714	0.988481474219	1.004740645260	0.992904659214	1.010978749640
$Q_{00}{}^{1}$	-0.162576177144	-0.163369077198	-0.166209660837	-0.165841693972	-0.172993745325
$Q_{10}{}^{0}$	0.001770037539	-0.006855277111	0.008910972432	-0.002407760923	0.007251403583
$Q_{00}{}^{2}$	0.643196749999	0.640275941805	0.651416903921	0.651400793158	0.663477581682
$Q_{02}{}^{0}$	0.466322916488	0.460038478653	0.463923587302	0.466664008585	0.462002798987
$Q_{10}{}^{1}$	-0.200628665599	-0.196163826601	-0.200769581981	-0.207328469408	-0.203843559597
$Q_{20}{}^{0}$	-0.147996788179	-0.159124320471	-0.151020661705	-0.155826786904	-0.155286417941
$Q_{00}{}^{3}$	0.156291571989	0.153930797417	0.155951762417	0.149702185463	0.149249839297
$Q_{02}{}^{1}$	-0.180710110522	-0.184955738256	-0.180678569224	-0.186740269710	-0.176188789974
$Q_{10}{}^{2}$	0.241713568633	0.248901860691	0.242121786389	0.242960688539	0.245880254423
$Q_{12}{}^{0}$	0.061082700110	0.049889474389	0.066442830107	0.064991679819	0.064758835369
$Q_{20}{}^{1}$	0.079507761936	0.085460611582	0.060589594825	0.096080001704	0.078134629452
$Q_{30}{}^{0}$	-0.194523147519	-0.207656148378	-0.191611934537	-0.189073221637	-0.188506427186
$Q_{00}{}^{4}$	0.537542204823	0.536298751170	0.540961498470	0.554215970268	0.561962109198
$Q_{02}{}^{2}$	0.085301813890	0.080954377515	0.086722185047	0.087796652378	0.084464692818
$Q_{04}{}^{0}$	-0.089768449271	-0.100568464130	-0.091231441901	-0.091925845469	-0.090770369156
$Q_{10}{}^{3}$	-0.380268958844	-0.395863933257	-0.397836338588	-0.387033640349	-0.383541942552
$Q_{12}{}^{1}$	-0.119547411691	-0.084977339804	-0.144917600338	-0.083563164378	-0.101796428894
$Q_{20}{}^{2}$	0.112855096839	-0.035941037802	0.045314553999	0.111361685939	0.132516712855
$Q_{22}{}^{0}$	0.366091329478	0.353118970142	0.369748086427	0.369968976370	0.369369085204
$Q_{30}{}^{1}$	-0.200007224160	-0.307122107927	-0.260971642542	-0.210586157733	-0.192365750026
$Q_{40}{}^{0}$	-0.200490148446	-0.237095761758	-0.218901555561	-0.215739112770	-0.215761852337
$Q_{00}{}^{5}$	0.392863139736	0.396367758652	0.395929908157	0.397310752872	0.398883887733
$Q_{02}{}^{3}$	-0.079334721369	-0.073347290072	-0.076458865441	-0.091588576245	-0.080765260333
$Q_{04}{}^{1}$	0.838957883584	0.867091981594	0.826255101239	0.870451450512	0.851753761752
$Q_{10}{}^{4}$	-0.178006858277	-0.173061338081	-0.178363221690	-0.154757793067	-0.176345351684
$Q_{12}{}^{2}$	0.495859829971	0.482497314792	0.519484871747	0.498368269142	0.479993374701
$Q_{14}{}^{0}$	0.171827901714	0.125667436915	0.181948088454	0.098431316336	0.136624831843
$Q_{20}{}^{3}$	-0.829156411703	-0.875652103717	-0.835489975742	-0.851773271035	-0.842870267504
$Q_{22}{}^{1}$	-0.447459698788	-0.476816503701	-0.474228091725	-0.473163222544	-0.467460732083
$Q_{30}{}^{2}$	0.238985666111	0.323204796240	0.485721397433	0.126377933500	0.228317850791
$Q_{32}{}^{0}$	0.302246734004	0.292532350361	0.312545922045	0.316714876708	0.300327902984
$Q_{40}{}^{1}$	0.167413349212	0.086099980194	0.354660582760	0.000000000000	0.132742219299
$Q_{50}{}^{0}$	-0.644630480002	-0.916276877016	-0.775127859528	-0.707369055235	-0.637225297177
$Q_{00}{}^{6}$	0.747695989919	0.750890168399	0.751561593219	0.730009002743	0.737357871636
$Q_{02}{}^{4}$	0.036930908227	0.048942014444	0.033640581295	0.065704357110	0.043722231572
$Q_{04}{}^{2}$	-0.450141963314	-0.401604470046	-0.475754468940	-0.455476261676	-0.472795768782
$Q_{06}{}^{0}$	-0.657954576228	-0.651361604356	-0.657274569487	-0.707132036203	-0.699418980284
$Q_{10}{}^{5}$	0.386018772852	0.305075044290	0.477712956796	0.279129415487	0.351475921230
$Q_{12}{}^{3}$	1.534465456990	1.800902850170	1.624677627330	1.370672488140	1.376697643060
$Q_{14}{}^{1}$	0.000000000000	0.000000000000	0.000000000000	0.000000000000	0.000000000000
$Q_{20}{}^{4}$	-0.088394690499	0.126900461822	-0.079504257036	-0.152529411366	-0.202851890535
$Q_{22}{}^{2}$	0.943472730745	1.022717131710	1.191625525550	0.464213215874	0.839349537967
$Q_{24}{}^{0}$	1.902770420330	2.907482095960	2.620298039860	2.764141508480	1.842628198110
$Q_{30}{}^{3}$	-1.095466638940	-1.130046884240	-1.088121628630	-1.182201424900	-1.222396406680
$Q_{32}{}^{1}$	-0.797493647988	-1.142111257580	-0.683686990407	-1.298156391490	-0.956249474325
$Q_{40}{}^{2}$	0.460679356811	2.274033062280	1.512660762480	0.673998854616	0.354839727469
$Q_{42}{}^{0}$	1.303710331360	1.210429538410	1.173551927950	1.158437000060	1.129472399890
$Q_{50}{}^{1}$	-1.067273116300	0.000000000000	0.000000000000	-1.273051518660	-1.116132863200
$Q_{60}{}^{0}$	-0.741706906581	-1.371383257870	-1.308813841180	-0.879007102168	-0.974970010235

Appendix B

Table 6: All the transitions with problems in positions and intensities in the polyad region 1. (powers of ten in parenthesis).

Vib. qun. #		Rot. qun. #						HITRAN		Our calculations			
upper	lower	upper			lower			Frequency	Intensity	Frequency	Intensity	$\lvert\nu_{Calc.} - \nu_{HITRAN}\rvert$	I_{Calc}/I_{HITRAN}
								(ν) cm^{-1}		(ν) cm^{-1}		cm^{-1}	
0 0 1	0 0 0	5	1	4	6	3	3	2339.344971	5.17(-24)	2340.833740	1.76(-27)	1.4888	3.41(-04)
0 0 1	0 0 0	6	1	6	5	1	5	2687.297119	1.90(-25)	2688.902832	6.66(-25)	1.6057	3.50(+00)
0 0 1	0 0 0	6	3	3	7	5	2	2334.693359	2.63(-23)	2332.399885	2.84(-25)	2.2935	1.08(-02)
0 0 1	0 0 0	7	1	7	6	1	6	2695.890381	8.47(-25)	2696.308594	2.38(-24)	0.4182	2.81(+00)
0 0 1	0 0 0	8	7	2	9	7	3	2338.359131	1.37(-24)	2336.270717	2.50(-25)	2.0884	1.82(-01)
0 0 1	0 0 0	9	6	4	10	6	5	2330.678223	5.62(-24)	2333.804490	4.44(-25)	3.1263	7.90(-02)
0 0 1	0 0 0	12	4	8	13	4	9	2433.326172	7.33(-25)	2432.062500	1.95(-25)	1.2637	2.65(-01)
0 0 1	0 0 0	12	9	3	13	7	6	2331.628174	2.07(-25)	2329.943848	7.56(-25)	1.6843	3.65(+00)
0 0 1	0 0 0	16	1	15	16	3	14	2331.515625	3.70(-25)	2328.724607	9.26(-28)	2.7910	2.50(-03)
0 0 1	0 0 0	16	2	15	16	2	14	2331.515625	1.23(-25)	2329.735107	3.06(-28)	1.7805	2.48(-03)
0 2 0	0 0 0	6	6	1	6	3	4	2332.512695	4.12(-25)	2333.043945	1.10(-25)	0.5313	2.67(-01)
0 2 0	0 0 0	7	3	4	6	4	3	2332.150391	5.35(-23)	2331.378174	9.74(-28)	0.7722	1.82(-05)
0 2 0	0 0 0	7	4	3	6	5	2	2336.127441	1.86(-23)	2340.327989	2.76(-28)	4.2005	1.48(-05)
0 2 0	0 0 0	7	4	4	6	3	3	2336.222900	2.09(-23)	2336.941650	8.01(-28)	0.7188	3.83(-05)
0 2 0	0 0 0	9	4	5	9	5	4	2333.036865	4.26(-24)	2331.616943	9.13(-27)	1.4199	2.14(-03)
0 2 0	0 0 0	9	4	5	10	5	6	2233.627441	3.25(-24)	2230.764102	2.43(-25)	2.8633	7.47(-02)
0 2 0	0 0 0	9	6	4	10	5	5	2233.564209	5.61(-25)	2231.075679	1.19(-25)	2.4885	2.12(-01)
0 2 0	0 0 0	11	2	10	10	1	9	2338.459229	9.11(-24)	2339.003906	3.62(-28)	0.5447	3.97(-05)
0 2 0	0 0 0	12	8	4	12	7	5	2433.573730	4.76(-25)	2432.067139	2.51(-26)	1.5066	5.30(-02)
0 2 0	0 0 0	12	10	2	12	9	3	2332.709229	3.05(-25)	2331.066895	4.06(-28)	1.6423	1.33(-03)
0 2 0	0 0 0	13	7	6	13	6	7	2336.806641	7.89(-25)	2336.157471	1.19(-27)	0.6492	1.51(-03)
0 2 0	0 0 0	16	2	14	15	3	13	2533.902588	2.79(-25)	2532.512695	2.46(-28)	1.3899	1.00(-03)
0 2 0	0 0 0	16	3	14	15	2	13	2533.902588	8.38(-25)	2532.512695	2.46(-28)	1.3899	2.93(-04)
0 3 0	0 1 0	4	3	2	3	0	3	2433.498779	1.51(-25)	2432.138672	1.20(-27)	1.3601	7.97(-03)
0 3 0	0 1 0	6	5	1	5	4	2	2339.141113	3.47(-25)	2337.550537	3.20(-26)	1.5906	9.20(-02)
0 3 0	0 1 0	7	5	3	6	4	2	2339.419189	1.91(-25)	2340.327881	2.76(-28)	0.9087	1.44(-03)
0 3 0	0 1 0	9	3	6	8	4	5	2338.429443	3.17(-25)	2340.185791	8.48(-28)	1.7563	2.67(-03)
0 3 0	0 1 0	9	4	6	8	3	5	2338.771240	1.07(-25)	2340.185791	8.48(-28)	1.4146	7.92(-03)
1 0 0	0 0 0	5	3	3	6	4	2	2339.716553	4.97(-25)	2340.833740	1.76(-27)	1.1172	3.54(-03)
1 0 0	0 0 0	7	7	1	8	8	0	2433.101318	1.54(-24)	2433.440186	1.19(-23)	0.3389	7.73(+00)
1 0 0	0 0 0	7	7	0	6	6	1	2733.503662	2.02(-22)	2734.030273	5.30(-23)	0.5266	2.62(-01)
1 0 0	0 0 0	8	5	4	9	4	5	2338.096924	1.06(-25)	2336.270752	2.50(-25)	1.8262	2.35(+00)
1 0 0	0 0 0	10	8	2	11	7	5	2339.953613	1.46(-25)	2340.795166	3.79(-26)	0.8416	2.60(-01)
1 0 0	0 0 0	11	1	10	12	2	11	2335.299072	2.89(-25)	2334.651855	1.79(-26)	0.6472	6.20(-02)
1 0 0	0 0 0	11	2	10	12	1	11	2335.298828	9.62(-26)	2334.651855	1.79(-26)	0.6470	1.86(-01)
1 0 0	0 0 0	12	0	12	13	1	13	2335.307129	1.04(-25)	2334.640137	4.33(-25)	0.6670	4.16(+00)
1 0 0	0 0 0	13	7	6	13	6	7	2633.861084	1.38(-24)	2632.537598	4.54(-27)	1.3235	3.00(-03)

Table 7: All the transitions with problems in intensities in the polyad region 1. (powers of ten in parenthesis).

Vib. qun. #		Rot. qun. #						HITRAN		Our calculations			
upper	lower	upper			lower			Frequency	Intensity	Frequency	Intensity	$\lvert\nu_{Calc.}-\nu_{HITRAN}\rvert$	I_{Calc}/I_{HITRAN}
								(ν) cm^{-1}		(ν) cm^{-1}		cm^{-1}	
0 0 1	0 0 0	0	0	0	1	0	1	2614.707764	1.45(-24)	2614.717041	6.47(-25)	0.0093	4.45(-01)
0 0 1	0 0 0	1	0	1	2	0	2	2604.052734	7.81(-25)	2604.058838	3.58(-25)	0.0061	4.58(-01)
0 0 1	0 0 0	1	1	1	2	1	2	2604.979492	1.39(-24)	2604.988525	5.22(-25)	0.0090	3.75(-01)
0 0 1	0 0 0	1	1	1	1	1	0	2623.901611	2.21(-24)	2623.910889	9.69(-25)	0.0093	4.38(-01)
0 0 1	0 0 0	2	0	2	3	0	3	2594.584961	2.05(-24)	2594.589355	7.59(-25)	0.0044	3.71(-01)
0 0 1	0 0 0	2	1	2	1	1	1	2651.114014	2.21(-25)	2651.119629	5.73(-25)	0.0056	2.59(+00)
0 0 1	0 0 0	2	2	1	2	2	0	2624.261230	4.58(-25)	2624.270996	9.30(-26)	0.0098	2.03(-01)
0 0 1	0 0 0	2	2	0	2	2	1	2630.733154	3.06(-25)	2630.739258	1.32(-24)	0.0061	4.31(+00)
0 0 1	0 0 0	3	1	3	4	1	4	2584.830322	1.50(-24)	2584.832520	4.04(-25)	0.0022	2.69(-01)
0 0 1	0 0 0	3	3	0	3	3	1	2628.549316	2.18(-25)	2628.555176	7.50(-25)	0.0059	3.44(+00)
0 0 1	0 0 0	4	0	4	5	0	5	2574.869629	9.43(-25)	2574.867676	1.45(-25)	0.0020	1.53(-01)
0 0 1	0 0 0	4	1	4	5	1	5	2574.871582	3.13(-25)	2574.867676	1.45(-25)	0.0039	4.62(-01)
0 0 1	0 0 0	4	4	0	4	4	1	2626.179199	1.59(-24)	2626.188477	3.95(-24)	0.0093	2.48(+00)
0 0 1	0 0 0	4	4	1	4	4	0	2623.777588	1.36(-25)	2623.791504	6.42(-25)	0.0139	4.74(+00)
0 0 1	0 0 0	5	0	5	6	0	6	2564.819824	1.54(-25)	2564.812988	4.26(-27)	0.0068	2.77(-02)
0 0 1	0 0 0	5	1	5	6	1	6	2564.819824	4.62(-25)	2564.813232	1.27(-26)	0.0066	2.76(-02)
0 0 1	0 0 0	5	1	5	4	1	4	2678.587158	2.86(-25)	2678.586670	1.28(-25)	0.0005	4.49(-01)
0 0 1	0 0 0	5	5	1	5	5	0	2622.499512	2.39(-24)	2622.519043	5.06(-24)	0.0195	2.12(+00)
0 0 1	0 0 0	6	0	6	7	0	7	2554.671631	1.58(-25)	2554.659180	1.61(-26)	0.0125	1.02(-01)
0 0 1	0 0 0	6	2	5	7	4	4	2433.660156	4.13(-24)	2433.942139	1.43(-24)	0.2820	3.46(-01)
0 0 1	0 0 0	6	5	2	6	5	1	2617.772949	3.71(-25)	2617.765381	1.25(-25)	0.0076	3.38(-01)
0 0 1	0 0 0	8	0	8	7	0	7	2704.367676	1.04(-24)	2704.342285	1.23(-25)	0.0254	1.18(-01)
0 0 1	0 0 0	8	1	8	7	1	7	2704.367676	3.47(-25)	2704.342285	1.23(-25)	0.0254	3.54(-01)
0 0 1	0 0 0	8	6	2	8	6	3	2627.153076	2.39(-25)	2627.062744	9.34(-26)	0.0903	3.91(-01)
0 0 1	0 0 0	8	7	1	8	7	2	2618.077393	4.50(-25)	2618.062012	9.34(-25)	0.0154	2.07(+00)
0 0 1	0 0 0	9	1	8	8	1	7	2720.906006	3.41(-25)	2720.866943	6.82(-25)	0.0391	2.00(+00)
0 0 1	0 0 0	9	2	7	10	2	8	2501.643066	1.01(-24)	2501.594238	2.11(-24)	0.0488	2.09(+00)
0 0 1	0 0 0	9	4	5	8	4	4	2733.579346	4.27(-24)	2733.310791	2.53(-23)	0.2686	5.93(+00)
0 0 1	0 0 0	9	7	3	9	7	2	2609.383057	3.37(-25)	2609.335938	1.49(-25)	0.0471	4.40(-01)
0 0 1	0 0 0	10	1	9	11	1	10	2501.830078	5.47(-25)	2501.778320	2.15(-25)	0.0518	3.93(-01)
0 0 1	0 0 0	11	0	11	10	0	10	2729.080811	3.14(-25)	2729.030273	7.22(-26)	0.0505	2.30(-01)
0 0 1	0 0 0	11	1	11	10	1	10	2729.080811	9.40(-25)	2729.030273	2.17(-25)	0.0505	2.31(-01)
0 0 1	0 0 0	11	2	10	12	2	11	2491.067871	2.57(-25)	2491.005615	7.92(-26)	0.0623	3.08(-01)
0 0 1	0 0 0	11	3	8	11	5	7	2544.793701	1.04(-24)	2544.754639	2.68(-24)	0.0391	2.57(+00)
0 0 1	0 0 0	12	0	12	11	0	11	2737.075439	7.62(-25)	2737.014648	1.88(-25)	0.0608	2.46(-01)
0 0 1	0 0 0	12	1	11	13	1	12	2480.218994	1.11(-25)	2480.145020	2.36(-26)	0.0740	2.12(-01)
0 0 1	0 0 0	13	1	13	12	1	12	2744.947021	5.79(-25)	2744.874756	1.50(-25)	0.0723	2.58(-01)
0 0 1	0 0 0	13	3	11	12	5	8	2589.262695	1.83(-25)	2589.182861	8.17(-26)	0.0798	4.47(-01)
0 0 1	0 0 0	13	4	9	13	6	8	2531.084717	2.06(-25)	2531.010010	5.17(-25)	0.0747	2.51(+00)
0 0 1	0 0 0	13	6	7	14	6	8	2415.131592	1.14(-25)	2415.014160	2.70(-25)	0.1174	2.37(+00)
0 0 1	0 0 0	15	0	15	14	0	14	2760.306641	8.54(-26)	2760.209229	2.10(-26)	0.0974	2.45(-01)
0 0 1	0 0 0	15	1	15	14	1	14	2760.306641	2.56(-25)	2760.209229	6.29(-26)	0.0974	2.46(-01)
0 0 1	0 0 0	15	3	12	15	5	11	2499.737549	1.02(-25)	2499.602783	2.55(-25)	0.1348	2.50(+00)
0 0 1	0 0 0	16	0	16	15	0	15	2767.795166	1.59(-25)	2767.684326	3.78(-26)	0.1108	2.38(-01)
0 0 1	0 0 0	17	1	17	16	1	16	2775.154541	9.24(-26)	2775.028076	2.10(-26)	0.1265	2.28(-01)
0 2 0	0 0 0	7	1	7	7	2	6	2288.590820	1.01(-24)	2288.564209	2.11(-24)	0.0266	2.09(+00)
0 2 0	0 0 0	7	3	4	7	6	1	2304.863281	1.01(-25)	2304.855713	2.03(-25)	0.0076	2.01(+00)
0 2 0	0 0 0	8	4	5	7	5	2	2438.833740	1.94(-25)	2438.851074	4.08(-25)	0.0173	2.10(+00)
0 2 0	0 0 0	9	0	9	9	1	8	2266.480225	5.57(-25)	2266.467529	2.02(-25)	0.0127	3.63(-01)
0 2 0	0 0 0	10	1	10	10	2	9	2255.109619	1.92(-25)	2255.105957	2.51(-26)	0.0037	1.31(-01)
0 2 0	0 0 0	10	2	9	10	3	8	2278.772705	4.73(-25)	2278.782959	1.71(-25)	0.0103	3.62(-01)
0 2 0	0 0 0	10	6	5	10	5	6	2433.197510	1.02(-23)	2433.460449	2.31(-24)	0.2629	2.27(-01)
0 2 0	0 0 0	11	1	10	11	2	9	2268.760010	1.56(-25)	2268.781006	2.28(-26)	0.0210	1.46(-01)
0 2 0	0 0 0	11	2	9	11	3	8	2291.752197	2.79(-25)	2291.785156	1.00(-25)	0.0330	3.59(-01)
0 2 0	0 0 0	11	10	2	11	9	3	2332.058838	5.84(-25)	2332.161865	1.10(-25)	0.1030	1.89(-01)
0 2 0	0 0 0	12	3	10	12	4	9	2282.982910	8.76(-26)	2283.028809	1.41(-26)	0.0459	1.61(-01)
0 2 0	0 0 0	12	4	9	12	5	8	2305.308105	1.36(-25)	2305.364014	4.83(-26)	0.0559	3.56(-01)
0 2 0	0 0 0	12	5	8	12	6	7	2325.826172	1.83(-25)	2325.888428	9.11(-26)	0.0623	4.96(-01)
0 2 0	0 0 0	12	10	3	12	9	4	2338.441162	1.00(-24)	2338.615479	1.57(-27)	0.1743	1.57(-03)
0 2 0	0 0 0	13	1	12	13	0	13	2339.850098	3.56(-24)	2339.714844	3.59(-26)	0.1353	1.00(-02)
0 2 0	0 0 0	13	2	12	13	1	13	2339.850098	1.19(-24)	2339.714844	3.59(-26)	0.1353	3.00(-02)
0 3 0	0 1 0	6	4	3	5	3	2	2433.959961	7.50(-25)	2434.051758	2.54(-24)	0.0918	3.39(+00)
1 0 0	0 0 0	7	7	0	8	8	1	2433.214600	4.88(-24)	2433.440186	1.19(-23)	0.2256	2.44(+00)
1 0 0	0 0 0	9	9	1	10	10	0	2404.224609	1.00(-24)	2404.143066	2.86(-24)	0.0815	2.86(+00)
1 0 0	0 0 0	9	9	1	10	10	0	2404.224609	1.00(-24)	2404.143066	2.86(-24)	0.0815	2.86(+00)
1 0 0	0 0 0	11	6	6	11	7	5	2533.497559	2.12(-25)	2533.598877	6.05(-27)	0.1013	2.90(-02)
1 0 0	0 0 0	12	8	5	12	9	4	2533.327637	1.61(-25)	2533.495605	5.27(-25)	0.1680	3.27(+00)
1 1 0	0 1 0	3	0	3	4	1	4	2552.917725	1.10(-25)	2552.942139	2.36(-25)	0.0244	2.14(+00)

Table 8: All the transitions with problems in positions in the polyad region 1. (powers of ten in parenthesis).

Vib. qun. #		Rot. qun. #						HITRAN		Our calculations			
upper	lower	upper			lower			Frequency	Intensity	Frequency	Intensity	$\lvert\nu_{Calc.} - \nu_{HITRAN}\rvert$	I_{Calc}/I_{HITRAN}
								(ν) cm^{-1}		(ν) cm^{-1}		cm^{-1}	
0 0 1	0 0 0	4	1	3	5	5	0	2337.944092	5.58(-25)	2335.956543	4.16(-25)	1.9876	7.46(-01)
0 0 1	0 0 0	6	0	6	5	0	5	2687.297852	5.72(-25)	2688.902832	6.66(-25)	1.6050	1.16(+00)
0 0 1	0 0 0	8	2	7	7	2	6	2712.733643	5.92(-25)	2713.446777	3.57(-25)	0.7131	6.03(-01)
0 0 1	0 0 0	9	1	9	8	1	8	2712.725098	1.12(-24)	2713.264160	8.64(-25)	0.5391	7.72(-01)
0 0 1	0 0 0	9	7	3	9	3	6	2733.165771	6.80(-25)	2731.701660	5.10(-25)	1.4641	7.50(-01)
0 0 1	0 0 0	10	0	10	9	0	9	2720.963867	1.07(-24)	2721.297119	1.25(-24)	0.3333	1.16(+00)
0 0 1	0 0 0	10	9	1	11	11	0	2349.943115	1.01(-24)	2348.889648	1.08(-24)	1.0535	1.07(+00)
0 0 1	0 0 0	11	1	10	10	1	9	2736.859863	9.26(-26)	2735.719971	1.29(-25)	1.1399	1.40(+00)
0 0 1	0 0 0	11	3	9	12	3	10	2339.940674	8.53(-25)	2341.077148	1.63(-24)	1.1365	1.91(+00)
0 0 1	0 0 0	12	5	8	13	5	9	2433.323975	2.44(-25)	2432.062500	1.95(-25)	1.2615	7.98(-01)
0 0 1	0 0 0	14	0	14	13	0	13	2752.687744	3.81(-25)	2753.639404	5.02(-25)	0.9517	1.32(+00)
0 0 1	0 0 0	15	10	5	14	10	4	2834.685791	1.95(-25)	2834.346924	1.94(-25)	0.3389	9.94(-01)
0 0 1	0 0 0	16	11	5	15	11	4	2843.103271	1.72(-25)	2842.737793	1.69(-25)	0.3655	9.85(-01)
0 1 1	0 1 0	4	2	2	5	2	3	2530.465576	8.58(-26)	2532.208252	8.22(-26)	1.7427	9.58(-01)
0 2 0	0 0 0	6	5	2	6	6	1	2333.270020	1.16(-23)	2332.310303	1.69(-23)	0.9597	1.45(+00)
0 2 0	0 0 0	7	3	4	8	2	7	2379.021973	1.77(-25)	2380.233887	1.05(-25)	1.2119	5.93(-01)
0 2 0	0 0 0	8	6	3	9	3	6	2333.780273	2.02(-25)	2332.948486	1.34(-25)	0.8318	6.65(-01)
0 2 0	0 0 0	10	7	4	9	2	7	2733.781006	8.54(-26)	2734.483398	4.94(-26)	0.7024	5.79(-01)
0 2 0	0 0 0	12	5	7	13	6	8	2229.733887	1.03(-25)	2228.594238	1.45(-25)	1.1396	1.40(+00)
0 2 0	0 0 0	13	5	9	14	4	10	2224.313965	1.03(-25)	2223.966309	1.11(-25)	0.3477	1.08(+00)
0 2 0	0 0 0	13	6	7	13	5	8	2483.852539	1.12(-24)	2484.238525	1.18(-24)	0.3860	1.05(+00)
0 2 0	0 0 0	13	9	4	13	10	3	2392.632568	1.19(-25)	2393.487549	1.26(-25)	0.8550	1.06(+00)
0 2 0	0 0 0	13	9	4	13	10	3	2392.632568	1.19(-25)	2393.487549	1.26(-25)	0.8550	1.06(+00)
0 2 0	0 0 0	16	5	12	15	2	13	2823.077637	1.89(-25)	2823.784912	1.40(-25)	0.7073	7.39(-01)
0 3 0	0 1 0	5	3	2	6	4	3	2233.029297	1.58(-25)	2233.657471	1.22(-25)	0.6282	7.71(-01)
0 3 0	0 1 0	8	2	6	8	1	7	2415.517090	1.23(-25)	2417.486328	1.11(-25)	1.9692	9.02(-01)
1 0 0	0 0 0	5	5	0	6	6	1	2490.621582	1.24(-24)	2489.279297	1.27(-24)	1.3423	1.03(+00)
1 0 0	0 0 0	6	3	4	7	4	3	2433.503662	1.82(-24)	2433.942139	1.43(-24)	0.4385	7.86(-01)
1 0 0	0 0 0	6	5	1	7	6	2	2336.516113	2.64(-25)	2332.399885	2.84(-25)	4.1162	1.08(+00)
1 0 0	0 0 0	7	7	1	6	6	0	2733.175293	6.54(-23)	2734.030273	5.30(-23)	0.8550	8.10(-01)
1 0 0	0 0 0	8	4	4	9	5	5	2335.675293	1.42(-25)	2336.270752	2.50(-25)	0.5955	1.76(+00)
1 0 0	0 0 0	10	2	8	11	3	9	2335.672607	9.71(-26)	2336.162354	8.65(-26)	0.4897	8.90(-01)
1 0 0	0 0 0	10	2	9	9	3	6	2579.025146	1.88(-25)	2580.792480	1.84(-25)	1.7673	9.79(-01)
1 0 0	0 0 0	10	3	8	11	2	9	2335.672607	2.91(-25)	2333.974609	2.37(-25)	1.6980	8.13(-01)
1 0 0	0 0 0	10	5	6	11	6	5	2333.337646	7.06(-25)	2334.468262	7.23(-25)	1.1306	1.02(+00)
1 0 0	0 0 0	10	10	1	11	9	2	2332.108643	1.89(-25)	2333.974609	2.37(-25)	1.8660	1.25(+00)
1 0 0	0 0 0	11	8	4	10	5	5	2845.959961	3.54(-25)	2845.396973	3.78(-25)	0.5630	1.07(+00)
1 0 0	0 0 0	12	1	12	13	0	13	2335.307129	3.12(-25)	2334.640137	4.33(-25)	0.6670	1.39(+00)
1 0 0	0 0 0	13	1	12	14	4	11	2224.024170	8.81(-26)	2224.389160	9.68(-26)	0.3650	1.10(+00)
1 0 0	0 0 0	13	9	5	13	8	6	2639.120605	1.46(-25)	2640.381836	1.52(-25)	1.2612	1.04(+00)
1 0 0	0 0 0	16	11	6	15	10	5	2843.627197	2.41(-25)	2843.295654	2.38(-25)	0.3315	9.87(-01)
1 1 0	0 1 0	7	2	5	7	1	6	2633.032959	1.70(-25)	2634.898438	2.30(-25)	1.8655	1.35(+00)
1 1 0	0 1 0	14	1	14	13	0	13	2715.986328	1.84(-25)	2715.666992	2.59(-25)	0.3193	1.41(+00)

Table 9: All the transitions with problems in positions and intensities in the polyad region 1.5. (powers of ten in parenthesis).

Vib. qun. #		Rot. qun. #						HITRAN		Our calculations			
upper	lower	upper			lower			Frequency	Intensity	Frequency	Intensity	$\lvert\nu_{Calc.} - \nu_{HITRAN}\rvert$	I_{Calc}/I_{HITRAN}
								(ν) cm^{-1}		(ν) cm^{-1}		cm^{-1}	
0 2 1	0 1 0	11	7	4	10	7	3	3933.934814	4.64(-26)	3932.190918	1.54(-25)	1.7439	3.32(+00)
0 3 0	0 0 0	10	10	1	11	11	0	3402.275146	2.04(-25)	3402.621094	1.85(-25)	0.3460	9.07(-01)
0 3 0	0 0 0	11	11	0	12	12	1	3402.333252	6.65(-26)	3402.763672	5.96(-26)	0.4304	8.97(-01)
0 3 0	0 0 0	11	11	0	10	6	5	4022.144287	2.71(-25)	4022.501221	3.71(-25)	0.3569	1.37(+00)
0 3 0	0 0 0	11	11	0	11	6	5	3819.482178	2.44(-25)	3819.834961	3.67(-25)	0.3528	1.50(+00)
0 3 0	0 0 0	11	11	0	10	8	3	3939.135010	2.53(-25)	3939.500244	3.85(-25)	0.3652	1.52(+00)
0 3 0	0 0 0	12	11	2	13	12	1	3395.206787	2.58(-26)	3395.569824	2.19(-26)	0.3630	8.48(-01)
0 3 0	0 0 0	14	13	2	13	10	3	4054.311768	1.26(-25)	4054.729980	1.30(-25)	0.4182	1.03(+00)
1 1 0	0 0 0	4	3	2	3	2	1	3833.305176	3.72(-22)	3832.777344	6.89(-22)	0.5278	1.85(+00)
1 1 0	0 0 0	12	8	4	12	9	3	3759.330566	2.11(-24)	3759.709229	2.16(-24)	0.3787	1.02(+00)
1 1 0	0 0 0	14	9	5	14	10	4	3758.355469	2.79(-25)	3758.661133	2.85(-25)	0.3057	1.02(+00)
1 1 0	0 0 0	14	9	5	13	10	4	3980.971436	1.77(-25)	3981.304443	1.82(-25)	0.3330	1.03(+00)
1 1 0	0 0 0	14	9	5	14	8	6	3828.231934	1.25(-25)	3828.533447	1.40(-25)	0.3015	1.12(+00)
1 1 0	0 0 0	15	9	6	14	10	5	4002.928711	3.09(-25)	4003.273682	3.21(-25)	0.3450	1.04(+00)
1 1 0	0 0 0	15	10	5	15	9	6	3828.358154	1.10(-25)	3828.658447	1.25(-25)	0.3003	1.14(+00)
1 1 0	0 0 0	15	10	5	14	9	6	4092.126709	3.12(-25)	4092.460938	3.03(-25)	0.3342	9.72(-01)
1 1 0	0 0 0	15	10	5	14	11	4	3988.310547	1.34(-25)	3988.668701	1.36(-25)	0.3582	1.01(+00)
1 1 0	0 0 0	15	11	4	14	12	3	3976.303467	5.94(-26)	3976.630371	5.91(-26)	0.3269	9.94(-01)
1 1 0	0 0 0	16	9	7	15	8	8	4145.444336	2.70(-26)	4145.775879	2.39(-26)	0.3315	8.87(-01)
1 1 0	0 0 0	16	10	6	15	9	7	4123.806641	2.55(-26)	4124.203125	2.38(-26)	0.3965	9.34(-01)
1 1 0	0 0 0	16	10	6	16	11	5	3756.213867	2.45(-26)	3756.573730	2.66(-26)	0.3599	1.08(+00)
1 1 0	0 0 0	16	11	5	15	10	6	4104.372559	3.85(-26)	4104.755859	3.83(-26)	0.3833	9.93(-01)
1 1 0	0 0 0	17	9	8	16	10	7	4034.105469	5.70(-26)	4034.478271	6.00(-26)	0.3728	1.05(+00)
1 1 0	0 0 0	17	10	7	16	9	8	4156.593262	2.15(-26)	4157.036621	1.90(-26)	0.4434	8.80(-01)
1 1 0	0 0 0	17	10	7	17	11	6	3752.000000	2.17(-26)	3752.358643	2.22(-26)	0.3586	1.02(+00)

Table 10: All the transitions with problems in intensities in the polyad region 1.5. (powers of ten in parenthesis).

Vib. qun. #		Rot. qun. #						HITRAN		Our calculations			
upper	lower	upper			lower			Frequency	Intensity	Frequency	Intensity	$\lvert\nu_{Calc.} - \nu_{HITRAN}\rvert$	I_{Calc}/I_{HITRAN}
								(ν) cm^{-1}		(ν) cm^{-1}		cm^{-1}	
0 1 1	0 0 0	7	2	6	7	4	3	3662.864014	2.98(-26)	3662.852051	1.13(-26)	0.0120	3.80(-01)
0 1 1	0 0 0	7	3	5	8	1	8	3826.407227	1.32(-25)	3826.390137	5.29(-26)	0.0171	4.00(-01)
0 1 1	0 0 0	7	7	1	7	5	2	3833.033936	1.60(-23)	3832.955811	5.70(-23)	0.0781	3.56(+00)
0 1 1	0 0 0	8	2	6	7	4	3	3817.737549	7.71(-26)	3817.719482	2.89(-26)	0.0181	3.75(-01)
0 1 1	0 0 0	8	3	5	9	1	8	3807.849121	1.90(-25)	3807.827637	7.36(-26)	0.0215	3.88(-01)
0 1 1	0 0 0	8	4	5	7	6	2	3835.639893	2.46(-26)	3835.625977	1.04(-26)	0.0139	4.21(-01)
0 1 1	0 0 0	8	7	1	8	3	6	3962.918701	2.85(-26)	3962.878906	1.20(-26)	0.0398	4.21(-01)
0 1 1	0 0 0	8	8	0	8	4	5	3946.660889	2.99(-26)	3946.600830	1.49(-26)	0.0601	4.99(-01)
0 1 1	0 0 0	9	3	7	10	1	10	3844.785400	5.28(-26)	3844.757812	9.65(-27)	0.0276	1.83(-01)
0 1 1	0 0 0	9	3	6	8	5	3	3842.813477	3.50(-26)	3842.788330	1.64(-26)	0.0252	4.69(-01)
0 1 1	0 0 0	9	4	6	10	2	9	3817.348633	1.07(-25)	3817.321289	2.85(-26)	0.0273	2.66(-01)
0 1 1	0 0 0	9	4	6	9	0	9	4008.999268	5.26(-26)	4008.970947	2.52(-26)	0.0283	4.80(-01)
0 1 1	0 0 0	9	5	5	10	3	8	3789.585938	1.59(-25)	3789.560059	5.74(-26)	0.0259	3.61(-01)
0 1 1	0 0 0	9	6	4	10	4	7	3762.310059	2.07(-25)	3762.283691	9.28(-26)	0.0264	4.48(-01)
0 1 1	0 0 0	10	2	8	11	0	11	3853.571045	3.23(-26)	3853.537842	3.34(-27)	0.0332	1.03(-01)
0 1 1	0 0 0	10	4	6	11	2	9	3798.903320	8.30(-26)	3798.871582	2.12(-26)	0.0317	2.55(-01)
0 1 1	0 0 0	10	4	6	10	2	9	4008.602783	8.97(-26)	4008.569824	4.35(-26)	0.0330	4.84(-01)
0 1 1	0 0 0	10	5	5	11	3	8	3770.135498	1.13(-25)	3770.107666	4.36(-26)	0.0278	3.86(-01)
0 1 1	0 0 0	10	7	4	11	5	7	3745.234131	3.75(-26)	3745.200439	1.56(-26)	0.0337	4.15(-01)
0 1 1	0 0 0	11	5	7	12	3	10	3808.108398	4.14(-26)	3808.069336	6.34(-27)	0.0391	1.53(-01)
0 1 1	0 0 0	11	5	7	11	1	10	4036.607666	4.67(-26)	4036.567383	1.92(-26)	0.0403	4.12(-01)
0 1 1	0 0 0	11	6	6	12	4	9	3780.645752	4.72(-26)	3780.608643	1.08(-26)	0.0371	2.29(-01)
0 1 1	0 0 0	11	6	5	12	4	8	3750.462646	2.21(-26)	3750.435059	9.22(-27)	0.0276	4.18(-01)
0 1 1	0 0 0	11	6	6	11	2	9	4008.105225	8.56(-26)	4008.066895	4.04(-26)	0.0383	4.72(-01)
0 1 1	0 0 0	11	7	5	12	5	8	3753.253418	4.96(-26)	3753.217285	1.48(-26)	0.0361	2.99(-01)
0 1 1	0 0 0	11	8	4	12	6	7	3729.260010	5.05(-26)	3729.217529	1.92(-26)	0.0425	3.80(-01)
0 1 1	0 0 0	11	9	3	12	7	6	3713.861328	4.31(-26)	3713.803955	1.91(-26)	0.0574	4.44(-01)
0 1 1	0 0 0	12	5	7	13	3	10	3789.698242	2.19(-26)	3789.652588	3.14(-27)	0.0457	1.43(-01)
0 1 1	0 0 0	12	5	7	12	3	10	4035.740234	4.12(-26)	4035.693359	1.71(-26)	0.0469	4.15(-01)
0 1 1	0 0 0	12	6	6	13	4	9	3761.428711	2.46(-26)	3761.386719	6.17(-27)	0.0420	2.51(-01)
0 1 1	0 0 0	13	7	7	13	3	10	4034.600830	2.58(-26)	4034.535645	1.03(-26)	0.0652	4.00(-01)
0 1 1	0 0 0	13	8	6	13	4	9	4006.066162	3.20(-26)	4005.998047	1.39(-26)	0.0681	4.36(-01)
0 1 1	0 0 0	13	9	5	13	5	8	3980.095703	3.82(-26)	3980.038574	1.85(-26)	0.0571	4.85(-01)
0 2 1	0 1 0	6	4	2	7	4	3	3633.118408	2.26(-24)	3633.025879	1.19(-25)	0.0925	5.20(-02)
0 2 1	0 1 0	8	7	1	7	5	2	3933.550049	4.65(-25)	3933.464600	7.96(-28)	0.0855	2.00(-03)
0 3 0	0 0 0	10	10	1	9	5	4	3937.446777	6.74(-26)	3937.737305	2.87(-26)	0.2905	4.26(-01)
0 3 0	0 0 0	12	9	3	12	6	6	3726.931885	8.76(-26)	3726.966309	3.10(-26)	0.0344	3.54(-01)
0 3 0	0 0 0	12	9	3	11	6	6	3950.146973	3.25(-25)	3950.183594	1.18(-25)	0.0366	3.64(-01)
0 3 0	0 0 0	12	9	3	11	4	8	4081.305908	1.71(-25)	4081.340576	8.43(-26)	0.0347	4.92(-01)
0 3 0	0 0 0	13	4	9	14	3	12	3616.694336	6.46(-26)	3616.776367	2.13(-26)	0.0820	3.30(-01)
0 3 0	0 0 0	14	6	8	13	5	9	3956.558838	5.93(-26)	3956.640869	1.41(-25)	0.0820	2.38(+00)
0 3 0	0 0 0	14	7	8	14	4	11	3881.419189	3.46(-26)	3881.491699	8.28(-27)	0.0725	2.39(-01)
0 3 0	0 0 0	16	3	14	15	2	13	3720.561768	2.15(-26)	3720.661133	1.04(-26)	0.0994	4.82(-01)
0 4 0	0 1 0	10	1	10	11	0	11	3363.156982	1.14(-25)	3363.128662	4.85(-26)	0.0283	4.24(-01)
0 4 0	0 1 0	10	2	9	11	1	10	3374.680664	5.75(-26)	3374.662354	2.48(-26)	0.0183	4.31(-01)
0 4 0	0 1 0	10	3	8	11	2	9	3382.920898	3.05(-26)	3382.907715	1.35(-26)	0.0132	4.43(-01)
0 4 0	0 1 0	12	1	12	13	0	13	3338.881348	4.89(-26)	3338.865723	1.74(-26)	0.0156	3.56(-01)
1 1 0	0 0 0	6	5	1	5	2	4	3965.657227	3.25(-26)	3965.687500	1.58(-26)	0.0303	4.87(-01)
1 1 0	0 0 0	7	0	7	6	3	4	3733.428711	1.95(-25)	3733.517334	5.78(-28)	0.0886	3.00(-03)
1 1 0	0 0 0	7	1	7	6	2	4	3733.657715	6.53(-26)	3733.517334	5.78(-28)	0.1404	9.00(-03)
1 1 0	0 0 0	7	6	1	6	3	4	3987.578369	1.34(-25)	3987.588135	5.58(-26)	0.0098	4.16(-01)
1 1 0	0 0 0	8	6	2	7	5	3	3933.607910	4.54(-23)	3933.464600	7.96(-28)	0.1433	1.75(-05)
1 1 0	0 0 0	8	7	1	7	4	4	4011.415283	2.91(-26)	4011.399170	7.56(-27)	0.0161	2.60(-01)
1 1 0	0 0 0	8	8	1	7	5	2	4002.406494	1.04(-25)	4002.275635	4.40(-26)	0.1309	4.23(-01)
1 1 0	0 0 0	9	8	1	8	5	4	4036.950684	2.34(-26)	4036.905762	1.95(-28)	0.0449	8.00(-03)
1 1 0	0 0 0	10	7	4	9	2	7	4131.452637	4.39(-26)	4131.488770	1.64(-26)	0.0361	3.73(-01)
1 1 0	0 0 0	10	7	4	10	4	7	3941.399658	8.36(-26)	3941.437012	3.19(-26)	0.0374	3.82(-01)
1 2 0	0 1 0	8	2	7	9	1	8	3633.552979	1.13(-24)	3633.498047	3.46(-25)	0.0549	3.05(-01)

Table 11: All the transitions with problems in positions in the polyad region 1.5. (powers of ten in parenthesis).

Vib. qun. #		Rot. qun. #						HITRAN		Our calculations			
upper	lower	upper			lower			Frequency	Intensity	Frequency	Intensity	$\lvert\nu_{Calc.} - \nu_{HITRAN}\rvert$	I_{Calc}/I_{HITRAN}
								(ν) cm^{-1}		(ν) cm^{-1}		cm^{-1}	
0 1 1	0 0 0	10	0	10	11	2	9	3337.123779	3.05(-25)	3336.419189	1.72(-27)	0.7046	6.00(-03)
0 1 1	0 0 0	10	1	10	11	3	9	3337.123779	1.02(-25)	3336.419189	1.72(-27)	0.7046	1.70(-02)
0 2 1	0 1 0	8	2	6	9	2	7	3633.901123	1.54(-24)	3633.498047	3.46(-25)	0.4031	2.25(-01)
0 2 1	0 1 0	8	3	6	9	3	7	3633.907227	5.15(-25)	3633.498047	3.46(-25)	0.4092	6.73(-01)
0 3 0	0 0 0	3	0	3	2	1	2	3533.909668	1.54(-23)	3532.450195	3.91(-26)	1.4595	3.00(-03)
0 3 0	0 0 0	3	3	0	4	4	1	3433.146484	1.35(-23)	3434.092773	1.19(-24)	0.9463	8.80(-02)
0 3 0	0 0 0	14	14	1	13	13	0	3967.855225	3.88(-26)	3968.180664	2.85(-26)	0.3254	7.35(-01)
0 4 0	0 1 0	6	3	4	6	2	5	3533.162598	5.38(-26)	3534.276855	1.53(-26)	1.1143	2.85(-01)
0 4 0	0 1 0	6	5	2	6	4	3	3533.019531	4.29(-26)	3534.276855	1.53(-26)	1.2573	3.57(-01)
1 1 0	0 0 0	4	0	4	5	3	3	3633.333008	3.43(-24)	3631.540039	1.91(-25)	1.7930	5.60(-02)
1 1 0	0 0 0	10	5	6	11	8	3	3330.591797	2.74(-26)	3329.363281	4.54(-28)	1.2285	1.70(-02)
1 1 0	0 0 0	11	6	6	11	9	3	3633.263916	2.47(-26)	3631.362305	2.88(-28)	1.9016	1.20(-02)
1 1 0	0 0 0	12	11	1	13	12	2	3533.483643	1.48(-25)	3534.354980	3.45(-28)	0.8713	2.00(-03)
1 1 0	0 0 0	13	5	8	12	8	5	3833.624023	6.91(-26)	3832.500488	4.64(-27)	1.1235	6.70(-02)
1 1 0	0 0 0	13	11	2	12	10	3	4033.270020	5.09(-24)	4034.083008	1.91(-24)	0.8130	3.74(-01)
1 1 0	0 0 0	13	31	3	13	12	2	3733.109131	3.41(-25)	3731.329346	6.20(-27)	1.7798	1.80(-02)
1 2 0	0 1 0	3	1	3	4	2	2	3633.011475	4.58(-26)	3631.978027	4.47(-27)	1.0335	9.70(-02)

References and index of citations

R. Aladro, S. Martin, J. Martin-Pintado, R. Mauersberger, C. Henkel, B. Ocana Flaquer, and M. A. Amo-Baladron. A $\lambda = 1.3$ mm and 2 mm molecular line survey towards M 82. *Astron. Astrophys.*, 535:A84, 2011. doi: 10.1051/0004-6361/201117397. 15, 16, 153

A. A. A. Azzam, S. N. Yurchenko, J. Tennyson, M.-A. Martin, and O. Pirali. Teraherzt spectroscopy of hydrogen sulfide. *J. Quant. Spectrosc. Radiat. Transf.*, 2013. (In press). 121, 134

R. J. Barber, J. Tennyson, G. J. Harris, and R. N. Tolchenov. A high accuracy computed water line list. *Mon. Not. R. Astr. Soc.*, 368:1087–1094, 2006. 16, 17, 46

P. Barletta, A. G. Császár, H. M. Quiney, and J. Tennyson. Higher order relativistic corrections to the vibration-rotation levels of H_2S. *Chem. Phys. Lett.*, 361:121–128, 2002. 68

Z. Bačić and J. C. Light. Theoretical methods for rovibrational states of floppy molecules. *Annu. Rev. Phys. Chem.*, 40:469–498, 1989. 36

S. P. Belov, K. M. T. Yamada, G. Winnewisser, L. Poteau, R. Bocquet, J. Demaison, O. Polyansky, and M. Yu. Tretyakov. Terahertz rotational spectrum of H_2S. *J. Mol. Spectrosc.*, 173:380–390, 1995. doi: 10.1006/jmsp.1995.1242. 18, 122, 124, 132, 135, 138

L. R. Brown, J. A. Crisp, D. Crisp, O. V. Naumenko, M. A. Smirnov, and L. N.

Sinitsa. The first hexad of interacting states of H_2S molecule. *SPIE*, 3090: 111–113, 1997. 18, 113

L. R. Brown, J. A. Crisp, D. Crisp, O. V. Naumenko, M. A. Smirnov, L. N. Sinitsa, and A. Perrin. The absorption spectrum of H_2S between 2150 and 4260 cm^{-1}: Analysis of the positions and intensities in the first ($2\nu_2$, ν_1, and ν_3) and second ($3\nu_2$, ν_1/ν_2, and ν_2/ν_3) triad regions. *J. Mol. Spectrosc.*, 188: 148–174, 1998. 18, 58, 59, 66, 87, 91, 108

L. R. Brown, O. V. Naumenko, E. R. Polovtseva, and L. N. Sinitsa. Hydrogen sulfide absorption spectrum in the 8400 - 8900 cm^{-1} spectral region. *Eleventh International Symposium on Atmospheric and Ocean Optics/Atmospheric Physics*, 5743:1–7, 2004. 18, 20, 113

J. B. Brubach, L. Manceron, M. Rouzières, O. Pirali, D. Balcon, F. Kwabia-Tchana, V. Boudon, M. Tudorie, T. Huet, A. Cuisset, and P. Roy. Performance of the ailes thz-infrared beamline at soleil for high resolution spectroscopy. In *WIRMS 2009*, volume 1214 of *AIP Conference Proceedings*, pages 81–84, 2010. 121

P. R. Bunker and P. Jensen. Variational calculations of rotation-vibration spectra. In P. Jensen and P. R. Bunker, editors, *Computational Molecular Spectroscopy*, pages 3–11. Wiley, 2000. 26

A. V. Burenin, T. M. Fevralskikh, A. A. Melnikov, and S. M. Shapin. Microwave spectrum of the hydrogen sulfide molecule $H_2{}^{32}S$ in the ground state. *J. Mol. Spectrosc.*, 109:1–7, 1985. 18, 122, 124

C. A. Burrus, JR., and W. Gordy. One-to-two millimeter wave spectroscopy. II. H_2S. *Phys. Rev.*, 92:274–277, 1953. 18, 122, 124, 135

A. Campargue and J. M. Flaud. The overtone spectrum of $H_2{}^{32}S$ near 13200 cm^{-1}. *J. Mol. Spectrosc.*, 194:43–51, 1999. 20

C. Camy-Peyret and J. M. Fiaud. in Molecular Spectroscopy: Modern Research. volume III. Academic, New York, 1985. 59

S. Carter, P. Rosmus, N. C. Handy, S. Miller, J. Tennyson, and B. T. Sutcliffe. Benchmark calculations of first principles rotational and ro-vibrational line strengths. *Comput. Phys. Commun.*, 55:71–75, 1989. 59

T. Cours, P. Rosmus, and V. G. Tyuterev. Ab initio dipole moment function of H_2S. *Chem. Phys. Lett.*, 331:317–322, 2000. 59, 60, 61, 63, 94

T. Cours, P. Rosmus, and V. G. Tyuterev. Ab initio dipole moment functions of (H_2S)-S-32 and intensity anomalies in rovibrational spectra. *J. Chem. Phys.*, 117:5192–5208, 2002. doi: 10.1063/1.1499487. 59, 60, 61, 63, 65, 66, 73

A. G. Császár, W. D. Allen, Y. Yamaguchi, and H. F. Schaefer III. Variational calculations of rotation-vibration spectra. In P. Jensen and P. R. Bunker, editors, *Computational Molecular Spectroscopy*, pages 16–68. Wiley, 2000. 8, 27, 28

R. E. Cupp, R. A. Keikpf, and J. J. Gallagher. Hyperfine structure in the millimeter spectrum of hydrogen sulfide electric spectroscopy on asymmetric-top molecules. *Phys. Rev.*, 171:60–69, 1968. 18, 122, 135, 138

C. de Bergh, V. I. Moroz, F. W. Taylor, D. Crisp, B. Bézard, and L. V. Zasova. The composition of the atmosphere of venus below 100 km altitude: An overview. *Planetary and Space Science*, 54:1389–1397, 2006. 17

Y. Ding, O. Naumenko, S.-M. Hu, Q. Zhu, E. Bertseva, and A. Campargue. The absorption spectrum of H_2S between 9540 and 10000 cm^{-1} by intracavity laser absorption spectroscopy with a vertical external cavity surface emitting laser. *J. Mol. Spectrosc.*, 217:222–238, 2003. 20

T. H. Dunning. *J. Chem. Phys.*, 90:1007–1023, 1989. 60, 68

T. H. Dunning, K. A. Peterson, and A. K. Wilson. Gaussian basis sets for use in correlated molecular calculations. x. the atoms aluminum through argon revisited. *J. Chem. Phys.*, 114:9244, 2001. 35, 75

T. H. Edwards, N. K. Moncur, and L. E. Snyder. Groundstate molecular constants of hydrogen sulfide. *J. Chem. Phys.*, 46:2139, 1967. 14, 71

J. M. Flaud, C. Camy-Peyret, and J. W. C. Johns. The far-infrared spectrum of hydrogen-sulfide - the (000) rotational-constants of $H_2{}^{32}S$, $H_2{}^{33}S$ and $H_2{}^{34}S$. *Can. J. Phys.*, 61:1462–1473, 1983. 18, 66, 106, 122, 124, 134, 135, 138, 139

J. M. Flaud, R. Großkloß, S. B. Rai, R. Struber, W. Demtroder, D. A. Tate, Liang guo Wang, and Th. F. Gallagher. Diode laser spectroscopy of $H_2{}^{32}S$ around 0.82 μm. *J. Mol. Spectrosc.*, 172:275–281, 1995. 20

J. M. Flaud, O. Vaittinen, and A. Campargue. The H_2S spectrum around 0.7 μm. *J. Mol. Spectrosc.*, 190:262–268, 1998. 20

J. R. Gillis and T. H. Edwards. Analysis of $2\nu_2$, ν_1, and ν_3 of H_2S. *J. Mol. Spectrosc.*, 85:55–73, 1981. 18, 58

A. Goldman and J.R. Gillis. Line parameters and line by line calculations for molecules of stratospheric interest. *University of Denver Progress Report*, 1984. 87, 108

M. Grechko, O. Aseev, T. R. Rizzo, N. F. Zobov, L. Lodi, J. Tennyson, O. L. Polyansky, and O. V. Boyarkin. Stark coefficients for highly excited rovibrational states of H_2O. *J. Chem. Phys.*, 136:244308, 2012. 62, 152

R. Großkloß, S .B. Rai, R. Stuber, and W. Demtroder. Diode laser overtone spectroscopy of hydrogen sulfide. *Chem. Phys. Lett.*, 229:609–615, 1994. 20

P. Helminger, Robert L. Cook, and Frank C. De Lucia. Microwave spectrum and centrifugal distortion effects of H_2S. *J. Chem. Phys.*, 56:4581–4584, 1972. 18, 122, 124, 132, 135, 138

P. Helminger, Frank C. De Lucia, and William H. Kirchhoff. Microwave spectra of molecules of astrophysical interest IV. hydrogen sulfide. *J. Phys. Chem. Ref. Data*, 2:215–223, 1973. 135, 138

E. Henon, T. Cours, and V. G. Tyuterev. A CASPT2 study of the dipole moment surfaces of hydrogen sulphide molecule. *Chem. Phys. Lett.*, 367:284–292, 2003. 59

B. A. Hess and C. M. Marian. Relativistic effects in the calculation of electronic energies. In P. Jensen and P. R. Bunker, editors, *Computational Molecular Spectroscopy*, pages 169–252. Wiley, 2000. 36

V. M. Horneman, R. Anttila, S. Alanko, and J. Pietila. Transferring calibration from CO_2 laser lines to far infrared water lines with the aid of the ν_2 band of OCS and the ν_2, ν_1-ν_2, and ν_1+ν_2 bands of CS_2-C-13: Molecular constants of CS_2-C-13. *J. Mol. Spectrosc.*, 234:238–254, 2005. 12, 125, 128, 130

G. Hoshyaripour, M. Hort, and B. Langmann. How does the hot core of a volcanic plume control the sulfur speciation in volcanic emission? *Geochem. Geophys. Geosys.*, 13:Q07004, 2012. doi: 10.1029/2011GC004020. 14

R. Hu, S. Seager, and W. Bains. Photochemistry in terrestrial exoplanet atmospheres. II. H_2S and SO_2 photochemistry in anoxic atmospheres. *Astrophysical Journal*, 769, 2013. doi: 10.1088/0004-637X/769/1/6. 16

C. Huiszoon. A high resolution spectrometer for the shorter millimeter wavelength region. *Rev. Sci. Instrum.*, 42:477–481, 1971. 18, 122, 124, 135, 138

C. Huiszoon and A. Dymanus. Stark effect of millimeter wave transitions, I. hydrogen sulfide. *Physica*, 31:1049–1052, 1965. 124, 132

C. Huiszoon and A. Dymanus. Magnetic hyperfine structure the rotational spectrum of H_2S. *Phys. Lett.*, 21:164–166, 1966. 18, 122, 124, 134, 135, 138

S. Huzinaga. *Technical Report: Approximate Atomic Functions.* Unversity of Alberta, 1965. 60

N. Jacquinet-Husson, L. Crepeau, R. Armante, C. Boutammine, A. Chédin, N. A. Scott, C. Crevoisier, V. Capelle, C. Boone, N. Poulet-Crovisier, A. Barbe, A. Campargue, D. Chris Benner, Y. Benilan, B. Bézard, V. Boudon, L. R. Brown, L. H. Coudert, A. Coustenis, V. Dana, V. M. Devi, S. Fally, A. Fayt, J. M. Flaud, A. Goldman, M. Herman, G. J. Harris, D. Jacquemart, A. Jolly, I. Kleiner, A. Kleinböhl, F. Kwabia-Tchana, N. Lavrentieva, N. Lacome, Li-Hong Xu, O. M. Lyulin, J.-Y. Mandin, A. Maki, S. Mikhailenko, C. E. Miller, T. Mishina, N. Moazzen-Ahmadi, H. S. P. Müller, A. Nikitin, J. Orphal,

V. Perevalov, A. Perrin, D. T. Petkie, A. Predoi-Cross, C. P. Rinsland, J. J. Remedios, M. Rotger, M. A. H. Smith, K. Sung, S. Tashkun, J. Tennyson, R. A. Toth, A.-C. Vandaele, and J. Vander Auwera. The 2009 edition of the GEISA spectroscopic database. *J. Quant. Spectrosc. Radiat. Transf.*, 112:2395–2445, 2011. 20

F. Jensen. *Introduction to Computational Chemistry, 2nd Edition.* Wiley, 2006. 28

P. Jensen and P. R. Bunker, editors. *Computational Molecular Spectroscopy.* Wiley, 2000. 28

P. Jensen and P. R. Bunker. *Molecular Symmetry and Spectroscopy.* NRC, Canada, 1998. 26, 42

U. G. Jørgensen and P. Jensen. The dipole-moment surface and the vibrational transition moments of h_2o. *J. Mol. Spectrosc.*, 161(1):219–242, SEP 1993. ISSN 0022-2852. doi: 10.1006/jmsp.1993.1228. 63

K. Justtanont, T. Khouri, M. Maercker, J. Alcolea, L. Decin, H. Olofsson, F. L. Schöier, V. Bujarrabal, A. P. Marston, D. Teyssier, J. Cernicharo, C. Dominik, A. de Koter, G. Melnick, K. M. Menten, D. Neufeld, P. Planesas, M. Schmidt, R. Szczerba, and R. Waters. Herschel/HIFI observations of O-rich AGB stars: molecular inventory. *Astron. Astrophys.*, 537:A144, 2012. doi: 10.1051/0004-6361/201117524. URL `http://dx.doi.org/10.1051/0004-6361/201117524`. 15, 153

I. N. Kozin and P. Jensen. Fourfold clusters of rotational energy levels for H_2S studied with a potential energy surface derived from experiment. *J. Mol. Spectrosc.*, 163:483–509, 1994. 122

F. L. Colomer, H. E. Morato, and E. M. Iglesias. Estimation of hydrogen sulfide emission rates at several wastewater treatment plants through experimental concentration measurements and dispersion modeling. *J. Air Waste Management Assoc.*, 62:758–766, 2012. doi: 10.1080/10962247.2012.674008. 14

WM. C. Lane, T. H. Edwards, J. R. Gillis, Francis S. Bonomo, and Frank J. Murcray. Analysis of ν_2 of H_2S. *J. Mol. Spectrosc.*, 95:365–380, 1982. 18, 122

WM. C. Lane, T. H. Edwards J. R. Gillis, Francis S. Bonomo, and Frank J. Murcray. Analysis of ν_2 of $H_2{}^{33}S$ and $H_2{}^{34}S$. *J. Mol. Spectrosc.*, 111:320–326, 1985. 122

C. R. Le Sueur, S. Miller, J. Tennyson, and B. T. Sutcliffe. On the use of variational wavefunctions in calculating vibrational band intensities. *Mol. Phys.*, 76:1147–1156, 1992. 59

L. Lodi and J. Tennyson. Theoretical methods for small-molecule ro-vibrational spectroscopy. *J. Phys.B: At. Mol. Opt. Phys.*, 43:133001, 2010. 62

L. Lodi and J. Tennyson. Line lists for $H_2{}^{18}O$ and $H_2{}^{17}O$ based on empirically-adjusted line positions and ab initio intensities. *J. Quant. Spectrosc. Radiat. Transf.*, 113:850–858, 2012. 62

L. Lodi, R. N. Tolchenov, J. Tennyson, A. E. Lynas-Gray, S. V. Shirin, N. F. Zobov, O. L. Polyansky, A. G. Császár, J. van Stralen, and L. Visscher. A new ab initio ground-state dipole moment surface for the water molecule. *J. Chem. Phys.*, 128:044304, 2008. 61, 68, 69, 81

L. Lodi, J. Tennyson, and O. L. Polyansky. A global, high accuracy ab initio dipole moment surface for the electronic ground state of the water molecule. *J. Chem. Phys.*, 135:034113, 2011. 62, 68, 152

F. Matsushima, H. Odashima, T. Iwasaki, S. Tsunekawa, and K. Takagi. Frequency-measurement of pure rotational transitions of H_2O from 0.5 to 5 THz. *J. Mol. Struct.*, 352:371–378, 1995. 12, 125, 128, 130

R. E. Miller, G. E. Leroi, and T. M. Hard. Analysis of the pure rotational absorption spectra of hydrogen sulfide and deuterium sulfide. *J. Chem. Phys.*, 50:677–684, 1969. 18, 122

Y. C. Minh, W. M. Irvine, and L. M. Ziurys. Detection of interstellar hydrogen sulfide in cold, dark clouds. *The Astrophysical Journal*, 345:L63–L66, 1989. 153

H. S. P. Müller, S. Thorwirth, D. A. Roth, and G. Winnewisser. The cologne database for molecular spectroscopy, cdms. *Astron. Astrophys.*, 370(3):L49–L52, MAY 2001. ISSN 1432-0746. 12, 13, 20, 122, 132, 135, 142, 143, 144

H. S. P. Müller, F. Schlöder, J. Stutzki, and G. Winnewisser. The cologne database for molecular spectroscopy, cdms: a useful tool for astronomers and spectroscopists. *J. Molec. Struct. (THEOCHEM)*, 742:215–227, 2005. doi: 10.1016/j.molstruc.2005.01.027. 20, 122, 132, 135

O. Naumenko and A. Campargue. $H_2{}^{32}S$: First observation of the (70,0) local mode pair and updated global effective vibrational hamiltonian. *J. Mol. Spectrosc.*, 210:224–232, 2001a. 20

O. Naumenko and A. Campargue. Local mode effects in the absorption spectrum of H_2S between 10780 and 11330 cm^{-1}. *J. Mol. Spectrosc.*, 209:242–253, 2001b. 20

H. R. Partridge. *NASA Technical Memorandum*, page 89449, 1987. 59

K. A. Peterson and T. H. Dunning. Accurate correlation consistent basis sets for molecular corevalence correlation effects: The second row atoms alar, and the first row atoms bne revisited. *J. Chem. Phys.*, 117:10548, 2002. 68, 73

H. M. Pickett. The fitting and prediction of vibration-rotation spectra with spin interactions. *J. Mol. Spectrosc.*, 148:371–377, 1991. 118, 132, 136, 137

H. M. Pickett, R. L. Poynter, E. A. Cohen, M. L. Delitsky, J. C. Pearson, and H. S. P. Muller. Submillimeter, millimeter, and microwave spectral line catalog. *J. Quant. Spectrosc. Radiat. Transf.*, 60:883–890, 1998. 13, 20, 116, 122, 135, 138, 143

E. R. Polovtseva, N. A. Lavrentiev, S. S. Voronina, O. V. Naumenko, and A. Z. Fazliev. Information system for molecular spectroscopy. 5. ro-vibrational transitions and energy levels of the hydrogen sulfide molecule. *Atmospheric and Oceanic Optics*, 25:157–165, 2012. 18, 20

O. L. Polyansky. One-dimensional approximation of the effective rotational hamiltonian of the ground-state of the water molecule. *J. Mol. Spectrosc.*, 112:79–87, 1985. doi: 10.1016/0022-2852(85)90193-6. 138

O. L. Polyansky, N. F. Zobov, I. I. Mizus, L. Lodi, S. N. Yurchenko, J. Tennyson, A. G. Császár, and O. V. Boyarkin. Global spectroscopy of the water monomer. *Phil. Trans. Royal Soc. London A*, 370:2728–2748, 2012. 62

M. Reiher and A. Wolf. *J. Chem. Phys.*, 121:2037–2047, 2004a. 36

M. Reiher and A. Wolf. *J. Chem. Phys.*, 121:10945–10956, 2004b. 36

L. S. Rothman, D. Jacquemart, A. Barbe, D. C. Benner, M. Birk, L. R. Brown, M. R. Carleer, C. Chackerian, K. Chance, L. H. Coudert, V. Dana, V. M. Devi, J. M. Flaud, R. R. Gamache, A. Goldman, J. M. Hartmann, K. W. Jucks, A. G. Maki, J. Y. Mandin, S. T. Massie, J. Orphal, A. Perrin, C. P. Rinsland, M. A. H. Smith, J. Tennyson, R. N. Tolchenov, R. A. Toth, J. Vander Auwera, P. Varanasi, and G. Wagner. The *HITRAN* 2004 molecular spectroscopic database. *J. Quant. Spectrosc. Radiat. Transf.*, 96:139–204, 2005. 11, 20, 62, 98, 103, 122

L. S. Rothman, I. E. Gordon, A. Barbe, D. Chris Benner, P. F. Bernath, M. Birk, V. Boudon, L. R. Brown, A. Campargue, J. P. Champion, K. Chance, L. H. Coudert, V. Dana, V. M. Devi, S. Fally, J. M. Flaud, R. R. Gamache, A. Goldman, D. Jacquemart, I. Kleiner, N. Lacome, W. J. Lafferty, J. Y. Mandin, S. T. Massie, S. N. Mikhailenko, C. E. Miller, N. Moazzen-Ahmadi, O. V. Naumenko, A. V. Nikitin, J. Orphal, V. I. Perevalov, A. Perrin, A. Predoi-Cross, C. P. Rinsland, M. Rotger, M. Simeckova, M. A. H. Smith, K. Sung, S. A. Tashkun, J. Tennyson, R. A. Toth, A. C. Vandaele, and J. Vander Auwera. The *HITRAN* 2008 molecular spectroscopic database. *J. Quant. Spectrosc. Radiat. Transf.*, 110:533–572, 2009. 11, 12, 13, 20, 62, 91, 94, 98, 103, 122, 129, 132, 142, 143, 144, 147, 148

L. S. Rothman, I. E. Gordon, Y. Babikov, A. Barbe, D. Chris Benner, P. F. Bernath, M. Birk, L. Bizzocchif, V. Boudon, L. R. Brown, A. Campargue, K. Chance, L. Couder, V. M. Devi, B. J. Drouin, A. Fayt, J. M. Flaud, R. R.

Gamache, J. Harrison, J. M. Hartmann, C. Hill, J. T. Hodges, D. Jacquemart, A. Jolly, J. Lamouroux, R. J. LeRoy, G. Li, D. Long, C. J. Mackie, S. T. Massie, S. Mikhailenko, H. S. P. Müllerr, O.V. Naumenko, A. V. Nikitin, J. Orphal, V. Perevalov, A. Perrin, E. R. Polovtseva, C. Richard, M. A. H. Smith, E. Starikova, K. Sung, S. Tashkun, J. Tennyson, G. C. Toon, V. G. Tyuterev, J. Vander Auwera, and G. Wagner. The HITRAN database: 2012 Edition. *J. Quant. Spectrosc. Radiat. Transf.*, 2013. (In press). 62, 121, 153

C. T. Russell and M. G. Kivelson. Evidence for sulfur dioxide, sulfur monoxide, and hydrogen sulfide in the io exosphere. *J. Geohphys. Res.*, 106:267–272, 2001. 16, 17

A. H. Saleck, M. Tanimoto, S. P. Belov, T. Klaus, and G. Winnewisser. Millimeter- and submillimeter-wave rotational spectra of rare hydrogen sulfide isotopomers. *J. Mol. Spectrosc.*, 171:481–493, 1995. 122, 124, 132, 133, 135, 139, 142

D. W. Schwenke and H. Partridge. Convergence testing of the analytic representation of an ab initio dipole moment function for water: Improved fitting yields improved intensities. *J. Chem. Phys.*, 113:6592, 2000. 62

J. Senekowitsch, S. Carter, A. Zilch, H. Werner, and N. C. Handy. Theoretical rotationalvibrational spectrum of H_2S. *J. Chem. Phys.*, 90:783, 1989. 23, 59, 60

M. Šimečková, D. Jacquemart, L. S. Rothman, R. R. Gamache, and A. Goldman. Einstein A coefficients and statistical weights for molecular absorption transitions in the HITRAN database. *J. Quant. Spectrosc. Radiat. Transf.*, 98: 130–155, 2006. 118, 133

L. E. Snyder and T. H. Edwards. Simultaneous analysis of the (110) and (011) bands of hydrogen sulfide. *J. Mol. Spectrosc.*, 31:347–361, 1969. 18

C. Sousa-Silva, S. N. Yurchenko, and J. Tennyson. A computed room temperature line list for phosphine. *J. Mol. Spectrosc.*, 288:28–37, 2013. 16

L. Larrabee Strow. Line strength measurements using diode laser: the ν_2 band of H_2S. *J. Quant. Spectrosc. Radiat. Transf.*, 29:395–406, 1983. 18, 58, 66, 122, 131

B. T. Sutcliffe and J. Tennyson. A generalised approach to the calculation of ro-vibrational spectra of triatomic molecules. *Mol. Phys.*, 58:1053–1066, 1986. 36

E. C. Sutton, C. R. Masson G. A. Blake, and T. G. Phillips. *Ap. J. Suppl.*, 58: 341, 1985. 153

G. Tarczay, A. G. Császár, o. L. Polyansky, and J. Tennyson. Ab initio rovibrational spectroscopy of hydrogen sulfide. *J. Chem. Phys.*, 115:1229, 2001a. 23

G. Tarczay, A. G. Császár, O. L. Polyansky, and J. Tennyson. Ab initio rovibrational spectroscopy of hydrogen sulphide. *J. Chem. Phys.*, 115:1229–1242, 2001b. 68

J. Tennyson. Variational calculations of rotation-vibration spectra. In P. Jensen and P. R. Bunker, editors, *Computational Molecular Spectroscopy*, pages 305–323. Wiley, 2000. 39

J. Tennyson. The calculation of vibration-rotation energies of triatomic molecules using scattering coordinates. *Computer Phys. Reports*, 4:1–36, 1986. 36

J. Tennyson and J. R. Henderson. Highly excited states using a discrete variable representation: the H_3^+ molecular ion. *J. Chem. Phys.*, 91:3815–3825, 1989. 36

J. Tennyson and B. T. Sutcliffe. Discretisation to avoid singularities in vibration-rotation hamiltonians: a bisector embedding for AB_2 triatomics. *Intern. J. Quantum Chem.*, 42:941–952, 1992. 42, 50

J. Tennyson and S. N. Yurchenko. ExoMol: molecular line lists for exoplanet and other atmospheres. *Mon. Not. R. Astr. Soc.*, 425:21–33, 2012. 15, 17

J. Tennyson, J. R. Henderson, and N. G. Fulton. DVR3D: programs for fully pointwise calculation of ro-vibrational spectra of triatomic molecules. *Comput. Phys. Commun.*, 86:175–198, 1995. 16, 23, 37, 99, 151

J. Tennyson, M. A. Kostin, P. Barletta, G. J. Harris, O. L. Polyansky, J. Ramanlal, and N. F. Zobov. DVR3D: a program suite for the calculation of rotation-vibration spectra of triatomic molecules. *Comput. Phys. Commun.*, 163:85–116, 2004. 8, 37, 38, 42, 43, 47, 71

P. Thaddeus, M. L. Kutner, A. A. Penzias R. W. Wilson, and K. B. Jefferts. *Ap. J. (Letters)*, 176:L73, 1972a. 153

P. Thaddeus, R. W. Wilson, M. L. Kutner, K. B. Jefferts, and A. A. Penzias. Interstellar hydrogen sulfide. *Astrophys. J.*, 176:L73, 1972b. doi: 10.1086/181023. 15

G. Tinetti, A. Vidal-Madjar, M-C. Liang, J-P. Beaulieu, Y. Yung, S. Carey, R. J Barber, J. Tennyson, I. Ribas, N. Allard, G. E. Ballester, D. K. Sing, and F. Selsis. Water vapour in the atmosphere of a transiting extrasolar planet. *Nature*, 448:169–171, 2007. 16

G. Tinetti, J.P. Beaulieu, T. Henning, M. Meyer, G. Micela, I. Ribas, D. Stam, M. Swain, O. Krause, M. Ollivier, E. Pace, B. Swinyard, A. Aylward, R. van Boekel, A. Coradini, T. Encrenaz, I. Snellen, M. R. Zapatero-Osorio, J. Bouwman, J. Y-K Cho, V. Coudé du Foresto, T. Guillot, M. Lopez-Morales, I. Mueller-Wodarg, E. Palle, F. Selsis, A. Sozzetti, P. A R Ade, N. Achilleos, A. Adriani, C. B Agnor, C. Afonso, C. Allende Prieto, G. Bakos, R. J Barber, M. Barlow, V. Batista, P. Bernath, B. Bézard, P. Bordé, L. R. Brown, A. Cassan, C. Cavarroc, A. Ciaravella, C. Cockell, A. Coustenis, C. Danielski, L. Decin, R. De Kok, O. Demangeon, P. Deroo, P. Doel, P. Drossart, L. N. Fletcher, M. Focardi, F. Forget, S. Fossey, P. Fouqué, J. Frith, M. Galand, P. Gaulme, J. L González Hernàndez, O. Grasset, D. Grassi, J. l Grenfell, M.j Griffin, C. A Griffith, U. Grözinger, M. Guedel, P. Guio, O. Hainaut, R. Hargreaves, P. H Hauschildt, K. Heng, D. Heyrovsky, R. Hueso, P. Irwin, L. Kaltenegger, P. Kervella, D. Kipping, T T. Koskinen, G. Kovács, A. La

Barbera, H. Lammer, E. Lellouch, G. Leto, M. Lopez Morales, M. A Lopez Valverde, M. Lopez-Puertas, C. Lovis, A. Maggio, J. P. Maillard, J. Maldonado Prado, J. B Marquette, F. Martin-Torres, P. Maxted, S. Miller, S. Molinari, D. Montes, A. Moro-Martin, J. L Moses, O. Mousis, N. Nguyen Tuong, R. Nelson, G. S. Orton, E. Pantin, E. Pascale, S. Pezzuto, D. Pinfield, E. Poretti, R. Prinja, L. Prisinzano, J. M. Rees, A. Reiners, B. Samuel, A. Sánchez-Lavega, J. Sanz Forcada, D. Sasselov, G. Savini, B. Sicardy, A. Smith, L. Stixrude, G. Strazzulla, J. Tennyson, M. Tessenyi, G. Vasisht, S. Vinatier, S. Viti, I. Waldmann, G. J White, T. Widemann, R. Wordsworth, R. Yelle, Y. Yung, and S. N Yurchenko. Exoplanet Characterisation Observatory. *Experimental Astronomy*, 34:311–353, 2012. 15

V. G. Tyuterev, S. A. Tashkun, and D. W. Schwenke. An accurate isotopically invariant potential function of the hydrogen sulphide molecule. *Chem. Phys. Lett.*, 348:223–234, 2001. doi: 10.1016/S0009-2614(01)01093-4. 52, 53, 54, 151

V. G. Tyuterev, L. Regalia-Jarlot, D. W. Schwenke, S. A. Tashkun, and Y. G. Borkov. Global variational calculations of high-resolution rovibrational spectra: isotopic effects, intensity anomalies and experimental confirmations for H_2S, HDS, D_2S molecules. *Comptes Rendus Physique*, 5:189–199, 2004. doi: 10.1016/j.crhy.2004.01.017. 23

O. N. Ulenikov, A. B. Malikova, M. Koivusaari, S. Alanko, and R. Anttila. High resolution vibrational.rotational spectrum of H_2S in the region of the ν_2 fundamental band. *J. Mol. Spectrosc.*, 176:229–235, 1996a. 13, 18, 122, 124, 132, 133, 138, 145, 146, 147, 149, 150

O. N. Ulenikov, G. A. Onopenko, M. Koivusaari, S. Alanko, and R. Anttila. High resolution fourier transform spectrum of H_2S in the 3300-4080 cm^{-1} region. *J. Mol. Spectrosc.*, 176:236–250, 1996b. 18

O. N. Ulenikov, A. W. Liu, E. S. Bekhtereva, O. V. Gromova, L. Y. Hao, and S. M. Hu. On the study of high-resolution rovibrational spectrum of H_2S in the region of 7300-7900 cm^{-1}. *J. Mol. Spectrosc.*, 226:57–70, 2004. 20, 113

O. N. Ulenikov, A.-W. Liu, E. S. Bekhtereva, O. V. Gromova, L.-Y. Hao, and S.-M. Hu. High-resolution fourier transform spectrum of H_2S in the region of the second hexade. *J. Mol. Spectrosc.*, 234:270–278, 2005. 18, 113

D. S. Underwood, J. Tennyson, and S. N. Yurchenko. An ab initio variationally computed room-temperature line list for SO_3. *Phys. Chem. Chem. Phys.*, 2013. 16

O. Vaittinen, L. Biennier, A. Campargue, J. M. Flaud, and L. Halonen. Local mode effects on the high-resolution overtone spectrum of H_2S around 12500 cm^{-1}. *J. Mol. Spectrosc.*, 184:288–299, 1997. 20

C. Visscher, K. Lodders, and Bruce Fegley, Jr. Atmospheric chemistry in giant planets, brown dwarfs, and low-mass dwarf stars. II. Sulfur and phosphorus. *Astron. Astrophys.*, 648:1181–1195, 2006. doi: 10.1086/506245. 14, 16

R. Viswanathan and T. R. Dyke. Electric dipole moments and nuclear hyperfine interactions for H_2S, HDS, and D_2S. *J. Mol. Spectrosc.*, 103:231–239, 1984. 71, 72, 73, 133, 138

V. Wakelam, A. Castets, C. Ceccarelli, B. Lefloch, E. Caux, and L. Pagani. Sulphur-bearing species in the star forming region L1689N. *Astron. Astrophys.*, 413:609–622, 2004. doi: 10.1051/0004-6361:20031572. 15

J. K. G. Watson. Vibrational Spectra and Structure. volume 6, pages 1–80. Elsevier, 1977. 131

H.-J. Werner, P. J. Knowles, G. Knizia, F. R. Manby, M. Schütz, P. Celani, T. Korona, R. Lindh, A. Mitrushenkov, G. Rauhut, K. R. Shamasundar, T. B. Adler, R. D. Amos, A. Bernhardsson, A. Berning, D. L. Cooper, M. J. O. Deegan, A. J. Dobbyn, F. Eckert, E. Goll, C. Hampel, A. Hesselmann, G. Hetzer, T. Hrenar, G. Jansen, C. Köppl, Y. Liu, A. W. Lloyd, R. A. Mata, A. J. May, S. J. McNicholas, W. Meyer, M. E. Mura, A. Nicklass, D. P. O'Neill, P. Palmieri, D. Peng, K. Pflüger, R. Pitzer, M. Reiher, T. Shiozaki, H. Stoll, A. J. Stone, R. Tarroni, T. Thorsteinsson, and M. Wang. Molpro, version 2012.1, a package of ab initio programs, 2012. see http://www.molpro.net. 27, 51, 61, 151

D. E. Woon and T. H. Dunning. Gaussian basis sets for use in correlated molecular calculations. iii. the atoms aluminum through argon. *J. Chem. Phys.*, 98:1358–1371, 1993. 34, 68, 75

B. Yadin, T. Vaness, P. Conti, C. Hill, S. N. Yurchenko, and J. Tennyson. ExoMol Molecular linelists: I The rovibrational spectrum of BeH, MgH and CaH the $X\,^2\Sigma^+$ state. *Mon. Not. R. Astr. Soc.*, 425:34–43, 2012. 16

K. M. T. Yamada and S. Klee. Pure rotational spectrum of H_2S in the far-infrared region measured by ftir spectroscopy. *J. Mol. Spectrosc.*, 166:395–405, 1994. 18, 122, 124, 131, 132, 134, 135, 138

K. E. Yousaf and K. A. Peterson. Optimized complementary auxiliary basis sets for explicitly correlated methods: aug-cc-pVnZ orbital basis sets. *Chem. Phys. Lett.*, 476:303–307, 2009. 72, 75

U. Von Zahn and V. I. Moroz. Composition of the venus atmosphere below 100km altitude. *Adv. Space Res.*, 5:173–195, 1985. 17

K. Zahnle, M. S. Marley, R. S. Freedman, K. Lodders, and J. J. Fortney. Atmospheric sulfur photochemistry on hot jupiters. *Astrophys. J.*, 701:L20–L24, 2009. doi: 10.1088/0004-637X/701/1/L20. 14, 16